HIGH-RESOLUTION FUNCTIONAL MAGNETIC RESONANCE IMAGING OF PERCEPTUAL EXPERTISE IN THE VENTRAL TEMPORAL CORTEX AT 7-TESLA

By

Nancy Rankin Williams McGugin

Dissertation
Submitted to the Faculty of the
Graduate School of Vanderbilt University
in partial fulfillment of the requirements
for the degree of

DOCTOR OF PHILOSOPHY

in
Psychology
December, 2011
Nashville, Tennessee

APPROVED:

Dr. Isabel Gauthier

Dr. J. Christopher Gatenby

Dr. Thomas J. Palmeri

Dr. Anna Roe

Dr. Adriane Seiffert

ACKNOWLEDGMENTS

This thesis would not have been possible without the moral and scientific support of many individuals. First, I would like to thank my advisor, Dr. Isabel Gauthier, for her leadership and guidance over the last five years. Her passion for science is contagious, and her integrity and honesty are inspirational. She approaches each day with energetic vigor, striving for perfection while always showing great patience and balance. Not only as a scientist, but equally as a mother, a wife, a chef, and a traveler, Isabel will always be a most respected role model.

I would like to thank each member of my committee for his or her advice and guidance over this work, and especially Dr. Chris Gatenby, with whom many long hours have been sweated at the 7T scanner over the last five years. I would also like to thank all members – past and present – of Dr. Gauthier's Object Perception Lab and Dr. Tom Palmeri's Category Lab, especially Dr. Mike Mack for his invaluable help creating scripts for analyzing 7T fMRI data. Additional thanks to all past and present members of the Perceptual Expertise Network for creative training sessions and encouraging discussions during my graduate study. I also want to thank Dr. Allen Newton for his collaboration in acquiring optimized 7T data, and the Vanderbilt University Institute of Imaging Science for training and opportunities to explore HR imaging.

I'd like to thank each and every member of my family for his or her unconditional love and support. My parents and siblings continuously challenge me to shoot for the stars, showing me through example what hard work and dedication can bring. They have taken great interest in my work. Making them proud is the greatest reward of what I do.

Finally, I would like to thank with love my husband, Bill. With the inevitable ups and downs of science, Bill is always there. When the MRI machine malfunctions, when my participants don't show, and when my data don't cooperate, Bill is there. He has supported my unnaturally early mornings, my complete take-over of the home office, and my sporadic urges to get home immediately to test a new analysis. Bill has taught me great balance and showed me how to love life in a way I never knew possible. He is my best friend and my soul mate, and I would be lost without him.

TABLE OF CONTENTS

Page

LIST OF TABLES

Table Page

LIST OF FIGURES

Figure Page

PREFACE

Overview of the dissertation

This dissertation aims to augment our understanding of the fine-grain neural architecture and functionality of object-selective regions of the ventral-temporal brain and, especially, the highly face-selective Fusiform Face Area (FFA). I begin in CHAPTER I with a brief discussion of the relevant literature, highlighting the ongoing debate regarding the modularity of face perception. CHAPTER II reports on Experiment 1 (E1), which includes a behavioral and a fMRI component. Behavioral measurements provide an index of individual differences in car and plane expertise, while the fMRI study tests the magnitude, selectivity and spatial extent of car and plane expertise effects within the lateral fusiform gyrus. E1 will primarily focus on the FFA and surrounding cortex, since the FFA is the center of the strongest arguments for modularity and the clearest predictions about expertise. CHAPTER III reports on Experiment 2 (E2) in which I measure behaviorally face and car expertise, and use fMRI to explore neural competition in the FFA and beyond. E2 will investigate the spatial distribution of expertise effects when car experts must simultaneous process multiple objects from expert and non-expert visual categories. Finally, in CHAPTER IV, I will offer a general discussion of E1 and E2. I will interpret the present findings in light of the research and propose new directions. For the rest of the dissertation, I will use “we” to describe the work I performed in collaboration with my advisor and collaborators at the Vanderbilt University Institute of Imaging Science.

CHAPTER I

INTRODUCTION

The Fusiform Face Area (FFA): Modularity vs. Perceptual expertise

Visual object recognition is a tremendous human feat. We effortlessly recognize objects despite dramatic variability in their appearance, whether in viewpoint, location, size, lighting, occlusion, illumination, etc. Among other techniques, functional magnetic resonance imaging (fMRI) has been employed to explore the underlying neural mechanisms of visual object recognition. Object recognition is to a great extent supported by the ventral pathway of the human cortex, extending from posterior occipital regions to anterior portions of the temporal lobe. Numerous fMRI studies have revealed object-selective regions in the lateral and ventral occipito-temporal cortex (Haxby 1994; 1996; Ishai et al; 1997; Kanwisher, McDermott & Chun, 1997; Malach et al., 1995; Martin, Wiggs, Underleider & Haxby, 1996; Sergent, Ohta & Macdonald, 1992).

Although category-selective responses in the visual system are observed for many categories, including limbs, scenes, words, letters and musical notation (Dehaene et al., 2010; Downing et al., 2001; Epstein & Kanwisher, 1998; Wong & Gauthier, 2010), face-selectivity often receives the greatest attention. Indeed, faces may be one of the most important categories of objects to which we are exposed. In recognizing others, we quickly identify them as individuals – Mom, Dad, Bill, stranger, etc. – from their faces. Even strangers' faces allow for rapid judgments of sex, age and ethnicity, while also eliciting judgments of attractiveness and of many personality traits that underlie first impressions (Ambday, Bernieri & Richeson, 2000; Bar, Neta & Linz, 2006; Willis & Todorov, 2006). The processing of faces has been linked to an area in the fusiform gyrus of the temporal lobe, the FFA, which shows remarkable anatomical consistency across participants. The right FFA is the most studied face-selective region of the human brain, because its robust selectivity allows for easy identification in individual participants and because its stable location across

participants facilitates easy detection even with relatively crude methods of averaging brain images across different individuals. An FFA is also observed in the left hemisphere, though typically smaller and more variable in its location than its right counterpart (Gauthier et al., 1999; 2000; Kanwisher et al., 1997; Harley et al., 2009; Xu, 2005).

Since the "discovery" of the FFA, the origins of selectivity in this area have been highly controversial. A plausible argument can be made that the FFA is a genetically determined and specialized brain module for the representation of faces. However, whether this pea-sized region of human cortex that selectively responds to faces also supports a more general function relevant for perceptual expertise is a source of debate. Specifically, arguments are made that activity in the FFA is (a) domain-specific for faces (Kanwisher, 2000; Kanwisher et al., 1997) or (b) process-specific for mechanisms automatically recruited by faces but which can also be engaged by non-face objects of expertise (Bukach, Gauthier & Tarr, 2006; Gauthier 2000; Tarr & Gauthier, 2000; Wong et al., 2009). Although both faces and objects of expertise engage many brain areas, whether *the FFA* responds to objects of expertise is especially critical in evaluating the modularity of face processing. This importance is derived from the fact that the FFA is the focus of the strongest claims of modularity (Kanwisher et al., 1997; McCarthy et al., 1997; Puce et al., 1996) and the clearest predictions regarding perceptual expertise (Gauthier et al., 1999; 2000; Harley et al., 2009; Xu 2005). Despite considerable neuroimaging work focusing on the FFA using faces and objects of expertise, this debate is yet unresolved.

Face modularity: domain specificity

One of the strongest arguments for the modularity of face perception is the domain-specificity of FFA responses (Kanwisher et al., 1997). The domain-specific hypothesis argues that activity in the FFA – or even a subset of cells in this region – exclusively codes the processing of faces. Some of the earliest claims for domain specificity of the FFA came from single-cell recordings in monkeys that revealed two populations of face cells, one in inferior temporal gyrus with cells differentially

tuned to the identity of faces, and one in the superior temporal sulcus that was more sensitive to eye gaze and facial expression (Bruce, Desimone & Gross, 1981; Desimone, Albright, Gross & Bruce, 1984; Desimone, 1991; Hasselmo, 1989; Perrett & Mistlin, 1990; Perrett et al., 1982; 1984; 1985; 1990). In humans, electrophysiological studies reveal a face-selective potential that peaks negatively at 170 ms post-stimulus onset and is typically strongest over the right hemisphere occipito-temporal electrodes near the FFA (Bentin et al., 1996; Carmel & Bentin, 2002; Tanaka & Curran, 2001). Converging evidence for claims of domain specificity are also found in patients with focal brain damage typically to the occipito-temporal cortex that results in face-selective deficits, which are collectively called "prosopagnosia" (Bodamer, 1947; see Bouvier & Engel, 2006 for a review).

Arguments for domain specificity are also based in part on standard resolution (or SR)-fMRI studies showing fusiform activation that is at least twice as strong for faces as for a diverse sampling of non-face categories (e.g., common objects, head-less animals, and letter strings; Allison et al., 1994; Downing et al., 2005; Kanwisher et al., 1997; McCarthy et al., 1997; Puce et al., 1996). More recent claims rely on advances in neuroimaging that have allowed for high resolution (or HR)-fMRI of the FFA, revealing that *only* faces elicit a reliable selective response in the FFA (Grill-Spector, Sayres & Ress, 2006; Tsao et al., 2006; Op de Beeck & Baker, 2010; McKone, Kanwisher & Duchaine, 2007; Baker, Hutchison & Kanwisher, 2007; Weiner & Grill-Spector, 2010; Tsao & Livingstone, 2008). This is consistent with electrophysiological recordings in the monkey showing that similar face patches consist almost solely of face-selective neurons (Tsao et al., 2006). Without actually studying objects of expertise, these authors conclude against the importance of expertise with objects for understanding FFA function based on near-absolute selectivity for faces (Op de Beeck & Baker, 2010; Tsao & Livingstone, 2008). Thus, FFA responses to objects in novices or in experts obtained with SR-fMRI are thought to be due to spatial blurring of non-face selective regions near face selective patches.

Expertise: process-specificity

To apply the modular account (see Fodor, 1983; 2000) to face specialization in the FFA is to suggest not only that the FFA is exclusive for face processing, but that this region processes faces in a way that cannot be used with non-face objects even with extensive experience (Robbins & McKone, 2003). As the main alternative to the modularity account, the expertise account of FFA functions suggests that this area responds to faces just as it does for other objects of expertise, although face responses may be stronger and more universal because of the ubiquity and extent of our experience with faces (Bukach et al., 2006; Gauthier & Bukach, 2007).

This idea that our expertise with faces can explain specialization for face perception in the FFA is a specific case of a more general account that has been called the process-map hypothesis (Gauthier, 2000). Here, "map" refers to the layout of visual areas in the brain, with each area best suited for a certain kind of processing. The process-map hypothesis suggests that category-selectivity observed in any given region (e.g., the selectivity of the FFA for faces) reflects task-driven differences even when this selectivity is measured in the absence of a task. Associations between a category and a task, and by extension between a category and the processes best suited for performing this task, as well as the brain areas that support these processes, arise from our prior history with a given category and tend to generalize to novel objects of the trained category.

In the case of expertise in face recognition, the task that is postulated to specialize regions of the occipito-temporal cortex and, especially the FFA, is individuation. Expertise at individuating objects from visually similar categories is thought to recruit similar processing strategies as face perception (Busey & Vanderkolk, 2005; Diamond & Carey, 1986; Gauthier & Tarr, 1997). One critical marker of individuation is holistic processing, or the tendency to process all parts of an object at once to maximize sensitivity to small configural changes (Farah et al., 1998; Hole, 1994; Tanaka & Farah, 1993; Richler, Wong & Gauthier, 2011; Young et al., 1987). While perceptual

expertise in any domain – faces and objects alike – likely engages a distinct set of processes, holistic processing in particular may be specifically supported by the FFA. Evidence for this comes from studies using a variety of stimulus sets and experimental tasks that show the FFA to be specifically involved whenever individuation of items depends on holistic processing. For example, increases in holistic processing during the acquisition of expertise correlate with activity in or very near the FFA (Gauthier et al., 1999; Gauthier & Tarr, 2000; Wong et al., 2009). Moreover, using various sets of novel objects, several studies have demonstrated higher activity in the FFA for objects following subordinate-level identification training than the same objects following basic-level categorization training (Gauthier et al., 1997; 1999; Gauthier & Tarr, 2002; Rossion, Kung & Tarr, 2004). Naturally acquired real-world expertise also recruits this region, as seen when bird watchers process birds, car experts process cars (Gauthier et al., 2000; 2005; Xu, 2005[1]), radiologists process radiographs (Harley et al., 2009), and chess experts process chessboards (Bilalić et al., 2011).

Competition in the FFA

Despite the emerging evidence that both faces and objects of expertise can lead to robust activation in the FFA, we still cannot rule out the existence of a domain-specific, information-encapsulated face processing module, since it is possible that faces and objects of expertise are represented by neighboring but functionally independent cortical areas. Recent competition studies have provided additional evidence against hypotheses of domain-specificity by demonstrating that objects of expertise can interfere with face processing. Specifically, behavioral competition between faces and non-face objects of expertise has been explored through paradigms requiring concurrent processing that taxes the perceptual system (McGugin et al., 2010; McKeeff et al., 2010). If faces and objects of expertise rely on common perceptual mechanisms, their concurrent processing may lead to mutual interference or competition, such that objects of expertise interfere with or limit the

[1] One study (Grill-Spector, Knouf & Kanwisher, 2004) that failed to obtain a car expertise effect in the FFA used images of antique cars when testing modern car experts, so the null effect could simply reflect testing outside of the boundaries of the participants' expertise (Bukach, Phillips, & Gauthier, 2010; Yue et al., 2006).

processing of other objects of expertise (McGugin et al., 2011; McKeeff et al., 2010; Wong et al., 2011).

For example, competition is observed between faces and cars in car experts when exemplars from both categories are simultaneously available for perceptual processing. In a recent study we asked participants to identify which of two targets (either two faces, watches or cars) appeared in rapid sequences of images alternating between items from the target category and items from a task-irrelevant category (McKeeff et al., 2010). With increasing car expertise (as measured in an independent task), participants required more time to identify a target car among distractor faces than watches, revealing that faces competed with car processing as a function of car expertise. In another recent study, participants viewed an alternating sequence of face and chessboard composites, judging whether the bottom half of an image was the same as the bottom half of the previous image. Holistic effects were reflected as the degree to which the top of the image influenced judgments on the bottom. Holistic processing of faces was reduced when chess masters represented the interleaved chessboards in a holistic manner (Boggan, Bartlett & Krawczyk, 2011).

Given, first, that expertise with non-face objects causes neural changes in the FFA representation of the expert category and, further, that expertise leads to behavioral competition during concurrent processing of objects from two domains of expertise, should we conclude that that FFA is the locus of this competition? If the magnitude of neural response or the number of voxels maximally selective for objects of expertise within the FFA increases with expertise, will there be costs to face processing? Expertise with a non-face object category may selectively limit face representation in the FFA if the development of expertise represents a shift from one type of processing strategy and/or representation to another that is characteristic of face processing, yet limited in availability (DiCarlo & Cox, 2007). Previous studies have anecdotally suggested costs of non-face expertise on FFA face-selectivity using SR imaging of dual experts with trained novel objects (Gauthier et al., 1999; Behrmann et al., 2005), as well naturally occurring car experts

(Gauthier et al., 2000). One study found a trend towards decreased neural activity for upright relative to inverted faces in the right FFA during training with novel objects ("Greebles"; Gauthier et al., 1999). Following Greeble training of approximately 7 hours over at least 4 days, face preference in FFA was no longer statistically greater than Greeble preference, due both to an increase in the response to upright relative to inverted Greebles and a decrease to upright relative to inverted faces. Competition was also suggested in a case study that used a Greeble-based training paradigm in a visual agnosic patient with an inferotemporal lesion (Behrmann et al., 2005). In this individual, small improvements in Greeble discrimination during an intensive training program were associated with significant costs in performance on face perception tasks, and Greeble-evoked increases in activity in the fusiform gyrus were associated with decreases in response to faces. Another study found greater activity for cars than faces in the FFA of individuals with very strong car expertise (Gauthier et al., 2005).

This work shows competition for the spatial representation of category-selective neural responses, which may or may not affect performance. Alternatively, *simultaneous* processing of objects from different domains of expertise can also compete in terms of online functional dependencies, which *will* affect performance. For example, neurophysiological evidence from EEG studies suggests that the early N170 event-related potential (ERP) component, a face-selective response thought to originate in or around the FFA (Bentin, McCarthy, Perez, Puce, & Allison, 1996; Rossion et al., 2000), is attenuated when faces are presented concurrently with objects of expertise (Rossion et al., 2004, 2007). In one study, ERPs were recorded while participants viewed an alternating sequence of face and car composites, and judged whether the bottom half of an image was the same as the bottom half of the previous image. As evidenced behaviorally in Boggan et al. (2011) with chess masters, here too holistic processing of faces was reduced when (car) experts represented the expert category (cars) holistically, and this interference effect was correlated with the amplitude of the face-evoked N170 (Gauthier et al., 2003). Moreover, two other studies reported that the N170 in response to faces is attenuated when observers concurrently fixate a

non-face object of expertise (Rossion et al., 2004; Rossion, Collins, Goffaux & Curran, 2007). Faces and objects of expertise compete for resources in a variety of situations. Theoretically, however, competition during simultaneous processing of faces and non-face objects of expertise may ensue in brain regions outside the FFA, wherever expert face and expert object processes overlap.

Beyond the FFA: Distributed brain networks for faces and objects of expertise

Face perception selectively engages a distributed network of small areas beyond the FFA, including an Occipital Face Area (OFA) that is often observed in both hemispheres (Gauthier et al., 1999), as well as face-selective regions in the posterior superior temporal sulcus (pSTS; Puce, Allison, Gore, & McCarthy, 1995; Haxby, Hoffman, & Gobbini, 2000) and an anterior temporal lobe area (aIT) (Kriegeskorte, Formisano, Sorger & Goebel, 2007). The FFA is believed to play an important role in the individuation of faces in concert with the OFA and aIT (Haxby et al., 2001; Hoffman & Haxby, 2000; O'Toole, Jiang, Abdi & Haxby, 2005; Sergent et al., 1992; Tong et al., 2000; Gauthier et al, 2000), whereas face-selective regions of the STS appear more important for processing eye gaze, expression, and dynamic facial movements (Beauchamp, 2004; Haxby et al., 2001; Hoffman & Haxby, 2000; Puce et al., 1998). Face perception also depends on other brain areas devoted to spatial attention, speech perception, and the processing of emotional and biographical information (Haxby et al, 2000). In addition, the mapping of white matter tracks between face selective areas in the human brain reveal that anomalies in the fibers that connect fusiform regions to the anterior temporal lobe and the frontal lobe are associated with congenital deficits in face processing (Thomas et al., 2006).

Strikingly, expertise individuating objects recruits a similarly distributed network. In the first expertise study using fMRI (Gauthier et al, 1999), training with novel objects recruited a region centered on the right FFA, in addition to the right OFA and a region that appears to be the right AFP1 reported for faces (Tsao et al., 2008). In the first study testing experts with familiar objects (cars and birds; Gauthier et al., 2000), expertise recruited the right FFA, the right OFA, a small part

of the parahippocampal gyrus bilaterally and a small focus in left aIT. Recent work using whole brain imaging reported an even more extensive brain network engaged by car experts attending to cars, beginning at V1, overlapping parts of the OFA and FFA, and also including nonvisual areas (Harel et al., 2010), in both hemispheres[2].

Therefore, while the presentation of a face image can trigger a number of unique processes, only some of which relevant to individuation or recruiting the FFA, the presentation of a car image for a car expert likely recruits many different processes and brain regions as well. Face and car activation maps may overlap in a car expert only to the extent that they rely on shared common processes, such as individuation. So, given faces and objects of expertise both recruit multiple processes and multiple areas, what is the value of a debate that centers on the FFA specifically? The FFA is specifically predicted to be involved whenever individuation of items depends on holistic processing, as is the case for face as well as car expertise (Bukach et al., 2010; Richler, Cheung, Gauthier, 2011). Theoretically, the FFA occupies a special position both in a modular account and in an expertise account of face processing, as the center of the strongest claims for modularity and the clearest predictions about expertise.

fMRI at 7T

Earlier HR-FFA studies imaged the FFA at 3T using a surface coil, so data collection was restricted to the right FFA (Grill-Spector et al., 2006, Baker et al., 2007). In contrast, we used a novel scanning paradigm with real-time slice alignment that allowed bilateral imaging of our regions of interest. Bilateral imaging with a wider field of view will be especially critical in addressing E2 hypotheses comparing the right FFA to other face- and object-selective regions. Relative to 3T scanners, 7T scanners offer a greater signal-to-noise ratio (SNR) and contrast-to-noise ratio (CNR),

[2]However, the spatial extent of these expertise effects may have been overestimated, as suggested by the fact that even car novices showed significantly more activity to cars than control stimuli in early visual areas. In addition, while several studies have reported large correlations between individual differences in expertise and activity to objects in the FFA (Gauthier et al., 2000, 2003; Xu, 2005), this study only reported group differences, making it difficult to assess how much variance was accounted for by expertise in different areas.

higher BOLD signal, improved spatial resolution, greater specificity, and enhanced sensitivity to tissue variation and neural activation. For instance, given a volume of brain matter, the maximum signal increases quadratically with field strength. At 3T the BOLD signal depends considerably upon large veins, while at 7T the confounding influence of these veins lessens and activation is more tightly coupled with true neural activity. As such, 7T imaging promotes not only a higher spatial resolution but also a more accurate localization of functional responses. Unfortunately, methods yielding high-quality and uniform image intensity necessarily yield non-uniform image noise. At higher fields, susceptibility variations lead to geometric distortion, imaging artifacts, blurring and signal losses. These effects are especially prominent in areas proximal to the air-filled cavities (e.g., the ear canal and nasal cavity) and, thus, have restricted the HR imaging to temporal lobe. To our knowledge, this is the first study to image inferior/anterior temporal lobe in humans at 7T.

Critically, high field imaging was not in and of itself a goal of the present study. Rather, we were interested in obtaining high-resolution brain images while maximizing brain coverage and minimizing noise artifacts. HR imaging enables us to look at the spatial overlap between face expertise and expertise for non-face objects at a finer scale. Another crucial aspect of our experimental design at 7T hinged upon our use of real-time HR slice alignment. This allowed us to first localize regions of interest based on individual functional patterns of activity combined with anatomical markers, and then ascribe HR slices directly covering these regions for each individual brain.

Specific goals of this dissertation

Here, I used HR-fMRI at 7T to explore the fine-grained spatial organization of expertise effects in and around the SR-FFA. E1 focuses primarily on expertise effects in the right FFA and neural competition for cortical representation for expert categories. Although prior HR-fMRI studies found no reliable selectivity to non-face objects in the FFA (Grill-Spector et al., 2006; Baker et al., 2007), objects of expertise were not specifically investigated. Would reliable selectivity arise

for objects of expertise? On one hand, expertise effects previously localized in (or at least near) FFA with SR-fMRI may only be found in the periphery of those highly face-selective voxels in FFA, suggesting that prior overlap of expertise with face-selectivity was due to spatial blurring. Alternatively, expertise effects could occur more generally within the SR-FFA, suggesting a more homogeneous organization of neurons that can be recruited for different categories of expertise.

If we find expertise effects that are not limited to face-specific voxels, then it becomes important to ask whether expertise effects within this region are spatially limited to a patch similar to face-selectivity, or whether face-selectivity is an island of specialization for faces within a much larger fusiform region recruited by expertise. The first of these options would suggest that expertise could explain the patchy selectivity observed for faces, whereas the second option could be explained by an increase in response due to visual attention by experts, independent of feature selectivity.

E2 investigates expertise in the FFA as well as other areas to test hypotheses for on-line neural competition. Here, we will test underlying competitive interactions in category-selective patches of the FFA during rapid visual presentations in which faces alternate with objects that recruit either similar or dissimilar processing mechanisms. Do face and expert-object sub-populations compete for neural representation in the FFA when faces and non-face objects of expertise are shown in mixed-category streams? Is competition limited to the FFA or observed more generally in expert-object selective region of the ventral pathway?

Foreshadowing our results

Here, with HR-fMRI, we characterized responses to faces, animals, cars and planes in and around the FFA. Group-average mean responses in two experiments replicated prior work, showing reliable selectivity in the FFA for faces and animals but not for non-face objects. More importantly, selectivity for non-face objects in the FFA increased with expertise, including in face-selective voxels. FFA responses to objects (of expertise) cannot be attributed to spatial blurring beyond the

scale at which modular claims have been made, and within the right lateral fusiform gyrus, they are restricted to a 200 mm^2 area centered on the FFA peak. Therefore, these results show that considering individual differences in expertise sheds critical light on FFA functions, suggesting that experience with a category with specific processing demands may be sufficient to explain the spatially-clustered selectivity for faces observed in this region.

While we find competition for spatial representation in the FFA in both E1 and E2, we do not find evidence for on-line neural competition when specifically probed in E2. However, taking into account individual differences in car expertise highlights an interesting dissociation between distributed effects of expertise during non-mixed category presentations and very focal effects when object categories are mixed and the perceptual system is taxed. Effects of expertise, similar to category-specific effects for faces or houses, are less distributed under conditions of divided attention. In other words, while both face-selectivity and responses to non-face objects of expertise can engage distributed networks of areas in the ventral pathway, attentional constraints lead both domains to be focally represented in anterior FFA.

CHAPTER II

EXPERIMENT 1 – EFFECTS OF CAR AND PLANE EXPERTISE WITHIN THE LATERAL FUSIFORM GYRUS AT HIGH RESOLUTION

Methods

Participants. Twenty-five healthy right-handed adults (eight females) aged 22-34 participated for monetary compensation. Informed written consent was obtained from each participant in accordance with the guidelines of the institutional review board of Vanderbilt University and Vanderbilt University Medical Center. All participants had normal or corrected-to-normal visual acuity.

Scanning. All imaging was performed on a Philips Medical Systems 7-Tesla (7T) human magnetic resonance scanner at the Institute of Imaging Science at the Vanderbilt University Medical Center (Nashville, TN).

HR anatomical scan. HR T1-weighted anatomical volumes were acquired using a 3D MP-RAGE-like acquisition sequence (FOV = 256 mm, TE = 1.79 ms, TR = 3.68 ms, matrix size = 256 x 256) to obtain 172 slices of 1 mm^3 isotropic voxels. HR anatomical images were used to align sets of functional data, for volume rendering (including grey matter – white matter segmentation for the purposes of inflating and flattening of the cortical surface), and for visualization of functional data.

SR functional scan. The experimental sequence began with a single-run SR functional localizer for real-time localization of the FFA and optimal positioning of our HR slices on an individual basis (Figure 1). We acquired 30 SR slices oriented in the coronal plane at a resolution of 2.2 x 2.2 x 2.5 mm. The BOLD-based signals were collected using a fast T2*-sensitive

radiofrequency-spoiled 3D PRESTO (PRinciples of Echo Shifting using a Train of Observations)[1] sequence sequence (FOV = 211.2 mm, TE = 22 ms, TR = 21.93 ms, volume repetition time = 2500 ms, flip angle = 62 degrees, matrix size = 96 x 96). For the final 5 participants we achieved full brain coverage (40 slices) in the axial/transverse plane at a resolution of 2.3 x 2.3 x 2.5 mm. Other than a reduced volume repetition time (from 2500 ms to 2000 ms), all scanning parameters remained the same.

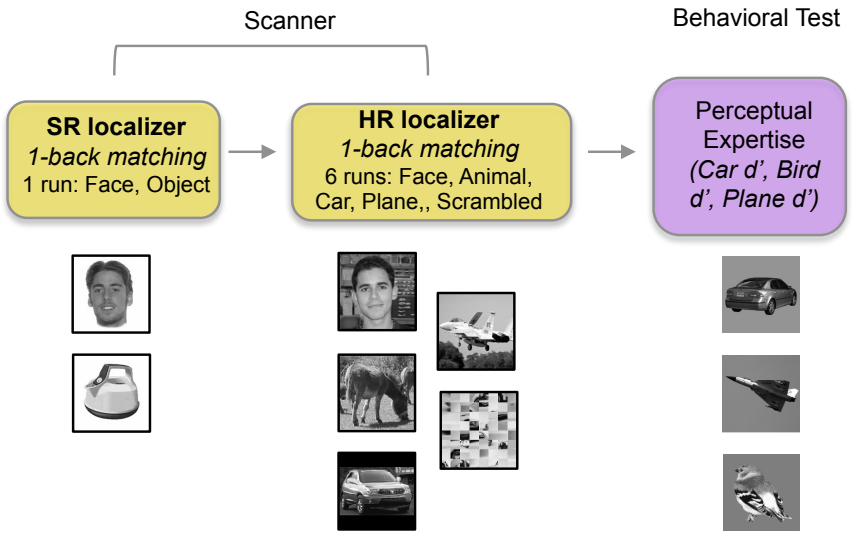

Figure 1: Experiment 1 (E1) design. 25 participants completed 1 SR Face-Object Localizer run, followed by 6 HR runs. Following the fMRI portion of the experiment, individuals completed a behavioral expertise test. One representative image from each object category is shown.

We applied real-time analysis on a participant-by-participant basis during the course of the SR functional scan. We used a linear regression (including a rudimentary motion correction) of the blocked face-object time course to return t-statistics. Only voxels that met a minimum signal threshold were displayed. We applied a very conservative threshold, since these analyses and

[1] PRESTO is an MR sequence that combines elements of echo-shifted, gradient-recalled MR imaging with the acquisition of multiple lines of k-space within a single TR, resulting in a faster imaging time relative to conventional gradient-echo MRI methods. It is a 3-dimensional ultrafast sequence providing higher temporal resolution and increased brain coverage compared to more traditional multi-slice imaging sequences. In addition, PRESTO presents an effective alternative to EPI techniques by minimizing sensitivity to susceptibility artifacts and confounding flow phenomena.

voxel-activation maps are only intended as a guide for subsequent HR acquisitions and not for actual signal extraction. Slice prescriptions that incorporated face-responsive voxels and also included the fusiform gyrus of the temporal lobe were then selected for the proceeding HR runs.

HR functional scans. Immediately following the SR scan, we acquired 24 HR slices oriented in the coronal plane. Signal drop-out typically occurred anterior to the ventral temporal cortex due to susceptibility artifacts in the region behind the ear canals. We also observed drop-out in cortex proximal to the nasal cavities. Thus, these regions were avoided as best as possible during slice prescription. The task is described below. We used a radiofrequency-spoiled 3-dimensional FFE (Fast Field Echo) acquisition sequence with sensitivity encoding (SENSE)[2] (FOV = 160 mm, TE = 21 ms, TR = 32.26 ms, volume repetition time = 4000 ms, flip angle = 45 degrees, matrix size = 128 x 128) to obtain 1.25 mm^3 isotropic voxels.

fMRI stimuli and display

All images were presented on an Apple Macintosh computer using Matlab (MathWorks, Natick, MA) with the Psychophysics Toolbox extension (Brainard, 1997; Pelli, 1997). An Avotec Incorporated "Silent Vision" LCD projector was used to project images on a translucent plastic screen positioned at the foot of the scanner bore. Participants wore prism glasses to view the presented images in their upright orientation. We used 72 grayscale images (36 faces, 36 objects) to localize face-selective regions in the SR run. Subsequent runs used another 110 grayscale face images, in addition to the same number of modern car images (taken in natural settings and in non-frontal views), animal images (all four-legged animal photographs in which the animal's face was typically in a non-frontal view and assumed less than 1/8 of the total image area) and planes (face, animal and plane images came from Dr. Kalanit Grill-Spector at Stanford). Scrambled images were

[2] SENSE is primarily used as a technique for scan time reduction. Importantly, SENSE – as other developments for decreasing imaging time – benefits greatly from the increase in SNR at higher field strengths, due to the intrinsic tradeoff between SNR and the speed of image acquisition.

created on-line during the scan by parsing a randomly selected image into 16 equally sized squares, then rearranging these squares to form a novel display of scrambled pieces. The stimuli were presented in the center of the screen and resized on each trial to subtend a visual angle that varied between 12.6° and 17.6° to discourage use of low-level visual information to perform the detection task. Images were square except for cars, because most of the original images had a landscape aspect ratio and we wanted to preserve the normal aspect ratio of the cars since disruption could disproportionately impede expert judgments. Rectangular images of cars were adjusted to match the area of the other square images.

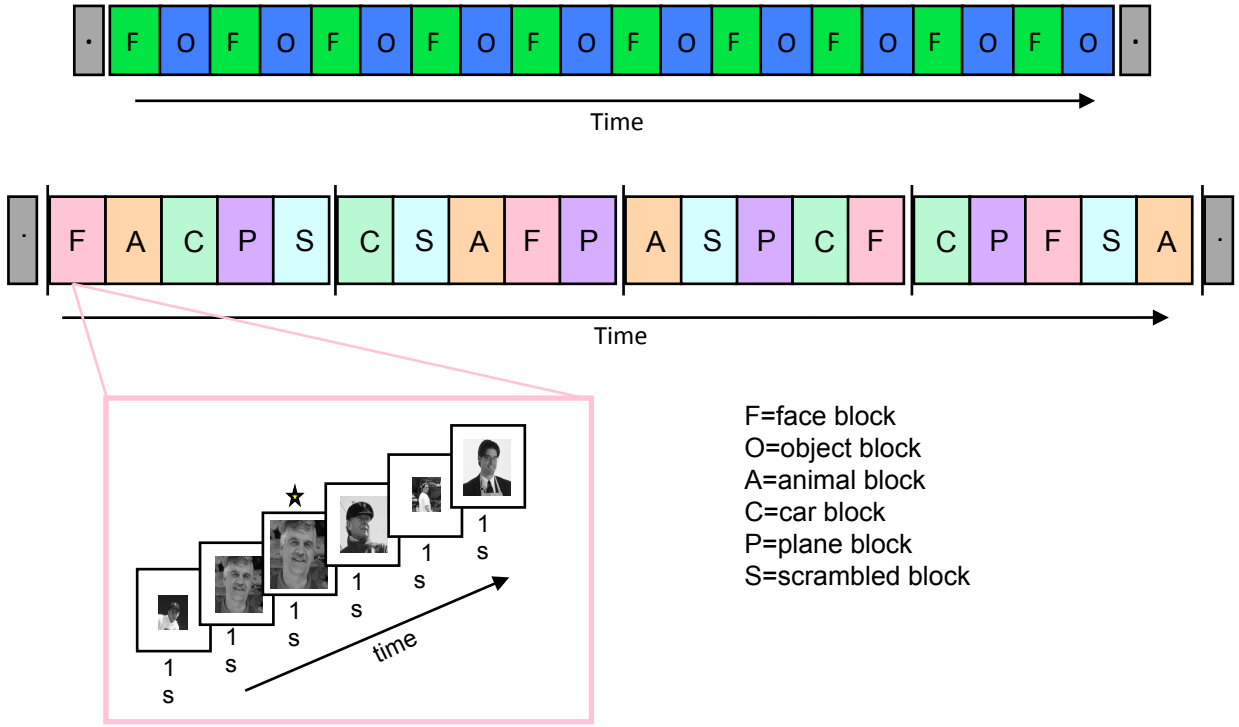

Figure 2. fMRI experimental design. The task in the scanner was identical for the SR localizer run and the 6 HR runs: 1-back identity matching. (a) Example experimental protocol for the SR localizer run: 20 20-s alternating face (F) and object (O) blocks with fixation periods to begin and end the run. (b) Example experimental protocol for the HR runs: 5 stimulus categories (face (F), object (O), animal (A), car (C), plane (P), and scrambled (S)) randomly presented within 4 sets of blocks. Each category occurred in 4 20-s blocks for 6 runs. One Face block is represented. The participant should respond when the second face is repeated in immediate succession.

fMRI tasks

Each participant participated in 7 functional scans: one SR localizer run followed by 6 HR experimental runs. All runs employed a blocked design using a 1-back detection task whereby individuals indicated the repetition of an identical image in immediate succession (Figure 2). Each image differed in size relative to the preceding image, and every block included 1-2 repeats.

1. ***SR localizer run****.* The localizer scan used 20 blocks of alternating faces and common objects (20 images shown for 1 s) with a 10 s fixation at the beginning and end, lasting 420 s in total duration. (In response to scanner upgrades, we adjusted the localizer in the final 5 participants to include 15 20-s blocks with 0 s fixation at the beginning and end of the run; scan duration was 300 s.) Average performance was 97% correct (range 69%-100%).

2. ***HR experimental runs***. Immediately following real-time alignment of the HR slices based on SR data, participants completed 6 experimental runs with 20 20-s blocks (4 each of faces, animals, cars, planes and scrambled, with 20 images sequentially presented for 1 s), with 8 s fixation at the beginning and end, lasting 416 s in total duration. Within a run of 20 blocks, each category occurred once every five blocks, was randomly selected within a set of five blocks, and two blocks of the same category never occurred in immediate succession. Average performance was 97% correct (range 81%-99%). Category-specific behavioral performance in the scanner was not related to indices of behavioral expertise administered outside the scanner (see Table 1 for average category-specific performance, and the relationship between block-specific performance and behavioral expertise measured outside the scanner).

Table 1. Behavioral performance during the 1-back identity-matching task in the scanner, by category. Paired t-tests comparing mean performance (*d'*) between object categories reveal no significant differences, apart from plane matching performance being lower than for face matching (p=0.012). Performance during all intact-object blocks was greater than during scrambled blocks (all ps<0.001). For no category was performance on these easy tasks in the scanner correlated with car or plane expertise. Data are represented for 24 participants, with one outlier omitted from analyses.

	d' (sem)	Correlation with expertise	
		Car d'	*Plane d'*
Face	3.96 (.14)	-0.32	-0.01
Animal	3.85 (.13)	-0.21	0.11
Car	3.84 (.11)	-0.28	0.07
Plane	3.71 (.15)	-0.2	0.09
Scrambled	0.95 (.13)	0.08	-0.03

Behavioral expertise

We sought to explore the effect of expertise on domain-specific patterns of response using individuals with a range of expertise with cars and planes. We quantified perceptual expertise by adapting a method that has successfully predicted both behavioral (Gauthier et al., 2003; Curby et al., 2009; McGugin & Gauthier, 2010) and neural (Gauthier et al., 2000; 2003; Rossion et al., 2004; Xu, 2005) effects of expertise in car experts. We adapted this method to index not only car expertise, but plane expertise as well (Figure 3). We predicted that individuals demonstrating superior interest in and knowledge of cars might show similar biases towards planes since, for example, these domains often co-occur in recreational magazines. Moreover, quantifying discrimination of planes in addition to cars allowed us to explore whether certain individuals were merely skilled at the matching task, itself, regardless of the images shown (e.g., similar to perceptual savants), or whether they actually had unique skill with one category more than others.

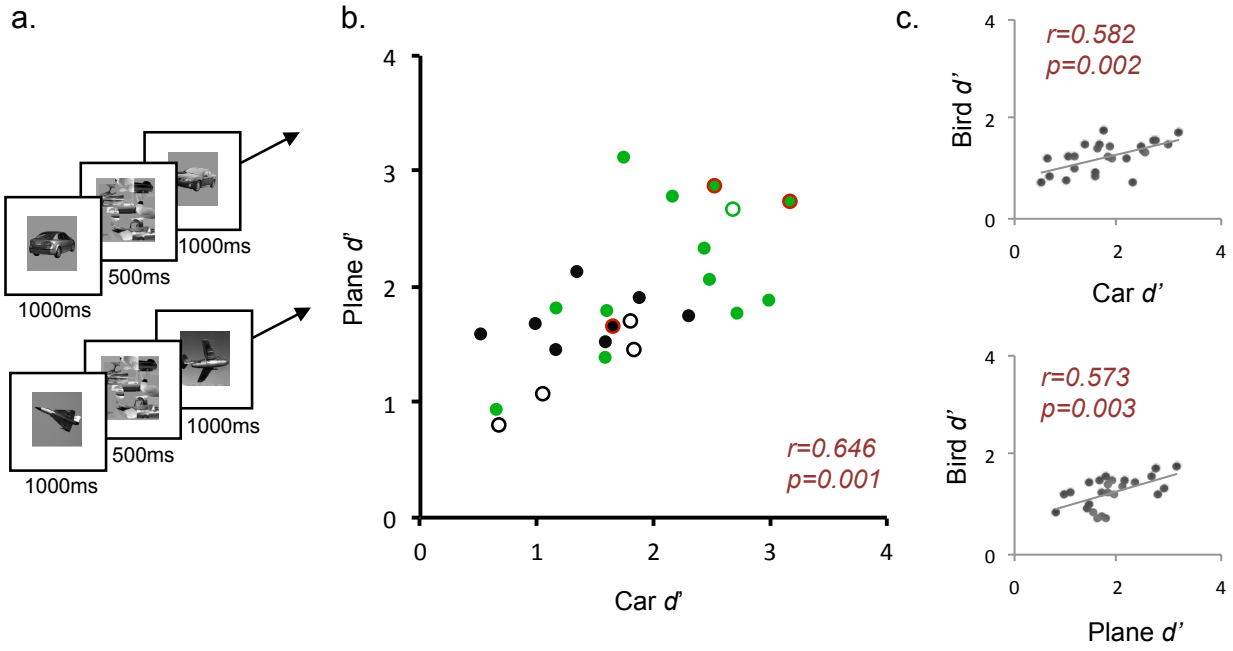

Figure 3. (a) Perceptual expertise test – blocked sequential matching of cars, planes and birds – administered outside the scanner. Category-specific performance was computed as sensitivity, *d'*. (b) Correlation between car expertise (Car *d'*) and plane expertise (Plane *d'*). Green fill shows participants with self-reported car expertise (13/25). Red outlines indicate participants with self-reported plane expertise (3/25). Hollow markers depict participants who did *not* have a right FFA with a minimal area of 100 mm^2. (c) Performance matching birds was correlated with car and plane performance and, thus, was not used as a baseline for car/plane expertise.

A behavioral task outside the scanner used grayscale images of 56 cars and planes (on a solid grey background) that were not used elsewhere in the experiment (Figure 3a). Participants performed 12 blocks (4 car, 4 plane, 4 bird) with 28 sequential matching trials per category. On each trial, the first stimulus appeared for 1000 ms, followed by a 500 ms mask. A second stimulus then appeared and remained visible until a same/different response was made or 5000 ms elapsed. Participants made same-different judgments on car and plane images (at the level of make and model, regardless of year) and bird images (at the level of species). An expertise sensitivity score was calculated for cars (Car *d'*, range 0.52-3.17), planes (Plane *d'*, range 0.80-3.13), and birds (Bird *d'*, range 0.70-1.80) for each participant. Car *d'* was positively correlated with Plane *d'* (r=0.65, p=0.0004), which may be expected if individuals with high interest and discriminatory perceptual

skills for cars also demonstrate such interests and skills for the related domain of planes, and vice versa (Figure 3b).

The measure of Bird *d*' was expected to serve as a baseline performance condition for individual differences in car- and plane-matching skill, as effectively employed in previous reports (e.g., Curby et al., 2009; Gauthier et al., 2000, 2005; Rossion et al., 2004; McGugin & Gauthier, 2010; McGugin et al., 2010; McKeeff et al., 2010; Xu, 2005). Surprisingly, however, performance on bird trials was positively correlated with both car performance (r=0.58, p=0.002) and plane performance (r=0.57, p=0.003) (Figure 3c). Thus, Bird *d*' was not an appropriate neutral baseline condition (in prior work Car d' – Bird d' was used as an index of expertise). Instead, we will here use the range of Car *d'* or Plane *d*' values (regressing out shared variance from the other category) for subsequent analyses relating brain activity to behavioral performance. This is also appropriate since we showed both cars and planes in the scanner.

In addition to these tests, we asked participants to rate their level of expertise with cars, planes and birds, as below average, average, or above average. In general, participants considered themselves most proficient with cars and least with birds. Thirteen participants reported expertise with cars and outperformed the others on car matching: (mean *d*' car experts=2.15, S.D.=0.72; car novices=1.40, S.D.=0.51). In contrast, reported skill with planes did not predict performance in sequential matching of planes: eleven participants reported below-average skill with planes, yet performance among this group ranged from Plane *d*' = 0.80 to 2.67.

Data analysis

Processing of raw fMRI data

The HR T1-weighted anatomical scan was used to create a 3D brain for which translational and rotational transformations ensured a center on the anterior commissure and alignment with the anterior commissure – posterior commissure (ACPC) plane. All brain data analyses were

performed in an effort to minimize interpolation and avoid non-rigid/non-linear transformation (i.e., warping through local expansion and contraction). Specifically, we applied landmark-based registration (using the anterior commissure and posterior commissure, as well as the anterior-, posterior-, inferior-, superior-, right-, and left-most cortical points) to the anatomical and functional data based on the six parameters of rigid body transformations, including translation in x, y, z and rotation over x-, y-, and z-axis. Rigid transformation are global in nature such that the same adjustment applies to all coordinates, in contrast to non-rigid/non-linear transformations which are locally defined and spatially varying. This allowed for maximum alignment in the initial registration of functional data to anatomy. For post-hoc analyses only, the anatomical brain was normalized using stereotaxic (Talairach) space (Talairach & Tournoux, 1988). This allowed us to confirm localization of functionally-defined ROIs with standardized Talairach brain coordinates that have been shown to correspond to face-selective patches.

Functional data were analyzed using the Brain Voyager (BV, http://www.brainvoyager.com) multi-study general linear model (GLM) procedure, as well as in-house scripts created in Matlab (http://www.themathworks.com). Data preprocessing included 3D motion correction and temporal filtering (using a high-pass criterion of 2.5 cycles/run) with linear trend removal. Data from HR functional runs were interpolated from 1.25mm isotropic voxels to a resolution of 1mm isotropic using sinc interpolation. No spatial smoothing was applied at any resolution. To relate functional brain activity with anatomical information in the brain, pre-processed functional slice-based data were aligned to the ACPC-adjusted brain. The hemodynamic response function was modeled from predictor variables represented as boxcar functions forward-shifted and convolved to account for the assumed hemodynamic shape and delay of the fMRI signal. We used standard (GLM) analyses to compute the correlation between predictor variables and actual neural activation, yielding voxel-by-voxel activation maps for each condition.

Table 2. Mean spatial coordinates for the peak of ROIs, and mean size when threshold was lowered until activity spread around the peak to a maximum area of 100mm^2 (right FFA), 50 mm^2 (left FFA, bilateral OFA) and 200mm^2 (bilateral medFG) on the cortical surface. These sizes were chosen on the basis of a review of the typical size of these regions in the literature (34 studies) and to maximize the number of participants for each ROI.

	Mean Talairach coordinates for peak voxel ± standard deviation	Maximum Area (mm^2)	Average Volume (mm^3) ± standard deviation
Right FFA (N=20)	37.3, -55.9, -16.7 (4.9, 9.0, 4.2)	100	729 (121)
Left FFA (N=21)	-35.9, -53.1, -15.6 (3.0, 8.1, 3.8)	50	382 (89)
Right OFA (N=15)	34,1, -71.2, -12.9 (4.3, 5.3, 5.7)	50	347 (74)
Left OFA (N=19)	-39.2, -68.4, -16.2 (5.0, 7.0, 5.2)	50	355 (95)
Right medFG (N=21)	26.0, -57.1, -11.8 (4.7, 5.0, 4.1)	200	1264 (196)
Left medFG (N=24)	-27.7, -59.6, -11.4 (3.8, 7.2, 3.9)	200	1260 (161)

All ROIs were defined in 2-dimensional space. First, BV's automatic segmentation algorithm was applied to disconnect the hemispheres and to separate tissue and ventricles based on approximate intensity peaks from the grey and white matter. Hemispheres were then manually corrected slice-by-slice to accurately distinguish the grey matter from the white matter, and this boundary was used to reconstruct the cortical surface for each hemisphere of each participant. When moving from the 3D volume space to the 2D surface space, we took extreme precaution in assessing the quality of our transformation. The grey matter – white matter boundary was segmented largely by hand to ensure precision. The 3D functional localizer data was transformed to a surface format to define ROIs optimally localized around the peak of face selectivity. Critically, SR surface-based mesh time course data were only employed to localize the peak of face > object

activity, and not to extract and analyze raw data. Once the voxels were selected for each ROI, HR data from the 3D volume was used to avoid potential blurring that can occur in surface space.

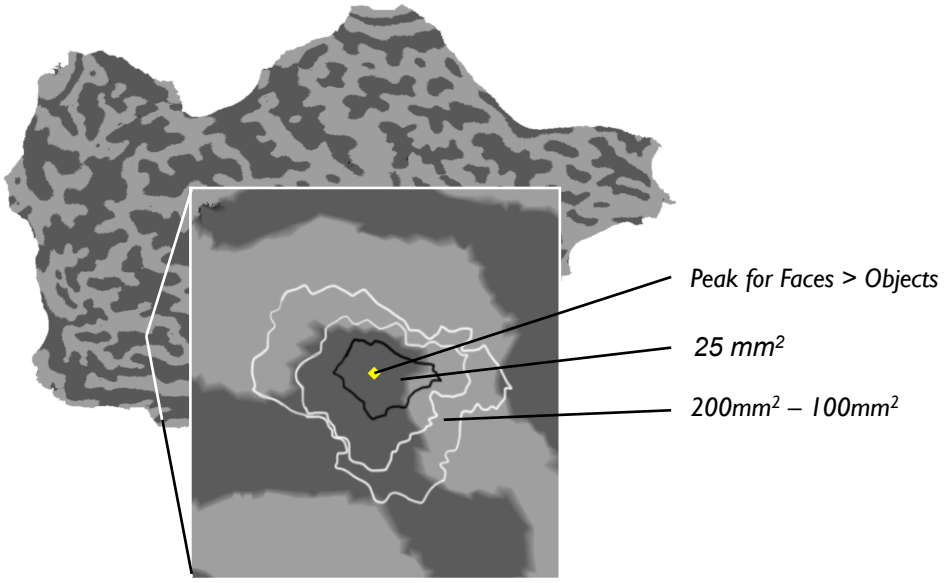

Figure 4. Example of a flattened right hemisphere, with an enlargement showing concentric ROIs and rings surrounding a central peak of face-selectivity, as determined using the SR face>object localizer data. For a ROI, up to five ROIs were defined (25 mm^2, 50 mm^2, 100 mm^2, 200 mm^2, 300 mm^2) and from these up to four rings were identified (50 mm^2 - 25 mm^2, 100 mm^2 – 50 mm^2, 200 mm^2 - 100 mm^2, and 300 mm^2 - 200 mm^2).

Category-selective ROIs were then defined in surface space using the face-object contrast in the SR localizer run: bilateral FFA and OFA included those voxels activated more to faces than objects, while bilateral medial FG included voxels more activated by objects than faces (Figure 4). First, the center of the ROI was defined as the peak of neural activity, then the ROI was expanded to achieve a fixed area across all individuals. Using a consistent number of voxels across participants and ROIs for classification analyses is particularly important since functionally-defined regions will vary in size across participants and classification accuracy improves asymptotically as more voxels are included (Cox & Savoy, 2003; Ku et al., 2008). In separate analyses we defined ROIs using a fixed effects analysis thresholded at q(FDR)<0.05; see Table 2) in standardized Talairach space. We confirmed the location and size of our ROIs as supported by the literature. Figure 5 shows how our

right face-selective fusiform ROIs fall relative to past studies using SR-fMRI. This surface-based peak of activity corresponded spatially to the peak of activity observed in the volume space. Surface rings were defined concentrically around this peak; indeed a major motivation for flattening the hemispheres was for ring creation, since such rings of activation cannot be readily defined in the volume due to folded cortex. However, it is important to note that all HR-analyses were performed in volume space and on volume time course data that had not been transferred into mesh/surface time course data format.

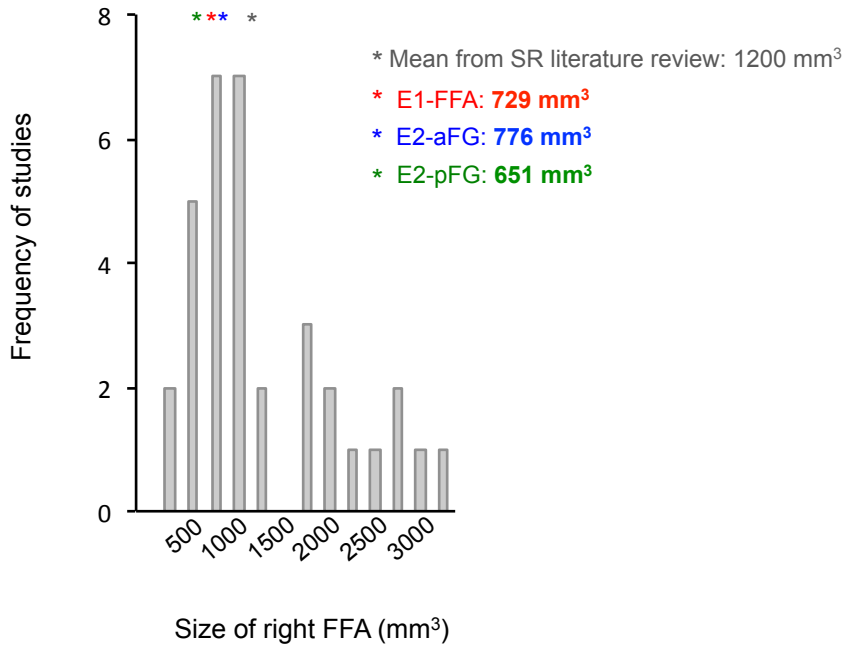

Figure 5. Histogram of select fMRI studies of the right FFA. An informal review of 34 studies represented in this histogram (selected based on a face > object localization and for which volumetric data was reported) revealed a mean FFA volume of 1200 mm^3. Asterisks denote mean volumes of the right FFA observed in the present dataset. See APPENDIX A for a complete list of these studies.

HR analyses were performed on 1 mm^3 voxels (interpolated from 1.5 isometric) of a given ROI that were activated significantly more to objects relative to the scrambled baseline (p<0.01). Voxels incorporated by the SR-defined ROI but failing to pass the HR-based Intact>Scrambled restriction were classified as "Scrambled" voxels.

Analysis of processed fMRI data

Response amplitudes. We first measured the average signal over all activated voxels from each ROI, an analysis that simulates the average SR response. We then computed HR response amplitudes. For each voxel, a percent signal change (PSC) estimate was computed for each category using scrambled blocks as the baseline: e.g., "Face" PSC = (Face – Scrambled)/Scrambled. Response amplitudes were computed in two steps. First, PSC values from the odd-numbered runs were used to determine the category preference of each voxel based on the category evoking the maximum response. Second, PSC values from the even-numbered runs were used to plot the average response amplitude for all 4 categories within each type of voxel. The reverse computations were performed – using data from *even*-numbered runs to sort voxels and data from *odd*-numbered runs to calculate response amplitudes – and the two computations were averaged.

Selectivity of response. We quantified selectivity on a voxel-by-voxel basis using the signal detection theory measure da, with cross validation. Selectivity was computed as $d_a = (\mu_{preferred} - \mu_{nonpreferred})/\sqrt{((\sigma^2_{preferred} + \sigma^2_{nonpreferred})/2)}$, where μ and σ represent the mean and standard deviation, respectively, of responses (Grill-Spector et al., 2006; Simmons et al., 2007)[3]. The mean and standard deviations were computed relative to a scrambled baseline: e.g., $\mu_{preferred} = ((\mu_{preferred} - \mu_{scrambled})/\mu_{scrambled}) * 100$. The preferred category for each voxel was the one that evoked the maximum response during odd-numbered runs, and da was calculated relative to this category using data from the even-numbered runs. These results were then averaged with results from the reverse computation (classification based on *even*-numbered runs and d_a calculation from *odd*-numbered runs). A d_a of 0 specifies no category preference, a $d_a < 0$ signifies that the category preference in even/odd runs did not match the category preference from odd/even runs, and a $d_a \geq 0$ indicates replicable category preference.

[3] As calculated here, d_a is mathematically equivalent to the so-called d' measure from earlier studies (Grill-Spector et al., 2006; Simmons et al., 2007). Because d' refers to the distance between the means of two equal variance Gaussian distributions in standard deviation units, it is not appropriate in cases of unequal variances (personal exchange with John Wixted). In such cases, d_a, is the appropriate discriminability measure.

Neural decoding and classification

Voxel-by-voxel correlations. We computed voxel-by-voxel correlation maps between the magnitude of PSC in even runs with that in odd runs. We computed the average correlation coefficient, *r*, for all voxels by comparing activation maps in two statistically independent datasets for all object categories (Haxby et al., 2001). The *replicability* of the pattern of response to each category is represented by the within-category correlation (e.g., "*Face within"* = correlation between the voxel-by-voxel face map on one dataset and the voxel-by-voxel face map on an independent dataset). The *confusability* of the pattern of response is represented by the between-category correlations (e.g., correlation between the face map on one dataset and the car or sofa map on the other dataset). Reliable classification of category-specific response for a given ROI is demonstrated by a higher replicabilty index (within-category correlation) relative to confusability index (between-category correlation). The cross-correlations for voxel-by-voxel pairwise contrasts comparing within- and between-category correlations were computed using independent datasets and averaged across orthogonal computations.

All statistical tests on correlations were conducted after performing a Fisher's transformation on the voxel-by-voxel within- and between-category correlations. The Fisher transformation is an approximate variance-stabilizing transformation for *r* and defined by z= ½ln((1_r)/(1-r)), where "ln" is the natural logarithm function and r is the sample correlation coefficient.

Winner-take-all (WTA) classifier. We implemented a WTA classifier to test whether a simple linear classifier could determine from the distributed activation patterns what category participants viewed. The classifier is trained with participant-specific activation patterns from one data set (e.g., odd runs), while receiving as input the distributed patterns from an independent data set of the corresponding participant (e.g., even runs). The cross correlation between the training set and input set is computed, and the "winner" is designated as the category that yields the highest correlation. We performed this analysis twice (training with odd, testing with even, and training

with even, testing with odd), then averaged results across these two computations. The WTA classifier was applied to progressive subsets of voxels in order to map the robustness of the classifier as a function of ROI size. Chance is 25%.

Results

We varied the threshold of relative object- and face-selectivity to produce concentric ROIs of incremental sizes (Figure 4, Figure 6a). With HR-fMRI we measured responses to faces, animals, cars, planes and scrambled matrices during a 1-back identity-discrimination task (Figure 6b, Table 1).

Replicating classical SR-FFA effects in participants varying in car expertise

First, we analyzed the results averaged over the entire rFFA, using the mean of category-selective responses and thereby simulating analyses performed earlier at SR-fMRI (Gauthier et al., 1999; 2000; Harley et al., 2009; Op de Beeck et al., 2006). As expected, the response to faces was twice that to inanimate objects, with an intermediate response to animals (Grill-Spector et al., 2006; Hanson & Schmidt, 2010; Kanwisher et al., 1997) (Figure 7a).

Because this was the first study to explore effects of expertise at HR, we first sought to replicate SR-fMRI effects of expertise (Gauthier et al., 1999; 2000; 2005; Gauthier & Tarr, 2002; Harley et al., 2009; Rossion et al., 2004; Wong et al., 2009; Xu 2005). We simulated a SR response using the average of category-selective HR responses. We replicated SR-fMRI effects of expertise, since our behavioral measure of car expertise predicted the average ROI percent signal change (PSC) to cars vs. animals when the signal was averaged over the entire SR-FFA (100mm^2 rFFA: r=0.604, p=0.005; Table 3).

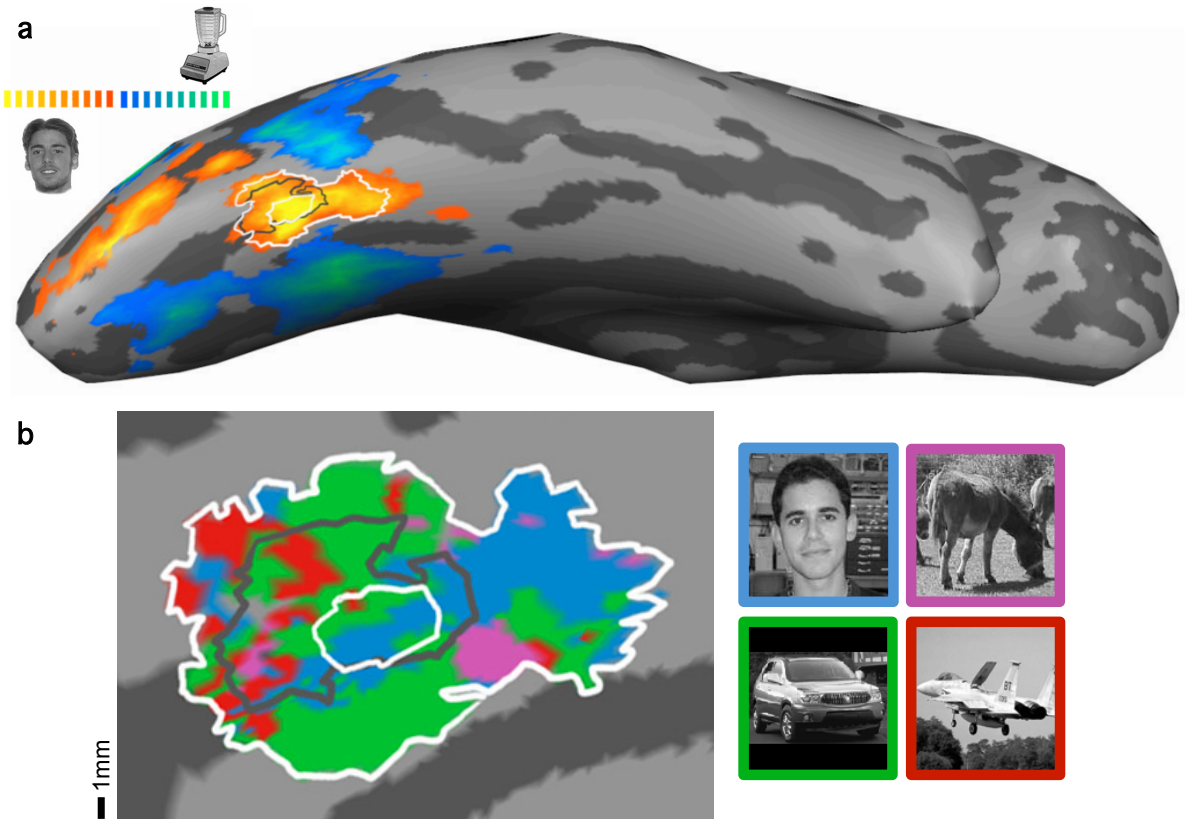

Figure 6. Patterns of functional response overlaid on anatomical maps for one representative car expert. (a) Data from the Face-Object SR-fMRI (2.2 x 2.2 x 2.5 mm) displayed on an inflated right hemisphere. A 25 mm^2 rFFA ROI was defined around the peak of face-selectivity in the lateral fusiform gyrus (innermost white circle). We varied the map threshold to define incrementally larger ROIs entered on the peak: the central black outline depicts the 100 mm^2 ROI, and the outermost white outline shows the 300 mm^2 ROI. An identical procedure was applied for intermediate sizes of the rFFA (50 mm^2 and 200 mm^2), and for all relevant sizes for other localized ROIs (lFFA, bilateral OFA, bilateral medFG). (b) An enhanced view of the SR-defined rFFA displayed on the flattened cortical sheet, with the 25 mm^2, 100 mm^2 and 300 mm^2 ROIs. The color map shows the HR- voxels (1.25 x 1.25 x 1.25 mm) sorted as a function of the maximal response in half the dataset.

Table 3. The table reports the correlations between the whole rFFA response to cars-animal and car expertise, or the rFFA response to planes-animal and plane expertise. Highlighted in grey are the partial correlations, with behavioral expertise from the other category partialled out. All correlations are significant (n=20, α = 0.05).

	ROI PSC	
	C-A	***P-A***
Zero-order correlation	**0.604**	**0.683**
Partial correlation	**0.529**	**0.634**

The neural response to animals serves as a high-level baseline to examine individual differences in activation because fixation alone is an insufficient baseline for a category-evoked signal, since the neural response to all categories is highly correlated. As a result, individual effects in behavior cannot be meaningful attributed to anything other than overall variance, which highlights how strong or weak an "activator" one is regardless of category.

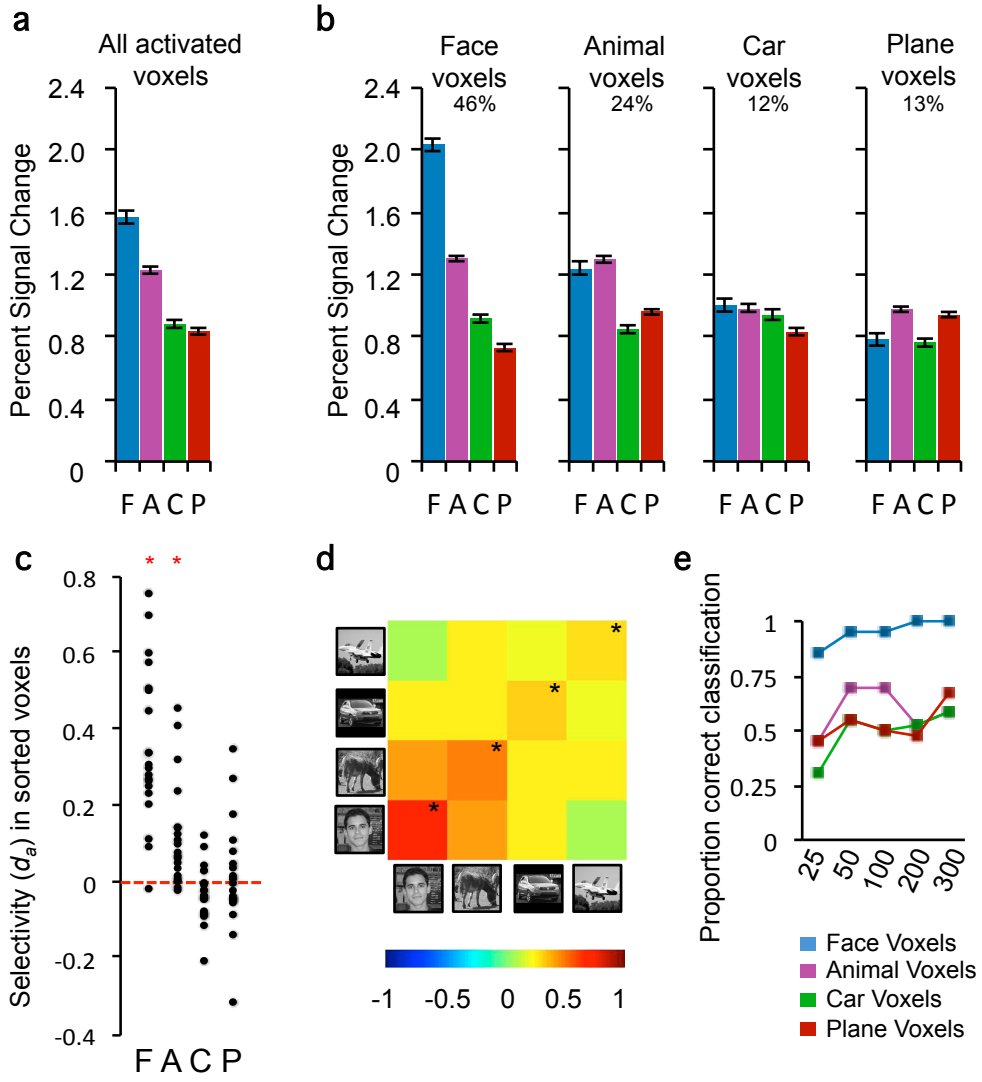

Figure 7. Category-specific response in 100 mm^2 area centered on peak of right FFA. (a) Average percent signal change (PSC) to faces, animals, cars and planes averaged over all HR voxels that were more active for objects than scrambled matrices. This is roughly equivalent to an SR-fMRI signal. (b) HR voxels were grouped by the category that elicited the maximal response in half of the data, and PSC for each category relative to scrambled matrices was plotted for the other half of the data. Error bars show SEM. (c) Voxel selectivity across participants measured using the signal detection theory measure d_a in sorted voxels, for half the data based in voxels sorted in the other half:

$$d_a = \frac{\mu_{preferred} - \mu_{nonpreferred}}{\sqrt{\frac{(\sigma^2_{preferred} + \sigma^2_{nonpreferred})}{2}}}$$

where μ and σ indicate the mean and standard deviation of responses, respectively. Category preference for each voxel was computed as the category yielding the maximal response during odd (or even) numbered runs, while d_a was computed relative to this category using data from the other runs. Negative d_a values suggest that voxels categorized by response to a category respond more to the average of the other categories. (d) Cross-correlation for the voxel-by-voxel pairwise contrasts between within-category and between-category correlations, computed across independent halves of the data and averaged. Asterisks denote cases where, after a Fischer transformation, the within-category (on-diagonal) correlation was significantly larger than the between-category (off-diagonal) correlations. (e) Winner-take-all (WTA) classifier hit rate as a function of ROI size. The WTA is trained with the distributed response profile for each category based on half the data, then computes the cross correlation between training set and the input to determine the winning category for the other half of the data. Chance is 25%.

HR amplitude selectivity analyses were supported using the signal detection theory measure, d_a, with cross validation (Figure 7c). We found reliable selectivity (i.e., mean $d_a > 0$) for faces (t=7.90, $p<0.0001$) and animals (t=3.91, $p=0.001$), but no reliability emerged for cars (t=1.39, *n.s.*) or planes (t=0.73, *n.s.*) (Table 4). Voxels that responded more to cars or to planes in one half of the data set were as likely to respond more to other categories than to cars or planes in the second half. This confirmed prior reports suggesting that FFA contains no reliable selectivity for non-face objects at this spatial scale.

Table 4. The first row shows reliability of category selectivity for the sorted voxels, using cross-validation for rFFA (100 mm²). Asterisks denote where selectivity (d_a) for a category is larger than 0 (α = 0.05). Below are the 0-order correlations (white rows) and partial correlations with expertise for the other category regressed out (grey rows) for car *d*' and plane *d*', respectively. Bold values indicate significant correlations (α = 0.05). Taking into account expertise reveals expertise-related increases in reliability for cars and for planes that is generally accompanied by a decrease in selectivity for animals.

Type of sorted voxel	F	A	C	P
Mean selectivity, d_a	*0.36**	*0.12**	*-0.02*	*0.02*
Correlation with Car expertise, r	-0.41	**-0.65**	**0.52**	-0.02
	-0.24	**-0.56**	0.42	-0.39
Correlation with Plane expertise, r	-0.42	-0.4	0.35	**0.48**
	-0.26	-0.06	0.09	**0.59**

However, we also tested for reliable *patterns* of non-face response within the right FFA. For each category, we compared category replicability to category confusabilty using multivoxel

pattern analysis (MVPA). Specifically, we used planned contrasts to test whether each category was significantly different from the average of the others. We found that the magnitude of category-specific PSC values in odd runs was highly correlated with PSC values in even runs *within* a category, but not *between* categories, for *all* four categories. Faces ($F_{1,19}$=112.00, p<0.0001), Animals ($F_{1,19}$=55.40, p<0.0001), Cars ($F_{1,19}$=18.23, p=0.0004), and Planes ($F_{1,19}$=16.33, p=0.0007) (Figure 7d-e). We further explored pattern replicability through a winner-take-all (WTA) classifier trained with the distributed patterns of response for each category using one half the data, then tested using an independent half of the data. The classifier computes the cross correlation between the training set and the testing set to conclude in an all-or-none fashion the 'winning' category, so chance performance is 25% correct. As seen in Figure 7e, the classifier performed above chance for all non-face categories in addition to faces. We have shown that MVPA can decode all 4 categories, confirming the existence of at least some distributed, sub-threshold information for non-face objects in the rFFA.

Thus far, our HR results correspond with the findings of Grill-Spector et al. (2006) and Baker et al. (2007): only the face voxels, on average, are reliably selective. We replicate these prior conclusions when ignoring expertise. However, as we will see next, a different picture emerges when we take into account individual differences in car and plane expertise.

Reliable selectivity of HR-voxels for objects increases with expertise in SR-FFA

For the first time, we examined the fine-scale organization of expertise effects. We began by examining the proportional representation of category-selective voxels within the rFFA. Expertise for cars predicted the proportion of car-selective voxels in the rFFA (r=0.52, p=0.009, see Table 5). Because the size of the FFA in the SR-fMRI localizer was not related to car expertise (r=0.27, *n.s.*) or plane expertise (r=0.11, *n.s.*), this suggests an expertise-related change of selectivity within at least a subset of FFA neurons. Even when we regressed out the shared variance associated with Plane *d'*,

car expertise (with plane expertise held constant) was able to predict the proportional representation of cars in the FFA (r=0.40, p=0.04).

Table 5. The top row gives the mean proportion of rFFA voxels maximally selective to faces, animals, cars and planes. Below are the zero-order correlations (in white rows) and partial correlations, with expertise for the other category regressed out (in grey rows) for the relationship between the proportion of voxels maximally selective to faces, animals, cars and planes with car (or plane) expertise. Significant correlations are shown in bold (α = 0.05).

	Face %	**Animal %**	**Car %**	**Plane %**
Mean Proportion, % (SD)	46 (17)	24 (10)	12 (7)	13 (8)
Correlation with Car expertise	0.14	**-0.62**	**0.52**	0.05
	0.35	**-0.5**	**0.4**	**-0.4**
Correlation with Plane expertise	-0.26	**-0.44**	**0.38**	**0.58**
	-0.4	-0.15	0.14	**0.66**

Interestingly, the proportional increase in car voxels comes at a cost in the proportion of voxels maximally selective to animals. As car expertise increased, the proportional representation of animals decreased (r=-0.62, p=0.002), even when plane expertise is regressed out (r=-0.50, p=0.01). We can visually compare activation maps between experts and novices to assess these tradeoffs, as well as the clustering and distribution of category-preferring voxels. Figure 8a shows the discrete category maps (sorted voxels) for the rFFA of one car novice and one car expert. These maps depict voxels activated significantly more to intact object categories relative to scrambled matrices at different surface sampling depths relative to the white matter–grey matter boundary. Within the SR-rFFA, HR imaging reveals discrete subsets of voxels that were maximally selective to faces, animals, cars and planes. Voxels preferring faces were spatially interdigitated amongst voxels responding maximally to non-face categories.

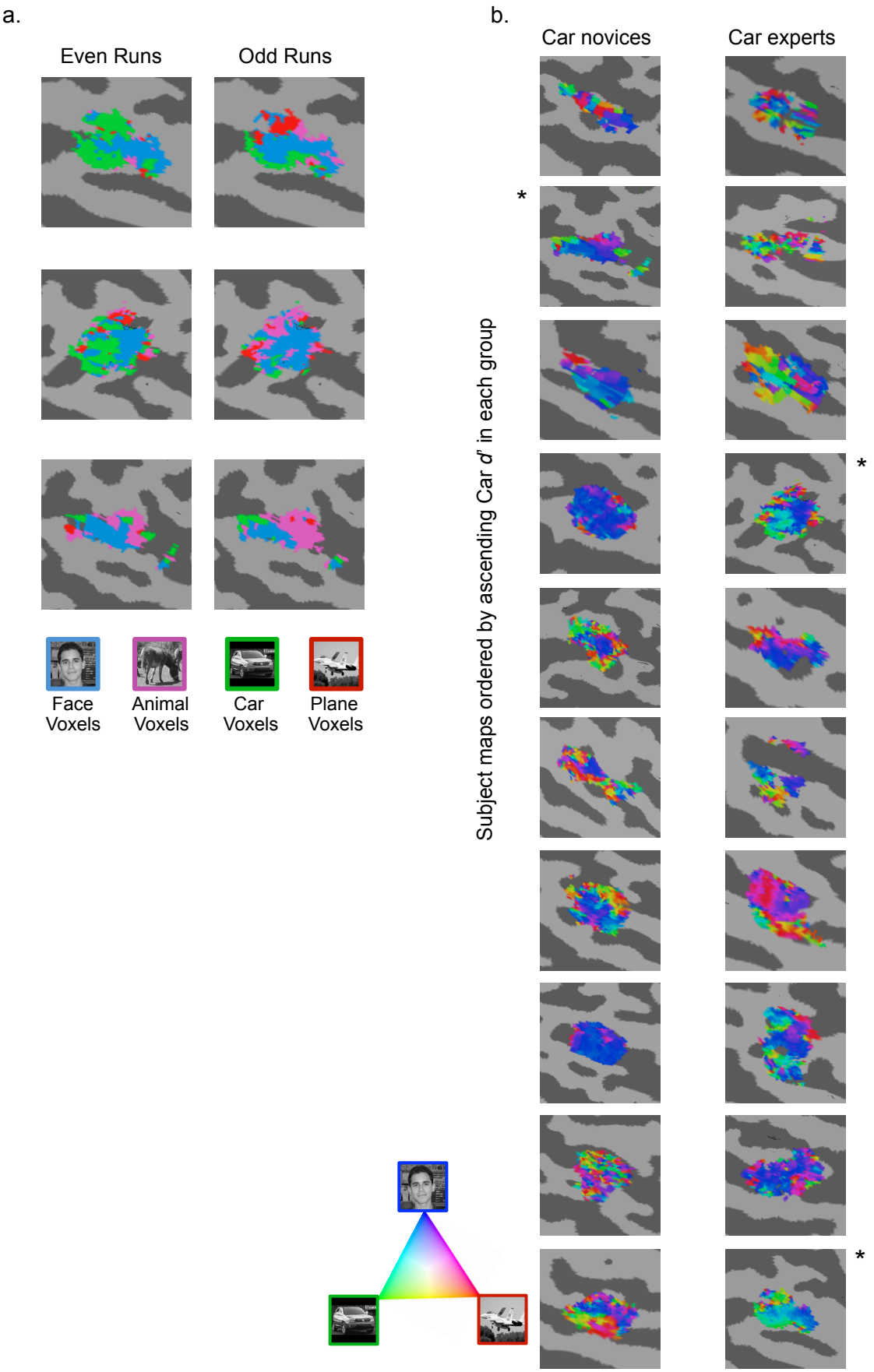
a.
Even Runs
Odd Runs
Face Voxels
Animal Voxels
Car Voxels
Plane Voxels
b.
Car novices
Car experts
Subject maps ordered by ascending Car d' in each group
*
*
*

Figure 8. Discrete and continuous activation maps. (a) Discrete activation maps for the rFFAs of three representative participants, showing active voxels maximally selective to faces, animals, cars or planes based on either even-run data or odd-run data. Within the area that was face-selective with SR-fMRI, different subsets of voxels were maximally responsive to each category. A comparison across these independent samples shows reliability for certain voxels but not others. (b) Continuous maps at the central layer of cortical sampling for the rFFA for all participants. Voxels were sorted according to their relative PSC for faces, cars and planes using an animal baseline, as discussed in the text. Participant maps are grouped into car novices (n=10) and car experts (n=10) based on a median split of car *d'* scores. Columns are ordered from low to high car *d'* values (novices: car *d'* = 0.52-1.65), experts: car *d'* = 1.74-3.17). Asterisks indicate continuous maps also shown for discrete category sorting in a.

However, in reality, HR voxels show a graded preference for *either* faces, animals, cars or planes. Rather, a given voxel responds to all categories though with a varying PSC magnitude. Figure 8b represents continuous category maps for all participants with a rFFA. Each voxel is color-coded based on the relative PSC for faces, cars and planes relative to an animal baseline. The RGB color space indexes the relative scale of "faceness", "carness", or "planeness" for each voxel. For example, voxels appearing dark blue in the participant maps are highly face-selective, while voxels appearing yellow in the maps show a similar response for cars and planes. Maps in Figure 8b are separated into two groups based on a median split for behavioral car *d'* scores (car novices (n=10): car *d'* = 0.52-1.65; car experts (n=10): car *d'* = 1.74-3.17), and sorted according to ascending car *d'* values within each group. These maps reveal an rFFA that is functionally heterogeneous, with highly face-preferring voxels interdigitated amongst voxels with weaker face preference and non-face category preference

With evidence for heterogeneity of rFFA response, we next examined the selectivity of the rFFA for different object categories using the signal detection measure, d_a. We find that d_a for cars in the rFFA HR-voxels increases with car expertise ($r=0.52$, $p=0.02$), while d_a for animals decreases ($r=-0.65$, $p=0.002$) (Figure 9 Table 4). Poor car performers show little evidence for any reliable car-selectivity, since sorted car voxels respond more to non-cars after cross-validation (i.e., Car $d_a < 0$). However, evidence for reliable car responses increase with car expertise. While this analysis averaged over all participants showed no voxels that are reliably car selective, we find a significant increase in the selectivity of car voxels with car expertise.

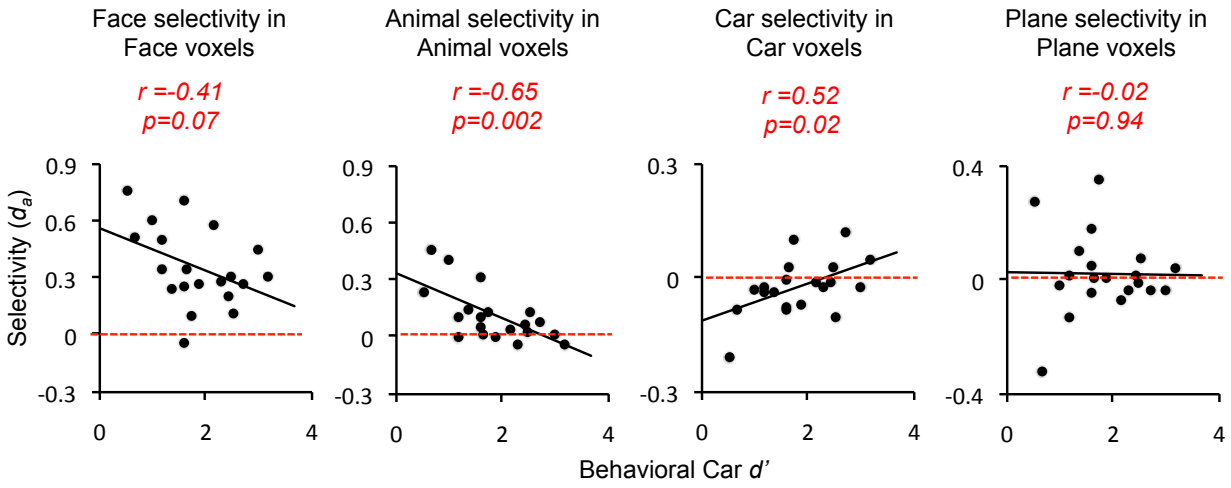

Figure 9. Scatterplots showing the correlations between behavioral car expertise and voxel selectivity, d_a, in a 100 mm² rFFA. Pearson's moment correlation (r) and statistical significance (p) are given. The horizontal red line depicts zero reliability.

Note that one individual appears to show no selectivity for faces, despite this region being defined based on a face>object activation (Figure 9). Although the SR face>object contrast localized a face-selective region expanding to 300mm² for this individual, HR data revealed that the 100 mm² rFFA was composed of only ~16% face voxels, with animal voxels having the highest proportional representation as well as a higher mean PSC across the entire rFFA relative to faces. It is possible that this individual does not have a true *peak* of face-selectivity, but rather has a widespread representation of object-selective clusters in the fusiform gyrus. Indeed, while this individual showed no face selectivity in the 25 mm² ROI (d_a=-0.093), face d_a was positive in the 200-100 mm² and 300-200 mm² rings (d_a=0.122 and d_a=0.081, respectively). When this individual is removed from the analyses, behavioral car *d'* is significantly and negatively correlated with Face d_a (r=-0.413, p=0.031), and there is no change for the other categories: Animal d_a (r=-0.650, p=0.003), Car d_a (r=0.5515, p=0.024), Plane d_a (r=-0.013, *n.s.*).

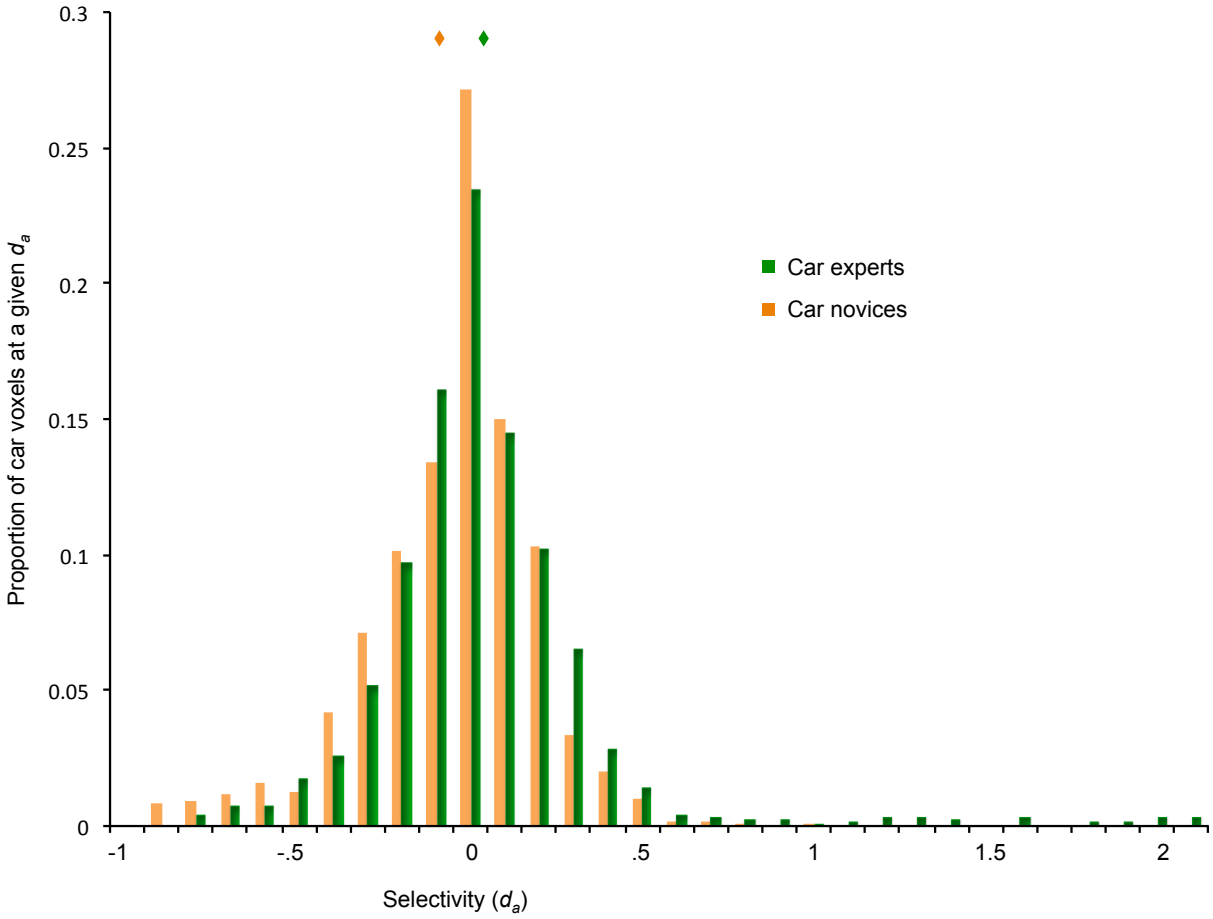

Figure 10. Mean voxel selectivity (d_a) for cars, in the 100 mm^2 rFFA car voxels for car novices (orange) and car experts (green), determined by a median split of car *d*' values. This shows how car expertise increases the proportion of voxels that are selective for cars.

The histogram in Figure 10 shows the distribution of d_a values for cars when participants are separated (median split) into two groups according to their car expertise. For car experts (n=10, green bars) relative to car novices (n=10, orange bars), we see a rise in the proportion of voxels selective to cars at increasing levels of selectivity: i.e., the selectivity profile appears right-shifted for car experts relative to novices. This histogram shows that car experts have more highly car-selective voxels than car novices.

While this index of selectivity reflects the reliability of category-specific responses across independent datasets of all voxels, it aggregates the response amongst the three non-preferred categories. This is because the preferred category mean (and variance) is compared to the average of all non-preferred category means (and variances). Consider, for example, the decrease in

selectivity for animals in animal voxels as a function of increasing car expertise (Figure 9). This trend could represent an expertise-related increase in the neural response for cars and/or planes within the maximally animal-selective voxels. In contrast, if we extract the response to cars or planes relative to the same baseline (the response to animals), they can be more independently compared. As discussed earlier, a high-level baseline is necessary to ensure effects specific to expertise. While d_a selectivity analyses used all other categories as a baseline (e.g., the mean response to cars is compared to the mean response for all other categories), amplitude analyses use animal PSC as a baseline for the other more theoretically relevant categories. In particular, we tested whether car expertise increased the neural response for cars (– animals) in voxels sorted using independent data.

We therefore measure BOLD PSC to cars minus animals in sorted voxels as a function of behavioral car expertise. Expertise for cars predicted PSC to cars in car voxels (r=0.738, p=0.0001), plane voxels (r=0.545, p=0.006), and most interestingly, within the most face-selective voxels (r=0.486, p=0.015) (Figure 11). The three significant correlations with Car *d'* are displayed, where each participant is represented by one point in the scatterplot. Moreover, when we regress out the influence of Plane *d'*, the effects largely remain comparable (Table 6). Amplitude analyses relying on Animal PSC as a baseline support d_a analyses using all non-preferred categories as a baseline, demonstrating that our findings and conclusions do not hinge on any single baseline.

Table 6. The zero-order correlations (in white rows) and the partial correlations, with expertise for the other category regressed out (in grey rows) between the response for cars – animals and car expertise, or the response for planes – animals and plane expertise (*d'*), in the four categories of voxels. Values in the white rows are also graphed in Figure 11. Significant correlations are shown in bold (α = 0.05).

	Face voxels		Animal voxels		Car voxels		Plane voxels	
	C-A	***P-A***	***C-A***	***P-A***	***C-A***	***P-A***	***C-A***	***P-A***
Zero-order correlation	**0.486**	**0.54**	0.32	**0.472**	**0.738**	**0.508**	**0.545**	**0.723**
Partial correlation	0.409	**0.497**	0.222	**0.448**	**0.695**	0.314	**0.467**	**0.636**

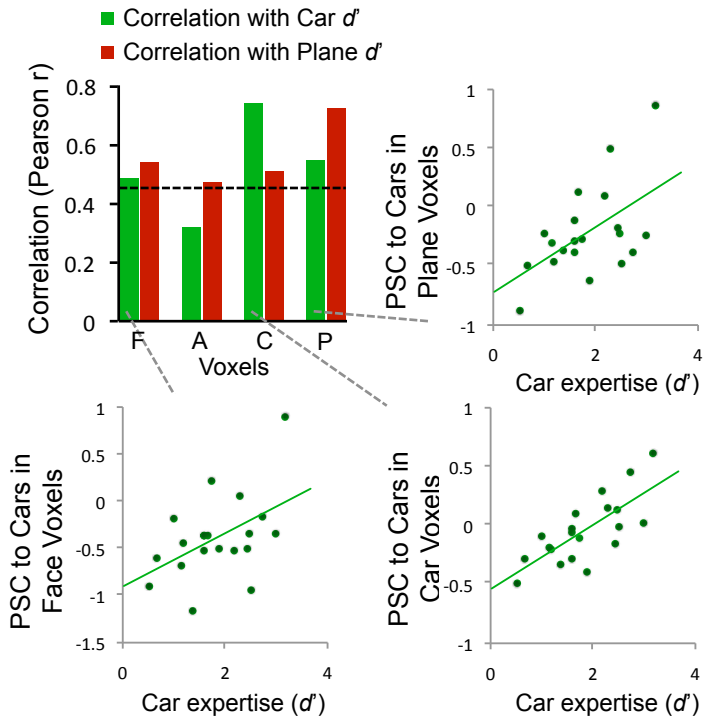

Figure 11. Car and plane expertise within 100 mm^2 ROI centered on the peak of rFFA (N=20). Correlation for behavioral Car *d'* with PSC to cars – animals (green bars) and behavioral Plane *d'* with PSC to planes – animals (red bars) within voxels sorted for their maximal response in the other half of the data. The horizontal dotted black line marks the Pearson r-value at which the correlations are significant (r=0.444). Three exemplar scatterplots are displayed.

Spatial extent of expertise effects in the right FG

We explored the spatial extent of expertise effects considering the patterns of response in concentric ROIs and ring-ROIs surrounding the peak of right face-selectivity. Note that without taking into account expertise, the results in concentric ROIs (25 mm^2, 100 mm^2) and ring-ROIs (200-100 mm^2 and 300-200 mm^2) were qualitatively similar across all neural measures including HR amplitude responses, d_a, Haxby correlations, and WTA analyses, which together highlighted the reliability of faces and, to a lesser extent, animals, but not of cars or planes (APPENDIX B).

However, when we consider expertise with cars, the uniformity of response across these ROIs changes. In particular, the general pattern of car expertise effects observed in the classical

100mm² rFFA is observed in the 25 mm² core and up to the 200-100 mm² ROI-ring, but then disappears. We investigated the spatial distribution of behavioral expertise effects looking at the selectivity of HR category-specific responses in concentric ROIs and ROI-rings centered on the peak of rFFA: 25 mm² ROI, 100 mm² ROI, 200 mm² – 100 mm² ring, and 300 mm² – 200 mm² ring. Figure 12a shows the PSC for Cars (relative to Animals) in sorted voxels correlated with behavioral car expertise in circular and concentric ROI-rings. These data represent only a subset of the group, since we only included individuals who had a rFFA of size 300 (N=12).

Expertise with cars leads to greater car selectivity in the most face-selective voxels of the 25 mm² peak, as well as in the face, car and plane voxels of the classical 100 mm² region, and the face and car voxels of the 200-100 mm² ring-ROI. Critically, HR car selectivity is spatially restricted to the 200-100mm² FG region.

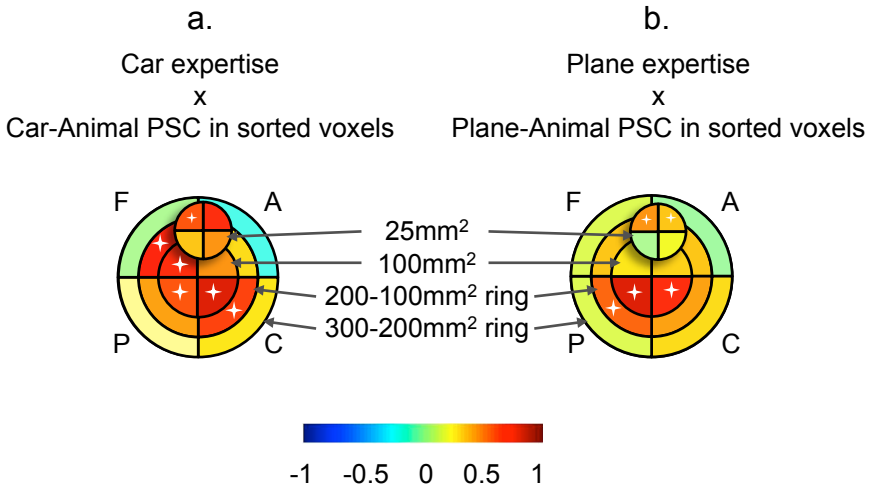

Figure 12. Spatial distribution of car and plane expertise in concentric ROIs and ROI-rings centered on the peak of rFFA: 25 mm² ROI, 100 mm² ROI, 200 mm² – 100 mm² ring, and 300 mm² – 200 mm² ring. (a) Pie charts show the correlation between behavioral car expertise (Car *d'*) and the Car-Animal PSC in sorted voxels. (b) Pie charts depict the correlations between behavioral plane expertise (Plane *d'*) and the Plane-Animal PSC in sorted voxels. Asterisks denote significant correlations ($p<0.05$). Note that the quadrants do not represent spatial information, but voxel categories, while rings illustrate spatial extent of ROIs.

Figure 12b shows the correlation between plane expertise and the Plane-Animal PSC in sorted voxels. Plane expertise increases the neural response to planes in the 25 mm² face and animal voxels, the plane and car voxels of the classical 100 mm² ROI, and the plane voxels of the

200-100 mm^2 ring-ROI. As with the car expertise effects, plane expertise effects fall off in the outermost ring-ROI. We show that without any spatial smoothing at high-resolution, expertise effects for objects cannot be dissociated from selectivity for faces.

These concentric ROIs centered on the rFFA peak reveal that overlap in face and expert-object activation is not simply due to a distributed increase in activity. Unlike the relatively spatially uniform MVPA effects, car and plane expertise effects were centered on the FFA and spatially limited (Figure 12). In the center of the rFFA (~25 mm^2), expertise effects remained detectable, but were not significant in a ring on average 8 to 10 mm away from the peak of face selectivity (300-200mm^2).

One concern in the comparison of activation from ROIs and rings of varying expanses is the overall signal level or time series signal-to-noise ratio (TSNR) of outer rings relative to inner ROIs. Because our HR slices were aligned centrally over the peak of the SR face > object signal, it is possible that growing areas of cortex around this central peak may show reduced TSNR. Thus, it is important to demonstrate that the absence of an expertise effect in the 300-200 mm^2 ring is not simply due to a decrease in signal. To look at this, we measured the TSNR (the mean signal intensity divided by the standard deviation of the signal time course) for the scrambled > fixation results in the HR experimental runs, within ROIs defined using the SR face > object localizer (Figure 13). Again, this analysis is performed only with participants who have a rFFA as large as 300 mm^2 (n=12). There was no evidence of a drop in signal in the 300-200 ROI compared to any of the other ROIs (vs. 200-100, p=0.20; vs. 100, p=0.60 and vs. 25, p=0.51), showing that the spatially-restricted expertise effect cannot be due to a decline in signal quality in the largest ring.

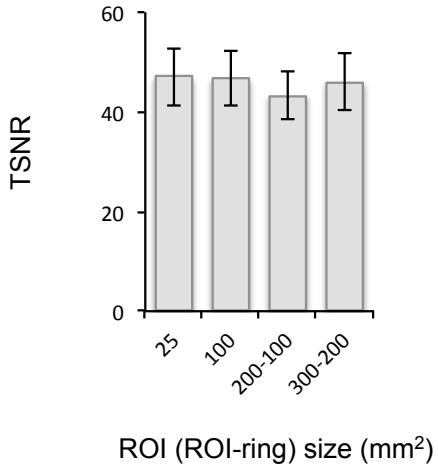

Figure 13. Time series signal-to-noise (TSNR) ratio for the right FFA, considering only those individuals with a 300 mm^2 ROI (N=12). The Scrambled > Fixation signal is compared across 2 ROIs and 2 ROI-ring, demonstrating consistent signal across varying expanses of cortex surrounding the peak.

Car expertise and Plane expertise

Even with only a subset of participants involved in the analysis (12 of the 20 participants with a 25 mm^2 rFFA), Figure 12b suggests that effects of plane expertise – relative to car expertise – are weaker at the centermost core of face selectivity. When considering the spatial extent of neural selectivity up to the 300-200 mm^2 ROI-ring (Figure 12), the car effect was as strong in the centermost peak of face-selectivity as in the 200-100 mm^2 ring, then dropped off. In contrast, the plane effect appears much weaker at the 25 mm^2 core relative to the 200-100 mm^2 ring, and in fact seems to drop off less abruptly passed 200 mm^2. We wanted to explore this further using a different measure of the change in selectivity, in particular looking at changes in the proportion of car-selective or plane-selective voxels as a function of distance from the peak of face-selectivity.

This measure may be particularly sensitive to the recruitment of additional neurons with expertise. Because neither plane nor car expertise recruited category-specific voxels in the outermost 300-200 mm^2 ring-ROI (car expertise: r=0.141, *n.s.*; plane expertise: r=0.120, *n.s.*), we

will contrast proportional representations in the 25 mm² and the 200-100 mm² ring for the two different domains of expertise.

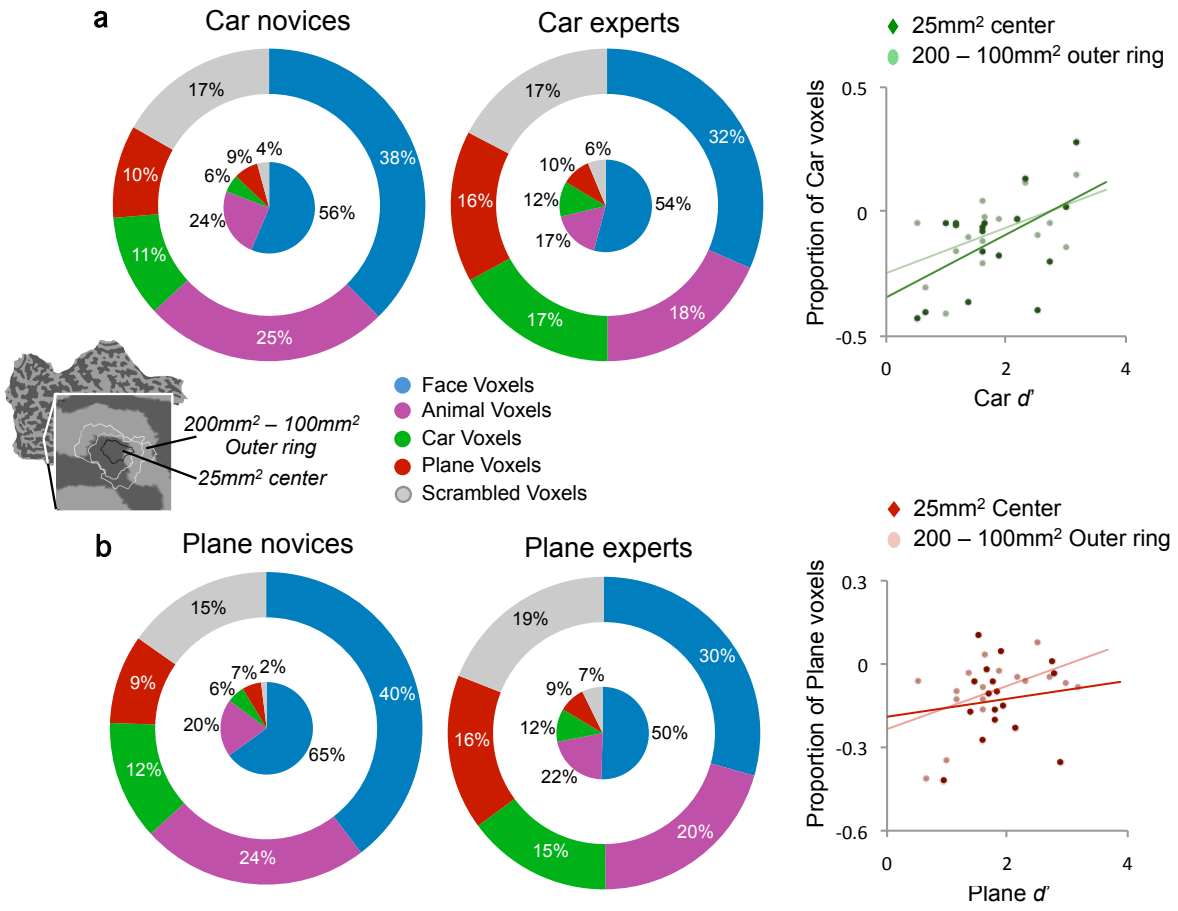

Figure 14. Proportion of category-selective voxels in a 25 mm² ROI and a 200 mm² – 100 mm² outer ring, both centered on the peak of the rFFA. Only participants whose FFA extended to the outer 200-100 mm² ring contributed to this analysis (N=17). (a) Participants grouped by car expertise (9 novices, 8 experts). Car *d'* predicts the proportion of car voxels in the center (r=0.513, p=0.035), as well as in the outer ring (r=0.523, p=0.031). (b) Participants grouped by plane expertise (9 novices, 8 experts). Plane *d'* predicts the proportion of plane voxels in the outer ring (r=0.601, p=0.012), but not in the center (r=0.120, *n.s.*). Inset depicts an enlarged example of center and ring ROI selection on the flattened hemispheric surface for one participant. This analysis reveals that the increase in proportion of selective voxels with plane expertise surrounds but does not invade the peak of the FFA, whereas for car expertise, the effect was found in any ROI equal or smaller than 200 mm².

Plane expertise only recruited additional voxels for planes in an outer 200-100 mm² ring-ROI (r=0.571, p=0.008) (Figure 14b), while for car expertise this effect was observed in the outer 200-100 mm² ring-ROI (r=0.419, p=0.459) as well as in the FFA's 25mm² center (r=0.443, p=0.036)

(Figure 14a). Only participants whose FFA extended to the outer 200-100 mm^2 ring contributed to this analysis (N=17). The increase in proportion of selective voxels with plane expertise surrounds but does not include the peak of the FFA, whereas for car expertise, the effect was found in any ROI equal or smaller than 200 mm^2.

Another interesting spatial dissociation between car and plane expertise occurred in the tradeoffs associated with increasing category-specific proportional representations. Behavioral expertise with cars predicted the proportion of voxels maximally selective to cars, and increasing proportions of car voxels with expertise were associated with a decreased representation for animal voxels in the 25 mm^2 center (r=-0.437, p=0.025), the classical 100 mm^2 (r=-0.619, p=0.002), and the 200-100 mm^2 ring (r=-0.420, p=0.045), but not in the 300-200 mm^2 (r=-0.269, *n.s.*). These data reveal the tradeoff between car and animal selectivity up to the 200-100 mm^2 region. On the other hand, plane expertise was only associated with a cost in the presentation of animals in the 100 mm^2 rFFA (r=-0.437, p=0.026) and marginally so in the 200-100 mm^2 ring (r=-0.368, p=0.072), but not in the core of face-selectivity. As there were no category-specific expertise effects in the 300-200 mm^2 region, neither were there costs in this outermost ring-ROI to non-expert category representations.

HR selectivity and expertise effects outside of the right FG

Left FFA

We asked the same questions in the left FFA as in the right and generally, we obtain similar results for car expertise, but not for plane expertise. To begin, we replicated results at SR with an average signal from all activated lFFA voxels. Considering all activated voxels, there was a main effect of category ($F_{1,20}$=16.18, p<0.001), which Scheffé's post-hoc test showed to be carried by a significantly greater response for faces relative to the response for other visual categories (all ps<0.0001) (Figure 15a). This main effect of category was also observed in a 25mm^2 center

($F_{1,20}$=17.74, p<0.0001; Scheffé's post-hoc test: face>animal, car, plane, all ps<0.001) as well as a 200-100mm outer ring ($F_{1,20}$=10.98, p<0.0001; Scheffé's post-hoc test: face>car, plane, ps<0.001; APPENDIX B). In contrast to the rFFA, the left counterpart has not demonstrated expertise effects when explored at SR-fMRI (Gauthier et al., 2000; Harley et al., 2009; Xu 2005). However, in our results obtained from averaging over the entire lFFA, behavioral car expertise predicts the mean car-animal PSC (r=0.479, p=0.028) (Table 7). This was observed even in the center 25mm^2 region centered on the peak of face selectivity (r=0.469, p=0.032), but fell off in a 200-100mm^2 ring (r=0.032, *n.s.*). This outer ring was only found in 12 of the 21 individuals with the standard 50mm^2 lFFA. Our finding of car expertise effects may be due to the fact that we have a larger number of participants than used in prior studies, as well as more carefully defined ROIs, which is critical since the left FFA is smaller than the right FFA. However, we did not observe effects of plane expertise in these mean PSC responses.

Next, we explore the pattern of HR responses, first independent of expertise, and then taking into account individual differences in behavioral car and plane expertise. Within face voxels of the standard lFFA (50mm^2), there was a main effect of category ($F_{1,20}$=32.97, p<0.001) due to a significantly greater response for faces relative to the response for other visual categories (Scheffé's post-hoc tests: all ps<0.0001) (Figure 15a). This effect was observed in a 25 mm^2 center (main effect: $F_{1,20}$=27.25, p<0.0001; Scheffé's post-hoc test: face>animal, car, plane, all ps<0.001) as well as a 200-100 mm^2 outer ring (main effect: $F_{1,20}$=26.80, p<0.0001; Scheffé's post-hoc test: face>animal, car, plane, all ps<0.001).

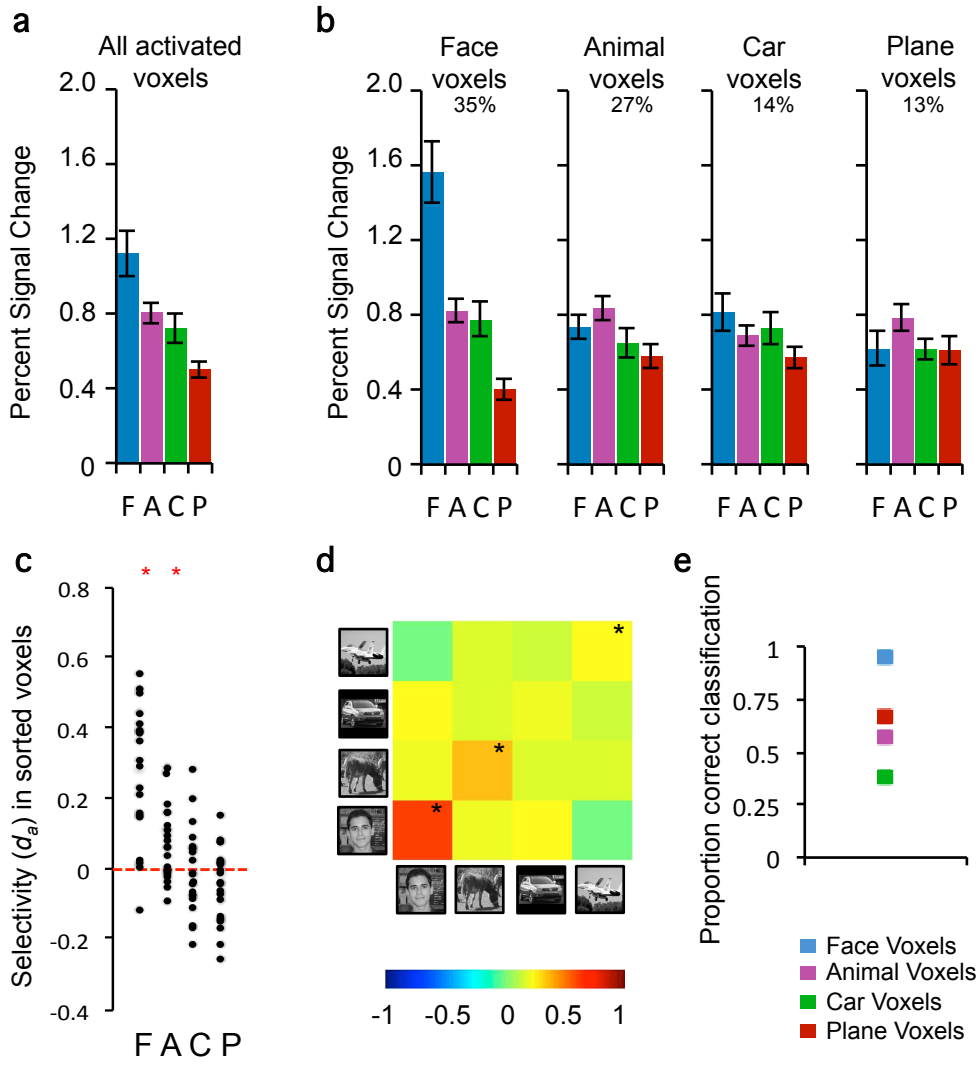

Figure 15. Category-specific response in 50 mm^2 area centered on peak of left FFA (N=21). (a) Average percent signal change (PSC) to faces, animals, cars and planes averaged over all HR voxels that were more active for objects than scrambled matrices. (b) HR voxels were grouped by the category that elicited the maximal response in half of the data, and PSC for each category relative to scrambled matrices was plotted for the other half of the data. Error bars show SEM. (c) Voxel selectivity across participants measured using the signal detection theory measure d_a in sorted voxels, for half the data based in voxels sorted in the other half. (d) Cross-correlation for the voxel-by-voxel pairwise contrasts between within-category and between-category correlations, computed across independent halves of the data and averaged. Asterisks denote cases where, after a Fisher transformation, the within-category (on-diagonal) correlation was significantly larger than the between-category (off-diagonal) correlations. (e) Winner-take-all (WTA) classifier hit rate. The WTA is trained with the distributed response profile for each category based on half the data, then computes the cross correlation between training set and the input to determine the winning category for the other half of the data. Chance is 25%.

Table 7. For each lFFA ROI, the table reports the zero-order correlations (in white rows) and partial correlations, with expertise for the other category regressed out (in grey rows) for the relationship between the response to cars (or planes)– animals in the whole ROI and car (or plane) expertise. Significant correlations are shown in bold (α = 0.05).

Size (mm²)	N	***C-A***	***P-A***
25	21	**0.469**	0.088
		0.278	-0.083
50	21	**0.479**	0.141
		0.319	0.158
200-100	12	0.032	0.037
		0.102	-0.012

Our data suggest that HR-fMRI may be able to detect influences of car or plane expertise. Indeed, car expertise led to a trend for increased recruitment of car voxels in the 25 mm² lFFA peak (r=0.310, *p*=0.084) as well as the standard 50 mm² region (r=0.330, *p*=0.071), but not in the 200-100 mm² ring-ROI (Table 8). Interestingly, in the 50 mm² lFFA, car expertise predicted the proportion of voxels maximally selective to faces (r=0.40, *p*=0.035), but this effect disappeared when we regressed out the influence of Plane *d*' (r=0.23, *n.s.*). As observed in the rFFA, car expertise is associated with a cost in the neural representations of maximally animal-selective voxels, in the 25mm² center (r=-0.60, *p*=0.002) and the 50mm² region (r=-0.60, *p*=0.002). Interestingly, although plane expertise did not recruit plane voxels in the lFFA, we did observe a trend towards smaller proportional representations of animals with increasing plane expertise in the 25mm² center (r=-0.52, *p*=0.012) and 50mm² ROI (r=-0.49, *p*=0.007). In the left hemisphere, as in the right, expertise effects are not observed when we test 8 to 10mm away from the peak of face selectivity.

Table 8. For each lFFA ROI, the table reports the zero-order correlations (in white rows) and partial correlations, with expertise for the other category regressed out (in grey rows) for the relationship between the proportion of face, animal, car, and plane voxels with car (or plane) expertise. The mean proportions are also given for the standard-sized lFFA of 50 mm^2. Significant correlations are shown in bold ($\alpha = 0.05$).

Size (mm^2)	N		**Face %**	**Animal %**	**Car %**	**Plane %**
25	21	Correlation with Car expertise	0.33	**-0.6**	0.31	-0.08
			0.27	-0.44	0.23	-0.16
		Correlation with Plane expertise	0.2	**-0.49**	0.19	0.09
			0.01	-0.21	0.004	0.17
50	21	*Mean Proportion, % (SD)*	*37 (16)*	*24 (12)*	*17 (11)*	*11 (9)*
		Correlation with Car expertise	**0.4**	**-0.6**	0.33	-0.06
			0.23	**-0.42**	0.3	-0.12
		Correlation with Plane expertise	**0.39**	**-0.52**	0.15	0.05
			0.21	-0.26	-0.05	0.11
200-100	12	Correlation with Car expertise	0.41	-0.3	0.36	0
			0.29	-0.39	0.16	-0.06
		Correlation with Plane expertise	0.31	-0.03	0.35	0.06
			0.03	0.26	0.16	0.09

Next, we considered expertise effects on category selectivity using d_a. When averaged over all participants, d_a analyses of selectivity revealed no voxels reliably selective to cars (Table 9). As seen in the rFFA, poor car performers show little evidence for true car-selective voxels, since sorted car voxels respond more to non-cars after cross-validation (i.e., Car $d_a < 0$; Figure 16). However, we find a significant increase in the selectivity of car voxels with car expertise in the standard 50 mm^2 area (r=0.625, p=0.002) as well as in the center-most 25 mm^2 peak (r=0.585, p=0.005). In both cases the observed increase for cars is accompanied by a decrease in selectivity for animals (25 mm^2: r=-0.607, p=0.004; 50 mm^2: r=-0.548, p=0.010) (Figure 16) (Table 9). Critically, this effect dropped off when we moved to a 200-100 mm^2 region surrounding the lFFA. As in the rFFA, in contrast to the relatively spatially uniform MVPA effects, expertise effects were centered on the peak of face selectivity and spatially limited: detectable in the center of the lFFA (~25 mm^2), but absent in a ring on average 6 to 8 mm away from the peak of face selectivity (200-100mm^2).

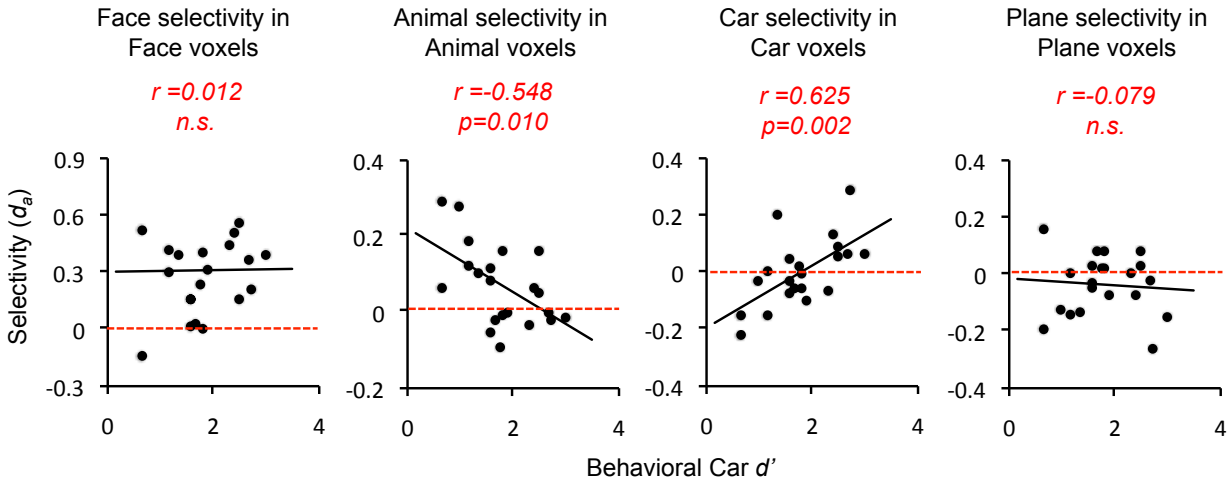

Figure 16. Scatterplots showing the correlations between behavioral car expertise and voxel selectivity, d_a, in sorted voxels in a 50 mm² lFFA. Pearson's moment correlation (r) and statistical significance (p) are given. The horizontal red line depicts zero reliability.

Table 9. For each lFFA ROI, the table reports the zero-order correlations (in white rows) and partial correlations, with expertise for the other category regressed out (in grey rows) for the relationship between the category-specific selectivity, d_a, and car or plane expertise. Mean selectivity values are given for the standard 50 mm² lFFA (red italicized). Before considering expertise, reliable responses are only observed for a faces and animals. Significant correlations are shown in bold ($\alpha = 0.05$).

Size (mm²)	N		F	A	C	P
25	21	Correlation with Car expertise	-0.09	**-0.61**	**0.59**	-0.14
			-0.05	-0.57	0.4	-0.09
		Correlation with Plane expertise	-0.08	-0.28	**0.53**	-0.11
			-0.03	0.12	0.28	-0.04
50	21	*Mean selectivity, d_a*	*0.31**	*0.07**	*0*	*-0.04*
		Correlation with Car expertise	0.01	**-0.55**	**0.63**	-0.08
			-0.04	-0.39	**0.47**	-0.15
		Correlation with Plane expertise	0.08	**-0.46**	**0.51**	0.08
			0.09	-0.21	0.23	0.15
200-100	12	Correlation with Car expertise	-0.36	-0.39	0.2	0.01
			-0.15	-0.3	0.05	0.07
		Correlation with Plane expertise	-0.38	-0.26	0.23	-0.06
			-0.19	0.01	0.14	-0.09

Moreover, in the standard lFFA (50 mm²), expertise with cars predicted the neural response to cars-animals in car voxels (r=0.548, p=0.010) (Figure 17; Table 10). Expertise effects were even

observed for cars in the car voxels of the 25 mm² center of face selectivity (r=0.531, p=0.013).

Expertise effects were not observed in the 200-100 mm² surrounding ring[4].

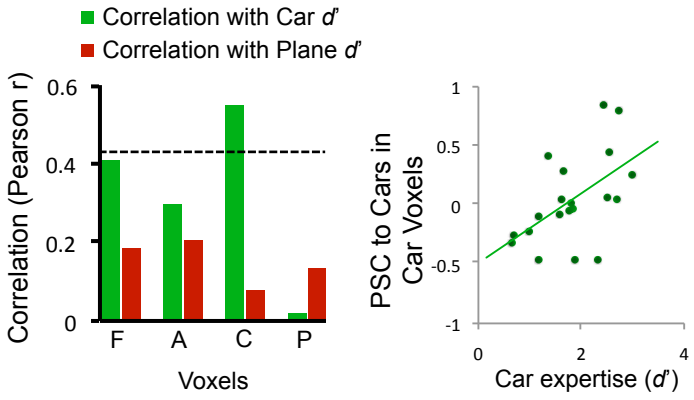

Figure 17. Car and plane expertise within the 50 mm² ROI centered on the peak of lFFA (N=21). Correlation for behavioral Car *d'* with PSC to cars – animals (green bars) and behavioral Plane *d'* with PSC to planes – animals (red bars) within voxels sorted for their maximal response in the other half of the data. The horizontal dotted black line marks the Pearson r-value at which the correlations are significant (r=0.433). One exemplar scatterplots are displayed.

Table 10. For each lFFA ROI, the table shows the zero-order correlations (in white rows) and the partial correlations, with expertise for the other category regressed out (in grey rows) between the response for cars – animals and car expertise, or the response for planes – animals and plane expertise (*d'*), in the four categories of voxels. Bold values are significant (α=0.05). Values in the white rows are also graphed in Figure 17.

		Face voxels		Animal voxels		Car voxels		Plane voxels	
Size (mm²)	N	***C-A***	***P-A***	***C-A***	***P-A***	***C-A***	***P-A***	***C-A***	***P-A***
25	21	0.372	0.054	0.392	0.386	**0.531**	-0.104	-0.081	-0.15
		0.081	-0.184	0.312	0.27	0.404	-0.252	0.082	-0.097
50	21	0.408	0.184	0.296	0.204	**0.548**	0.078	0.02	0.133
		0.198	0.217	0.045	0.075	0.411	0.066	0.072	0.234
200-100	12	-0.081	0.085	-0.143	-0.162	0.39	0.231	0.284	0.215
		-0.026	0.116	0.113	-0.114	0.186	0.145	0.229	0.089

We observed an interesting hemispheric difference in fusiform activations, showing bilateral expertise effects for cars but right-lateralized expertise effects for planes. This observation, along with the finding of right lateralized plane expertise effects that were often restricted from the

[4] We did not consider the spatial extent of expertise effects in the left hemisphere beyond the 200-100 mm² ROI-ring, since the standard lFFA is smaller than the rFFA and only three individuals showed SR face-selective activation extending to the outermost 300-200 mm² ROI-ring.

centermost rFFA core, together suggest that effects for planes may reflect the weaker neural changes associated with relatively limited experience, as addressed in the E1 interim discussion.

Right OFA and Left OFA

In prior work, expertise effects were also observed in other areas beyond the FFA, including OFA and medFG (Gauthier et al., 1999; 2000; Harel et al., 2010). Here, the OFA on the right and on the left were defined in 15 and 19 participants respectively, localized using the SR face>object contrast. Expertise effects in the rOFA have been reported at SR for novel and real-world categories (Gauthier et al., 1999; 2000; but see Harley et al., 2009), but to a lesser extent relative to the effects observed in the fusiform gyri. Whether expertise influences patterns of neural activity in the lOFA is less clear.

Our analyses in OFA generally revealed that car and plane expertise affect car and plane selectivity, respectively, within the rOFA, with trends resembling those observed in the rFFA. In contrast, expertise effects are not found in the lOFA. These conclusions are supported by the following analyses.

We began by testing replication of earlier work using SR-fMRI of bilateral OFAs. We computed averages of our HR data to simulate the response obtained at SR-fMRI. Even though these ROIs were defined from the SR face>object contrast, a 1-way ANOVA comparing category means in the rOFA did not reveal a higher response for faces ($F_{1,14}$=1.814, p=0.159) (Figure 18a). However, we replicated SR effects of expertise when we consider the mean car-animal PSC as a function of behavioral Car *d*' with Plane *d*' regressed out (r=0.508, p=0.053) (Table 11). On the other hand, the lOFA showed the expected main effect of category on mean PSC ($F_{1,18}$=4.220, p=0.009) (Figure 19a) yet no evidence for an expertise effect (r=0.192, *n.s.*).

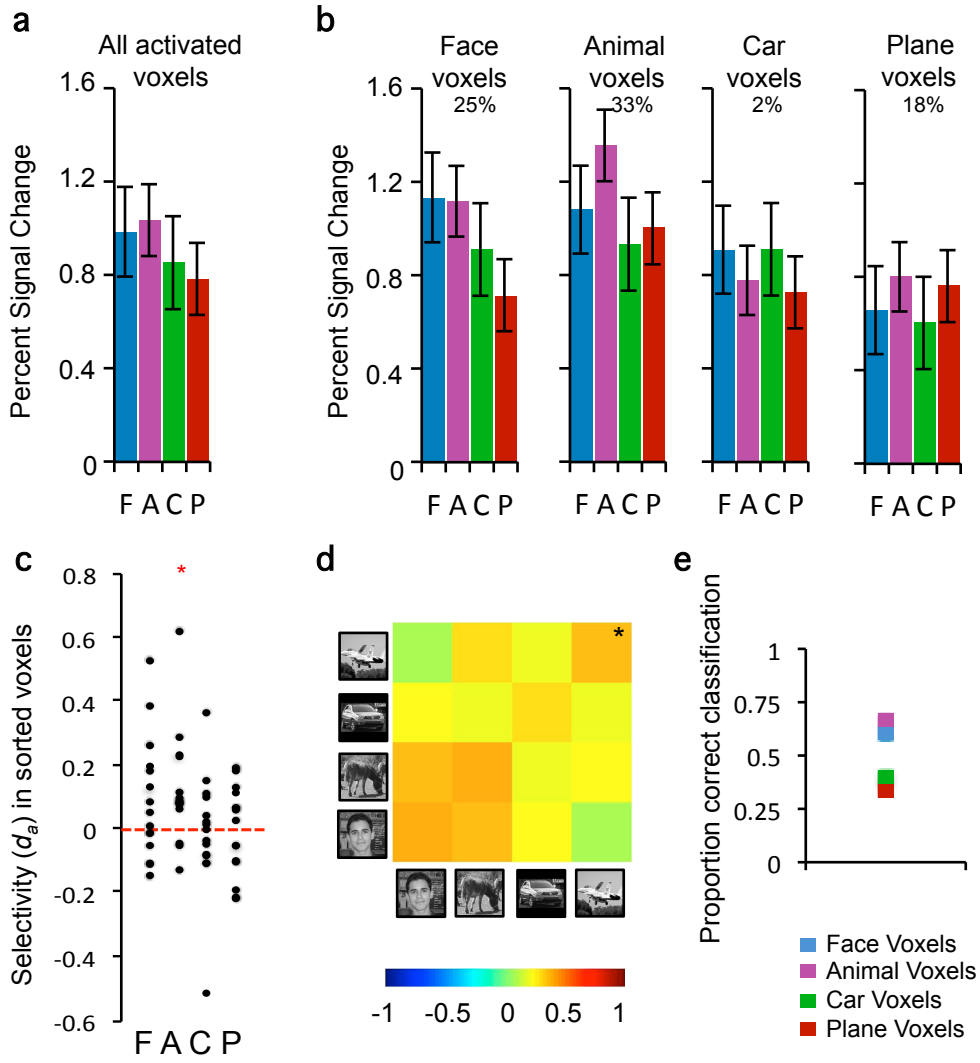

Figure 18. Category-specific response in 50 mm^2 area centered on peak of right OFA (N=15). (a) Average percent signal change (PSC) to faces, animals, cars and planes averaged over all HR voxels that were more active for objects than scrambled matrices. (b) HR voxels were grouped by the category that elicited the maximal response in half of the data, and PSC for each category relative to scrambled matrices was plotted for the other half of the data. Error bars show SEM. (c) Voxel selectivity across participants measured using the signal detection theory measure d_a in sorted voxels, for half the data based in voxels sorted in the other half. (d) Cross-correlation for the voxel-by-voxel pairwise contrasts between within-category and between-category correlations, computed across independent halves of the data and averaged. Asterisks denote cases where, after a Fisher transformation, the within-category (on-diagonal) correlation was significantly larger than the between-category (off-diagonal) correlations. (e) Winner-take-all (WTA) classifier hit rate. The WTA is trained with the distributed response profile for each category based on half the data, then computes the cross correlation between training set and the input to determine the winning category for the other half of the data. Chance is 25%.

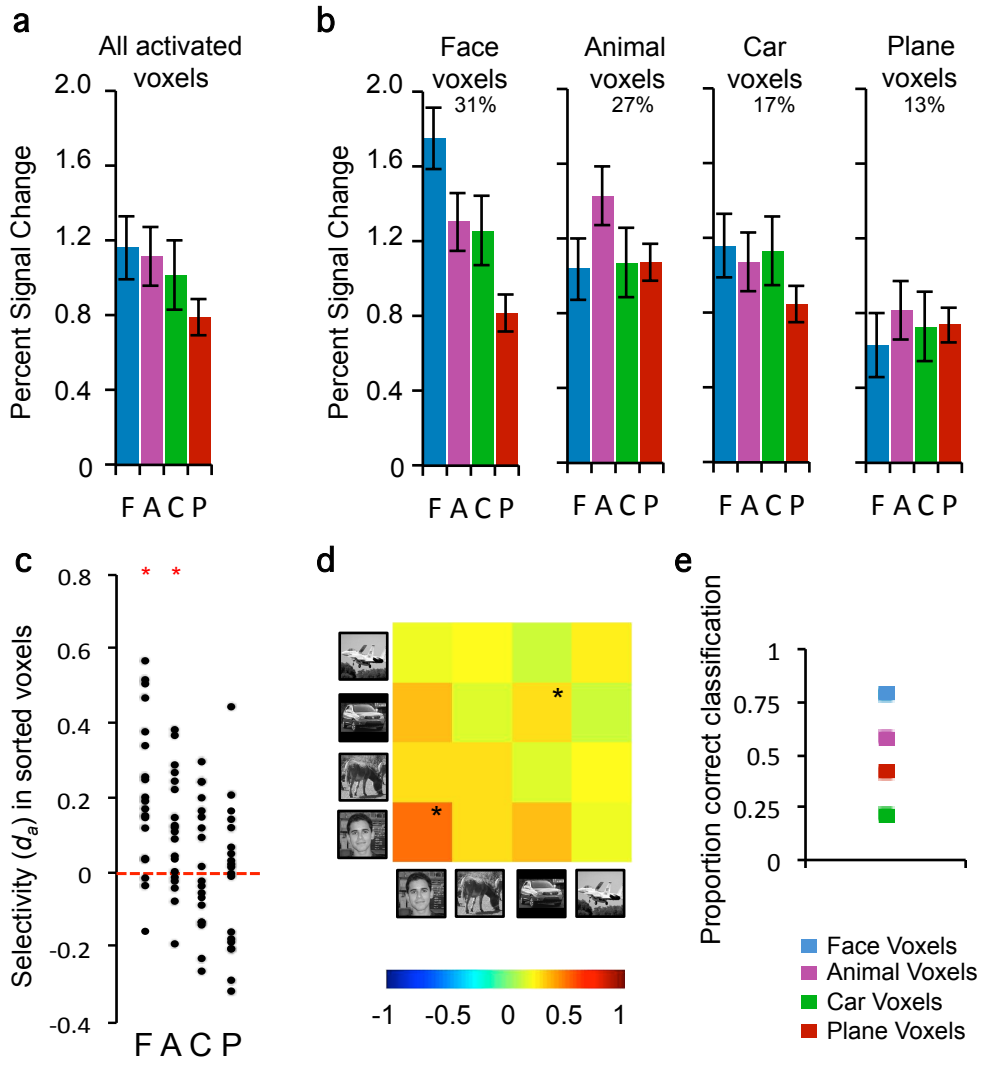

Figure 19. Category-specific response in 50 mm^2 area centered on peak of left OFA (N=19). (a) Average percent signal change (PSC) to faces, animals, cars and planes averaged over all HR voxels that were more active for objects than scrambled matrices. (b) HR voxels were grouped by the category that elicited the maximal response in half of the data, and PSC for each category relative to scrambled matrices was plotted for the other half of the data. Error bars show SEM. (c) Voxel selectivity across participants measured using the signal detection theory measure d_a in sorted voxels, for half the data based in voxels sorted in the other half. (d) Cross-correlation for the voxel-by-voxel pairwise contrasts between within-category and between-category correlations, computed across independent halves of the data and averaged. Asterisks denote cases where, after a Fisher transformation, the within-category (on-diagonal) correlation was significantly larger than the between-category (off-diagonal) correlations. (e) Winner-take-all (WTA) classifier hit rate. The WTA is trained with the distributed response profile for each category based on half the data, then computes the cross correlation between training set and the input to determine the winning category for the other half of the data. Chance is 25%.

Table 11. For bilateral OFA, the table reports the zero-order correlations (in white rows) and partial correlations, with expertise for the other category regressed out (in grey rows) for the relationship between the response to cars (or planes)– animals in the whole ROI and car (or plane) expertise. Significant correlations are shown in bold (α = 0.05).

		ROI PSC	
hem/size	N	***C-A***	***P-A***
right/50	15	0.284	0.45
		0.508	0.11
left/50	19	-0.017	0.018
		0.192	-0.005

Next, we investigated HR patterns of neural activity without spatial smoothing and without regards to behavioral expertise. In the rOFA, reliable responses were only found for animals ($F_{1,14}$=16.135, p=0.0013) (Figure 18b-c), while in the lOFA both faces ($F_{1,18}$=25.695, p<0.0001) and animals ($F_{1,18}$=29.083, p<0.0001) showed reliability of neural response, but not cars or planes (Figure 19b-c; Table 13). When considering the patterns of neural activity using multi-voxel analysis, both the right and left OFAs revealed replicable information for the other categories (Figure 18d-e; Figure 19d-e)

With evidence for at least some information for non-face categories in bilateral occipital regions, we tested for HR effects of behavioral expertise on category-specific responses, using identical methods as applied in bilateral fusiform ROIs. First, we find evidence for a tradeoff between car and animal representations in the rOFA (car % - animal %: r=0.543, p=0.036), but this relation seems carried by the significant decrease in animal representation with car expertise (Table 12). Similarly, in the rOFA, plane expertise predicts an increasing proportion of plane voxels (r=0.621, p=0.012) at the cost of animal voxels (r=-0.520, p=0.044), however this relationship is not sustained when the variance shared with plane expertise is regressed out. The lOFA region shows no evidence for expertise with either category (Table 12).

Table 12. For bilateral OFA, the table reports the zero-order correlations (in white rows) and partial correlations, with expertise for the other category regressed out (in grey rows) for the relationship between the proportion of category-selective voxels and car (or plane) expertise. Significant correlations are shown in bold ($\alpha = 0.05$).

Size (mm^2)	N		**Face %**	**Animal %**	**Car %**	**Plane %**
right/50	15	Correlation with Car expertise	0.195	**-0.754**	0.243	0.486
			0.21	**-0.64**	0.379	0.063
		Correlation with Plane expertise	0.07	**-0.52**	-0.024	**0.621**
			-0.106	0.061	-0.301	0.447
left/50	19	Correlation with Car expertise	0.084	-0.095	-0.044	0.279
			-0.137	0.078	-0.098	0.225
		Correlation with Plane expertise	0.243	-0.204	-0.152	0.174
			0.265	-0.196	-0.175	-0.042

Although we do not initially observe an effect of car *d'* on car d_a in the rOFA, a significant influence emerged when plane expertise was regressed out, highlighting an increase in car d_a (r=0.505, *p*=0.012) with a corresponding decrease in animal d_a (r=-0.449, *p*=0.040) (Table 13). We observed an increase in plane selectivity as a function of plane expertise, regardless of whether car expertise is held constant. In contrast to the rOFA, the lOFA showed no evidence for category-specific increases in selectivity with expertise for either category (Table 13).

As observed in selectivity – d_a – analyses, with amplitude PSCs we see that car *d*' scores do not initially appear to predict the PSC for car-animal in sorted voxels. However, by considering the partial-order correlations for car expertise (Car *d*' with Plane *d*' regressed out), we see a positive relationship between car performance and car-animal PSC in face voxels (r=0.541, *p*=0.045) and marginally so in car voxels (r=0.471, *p*=0.089) (Table 14).

Table 13. For bilateral OFA, the table reports mean selectivity values without considering expertise (red italicized). Asterisks denote reliable category-specific responses (d_a>0). The second and third rows for each ROI give the zero-order correlations (in white rows) and partial correlations, with expertise for the other category regressed out (in grey rows) for the relationship between the category-specific selectivity, d_a, and car or plane expertise. Before considering expertise, reliable responses are only observed for a faces and animals. Significant correlations are shown in bold (α = 0.05).

Size (mm²)	N		F	A	C	P
right/50	15	*Mean selectivity, d_a*	*0.1*	*0.13**	*-0.01*	*0*
		Correlation with Car expertise	-0.224	-0.364	0.221	**0.591**
			-0.185	**-0.449**	**0.505**	0.2
		Correlation with Plane expertise	-0.136	-0.077	-0.167	**0.673**
			0.041	0.293	**-0.489**	**0.439**
left/50	19	*Mean selectivity, d_a*	*0.22**	*0.12**	*0.02*	*-0.01*
		Correlation with Car expertise	0.083	**-0.473**	-0.34	-0.071
			-0.035	-0.342	-0.022	-0.022
		Correlation with Plane expertise	0.148	-0.348	**-0.451**	0.08
			0.128	-0.008	-0.315	-0.315

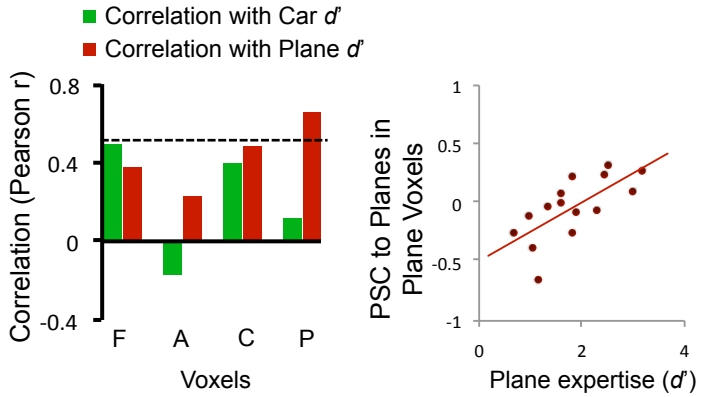

Figure 20. Car and plane expertise within the 50 mm² ROI centered on the peak of rOFA (N=15). Correlation for behavioral Car *d'* with PSC to cars – animals (green bars) and behavioral Plane *d'* with PSC to planes – animals (red bars) within voxels sorted for their maximal response in the other half of the data. The horizontal dotted black line marks the Pearson r-value at which the correlations are significant (r=0.514). One exemplar scatterplots are displayed.

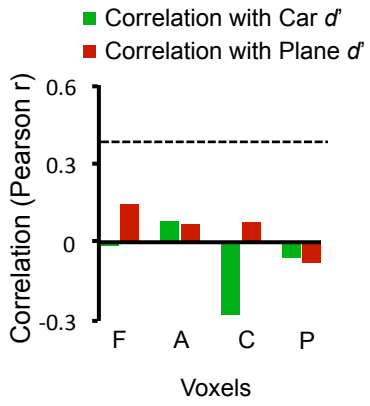

Figure 21. Car and plane expertise within the 50 mm² ROI centered on the peak of lOFA (N=19). Correlation for behavioral Car *d'* with PSC to cars – animals (green bars) and behavioral Plane *d'* with PSC to planes – animals (red bars) within voxels sorted for their maximal response in the other half of the data. The horizontal dotted black line marks the Pearson r-value at which the correlations are significant (r=0.456).

Table 14. For bilateral OFA, the table gives the zero-order correlations (in white rows) and the partial correlations, with expertise for the other category regressed out (in grey rows) between the response for cars – animals and car expertise, or the response for planes – animals and plane expertise (*d'*), in the four categories of voxels. Bold values are significant (α=0.05). Values in the white rows are also graphed in Figures 20-21.

		Face voxels		Animal voxels		Car voxels		Plane voxels	
hem/size	N	***C-A***	***P-A***	***C-A***	***P-A***	***C-A***	***P-A***	***C-A***	***P-A***
right/50	15	0.497	0.38	-0.171	0.23	**0.4**	0.485	0.116	**0.657**
		0.541	0.132	0.231	0.071	0.471	-0.19	0.306	0.303
left/50	19	-0.014	0.145	0.079	0.07	-0.277	0.076	-0.06	-0.079
		0.139	0.157	0.239	-0.097	-0.265	0.05	0.042	0.079

Right medFG and Left medFG

Expertise effects at SR have not been limited to face-selective regions but, rather, have also been reported in object-selective areas medial to the FFA (e.g., Gauthier 2000; Harel et al., 2010).

Here we consider bilateral regions in the medial fusiform gyri (medFG) that were activated significantly more to common objects relative to faces in the SR localizer run. Right and left medFG were observed in 21 and 24 participants, respectively. Our analyses in the medFG generally revealed expertise effects for both cars and planes in the right medFG region, but only for cars in the left medFG. These conclusions are supported by the following analyses.

First we tested replication of SR results using means across all activated voxels. Object selectivity was confirmed in both the right medFG ($F_{1,20}$=22.37, p<0.0001) and the left medFG ($F_{1,23}$=16.51, p<0.0001) ROIs (Figure 22a, 23a). We then replicated bilaterally effects of car expertise on the average car-animal PSC arising from all activated voxels (right: r=0.614, p=0.003; left: r=0.405, p=0.050), and the effect persisted regardless of whether we used Car *d*' alone or Car *d*' with the influence of planes regressed out (Table 15).

Table 15. For bilateral OFA, the table reports the zero-order correlations (in white rows) and partial correlations, with expertise for the other category regressed out (in grey rows) for the relationship between the response to cars (or planes)– animals in the whole ROI and car (or plane) expertise. Significant correlations are shown in bold (α = 0.05).

		ROI PSC	
hem/size	N	***C-A***	***P-A***
right/200	21	**0.614**	**0.575**
		0.609	0.306
left/200	24	**0.405**	0.203
		0.513	-0.07

Next we explored the HR fine-grain organization of object-selective areas without spatial smoothing and without regards to expertise. In the right medFG, we observed reliable responses for animals ($F_{1,20}$=8.749, p=0.008) and planes ($F_{1,20}$=50.81, p<0.0001) using mean amplitude PSC (Figure 22b), or just for planes when considering voxel selectivity index d_a (Table 17) (Figure 22c). MVPA revealed uniform replicability across categories (Figure 22d-e). The left medFG shows a similar pattern, with reliable signal for all categories through a combination of amplitude (face: $F_{1,23}$=10.69, p=0.003; animal: $F_{1,23}$=5.39, p=0.030; car: $F_{1,23}$=4.55, p=0.045; plane: $F_{1,23}$=52.04, p<0.0001), d_a selectivity (Table 17), and multi-voxels pattern analyses (Figure 23). Given this, we asked whether the expertise effects observed in the SR-simulated data would persist in these HR analyses.

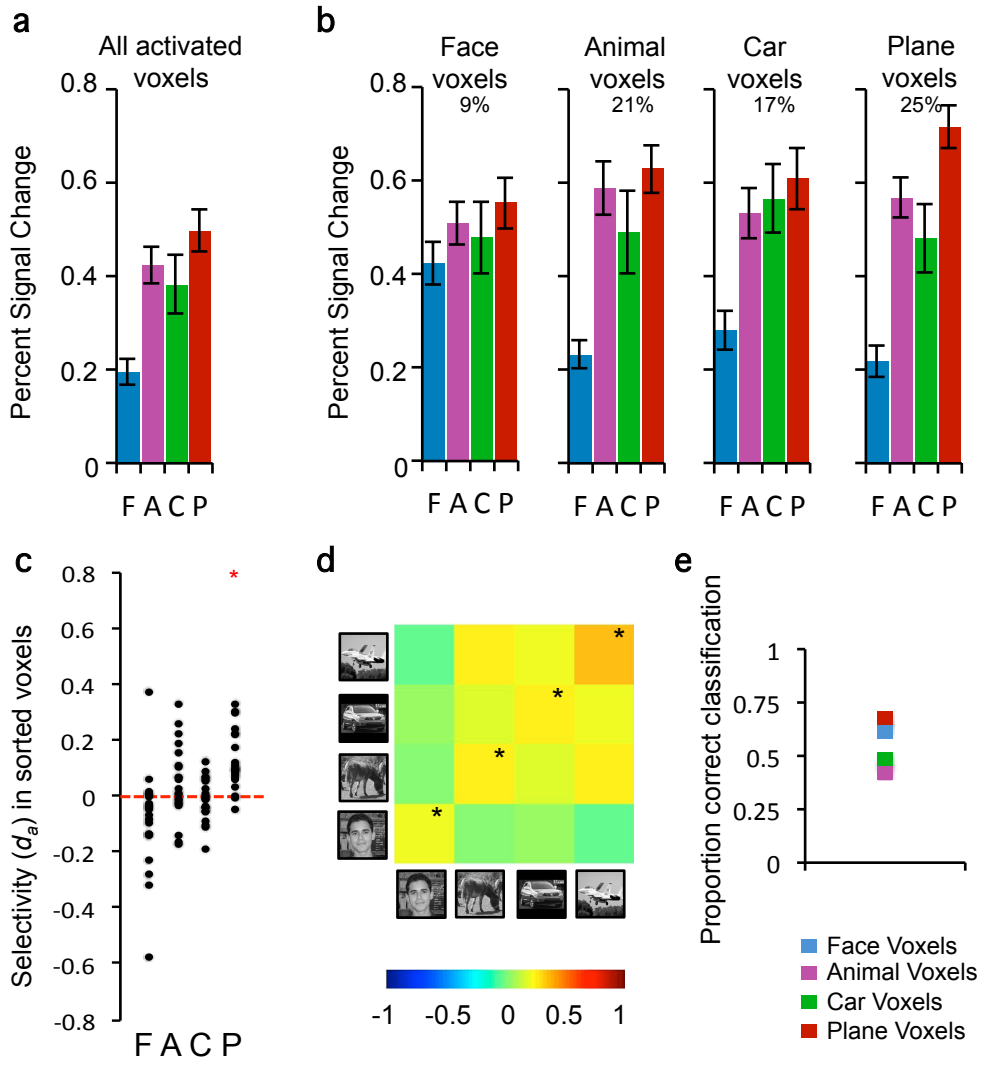

Figure 22. Category-specific response in 200 mm² area centered on peak of right medFG (N=19). (a) Average percent signal change (PSC) to faces, animals, cars and planes averaged over all HR voxels that were more active for objects than scrambled matrices. (b) HR voxels were grouped by the category that elicited the maximal response in half of the data, and PSC for each category relative to scrambled matrices was plotted for the other half of the data. Error bars show SEM. (c) Voxel selectivity across participants measured using the signal detection theory measure d_a in sorted voxels, for half the data based in voxels sorted in the other half. (d) Cross-correlation for the voxel-by-voxel pairwise contrasts between within-category and between-category correlations, computed across independent halves of the data and averaged. Asterisks denote cases where, after a Fisher transformation, the within-category (on-diagonal) correlation was significantly larger than the between-category (off-diagonal) correlations. (e) Winner-take-all (WTA) classifier hit rate. The WTA is trained with the distributed response profile for each category based on half the data, then computes the cross correlation between training set and the input to determine the winning category for the other half of the data. Chance is 25%.

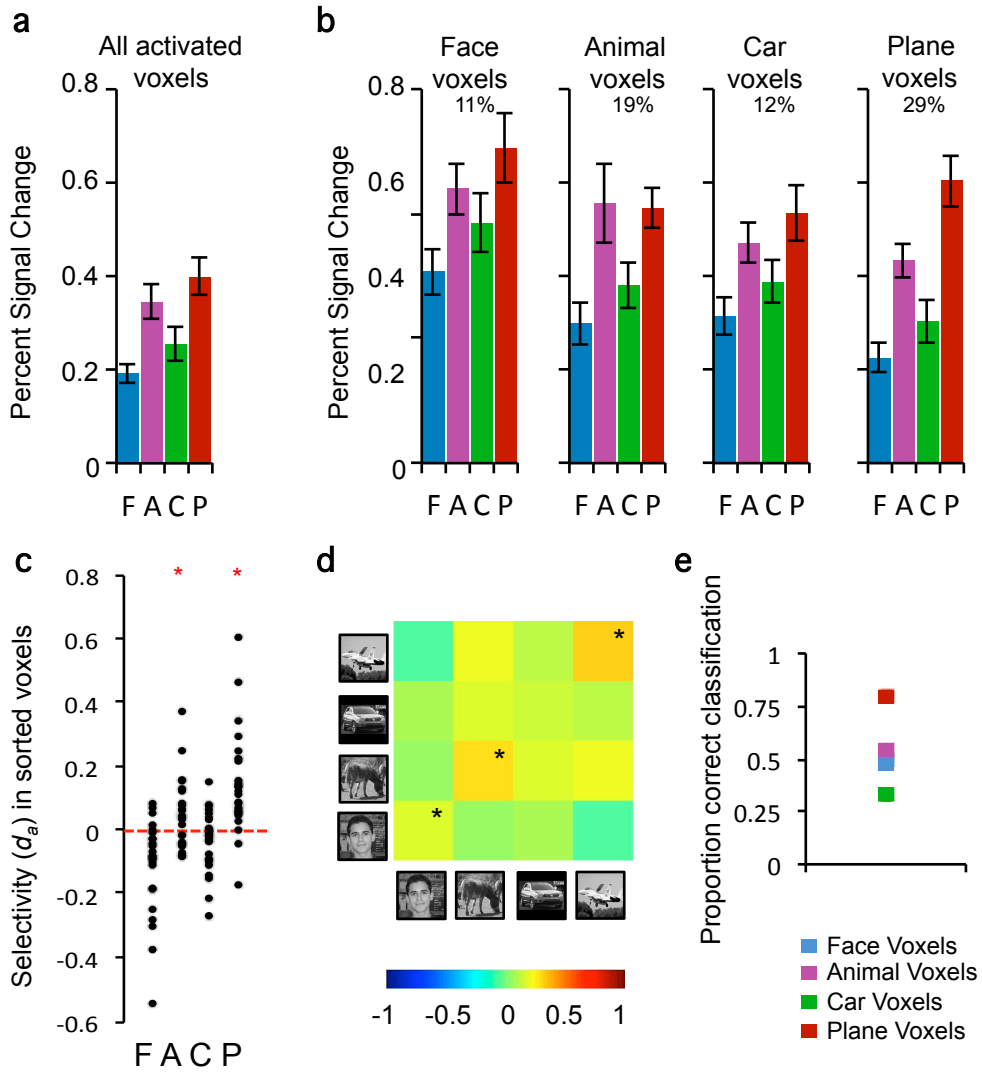

Figure 23. Category-specific response in 200 mm^2 area centered on peak of left medFG (N=24). (a) Average percent signal change (PSC) to faces, animals, cars and planes averaged over all HR voxels that were more active for objects than scrambled matrices. (b) HR voxels were grouped by the category that elicited the maximal response in half of the data, and PSC for each category relative to scrambled matrices was plotted for the other half of the data. Error bars show SEM. (c) Voxel selectivity across participants measured using the signal detection theory measure d_a in sorted voxels, for half the data based in voxels sorted in the other half. (d) Cross-correlation for the voxel-by-voxel pairwise contrasts between within-category and between-category correlations, computed across independent halves of the data and averaged. Asterisks denote cases where, after a Fisher transformation, the within-category (on-diagonal) correlation was significantly larger than the between-category (off-diagonal) correlations. (e) Winner-take-all (WTA) classifier hit rate. The WTA is trained with the distributed response profile for each category based on half the data, then computes the cross correlation between training set and the input to determine the winning category for the other half of the data. Chance is 25%.

Even with the influence of planes regressed out, expertise with cars recruited a greater proportion of car voxels in the right medFG (r=0.578, p=0.007) and the left medFG (r=0.441,

p=0.030). As we have seen in other regions, here the increased car representation came with a cost in the representation of animals, in the right medFG (r=-0.470, *p*=0.030) and marginally in the left medFG (r=-0.371, *p*=0.073). Plane expertise effects were restricted to the right hemisphere, and were no longer present when the influence of car performance was regressed out (Table 16).

Table 16. For bilateral medFG regions, the table reports the zero-order correlations (in white rows) and partial correlations, with expertise for the other category regressed out (in grey rows) for the relationship between the proportion of category-selective voxels and car (or plane) expertise. Significant correlations are shown in bold (α = 0.05).

Size (mm²)	N		**Face %**	**Animal %**	**Car %**	**Plane %**
right/200	21	Correlation with Car expertise	**-0.457**	**-0.651**	**0.461**	0.357
			-0.331	**-0.47**	**0.578**	0.059
		Correlation with Plane expertise	-0.348	**-0.569**	-0.001	**0.527**
			-0.102	-0.292	-0.393	0.418
left/200	24	Correlation with Car expertise	-0.069	**-0.418**	0.296	-0.107
			-0.074	-0.371	**0.441**	-0.044
		Correlation with Plane expertise	-0.018	-0.216	-0.075	-0.116
			0.032	0.064	-0.35	-0.063

Table 17. For bilateral PHG, the table reports mean selectivity values without considering expertise (red italicized). Asterisks denote reliable category-specific responses (d_a>0). The second and third rows for each ROI give the zero-order correlations (in white rows) and partial correlations, with expertise for the other category regressed out (in grey rows) for the relationship between the category-specific selectivity, d_a, and car or plane expertise. Before considering expertise, reliable responses are only observed for a faces and animals. Significant correlations are shown in bold (α = 0.05).

Size (mm²)	N		**F**	**A**	**C**	**P**
right/200	21	*Mean Selectivity, d_a*	*-0.08*	*0.05*	*-0.01*	*0.13**
		Correlation with Car expertise	-0.207	**-0.592**	**0.761**	-0.039
			-0.146	**-0.486**	**0.694**	**-0.456**
		Correlation with Plane expertise	-0.152	-0.391	**0.434**	**0.469**
			-0.036	-0.053	-0.046	**0.617**
left/200	24	*Mean Selectivity, d_a*	*-0.1*	*0.06**	*-0.03*	*0.15**
		Correlation with Car expertise	-0.022	**-0.423**	0.163	**-0.42**
			0.082	**-0.478**	0.249	**-0.547**
		Correlation with Plane expertise	-0.136	-0.083	-0.05	0.01
			-0.156	0.258	-0.198	0.386

Moreover, using the signal detection measures d_a, we found that behavioral expertise with cars (with the influence of plane performance held constant) predicted the selectivity of cars-animals in the right medFG (r=0.608, *p*=0.005) and the left medFG (r=0.423, *p*=0.044) (Table 17). Except for proportion-based analyses, effects of plane expertise on selectivity for planes in all other neural measures were restricted to the right medFG.

As shown in Figure 24, expertise effects associated with both cars and planes occurred with near uniformity across sorted voxels in the right medFG (Table 18). Effects were present but less strong in the corresponding left region, and were especially lessened for planes (Figure 25).

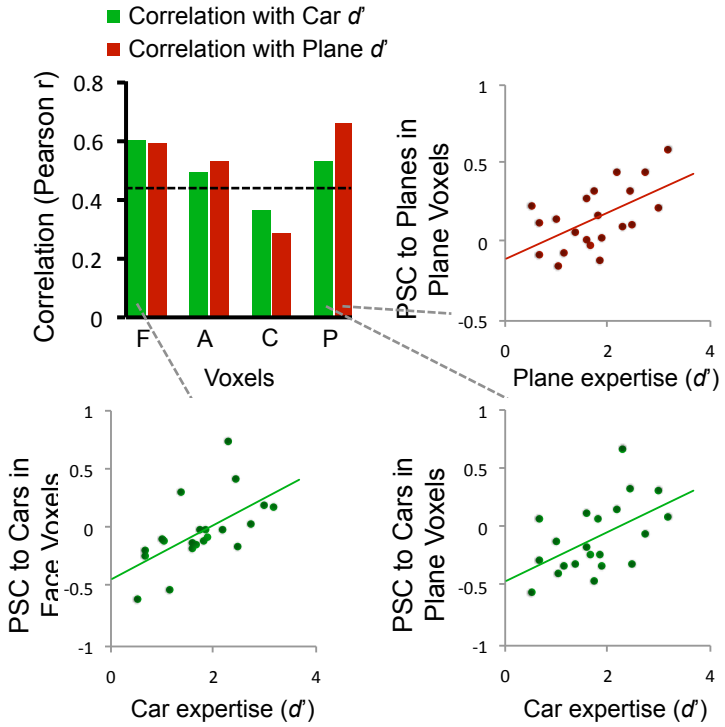

Figure 24. Car and plane expertise within the 200 mm^2 ROI centered on the peak of right medFG (N=19). Correlation for behavioral Car *d'* with PSC to cars – animals (green bars) and behavioral Plane *d'* with PSC to planes – animals (red bars) within voxels sorted for their maximal response in the other half of the data. The horizontal dotted black line marks the Pearson r-value at which the correlations are significant (r=0.433). Three exemplar scatterplots are displayed.

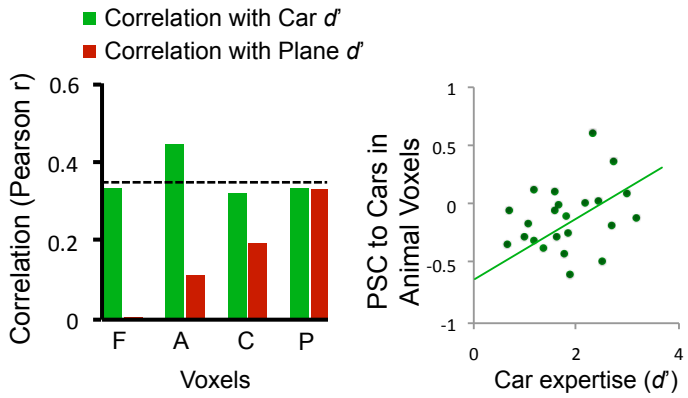

Figure 25. Car and plane expertise within the 200 mm² ROI centered on the peak of left medFG (N=24). Correlation for behavioral Car *d'* with PSC to cars – animals (green bars) and behavioral Plane *d'* with PSC to planes – animals (red bars) within voxels sorted for their maximal response in the other half of the data. The horizontal dotted black line marks the Pearson r-value at which the correlations are significant (r=0.388). One exemplar scatterplots are displayed.

Table 18. For bilateral medFG regions, the table gives the zero-order correlations (in white rows) and the partial correlations, with expertise for the other category regressed out (in grey rows) between the response for cars – animals and car expertise, or the response for planes – animals and plane expertise (*d'*), in the four categories of voxels. Bold values are significant (α=0.05). Values in the white rows are also graphed in Figures 24-25.

		Face voxels		Animal voxels		Car voxels		Plane voxels	
hem/size	N	***C-A***	***P-A***	***C-A***	***P-A***	***C-A***	***P-A***	***C-A***	***P-A***
right/200	21	**0.602**	**0.59**	**0.493**	**0.528**	**0.365**	0.285	**0.53**	**0.659**
		0.501	0.394	**0.438**	0.366	0.299	-0.013	**0.594**	**0.483**
left/200	24	0.335	0.002	**0.446**	0.112	0.322	0.193	0.335	0.332
		0.324	-0.24	**0.582**	-0.279	0.333	0.055	**0.513**	0.294

Partial correlation for car and plane expertise

In most cases, partial correlations were very similar to the zero-order correlations, suggesting that effects could not be explained by a factor common to both categories: performance discriminating cars predicted FFA responses to cars independently of performance discriminating planes and vice-versa.

A striking pattern emerges when we compare the zero-order and partial correlations with selectivity, d_a, across all ROIs (Table 19). First, we note that expertise effects within categories (car expertise predicting Car d_a and plane expertise predicting Plane d_a) generally survives the

partialling out of expertise with the other category. Second, cross category expertise effects (car expertise predicting Plane d_a and plane expertise predicting Car d_a) generally drop out or reverse when partialling out expertise with the other category. This pattern of results reveals that despite the correlation between the two kinds of expertise, it is mainly variance that is unique to performance for each category that predicts changes in their selectivity in the brain.

Table 19. Comparing zero-order correlations (a) and partial correlations (b) for behavioral car and plane expertise with or without controlling for the other factor, on face (F), animal (A), car (C) and plane (P) selectivity, d_a, of six SR-defined ROIs. In the tables, positive and negative correlations are represented by green and red, respectively. The color gradients are scaled from 0 to 1 or 0 to -1, with strongest correlations represented by the boldest colors. Significant correlations (zero-order df=n-1 and partial df=n-2) are outlined in a black box (α=0.05).

a. Zero-order correlations

	Correlation with Car expertise				***Correlation with Plane expertise***			
	F d_a	A d_a	C d_a	P d_a	F d_a	A d_a	C d_a	P d_a
rFFA	-0.41	**-0.65**	**0.52**	-0.02	-0.42	-0.4	0.35	**0.48**
lFFA	0.01	**-0.55**	**0.63**	-0.08	0.08	-0.46	0.51	0.08
rOFA	-0.22	-0.36	0.22	**0.59**	-0.14	-0.08	-0.17	**0.67**
lOFA	0.08	**-0.47**	**-0.34**	-0.07	0.15	-0.35	**-0.45**	0.08
rmedFG	-0.21	**-0.59**	**0.76**	-0.04	-0.15	-0.39	**0.43**	**0.47**
lmedFG	-0.02	-0.42	0.16	**-0.42**	-0.14	-0.08	-0.05	0.01

b. Partial correlations

	Correlation with Car expertise				***Correlation with Plane expertise***			
	F d_a	A d_a	C d_a	P d_a	F d_a	A d_a	C d_a	P d_a
rFFA	-0.24	**-0.56**	0.42	-0.39	-0.26	-0.06	0.09	**0.59**
lFFA	-0.04	-0.39	**0.47**	-0.15	0.09	-0.21	0.23	0.15
rOFA	-0.19	-0.45	0.51	0.2	0.04	0.29	-0.49	0.44
lOFA	-0.04	-0.34	-0.02	-0.19	0.13	-0.01	-0.32	0.19
rmedFG	-0.15	**-0.49**	**0.69**	**-0.46**	-0.04	-0.05	-0.05	**0.62**
lmedFG	0.08	**-0.48**	0.25	**-0.55**	-0.16	0.26	-0.2	0.39

The other interesting pattern concerns the reductions in selectivity for animals with expertise. To begin with, this reduction in animal selectivity effect was only significantly predicted by car expertise and not plane expertise. But in addition, the effect clearly appears related to unique variance associated with car expertise, since even trends are no longer present for plane expertise

when car expertise is regressed out. It is unclear why this is the case, but it is possible that it is related to the greater similarity of the environments in which cars and animals were found, relative to planes. A replication with images on a solid background could verify this possibility.

Discussion of E1 results

Expertise effects in the FFA have been observed at SR using complex objects trained to levels of expert discrimination (Gauthier et al., 1999; Gauthier & Tarr, 2002; Rossion et al., 2004; Wong et al., 2009), and for real-word domains of expertise (Gauthier et al., 2000; 2005; Harley et al., 2009; Xu 2005; but see Grill-Spector et al., 2004; Rhodes et al., 2004). Using HR-fMRI, our results challenge the view that the FFA is a "private patch of real estate in the brain" for faces (Kanwisher, 2010), suggesting that its function extends to the processing of objects of expertise. Neurons are recruited in that neighborhood whenever expert object processing mechanisms[5] are recruited.

Spatially distributed effects of expertise

The distributed effects of expertise observed here in bilateral OFA and medFG are not novel. Previous work on expertise using standard resolution fMRI also found areas in the visual system besides FFA that showed an expertise effect (Gauthier et al., 1999; 2000; Harel et al., 2010)[6]. Indeed, we would expect objects of expertise to engage many areas, since, like faces, objects of expertise engage a multiplicity of processes, some perceptual, semantic, social etc. However, these effects are not *uniformly* distributed: there is not higher activity for experts than novices (or, similarly, faces versus objects) *everywhere* in the visual system. A very general increase in category-selective brain

[5] Or more specifically, expertise individuating objects and which relies on holistic processing.
[6] Harel et al. (2010) also show a sparsely distributed effect for car expertise, though of far greater extent relative to previous work. In particular, large effects of expertise are reported in areas V1-V2. We believe that these effects are problematic, likely confounded by low-level stimulus differences, as the cars were much larger than their control plane stimuli. Indeed, the authors reported significantly greater activation in V1/V2 for cars than planes in *car novices.* It is therefore likely that the effects of expertise they obtained in V1/V2 and later visual areas reflect a combination of low-level differences that may interact with expertise. As such, this SR-fMRI study may overestimate the spatial spread of expertise effects.

activity throughout the ventral pathway could reflect a top-down control on neural activity, reflecting increases in activity with car expertise occur because car experts pay more attention to car images (Harel et al., 2010). On the other hand, our expertise effects were restricted to specific regions, suggesting that expertise leads to changes in perceptual processing whereby expert objects recruit face-like processing resources and face-selective regions in the brain. Critically, the expertise account of the origins of face selectivity in the FFA does not predict that *all* face-selective areas and *only* face-selective areas should be engaged by expertise individuating other objects, and especially not in cases of real-world expertise that entails much more than object individuation.

Indeed, while many areas engaged by non-face objects of expertise are also likely engaged by faces, this is clearly not always the case. Apart from requiring a common perceptual strategy for individuation (i.e., holistic processing, Bukach et al., 2010) other processes may be engaged only for faces (e.g., those associated with facial expressions) or only for cars (e.g., those associated with outdoor scenes). The neural response observed in object-selective medFG, for example, may reflect processes engaged in experts when viewing car and plane images, which are large objects typically processed in a scene context. In the same manner, some areas (e.g., the STS) could respond to faces and not to cars due to the processing of facial expression.

Accounting for the influence of attention

An alternative explanation for our results suggests that expertise recruits the FFA simply because experts attend to objects of interest (Wojciulik et al. 1998; Kanwisher 2000; McKone et al. 2007), as attention is known to boost visual signals (McAdams & Maunsell, 1999; Seidermann & Newsome, 1999; Treue & Martinez-Trujillo, 1999). But attention should only amplify existing patterns of category selectivity (Treue & Martinez-Trujillo, 1999; Puri et al., 2009; Reddy & Kanwisher, 2007), such that even if expertise is associated with more attention, and attention boosts the responses to objects of expertise, this would be expected to occur in regions of

selectivity for cars. In other words, if a region contains face-selective neurons and no car-selective neurons, attention to cars should not increase the response to cars.

Critically, within the latFG, we find expertise effects that are centered on the peak of face-selectivity and limited to the FFA.. When car and plane experts look at cars, attention may account for the magnitude of activation in a given area, but the location of the effect can still reveal that attention to *cars* is specifically linked with the location of *face*-selectivity. The expertise effect for cars and for planes was observed in the 25 mm^2 ROI, the 100 mm^2 ROI, the 200-100 mm^2 ROI but not in the 300 mm^2 ROI. This analysis offers two novel results. First, the expertise effect is present in the core of the FFA, even in those voxels that are highly face selective. For example, within the core 25mm^2 ROI, the number of car-selective voxels depends on car expertise ($r=0.513$, $p=0.035$), suggesting that the car responsive neurons and the face responsive neurons are intermingled at a very fine scale, because expertise effects are obtained even in face voxels. Second, the expertise effect in the fusiform gyrus is centered on the peak of face selectivity and restricted to a 200 mm^2 region.

Expertise with multiple domains

Our results highlight the need for the manipulation of various aspects of experience to examine how different patterns of selectivity emerge. We observed interesting and unexpected differences between the selectivity for cars and planes. While expertise effects were bilateral for cars, they were restricted to the right hemisphere for planes. In addition, even in the rFFA that showed expertise effects for both categories, the spatial extent of these effects differed. The difference was most pronounced in the proportion of selective voxels, a measure that should be particularly sensitive to the recruitment of additional neurons with expertise. Plane expertise only recruited additional voxels for planes in an outer ring-ROI, while for car expertise this effect was also observed in FFA's center. Effects for planes in our participants may reflect neural changes following relatively limited experience (Wong et al., 2009), or visual abilities without the

considerable semantic associations that may arise in a domain with which one claims expertise. Regardless of the specific explanation, the overlap of expertise effects for faces and objects in the FFA and the differences observed between expertise effects for cars and planes suggest that not even the FFA is solely dedicated to a single category, and that different domains of expertise can produce different patterns of selectivity in the visual system.

Implications for neural competition

Perceptual expertise as measured here likely occurs in most people as they learn to individuate objects related to professional activities or hobbies. Thus, most people will have several brain regions that contain populations of neurons selective for objects of expertise. Prior studies revealing only face-selective responses in the FFA (Grill-Spector et al., 2006) or in face patches (Tsao et al., 2006) relied on non-face categories which their participants likely had little experience individuating. While our results do not rule out an influence of genetics on specialization of the FFA, they suggest that the function itself is not specific to the face domain but rather supports learning more generally. Our effects could still be due to spatial averaging of different populations for faces and objects within our HR voxels, and whether the same neurons respond to faces and objects of expertise remains an interesting question. Previous work suggests that objects of expertise can compete specifically with the perception of faces (McGugin et al., 2010; McKeeff et al., 2010; Rossion et al., 2004), suggesting common perceptual resources.

Indeed, an intriguing result from E1 is the tradeoff for spatial representation suggested by various analyses: less selectivity for animals, and perhaps also faces, as a function of increasing car expertise. Expertise with a non-face object category may limit face (or other expert category) representation if the development of expertise represents a shift from one type of processing strategy and/or representation to another that is characteristic of face/expert processing yet limited in availability (DiCarlo & Cox, 2007). Indeed, previous studies have suggested *costs* – in terms of a tradeoff in the number and/or magnitude of category-selective neural representations –

of non-face expertise on FFA face-selectivity using SR imaging of dual experts (Gauthier et al., 1999; Gauthier et al., 2006; Behrmann et al., 2005). However, with so few categories investigated in the current study, the observed tradeoffs are almost a feature of the analysis: when one category in the baseline increases, the selectivity of the others must decrease. On the other hand, this evidence of competition for spatial representation could also reflect true competition. A more direct assessment, as employed in E2, is needed for a better understanding of competition.

In addition to this evidence of competition for spatial representation, concurrent processing of objects from different domains of expertise can also compete *on-line*, in a task where objects from different domains needs to be processed concurrently (Gauthier et al., 2003; McGugin et al., 2010; McKeeff et al., 2010; Rossion et al., 2004; 2007; Wong et al., 2011). Experiment 2 will specifically test competition for common perceptual resources. The goal of E2 is to use HR-fMRI to study concurrent multi-object processing during rapid serial image presentations. For car experts that are experts with faces *and* cars, what fine-grain pattern of response can be expected during simultaneous processing of faces and cars? We will compare neural patterns of response when objects are shown in isolation (as in E1) versus when they are seen in competitive sequences of alternating categories, and test how expertise effects differ across these conditions. To date no fMRI study – neither SR nor HR – has investigated individual differences in competition during concurrent processing of faces and objects of expertise.

CHAPTER III

EXPERIMENT 2 – SPATIAL DISTRIBUTION OF CAR EXPERTISE EFFECTS DURING CONDITIONS OF STRESSED PERCEPTUAL PROCESSING

Experiment 2 (E2) will explore HR effects of expertise and competition within ROIs defined with an independent SR face>object localizer, and in voxels sorted based on maximal category-specific response from independent HR runs with faces, cars and sofas. Specifically, we will compare neural responses during concurrent processing of faces and cars (FC), faces and sofa (FS), and cars and sofas (CS). If objects of expertise compete with face processing, the neural response during FC (but not CS or FS) conditions should become increasingly attenuated as a function of car expertise. Attenuation may be greatest where selectivity is greatest, in the maximally face-selective voxels or in the car voxels of car experts. Results from neurophysiology show competition between faces and non-face objects of expertise through attenuation of the early N170 event-related potential (ERP) component – a face-selective response thought to originate in or around the FFA – during concurrent face and expert object processing (Bentin et al., 1996; Gauthier et al., 2003; Rossion et al., 2004; 2007). Behavioral evidence of expert competition also suggests shared processing mechanisms between faces and objects of expertise, finding perceptual interference when individuals must discriminate faces and objects of expertise in dual-task conditions (McGugin et al., 2010; McKeeff et al., 2011; Rossion et al., 2004). Here, for the first time, we will explore these effects using HR fMRI.

HR fMRI will allow us to probe the response of face-selective regions during heterogeneous RSVP streams in which faces alternate with objects that recruit either similar or dissimilar processing mechanisms. We will ask how neural response profiles differ during single-category presentations relative to more taxing mixed-category RSVP sequences. Will objects from alternating categories compete for neural representation in the right FG in a manner that is

dependent on car expertise, and will the observed pattern vary across voxels maximally selective to faces, cars and sofas?

Methods

Participants

We scanned 26 individuals (6 females, ages 22 to 41 with an average of 27) at both SR and HR. All participants completed the Edinburgh Handedness Inventory (see APPENDIX C) and had a Laterality Quotient greater than or equal to +40 (implying right handedness; scores ranged from 54 to 100 with an average of 89). Following the fMRI portion of the experiment, behavioral expertise was assessed outside the scanner. All individuals had normal or corrected-to-normal vision. Prior to beginning the experiment, participants gave informed written consent in accordance with the guidelines of the institutional review board of Vanderbilt University and Vanderbilt University Medical Center.

Scanning

All imaging was performed on a Philips Medical Systems 7-Tesla (7T) human magnetic resonance scanner at the Institute of Imaging Science at the Vanderbilt University Medical Center (Nashville, TN). Participants completed one SR face-object localizer scan, three HR face-car-sofa localizer scans, six HR competition scans, and one HR anatomical scan.

Standard resolution face-object localizer scan. We first acquired 30 SR slices oriented in the coronal plane at a resolution of 2.3 x 2.3 x 2.5 mm. The BOLD-based signals were collected using a fast T2*-sensitive radiofrequency-spoiled 3D PRESTO (PRinciples of Echo Shifting using a Train of Observations) sequence (FOV = 211.2 mm, TE = 21.93 ms, TR = 2500 ms, flip angle = 78 degrees and matrix size = 96 x 96).

High resolution scans. Immediately following the SR scan, we acquired 24 HR slices oriented in the coronal plane. We used a radiofrequency-spoiled 3-dimensional FFE (Fast Field Echo) acquisition sequence with sensitivity encoding (SENSE) (FOV = 160 mm, TE = 21.93 ms, TR = 4000 ms, flip angle = 78 degrees and matrix size = 128 x 128) to obtain 1.25 mm^3 isotropic voxels. Nine functional scans with these parameters were acquired in each participant: 3 runs dedicated to localization of face, car and sofa-preferring voxels, and 6 runs for testing competition. (Due to time restrictions, one participant only completed four of the six HR competition scans.)

High resolution anatomical scan. HR T1-weighted anatomical volumes were also acquired using a 3-dimensional TFE (Turbo Field Echo) acquisition sequence with sensitivity encoding (SENSE) (FOV = 246 mm, minimum TE, TR = 3.152 ms, matrix size = 352 x 352) to obtain 249 slices of 0.7 mm^3 isometric voxels. These HR anatomical images were used to align the SR and HR functional data.

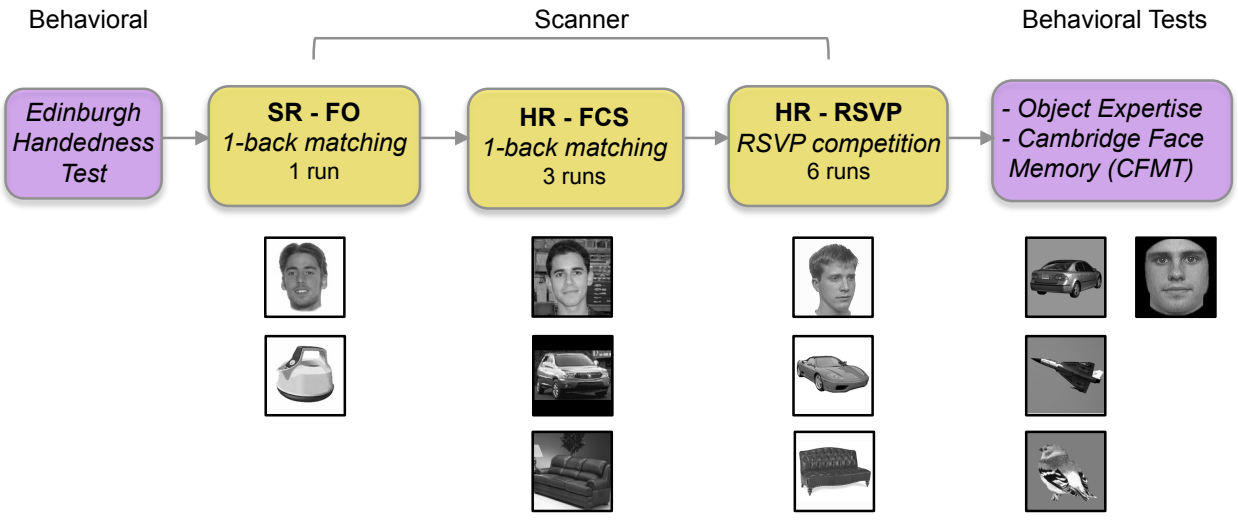

Figure 26. Experiment 2 design. 26 participants completed 1 SR Face-Object Localizer run, 3 HR Face-Car-Sofa Localizer runs, then 6 HR competition runs. Following the fMRI portion of the experiment, individuals completed behavioral tests assessing individual levels of face and object expertise. One representative image from each object category is presented.

fMRI design

The experimental design in the scanner consisted of three parts. The first was a SR face-object localizer to identify face- and object-selective regions on an individual basis. The second part was designed to localize HR voxels maximally selective to faces, cars and sofas, and to replicate expertise effects in HR data. The third and final part of the fMRI experiment measured the neural response in HR sorted voxels during conditions where two separate domains required simultaneous processing. We compared patterns of neural activity during single-category presentations (part two) relative to mixed-category presentations (part three).

Stimuli and display. All images were presented on an Apple Macintosh computer using Matlab (MathWorks, Natick, MA) with the Psychophysics Toolbox extension (Brainard, 1997; Pelli, 1997). The SR face-object localizer run used 72 grayscale images (36 faces, 36 objects). The three HR face-car-sofa localizer runs used grayscale images of faces (from Dr. Kalanit Grill-Spector at Stanford), cars (non-frontal views) and sofas. Images were selected randomly from 102 unique exemplars per category (Figure 26). Scrambled images were created on-line during the scan by parsing a randomly selected image into 64 equally sized squares, then rearranging these squares to form a novel display of scrambled pieces. All stimuli used in the SR face-object run and HR face-car-sofa runs were presented in the center of the screen and resized on each trial to subtend a visual angle of ~12.6, ~15.1, or ~17.6. The stimuli were presented at different sizes to discourage the use of low-level visual properties to perform the task. The six HR competition runs used grayscale face, car and sofa images cropped of all background and presented in isolation. Images for competition runs were selected from 48 unique exemplars per category. All images were presented in the center of the screen, subtending a 12° visual angle.

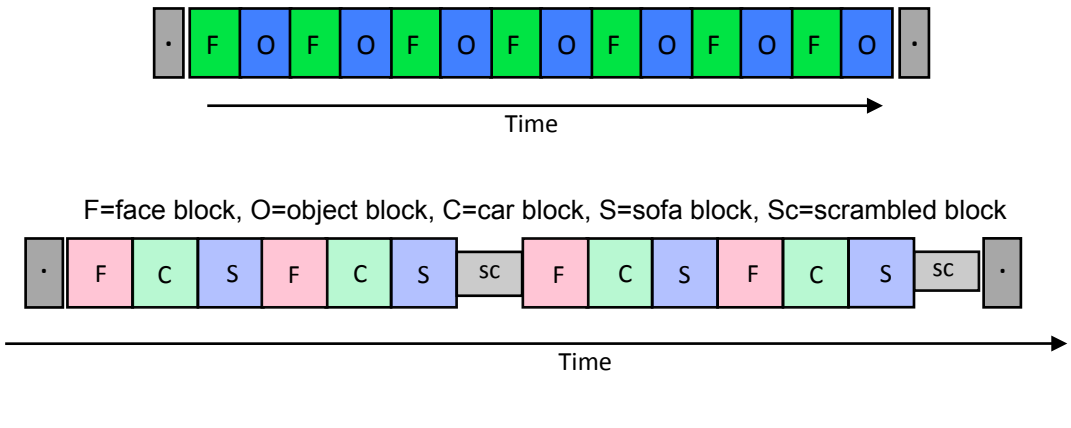

Figure 27. fMRI experimental design. All runs began end ended with fixation. The task in the scanner was identical for the SR Face-Object localizer run and the 3 HR Face-Car-Sofa Localizer runs: 1-back matching. (a) Example experimental protocol for the SR localizer run: 14 20-s blocks of alternating faces (F) and objects (O). (b) Example experimental protocol for the HR-FCS runs: 14 16-s blocks (4 each of faces (F), cars (C) and sofas (S), and 2 scrambled (sc)). (b) Example experimental protocol for the HR RSVP runs: 9 24-s blocks alternating Face/Car (FC), Face/Sofa (FS) and Car/Sofa (CS) presentation conditions. One FC trial is shown. The relevant 2 targets are cued, and participants search the RSVP stream for one or both of these targets, responding at the end of the 6-s sequence if they saw the face, the car, both, or neither.

SR Face-Object (SR-FO) Localizer run. The localizer scan used a 1-back detection task with 14 blocks of alternating faces and common objects (20 images shown for 1s) with a 2.5 s fixation at the beginning and end, lasting 285 s in total duration (Figure 27). This scan helped identify face-selective voxels (faces > objects) in the inferior-temporal and occipital cortices, thereby guiding the prescription of HR slices. Accuracy did not differ for Face and Object blocks: (hit rate, false alarm rate) Face (0.89, 0.01), Object (0.88, 0.01).

HR Face-Car-Sofa (HR-FCS) Localizer runs. Following real-time alignment of the HR slices based on SR data, participants completed 3 additional runs using a 1-back detection task. Each run contained 14 blocks (4 each of faces, cars and sofas, and 2 scrambled) of 16 s duration each (16 images sequentially presented for 1 s each), with 4 s fixation at the beginning and end. Each experimental run lasted 232 s. A one-way ANOVA revealed a main effect of category ($F_{1,25}$=105.74, p>0.0001), which was carried by significantly poorer detection during Scrambled blocks relative to the intact-object blocks, but no difference between Faces, Cars and Sofas (Scheffé test pairwise comparisons, p<0.0001): (hit rate, false alarm rate) Face (0.93, 0.007), Car (0.93, 0.005), Sofa (0.91, 0.01), Scrambled (0. 24, 0.03). See Table 20 for average accuracy rates and correlations with behavioral Car *d*'.

Table 20. (a) Behavioral performance during the 1-back HR-FCS identity-matching task in the scanner, by category. Paired t-tests comparing mean performance (*d*') between object categories reveal no significant differences. Performance during all intact-object blocks was greater than during scrambled blocks (all *p*s < 0.001). For no category was performance correlated with car expertise. (b) Behavior performance during the HR-RSVP detection task in the scanner, by condition. Chance is 25%. Paired t-tests comparing mean performance for trial where participants responded within the allotted time window report significantly poorer detection rates during Car/Sofa sequences relative to both Face/Car and Face/Sofa sequences (*p*s < 0.0001). There were no differences in performance during Face/Car and Face/Sofa conditions. For no condition was performance correlated with car expertise. Data are presented for all 26 participants.

a. HR-FCS

	d' (sem)	Correlation with Car d'
Face	3.92 (0.09)	-0.277
Car	3.94 (0.1)	-0.312
Sofa	3.83 (0.13)	-0.118
Scrambled	1.17 (0.14)	-0.206

b. HR-RSVP

	Accuracy	Correlation with Car d'
FC	0.58 (0.05)	0.053
FS	0.53 (0.04)	0.043
CS	0.38 (0.04)	-0.059

HR-RSVP Competition runs. The final segment of the fMRI experiment involved six runs with a rapid serial visual presentation (RSVP) of alternating images, which immediately following the three HR Face-Car-Sofa localizer runs in the MRI (due to time constraints, one individual only

completed four RSVP runs). Images were presented at a rate of 6 images/s for 6 s trials, and always alternated between two categories. This presentation rate was determined from a pilot experiment aimed at selecting a presentation rate that corresponds to behavioral performance of ~65% correct discrimination.

In the MRI experiment, three conditions were used: faces and cars (FC), faces and sofas (FS), and cars and sofas (CS). Each participant was randomly assigned a target face, car and sofa and studied these three images at least one day prior to beginning the experiment (all participants were emailed a slideshow with instructions and images for the fMRI experiment). A block consisted of a cue (1.5s) indexing the two (of three) target images that would be relevant for the upcoming trials, then three 6-s RSVP sequences each followed by a 1.5-s response window. Each block was 24 s in total duration. One run contained 9 blocks alternating FC, FS, and CS conditions in random order, lasting 224 s in total duration. Participants could also inspect the target images between runs.

In each trial, participants were instructed to maintain central fixation while monitoring the 6-s RSVP sequence of 36 rapidly alternating images for the two current targets: i.e., in FC trials, participants searched for the studied face and car, in FS trials participants searched for the studied face and sofa, and in CS trials participants searched for the studied car and sofa (Figure 27). At the end of each RSVP sequence, participants made a button response indicating one of four possible outcomes: they found (1) category one target only, (2) category two target only, (3) both category one and two targets, or (4) neither category one nor two targets. In target-present trials, the serial position of the target(s) was randomly determined, but never occurred first or last in the stream. Chance was 25%.

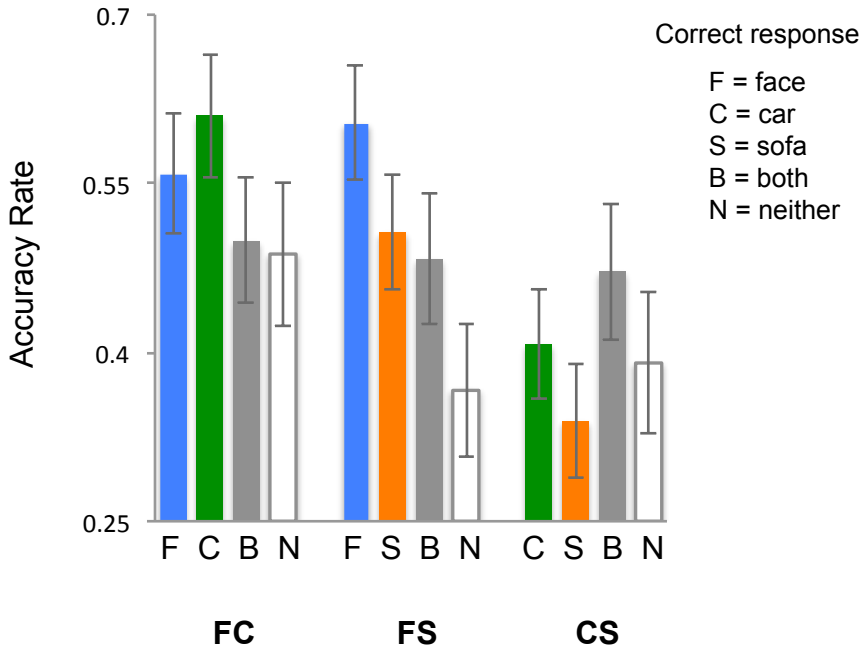

Figure 28. Behavioral data from the HR-RSVP runs. Participants searched for two targets in a rapidly presented stream of images alternating amongst two targets: faces and cars (FC), faces and sofas (FS), or cars and sofas (CS). At the end of the RSVP sequence, they indicated whether they found target 1, target 2, both targets, or neither targets. Overall, accuracy in FC blocks was better than CS blocks (main effect of condition: $F_{1,25}$=5.177, p=0.009), and performance when faces were present alone (i.e., correct response = 'face') was greater than when neither target appeared (main effect of response: $F_{1,25}$=4.409, p=0.003).

Participants were only allotted 1.5 s to make their response at the end of each trial. The response window was restricted to maximize the percentage of scan time occupied by visual presentations. Given such a brief window, however, participants responded during the time window on only ~50% of the trials. The percentage of responses made within the allotted time regardless of accuracy was submitted to a 2-way ANOVA using Condition (FC, FS, CS) and Response ('face', 'car', 'sofa', 'both', 'neither') as within-subject factors. There was a main effect of response ($F_{1,25}$=10.78, p<0.0001) as well as an interaction effect between condition and response ($F_{1,25}$=3.21, p=0.009). These tests revealed more accurate responses (or potentially faster responses, made within the allotted 1.5 s) when faces were present (i.e., response = 'face' or 'both') relative to absent, and this was especially pronounced in FS blocks. A 2-way ANOVA on total accuracy rates revealed main effects of both Condition ($F_{2,25}$=5.18, p=0.009) and Response ($F_{2,25}$=3.92, p=0.005), showing better search performance in FC blocks relative to CS blocks (p=0.02), and for 'face' target

responses relative to 'neither' responses (p=0.01). We also computed separate 1-way ANOVAs for each condition and found that while there was no difference in accuracy as function of correct response in FC ($F_{1,25}$=0.910, *n.s.*) and CS ($F_{1,25}$=0.877, *n.s.*), there was a significant main effect of response for FS ($F_{1,25}$=5.58, p=0.002), which was carried by higher accuracy for 'face' trials relative to 'neither' (Scheffé's post-hoc test: p=0.003) (Figure 28).

Behavioral tests

All participants completed two behavioral assessment tests following their fMRI session (Figure e2-3): the *sequential matching expertise test* used to quantify individual skill at matching cars and planes (Curby et al., 2009; Gauthier et al., 2000; 2005; Grill-Spector et al., 2004; Rossion et al., 2004; Xu, 2005), and the Cambridge Face Memory Test (CFMT; Duchaine & Nakayama, 2005).

Sequential matching expertise test: participants made same-different judgments on car and plane images (at the level of make and model, regardless of year) and bird images (at the level of species) (Figure 3). An expertise sensitivity score was calculated for cars (Car *d'*, range 0.64-3.17), planes (Plane *d'*, range 0.59-2.73), and birds (Bird *d'*, range 0.21-2.32) for each participant. As in E1, Car *d'* and Plane *d'* were significantly correlated (r=0.73, p<0.0001) (Figure 29). It is likely that individuals showing interest in cars also have interest in planes, considering their co-occurrence in sporting magazines, for example.

However, while in E1 sensitivity to birds was positively related to both car and plane sensitivity, here no such relationships were found (Figure 29). This pattern is consistent with previous work comparing car and bird matching, which has never revealed a positive correlation between these two variables (Gauthier et al. 1999; McGugin et al., 2010; McKeef et al., 2010). Although we would expect all object categories to share some degree of variance, which is the motivation behind using a baseline to remove non-domain specific variability, E1 results showing a significant correlation amongst all variables suggested more shared variance than we typically

observe, a difference for which we have no explanation. In E1 we were able to use the neural measure of plane expertise to verify that the variance associated with behavioral plane *d'* was related to brain activity, and we were able to use plane expertise as a control for shared effects.

In E2, we observed a more standard pattern between car and bird matching performance (i.e., no significant correlation). Given that E2 does not include a brain measure of plane expertise (thereby deeming behavioral plane *d'* less relevant), we will use bird *d'* as regressor when considering partial correlations that are specific to car expertise. This also adds to the validity of the neural car expertise effects that they can be shown to be specific to car recognition skills given different control variables.

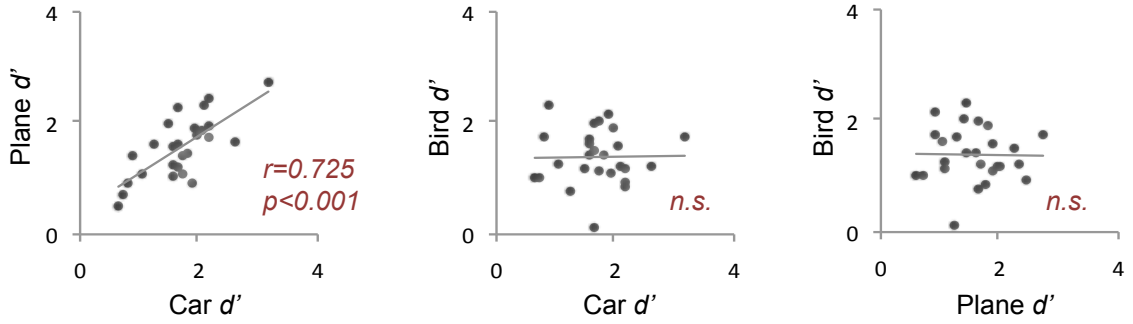

Figure 29. Behavioral performance during the same-different matching task. Scatterplots show the relationship amongst Car *d'*, Plane *d'* and Bird *d'*.

Cambridge Face Memory Test (CFMT): The CFMT provides a measure of face memory through learning to recognize six target faces. After participants are introduced to the target faces, they are tested with forced choice triplets of which one is the target. Trials are blocked in four stages: practice trails, faces identical to those studied (introduction trials), faces in novel views (average accuracy rate=0.79, range 0.47-1.00), and faces in novel views with noise (average accuracy rate=0.70, range 0.29-1.00). Memory for faces did not predict matching performance for cars (r=0.299, *n.s.*), planes (r=0.267, *n.s.*), or birds (r=0.304, *n.s.*). This suggests that the CFMT measures a memory skill for faces that is to some extent distinct from the perceptual skill observed for other objects, at least as assessed through the same-different matching task.

We also had participants self-rate their level of expertise, from 1, "zero knowledge of the category" to 9, "highly experienced in recognition and knowledge of the category". They were instructed to make these judgments considering interest in, years exposure to, knowledge of, and familiarity with each category. Self-reported skill with cars predicted Car *d'* scores (r=0.538, *p*=0.005).

Data analysis

Processing of raw data

The HR T1-weighted anatomical scan was used to create a 3D brain normalized on an individual basis according to the Talairach atlas of brain anatomy (Talairach & Tournoux, 1988). The Talairach coordinate system was defined by first using the anterior and posterior commissure points to vertically align the midsagittal plane. Six other standard anatomical landmarks (anterior-, posterior-, superior-, inferior-, right-, and left-most points) are then used to rotate and translate the brain in stereotaxic space. This transformation allowed us to confirm localization of functionally-defined ROIs with standardized Talairach brain coordinates that have been shown to correspond to face-selective patches.

Functional data were analyzed using the Brain Voyager (BV) (http://www.brainvoyager.com) multi-study general linear model (GLM) procedure, as well as in-house scripts created in Matlab (http://www.themathworks.com). In BV the raw functional data files were used to create 2-dimensional functional slice-based projects to which an experimental protocol was linked. Data preprocessing included 3D motion correction and temporal filtering (using a high-pass criterion of 2.5 cycles/run) with linear trend removal for all scans. Slice-time correction with sinc interpolation was applied to the SR Face-Object localizer run only, since the HR runs employed a 3D imaging sequence. Data from HR functional runs were interpolated from 1.25mm isotropic voxels to a resolution of 1mm isotropic using sinc interpolation. No spatial

smoothing was applied at any resolution. To relate functional brain activity with anatomical information in the brain, pre-processed functional slice-based data were aligned to the Talairach-transformed brain. The hemodynamic response function was modeled from predictor variables represented as boxcar functions forward-shifted and convolved to account for the assumed hemodynamic shape and delay of the fMRI signal. In both SR and HR runs, we used standard (GLM) analyses to compute the correlation between predictor variables and actual neural activation, yielding voxel-by-voxel activation maps for each condition.

Table 21. Mean spatial coordinates for the peak of ROIs, and mean size using a fixed effects analysis with a threshold of q(FDR)<0.05.

	Mean Talairach coordinates for peak voxel (standard deviation)	Average Volume (mm^3) (standard deviation)
Right aFG (N=21)	*36.3, -45.7, -17.8 (4.8, 7.3, 5.2)*	776 (155)
Right pFG (N=23)	*36.4, -61.5, -17.0 (4.7, 7.6, 5.7)*	651 (198)
Left aFG (N=20)	*-38.0, -43.8, -19.8 (4.1, 8.2, 4.1)*	530 (170)
Left pFG (N=19)	*-37.9, -58.2, -17.6 (3.1, 6.2, 5)*	670 (247)
Right OFA (N=16)	*29.3, -82.5, -11.9 (9.5, 7.1, 4.6)*	479 (229)
Left OFA (N=13)	*-38.6, -75.7, -13.6 (5.3, 7.5, 4.1)*	416 (160)
Right PHG (N=26)	*24.7, -47.9, -14.0 (3.5, 8.6, 4.8)*	1231 (396)
Left PHG (N=24)	*-26.9, -49.8, -14.1 (2.3, 8.2, 4.2)*	1270 (327)

All ROIs were defined in 3-dimensional space using the face-object contrast in the SR localizer run. Significantly activated voxels were classified using a fixed effects analysis with a threshold of p(FDR) < 0.05. We identified bilateral fusiform and occipital areas as those voxels more

activated by faces than objects, and bilateral medial parahippocampal regions as voxels more activated by objects than faces (Table 21). Not all ROIs were observed in all participants, and ROIs were only considered if fully incorporated by the HR slice prescription. The goal of our real-time alignment of HR slices based on the SR Face>Object activation map was to capture face-selective regions in the right fusiform gyrus, and in certain cases inclusion of these areas limited our ability to also capture more posterior regions of selectivity. Across 26 participants, SR-defined ROIs fully incorporated by the HR slices were isolated in eight locations (see Table 21).

In E1 we localized a single face-selective fusiform ROI bilaterally in relevant participants. Here, however, we isolated two distinct face-selective regions on the fusiform gyrus, one more anterior (aFG) and the other more posterior (pFG) (Table 21). Because E1 and E2 ROIs were defined in 2D space and 3D space, respectively, it is possible that clusters appearing as a single unit on an unfolded flattened hemisphere in surface space may appear discrete in a corresponding volume view. Using 3D space, we localized two discrete peaks of face selectivity in the FG of 20 participants, and another four participants had one peak, which we classified as either anterior or posterior according to its Talairach coordinates. Interestingly, comparing Talairach coordinates along the antero-posterior y-dimension, we see that the FFA from E1 falls between the aFG and the pFG from the current experiment, bilaterally. Position along the x- and z-dimensions are more similar for E1 FFA and E2 aFG and pFG, bilaterally. Across all ROIs from both experiments, variability is greatest in the antero-posterior direction, a trend observed in many studies of face-selective fusiform regions. Simply based on mean Talairach coordinates, it is unclear whether the currently designated aFG or pFG represents the classical FFA. We will present data for both regions and highlight interesting comparisons and dissociations.

We localized an object-selective region in each hemisphere in addition the six face-selective areas. In contrast to E1, where the localized object-selective regions fell on the medial portion of the FG gyrus, here object-selective regions were localized to the more anterior parahippocampal gyri bilaterally. The mean Talairach coordinates for the right and left medFG regions in E1 were

approximately 26, -57, -12 and -28, -60, -12, respectively. In contrast, mean Talairach coordinates for the right and left PHG regions in E2 were approximates 25, -48, -14 and -27, -50, -14, respectively, placing them along the parahippocampal gyri. The parahippocampal regions occurred anterior to the medFG regions. Because these object-selective areas represent relatively large category-selective regions of ~1250 mm^3 volume, it is possible that they actually span from the parahippocampal cortex to the medial fusiform cortex. However, since here the mean of the peak of object-selectivity occurred on the parahippocampal gyri, we will refer to these regions with "PHG".

Analyses were performed on all 1 mm^3 voxels with each ROIs that were activated significantly more to objects relative to the scrambled baseline ($p<0.01$). Voxels incorporated by the SR-defined ROI but failing to pass the HR-based Intact > Scrambled restriction were classified as "Scrambled" voxels.

Note, whereas E1 analyses were performed on flattened 2D non-transformed brains, all analyses for E2 were performed in 3D. A primary goal of flattening hemispheres in E1 was to map the spatial distribution of expertise effects in the lateral FG through the creation and comparison of concentric ROI-rings around points of peak activation. This was not a goal of E2, where we sought to replicate HR selectivity analyses in standard-sized ROIs in volume space, and subsequently compare activation for single-category and mixed-category presentations in various ROIs. Thus, participant hemispheres were not segmented and flattened, as this procedure requires approximately 10 hours of manual labor per hemisphere. For E2, all brains were transformed into a standard space in an effort to anchor our analyses in the SR-fMRI literature (which is quite large and with established standards), allowing for confident dissociations across face-selective regions in adjacent patches of cortex: e.g., aFG, pFG and OFA.

Analysis of processed data

Response amplitudes (HR-FCS and HR-RSVP): Response amplitude for the contrast between pairs of conditions, for instance C–F in the HR-FCS runs and (C–F)S in the HR-RSVP runs was calculated.

(a) HR-FCS: We computed the response amplitudes in HR-FCS localizer runs. For each voxel, a percent signal change (PSC) estimate was computed for each category using scrambled blocks as the baseline: e.g., "Face" PSC = (Face–Scrambled) / Scrambled. Response amplitudes were computed in two steps. First, PSC values from two runs were used to determine the category preference of each voxel based on the category evoking the maximum response. Second, PSC values from the third run was used to plot the average response amplitude for all three categories within each type of voxel. Three such complementary computations were performed – runs 1 & 2 to sort voxels and run 3 to calculate response amplitudes; runs 1 & 3 to sort and run 2 for amplitudes; runs 2 & 3 to sort and run 1 for amplitudes – and the three computations were averaged. These values were used to estimate the mean SR response from each ROI as the average of category-selective HR responses.

(b) HR-RSVP: We computed the response amplitudes in HR-RSVP runs by comparing the voxel-by-voxel differences across conditions: CS-FS, FC-FS, FC-CS. Since we are interested in comparing patterns of neural response in these mixed-category runs with activity in the single-category HR-FCS runs, condition differences will be referred to in terms of category difference relative to context: CS-FS = (C-F)S , FC-FS = (C-S)F and FC-CS = (F-S)C. As an example, (C-F)S should be read as "car minus face in the context of sofas". For each voxel, a PSC estimate was computed for each difference using the average of the other three as a baseline. For example, "(C-F)S PSC" = (CS–FS) / ((FC+FS+CS)/3). These means were calculated using data from all 6 RSVP runs. HR voxels were sorted based on their maximal response during HR-FCS voxels (considering the average over all three runs), and RSVP means were computed within the sorted voxels.

Selectivity of response (HR-FCS). Selectivity was quantified on a voxel-by-voxel basis using the signal detection theory measure d_a, with cross validation. See E1 for details. The only departure here from d_a analyses performed in E1 concern the partitioning of data for cross-validation. Here, the preferred category for each voxel was the one that evoked the maximum response during *two* runs, and d_a was calculated relative to this category using data from the *third* run. Three such orthogonal computations were averaged (runs 1 & 2 for classification, run 3 for d_a calculation; runs 1 & 3 for classification, run 2 for da calculation, and runs 2 & 3 for classification, run 1 for d_a calculation).

Multivoxel pattern analysis (MVPA) (HR-FCS)***.*** We considered neural decoding and classification across distributed patterns of activation. This analysis was done to explore whether there was distributed category information for objects even when an ROI showed no reliable selectivity for objects. We computed voxel-by-voxel correlation maps between the magnitude of PSC in two runs with that of the independent run. As in E1, all statistical tests on correlations were conducted after performing a Fisher's transformation on the correlation values.

All statistical tests of expertise conducted on the HR-FCS runs will use a 1-tail test, since we are testing replication of E1 results. All statistical tests of expertise conducted on the HR-RSVP runs will use a 2-tail test, since we are testing new predictions associated with mixed-category visual presentations.

Results & Discussion – HR-FCS runs

Replicating classical SR-FFA effects in participants varying in car expertise

In the HR 1-back matching runs, where Faces, Cars, Sofas, and Scrambled matrices were shown in a blocked format, we expected to replicate the patterns observed in E1. Identical analyses were applied to all regions, including six face-selective areas (bilateral aFG, bilateral pFG, bilateral OFA) and two object-selective areas (bilateral PHG). As before, we began by analyzing the results

averaged over the entire ROI. We calculated the average SR response from each ROI as the mean of category-selective HR responses. This simulation represents analyses performed earlier at SR-fMRI. In right fusiform regions (aFG and pFG), the response to faces was nearly twice that to inanimate objects (Figure 30a, 31a). Corroborating this observation, one-way ANOVAs performed on mean PSC values revealed a main effect of Category (aFG: $F_{1,20}$=17.48, p<0.0001; pFG: $F_{1,22}$=16.04, p<0.0001), which post-hoc tests showed to be the result of a greater response for faces relative to cars (Scheffé: aFG: p=0.0002; pFG: p=0.0007) *and* sofas (Scheffé: aFG: p<0.0001; pFG: p<0.0001), with no difference between responses of the non-face categories themselves.

We also considered expertise in the PSC category means. E1 replicated SR-fMRI effects of expertise, as performance discriminating cars predicted the average ROI PSC to cars vs. animals. To explore expertise in E2, it is also necessary to compare category-specific responses to a high-level baseline. However, our three categories are equally homogeneous and each theoretically interesting. Thus, we will present correlations between car expertise and each category comparison: Cars–Sofas, Cars–Faces, and Faces–Sofas. We would expect the response for Cars – Sofas to increase with car expertise, although as we will see below, this was to some degree complicated by the overall similarity of cars and sofas. Indeed, in the mixed runs, cars were much harder for participants to spot in the CS stream and the FC stream (Figure 28). Luckily, we would also expect Cars – Faces to increase with expertise, as this contrast as been used in prior SR studies. For example, Gauthier et al. (2005) and Xu (2005) compared the BOLD response of cars to that of faces when correlating with behavioral car expertise. Similarly, Furl et al. (2010) compared the BOLD response for faces to that of cars when correlating with behavioral face recognition. In contrast, we would not expect Faces – Sofas to depend on car expertise.

Table 22. For the right aFG and pFG, the zero-order correlations with Car *d*' (in white rows) and partial correlations with Car *d*' controlled for Bird *d*' (in grey rows) for the relationship between the mean PSC response to cars–faces, cars-sofas, and faces-sofas in the whole ROI. Significant correlations are shown in bold (α = 0.05).

	ROI PSC		
	Av Car-Face PSC	***Av Car-Sofa PSC***	***Av Face-Sofa PSC***
Right aFG (N=21)	0.357	0.269	-0.213
	0.334	0.259	-0.181
Right pFG (N=23)	**0.367**	0.157	-0.124
	0.379	0.177	-0.115

The relationship between Car *d*' (with Bird *d*' held constant) and the mean PSC for Cars vs. Faces is marginally significant in the aFG (r=0.334, *p*=0.075) and significant in the pFG (r=0.379, *p*=0.041) (Table 22). These results suggest that when we consider the entire SR-defined ROI, the fMRI PSC for Cars increases relative to Faces as behavioral expertise with cars increases. This finding replicates our E1 results, as well as earlier studies exploring expertise at SR.

Replicating prior cross-validation selectivity for faces

Response amplitudes: Next, we performed HR-analyses of selectivity for each category without spatial smoothing and without regards to expertise, as in E1. HR voxels were sorted into bins based on maximum response in 2/3 of the data, and PSC was computed using the independent 1/3 of the data. A comparison of responses for preferred and non-preferred categories provided evidence of reliable selectivity for faces, while voxels that initially responded most to cars or sofas responded equally to faces and non-face objects. This pattern of main effects was observed in the right aFG (Face voxels ($F_{1,20}$=49.43, *p*<0.0001), Car voxels ($F_{1,20}$=2.26, n.s.), Sofa voxels ($F_{1,20}$=0.003, n.s.)) as well as the right pFG (Face voxels ($F_{1,22}$=87.15, *p*<0.0001), Car voxels ($F_{1,22}$=2.21, n.s.), Sofa voxels ($F_{1,22}$=0.07, n.s.)) (Figure 30b, 31b).

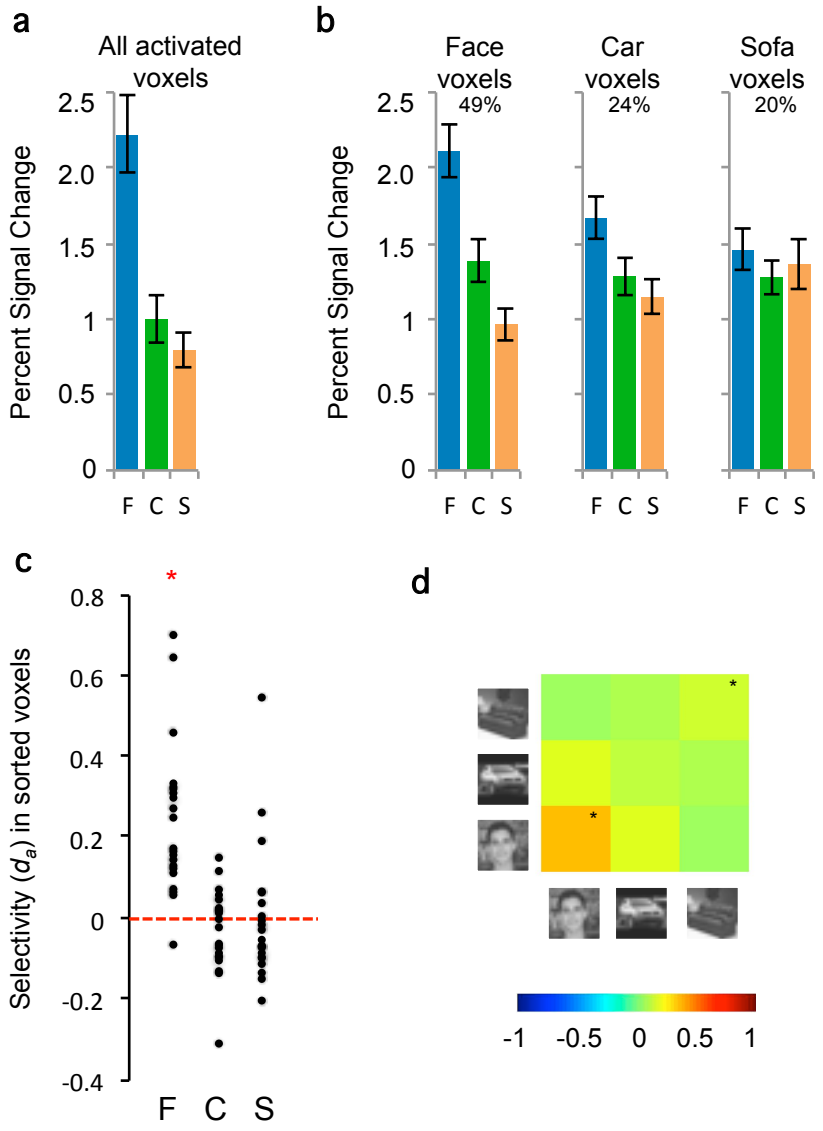

Figure 30. Category-specific response in the right aFG (n=21). (a) Average percent signal change (PSC) to faces, cars and sofas averaged over all HR voxels that were more active for objects than scrambled matrices. This is roughly equivalent to an SR-fMRI signal. (b) HR voxels were grouped by the category that elicited the maximal response in 1/3 of the data, and PSC for each category relative to scrambled matrices was plotted for the other 2/3 of the data. Error bars show SEM. (c) Voxel selectivity across participants measured using the signal detection theory measure d_a in sorted voxels, for half the data based in voxels sorted in the other half. (d) Cross-correlation for the voxel-by-voxel pairwise contrasts between within-category and between-category correlations, computed across independent datasets and averaged. Asterisks denote cases where, after a Fisher transformation, the within-category (on-diagonal) correlation was significantly larger than the between-category (off-diagonal) correlations.

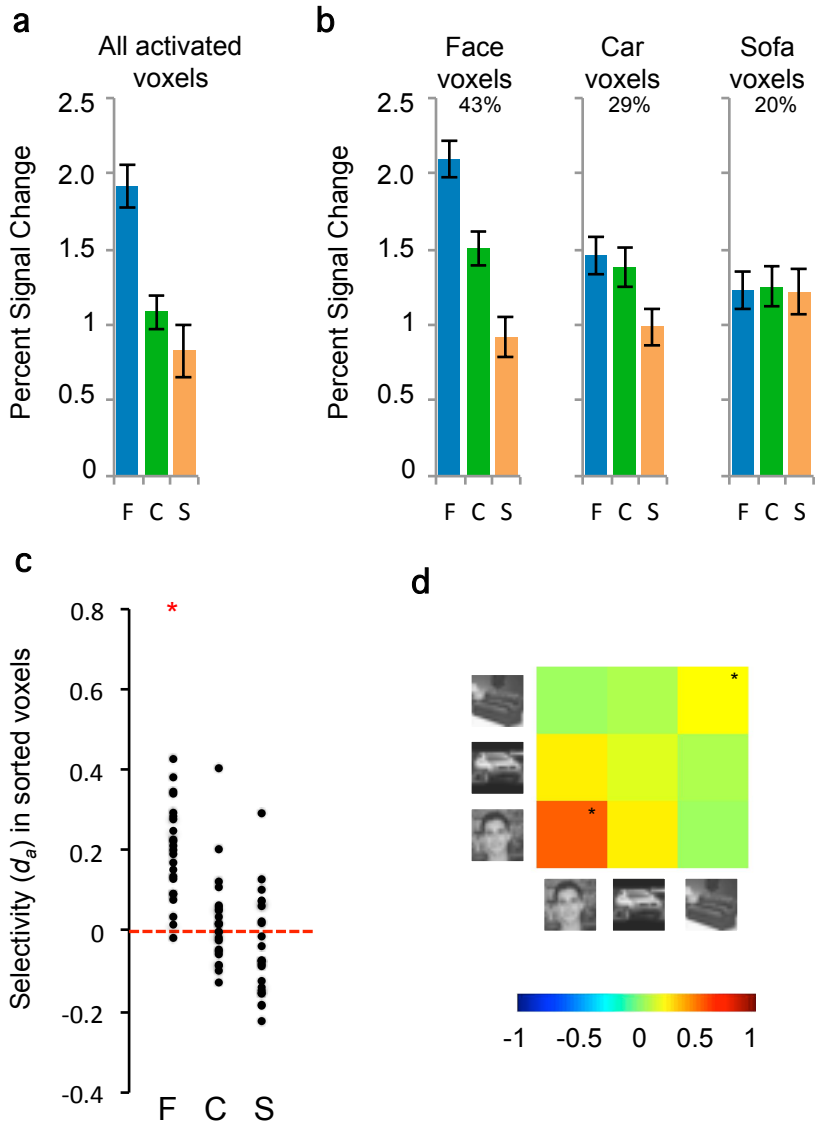

Figure 31. Category-specific response in the right pFG (n=23). (a) Average percent signal change (PSC) to faces, cars and sofas averaged over all HR voxels that were more active for objects than scrambled matrices. This is roughly equivalent to an SR-fMRI signal. (b) HR voxels were grouped by the category that elicited the maximal response in 1/3 of the data, and PSC for each category relative to scrambled matrices was plotted for the other 2/3 of the data. Error bars show SEM. (c) Voxel selectivity across participants measured using the signal detection theory measure d_a in sorted voxels, for half the data based in voxels sorted in the other half. (d) Cross-correlation for the voxel-by-voxel pairwise contrasts between within-category and between-category correlations, computed across independent datasets and averaged. Asterisks denote cases where, after a Fisher transformation, the within-category (on-diagonal) correlation was significantly larger than the between-category (off-diagonal) correlations.

Neural selectivity: Category selectivity was also quantified on a voxel-by-voxel basis using the signal detection theory measure d_a. We computed a mean for each category in all participants to determine the center of mass of each category-specific distribution of d_a values. Figures 30c, 31c

display the distribution of selectivity for Faces, Cars and Sofas, where each point represents a single participant and red asterisks denote significant selectivity of response for a given category (i.e., mean $d_a > 0$, where 0 reflects the absence of category preference). In both right fusiform ROIs, reliable selectivity emerged for faces (aFG: t=5.92, $p<0.0001$; pFG: t=8.19, $p<0.0001$), but not cars or sofas (Table 23). This pattern replicates results from E1.

Table 23. Reliability of category selectivity for the sorted voxels, using cross-validation. Asterisks denote where selectivity (d_a) for a category is larger than 0 ($\alpha = 0.05$). There was no reliable selectivity for cars (or sofas) in bilateral ventral face- or object-selective regions when perceptual expertise was not considered.

	Mean selectivity, d_a		
	Face	**Car**	**Sofa**
Right aFG	0.24*	-0.02	0.01
Right pFG	0.2*	0.03	-0.03
Left aFG	0.31*	-0.01	-0.04
Left pFG	0.24*	0	-0.05
Right OFA	0.2*	0.09	-0.02
Left OFA	0.18*	0.07	0.07
Right PHG	-0.03	0.01	0.13*
Left PHG	-0.04	0	0.14*

Multivoxel pattern analysis: Using MVPA, we compared the Fisher transformed voxel-by-voxel within- and between-category correlations using category-specific activation maps from independent datasets. The correlation matrices in Figures 30d, 31d display average replicability (within-category, on-diagonal) and confusability (between-category, off-diagonal) for Faces, Cars and Sofas across all participants. Positive correlations indicate reliability across independent datasets. MVPA successfully decodes Faces and Sofas in the right aFG (face: $F_{1,20}=45.98$, $p<0.0001$; sofa: $F_{1,20}=8.03$, $p=0.01$) and pFG (face: $F_{1,22}=50.73$, $p<0.0001$; sofa: $F_{,122}=7.08$, $p=0.01$). In neither case were Cars accurately decoded, which contrasts with the findings from E1. This is not surprising considering that the confusability of cars is derived from correlations with only two other categories, one of which – Faces – shows high confusability (i.e., positively correlated voxel-by-voxel activation maps) with cars.

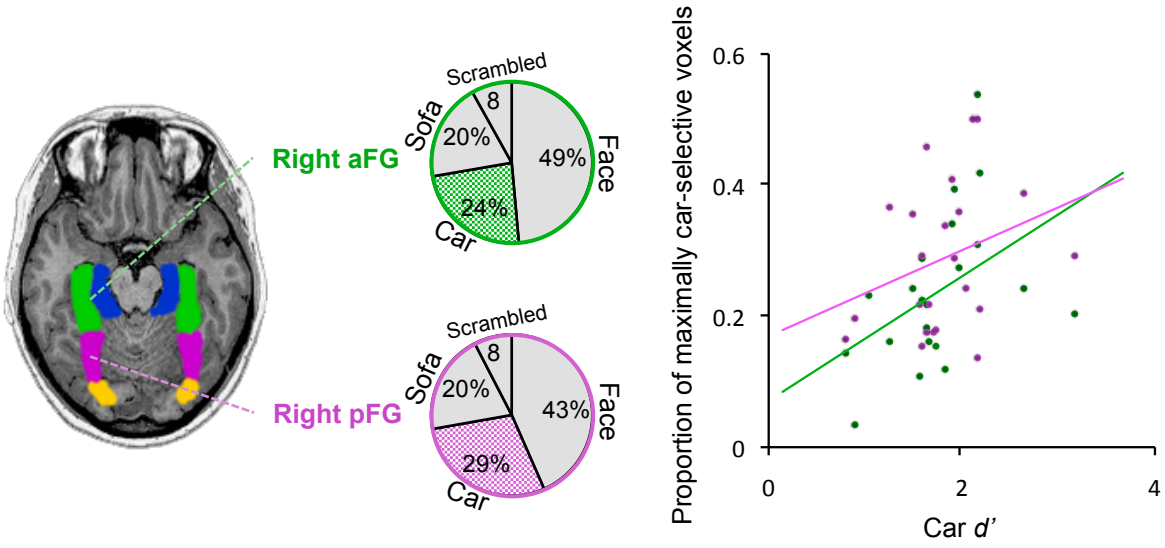

Figure 32. The proportional representation of category-selective voxels in the right FG. Pie charts show the proportion of total voxels maximally selective to faces, cars, sofas, or scrambled matrices in the right aFG (green) and pFG (magenta). The shaded regions of the corresponding pie charts represent the average proportional representation of car voxels in the associated ROIs, which is plotted in the scatterplots. Overlapping scatterplots show the proportion of car voxels as a function of a behavioral car expertise. Each point represents one individual. Car expertise recruits car-selective voxels in the right aFG (r=0.444, p=0.021) and marginally in the right pFG (r=0.294, p=0.086). Note that the colored regions are illustrative, the ROIs being defined functionally and individually in each participant.

Replicating increased reliable selectivity of HR voxels for objects with expertise in SR-FG

Proportional representation: In the HR-FCS runs of the present experiment, we tested whether expertise with cars (behavioral Car *d*') predicts the proportional representation of maximally selective car voxels in the right fusiform regions. Overlapping scatterplots in Figure 32 show the proportion of voxels maximally selective to cars as a function of behavioral Car *d*', for the aFG (green) and the pFG (pink). When we regress out Bird *d*', these trends with Car d' persist, showing that behavioral expertise selectively predicts the proportion of voxels maximally selective for cars in the left aFG (r=0.427, p=0.026) and marginally in the left pFG (r=0.305, p=0.0779) (Table 24). Note, the decrease in proportional representation of faces with car expertise is larger here than it was in E1. This demonstrates a critical point: proportion analyses will be highly dependent on the number and kinds of other categories included. Therefore, what is most important is not necessarily the absolute values, but rather how they vary with expertise.

Table 24. For the right aFG and pFG, the zero-order correlations with Car *d*' (in white rows) and partial correlations with Car *d*' controlled for Bird *d*' (in grey rows) for the proportion of voxels maximally selective to faces, cars, and sofas. Significant correlations are shown in bold (α = 0.05).

	ROI PROPORTION		
	Face %	***Car %***	***Sofa %***
Right aFG (N=21)	**-0.424**	**0.444**	0.143
	-0.409	**0.427**	0.122
Right pFG (N=23)	-0.307	0.294	-0.004
	-0.356	0.305	0.029

HR neural selectivity, d_a*:* Next, we tested whether the voxel-by-voxel selectivity, d_a, is related to car expertise. Without considering the role of expertise, we found reliable selectivity for faces (mean $d_a > 0$), but not cars or sofas (Figure 30c, 31c). Figure 33 shows the correlation between car expertise and d_a for each category, where each data point represents one participant. Many participants show zero or negative selectivity for cars and sofas in car and sofa voxels, respectively, because the voxels sorted as maximally selective to cars or sofas respond more to other categories following cross-validation, than they did in E1. Critically, however, poor car performers show the weakest evidence for true car-selective voxels. As behavioral car expertise increases, reliable selectivity of car voxels also increases (aFG: r=0.49, *p*=0.01; pFG: r=0.47, *p*=0.01). These results using d_a replicate E1. Moreover, when we regress out the influence of Bird *d*', the partial correlations with car expertise remain significant (Table 25).

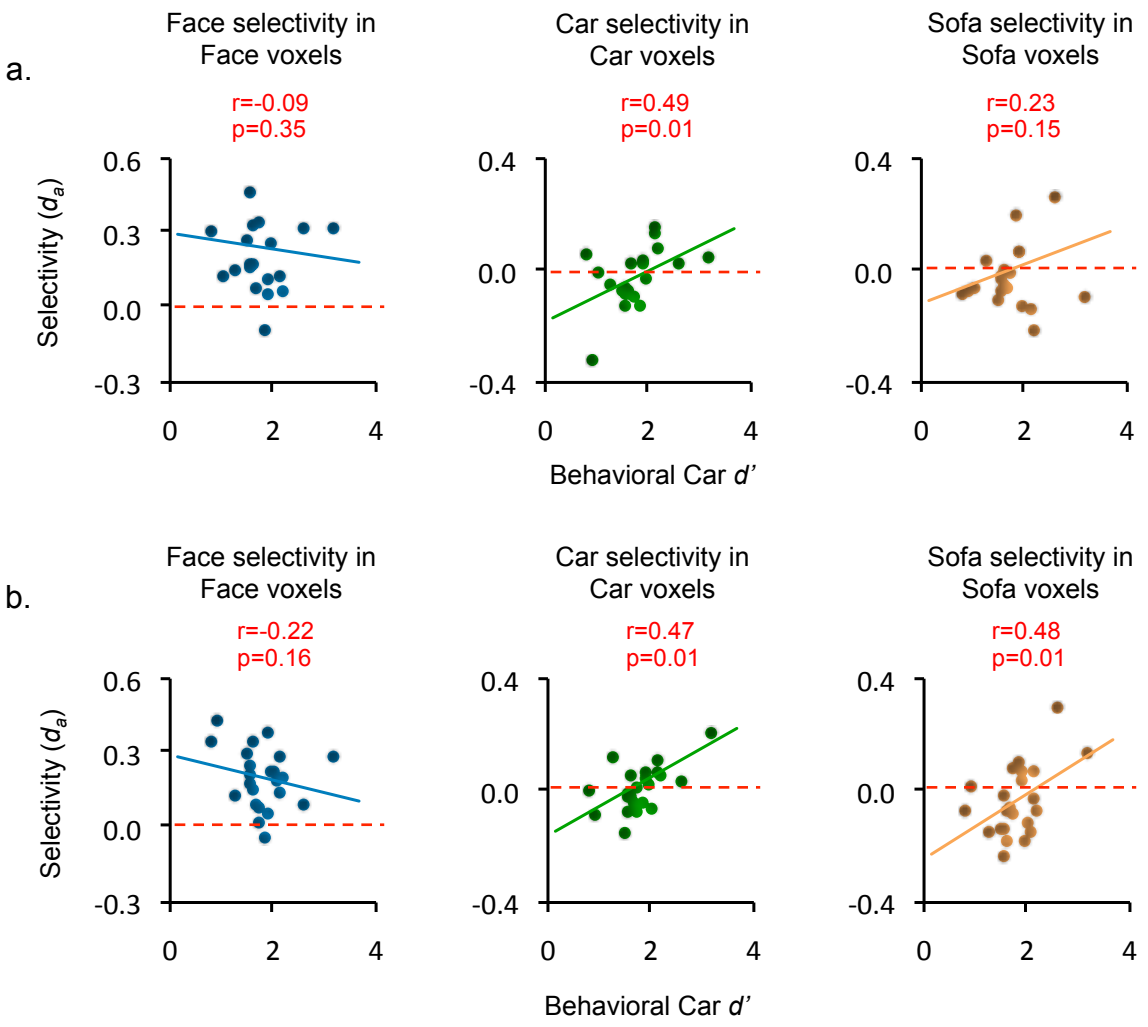

Figure 33. Scatterplots showing the correlations between behavioral car expertise and voxel selectivity, d_a, in sorted voxels for (a) the right aFG and (b) the right pFG. Pearson's moment correlation (r) and statistical significance (p) are given. The horizontal red line depicts zero reliability.

Car performance is also associated with increased selectivity of *sofa* voxels in the pFG (r=0.48, p=0.01), supporting a relationship suggested in HR amplitude calculations (Figure 33). As discussed relative to E1 data, d_a can be difficult to interpret because it depends on all categories as a baseline. This problem is especially pronounced in E2 since we have only three categories to compare. It is possible that the similarity of expertise effects observed for Car d_a and Sofa d_a are due to the fact that in each case the response to faces is subtracted out. We will investigate the relationship between cars and sofas relative to car expertise more directly using pairwise amplitude comparisons.

Table 25. For the right aFG and pFG, the zero-order correlations with Car *d*' (in white rows) and partial correlations with Car *d*' controlled for Bird *d*' (in grey rows) for face, car and sofa selectivity (d_a). Significant correlations are shown in bold (α = 0.05).

	ROI d_a		
	***Face* d_a**	***Car* d_a**	***Sofa* d_a**
Right aFG (N=21)	-0.092	**0.492**	0.234
	-0.06	**0.478**	0.211
Right pFG (N=23)	-0.216	**0.467**	**0.48**
	-0.233	**0.445**	**0.49**

HR amplitude selectivity: Next, data from the HR-FCS runs was used to examine the fine-scale organization of expertise effects at HR. We tested whether the PSC to cars in sorted voxels was predicted by behavioral measures of car expertise. To ensure effects specific to objects of expertise, we compared Car PSC to the high-level baseline of both Faces and Sofas as before. Using an animal baseline, E1 showed that expertise for cars predicted PSC to cars in car voxels, plane voxels, and even in the most highly face-selective voxels of a SR-defined rFFA. Using less than half the amount of data per participant as E1, we replicated this effect of expertise in the two right fusiform regions (Figure 34).

The effect of car expertise was greatest when using the signal for faces as a baseline. Expertise for cars (Car *d*' with Bird *d*' regressed out) predicted the Car – Face PSC in the right aFG in car voxels (r=0.425, *p*=0.031), in sofa voxels (r=0.454, *p*=0.022), and marginally so in the most face selective voxels (r=0.355, *p*=0.062) (Table 26). This suggests that as behavioral expertise with cars increases, so does the sorted HR neural response to cars relative to faces in sorted voxels. If we consider Car PSC relative to the Sofa PSC baseline, expertise effects are not as clear. Behavioral car expertise predicts Car – Sofa PSC only marginally in the face voxels (r=0.320, *p*=0.085), and not at all in car or sofa voxels. However, the face voxels show marginal correlations of expertise with both Car – Face and Car – Sofa, and a near correlation with Face – Sofa, so the most face-selective part of the right aFG shows what could be the most selective expertise effect. Previous work suggested that car expertise effects are due to an increase in activation for cars (Gauthier et al., 2000; Xu 2005),

and other work saw a decrease in the activation for faces (Harel et al., 2010). Our data support the first claim when we consider the most face-selective voxels of the anterior FG region, but the latter claim in non-face aFG voxels and in the pFG. We will later explore how this effect may reflect competition between faces and nonface objects of expertise for neural resources within face-selective FG.

Indeed, in non-face right aFG voxels and in right pFG, the signal for Sofas is surprisingly correlated with car expertise, as suggested by d_a analyses in the right pFG (Figure 33; Table 25). It is improbable that car experts would have greater interest in sofas than car novices, so this result is unlikely to be due to attention. More likely, this can be attributed to the low-level visual similarity between cars and sofas. Not only do cars and sofas share a similar basic configuration (oblong/horizontal), but they also contain similar visual features (e.g., car wheels are comparable to sofa legs, car windows are comparable to sofa pillows, etc).

Considering car expertise, the posterior fusiform region shows a similar pattern of response to the car and sofa aFG voxels (Figure 34). Specifically, behavioral performance with cars (Car *d*' with Bird *d*' held constant) predicts the Car – Face PSC in voxels maximally selective to cars (r=0.452, p=0.017), sofas (r=0.524, p=0.006), and even faces (r=0.371, p=0.045). The patterns observed with Car *d*' correlations persist when we regress out the influence of the Bird *d*' (APPENDIX C).

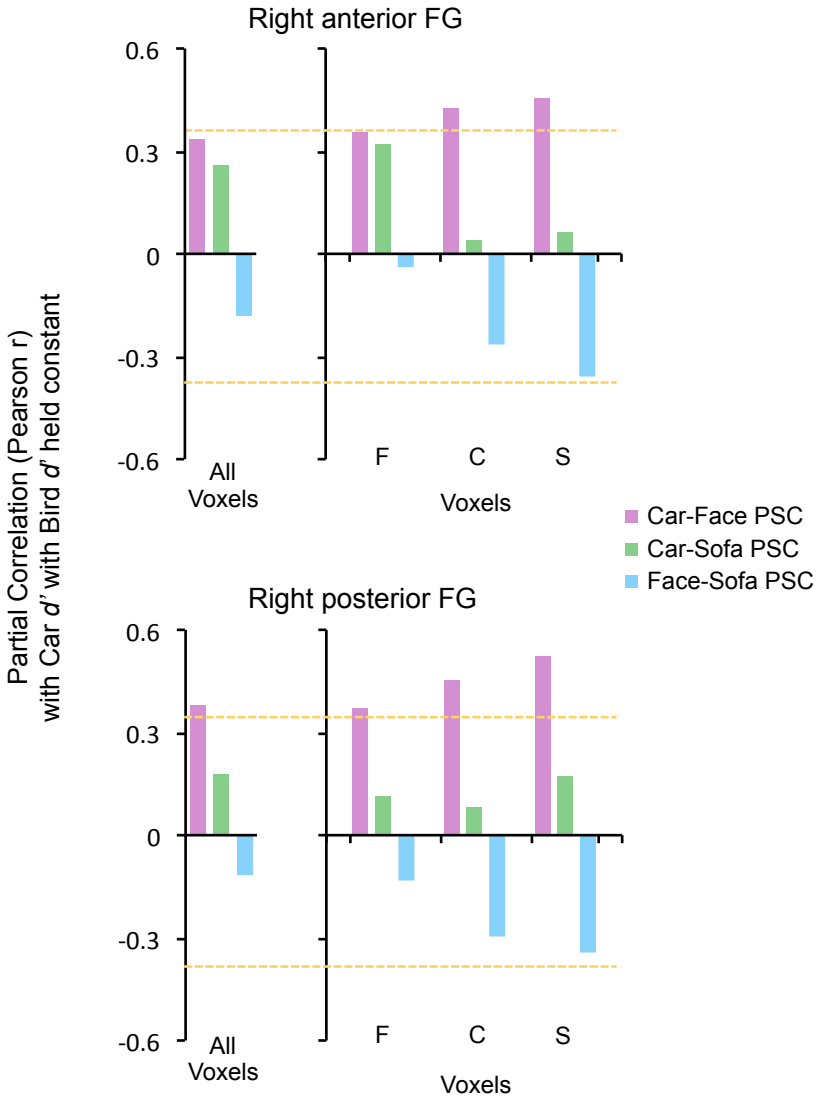

Figure 34. The partial correlations (Pearson r) between behavioral Car *d*' (with Bird *d*' regressed out) and Car–Face PSC, Car–Sofa PSC, and Face–Sofa PSC in all activated voxels (left most bars graphs) and voxels maximally responsive to faces (F), cars (C), and sofas (S) for the right aFG (N=21; top) and the right pFG (N=23; bottom). The horizontal dotted yellow lines mark the critical r-values for the aFG (r_{crit} = 0.378) and pFG (r_{crit} = 0.360) using a 1-tail test and *N-3* degrees of freedom for partial regression analysis.

Face expertise. In addition to exploring effects of car expertise, we also investigated how individual differences in performance on the Cambridge Face Memory Test (CFMT) relate to the neural response to faces in right fusiform regions. In contrast to previous work (Furl et al., 2010), we found no evidence for increased face selectivity with better face matching accuracy on the CFMT in either face-selective fusiform region.

Expertise effects outside of the right FG

Analyses of SR-simulated and HR selectivity for all other ROIs are presented below.

Left Face-selective fusiform regions

In most previous work, face-selective areas in the left hemisphere fusiform gyrus either showed no effect of expertise (Gauthier et al., 2000; Harley et al., 2009; Xu, 2005), or showed a small effect relative to the right hemisphere (Gauthier et al., 1999; Harel et al., 2010). However, in E1 we found an effect in the left FFA comparable to that on the right. We therefore expected to find again in E2 robust expertise effects in left aFG and pFG.

In general, expertise effects in the left aFG and pFG reflect the patterns observed in the right aFG and pFG. Effects of car expertise in the left pFG are slightly more robust than the in the aFG.

Response amplitudes: As observed in right fusiform regions, in left anterior and posterior fusiform regions (aFG and pFG), the response to faces was approximately twice that to inanimate objects (Figure 35a, 36a). One-way ANOVAs performed on mean PSC values revealed a main effect of Category (aFG: $F_{1,20}$=35.32, p<0.0001; pFG: $F_{1,19}$=18.43, p<0.0001), carried by greater response for faces relative to cars (Scheffé Post-hoc tests, aFG: p<0.0001; pFG: p=0.0003) *and* sofas (Scheffé Post-hoc tests, aFG: p<0.0001; pFG: p<0.0001), with no difference between responses for the two non-face categories. When we consider these data with regards to individual differences, an effect of car expertise is observed for Car – Face in the left pFG (r=0.435, p=0.035), but is not significant in the left anterior region (r=0.279, p=0.122) (Figure 34; Table 26).

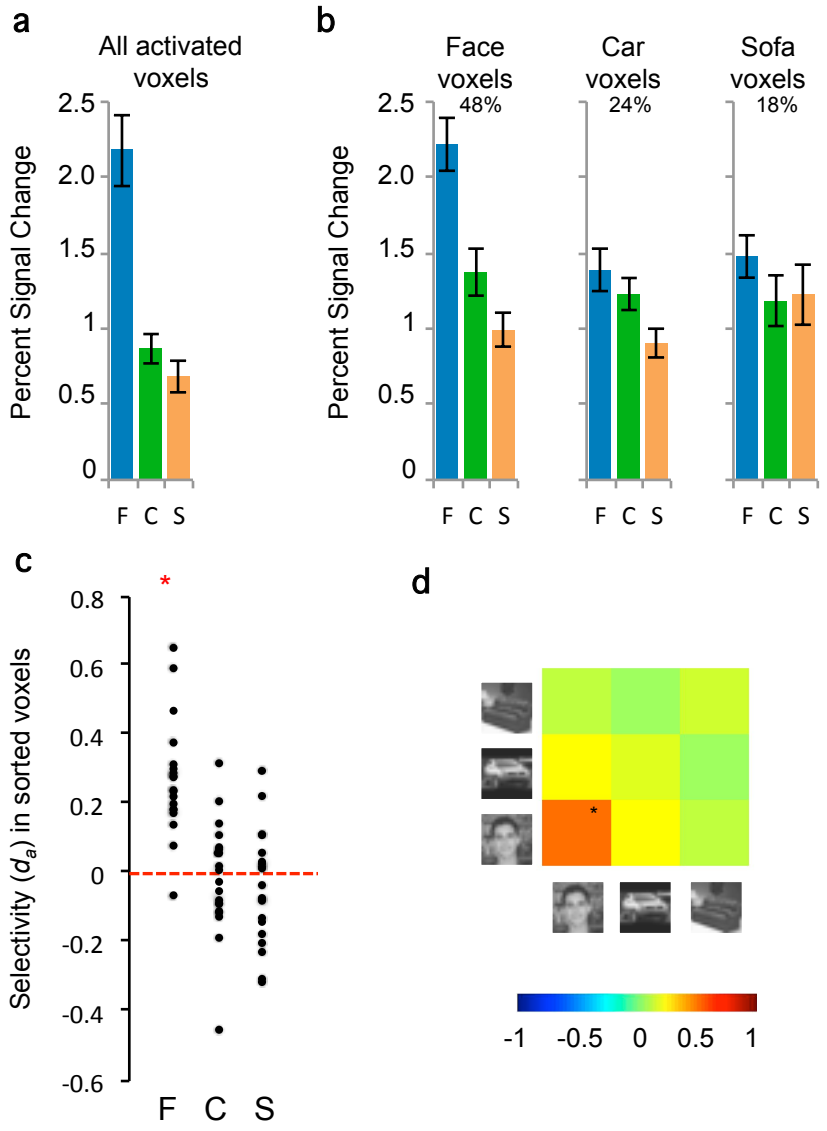

Figure 35. Category-specific response in the left aFG (n=20). (a) Average percent signal change (PSC) to faces, cars and sofas averaged over all HR voxels that were more active for objects than scrambled matrices. This is roughly equivalent to an SR-fMRI signal. (b) HR voxels were grouped by the category that elicited the maximal response in 1/3 of the data, and PSC for each category relative to scrambled matrices was plotted for the other 2/3 of the data. Error bars show SEM. (c) Voxel selectivity across participants measured using the signal detection theory measure d_a in sorted voxels, for half the data based in voxels sorted in the other half. (d) Cross-correlation for the voxel-by-voxel pairwise contrasts between within-category and between-category correlations, computed across independent datasets and averaged. Asterisks denote cases where, after a Fisher transformation, the within-category (on-diagonal) correlation was significantly larger than the between-category (off-diagonal) correlations.

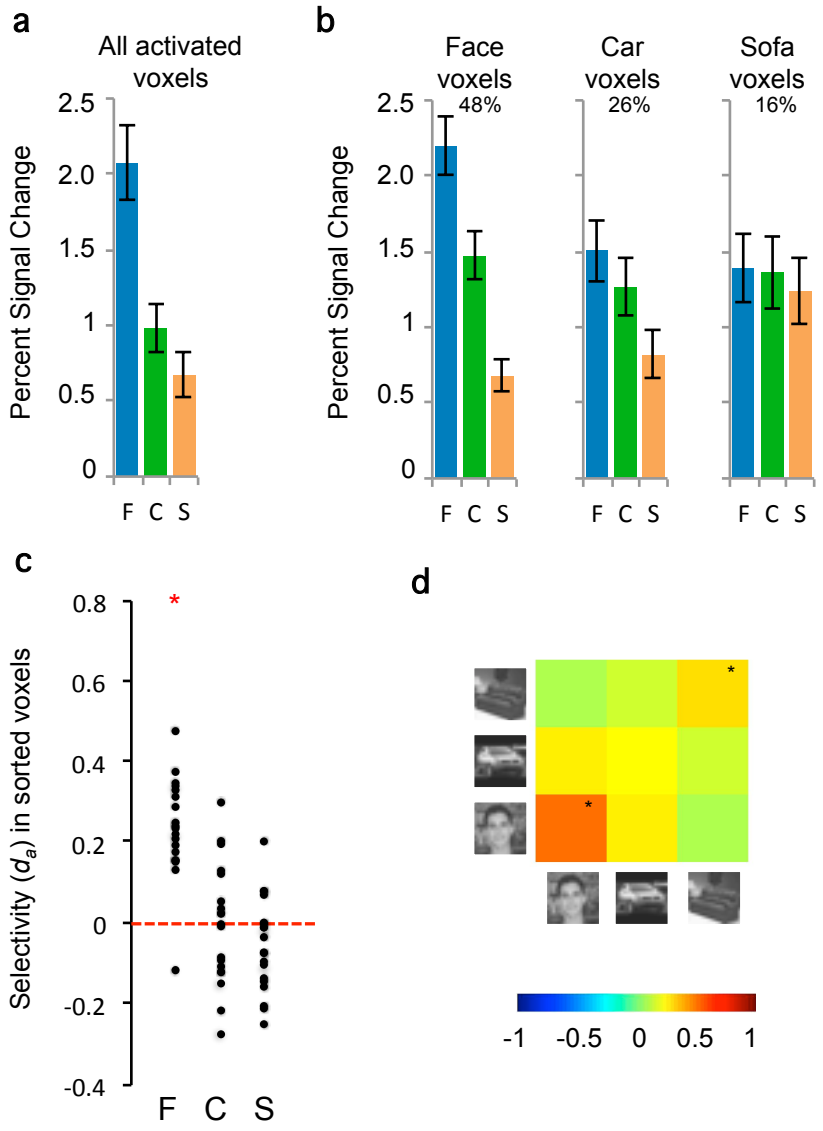

Figure 36. Category-specific response in the right pFG (n=19). (a) Average percent signal change (PSC) to faces, cars and sofas averaged over all HR voxels that were more active for objects than scrambled matrices. This is roughly equivalent to an SR-fMRI signal. (b) HR voxels were grouped by the category that elicited the maximal response in 1/3 of the data, and PSC for each category relative to scrambled matrices was plotted for the other 2/3 of the data. Error bars show SEM. (c) Voxel selectivity across participants measured using the signal detection theory measure d_a in sorted voxels, for half the data based in voxels sorted in the other half. (d) Cross-correlation for the voxel-by-voxel pairwise contrasts between within-category and between-category correlations, computed across independent datasets and averaged. Asterisks denote cases where, after a Fisher transformation, the within-category (on-diagonal) correlation was significantly larger than the between-category (off-diagonal) correlations.

Table 26. For the left aFG and pFG, the zero-order correlations with Car *d*' (in white rows) and partial correlations with Car *d*' controlled for Bird *d*' (in grey rows) for the relationship between the mean PSC response to cars–faces, cars-sofas, and faces-sofas in the whole ROI. Significant correlations are shown in bold (α = 0.05).

	ROI PSC		
	Av Car-Face PSC	***Av Car-Sofa PSC***	***Av Face-Sofa PSC***
Left aFG (N=20)	0.229	0.055	-0.186
	0.279	0.026	-0.25
Left pFG (N=19)	**0.421**	0.373	-0.174
	0.435	0.377	-0.185

Next, we computed category selectivity in sorted voxels. Comparing responses for preferred to average of the non-preferred categories in the sorted voxels revealed reliable selectivity for faces in face voxels, but not cars or sofas in car or sofa voxels, respectively (Figure 35b, 36b). This pattern was observed in the left aFG (Face voxels ($F_{1,19}$=52.46, p<0.0001*)*, Car voxels ($F_{1,19}$=1.02, n.s.), Sofa voxels ($F_{1,19}$=0.41, n.s.)) as well as the left pFG (Face voxels ($F_{1,18}$=132.95, p<0.0001), Car voxels ($F_{1,18}$=0.90, n.s.), Sofa voxels ($F_{1,18}$=1.19, n.s.)).

Neural selectivity: Figures 35c, 36c illustrate neural selectivity (d_a) in sorted voxels, using cross-validation. A similar pattern emerged in left anterior and posterior fusiform regions as was found in the comparable right-hemisphere ROIs. In both left fusiform areas, reliable selectivity emerged for faces (aFG: t=6.19, p<0.0001; pFG: t=8.47, p<0.0001), but not cars or sofas. This finding supports HR-analyses of category selectivity as shown in Figure 38b. We also replicate here category-specific voxel selectivity from E1 that was restricted to animate objects (faces and animals) and absent for cars and planes.

Multivoxel pattern analysis: We used a planned contrast to test whether each category (within-category comparison) was different from the average of the others (between-category comparisons). As expected, MVPA accurately decoded faces in both the left aFG ($F_{1,19}$=31.24, p<0.0001) and the left pFG ($F_{1,18}$=24.32, p=0.0001). However, while MVPA in the anterior region gave no evidence of non-face replicability, MVPA in the posterior region was able to decode sofas

($F_{1,18}$=19.99, p=0.0003) but not cars. Despite limited power, we nonetheless see evidence for the existence of face *and* non-face information in at least one left fusiform region.

Replicating increased reliable selectivity of HR voxels for objects with expertise in left SR-FG

Proportional representation: First, we consider the proportional representation of maximally car-selective voxels, asking whether this representation increases as a function of perceptual expertise with cars. When we regress out the influence of Bird *d*' on Car *d*', we see that car expertise predicts the proportion of voxels maximally selective to cars versus faces in both the left aFG (r=0.481, p=0.018) and the left pFG (r=0.397, p=0.051) (Figure 37). See Table 27 for the zero-order and partial correlations for all comparisons. It is surprising that car expertise predicts the proportion of sofa voxels, but may occur if the left aFG response is related to visual similarity between cars and sofas.

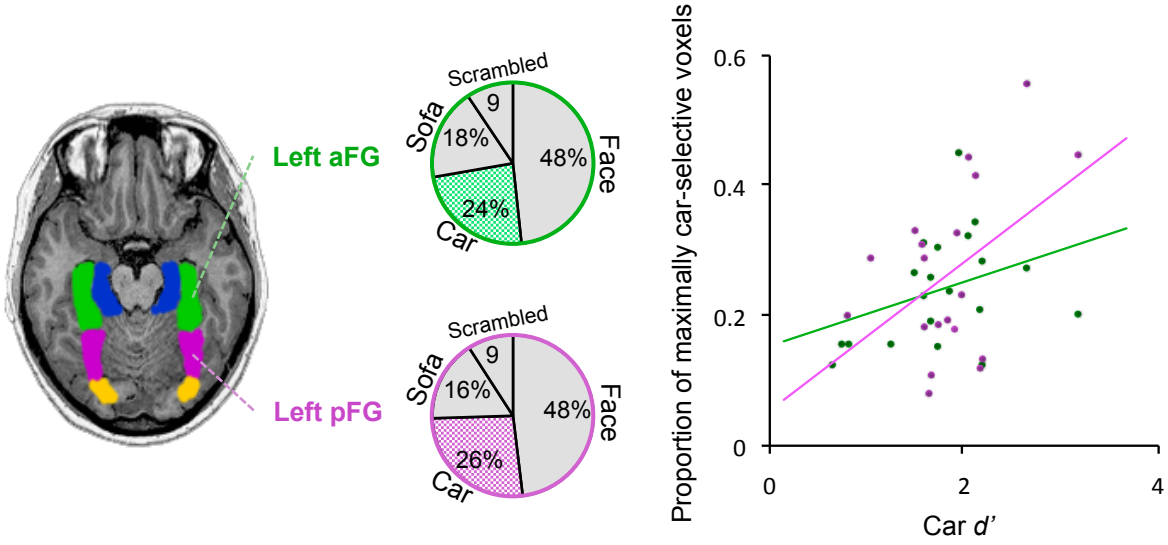

Figure 37. The proportional representation of category-selective voxels in the left FG. Pie charts show the proportion of total voxels maximally selective to faces, cars, sofas, or scrambled matrices in the right aFG (green) and pFG (magenta). The shaded regions of the corresponding pie charts represent the average proportional representation of car voxels in the associated ROIs, which is plotted in the scatterplots. Overlapping scatterplots show the proportion of car voxels as a function of a behavioral car expertise. Each point represents one individual.

Table 27. For the left aFG and pFG, the zero-order correlations with Car *d*' (in white rows) and partial correlations with Car *d*' controlled for Bird *d*' (in grey rows) for the proportion of voxels maximally selective to faces, cars, and sofas. Significant correlations are shown in bold (α = 0.05).

	ROI PROPORTION		
	Face %	***Car %***	***Sofa %***
Left aFG (N=20)	**-0.464**	0.361	**0.406**
	-0.481	0.349	**0.425**
Left pFG (N=19)	-0.286	**0.452**	0.198
	-0.287	**0.455**	0.198

HR neural selectivity, d_a: Without considering individual differences in car expertise, we found reliable selectivity for faces (mean $d_a > 0$), but not cars or sofas. Now we test whether behavioral Car *d*' predicts selectivity, d_a (Figure 38). Relative to participant selectivity in face voxels, the average participant means in car and sofa voxels often falls below the d_a=0 mark (horizontal red line), suggesting car and sofa voxels respond more to non-cars or non-sofas, respectively, after cross-validation. However, in both FG regions, car performance marginally predicts an increase in the selectivity of car voxels (aFG: r=0.29, *p*=0.11; pFG: r=0.36, *p*=0.06) (Table 28). As observed in the right hemisphere, good car performers show more evidence for true car-selective voxels.

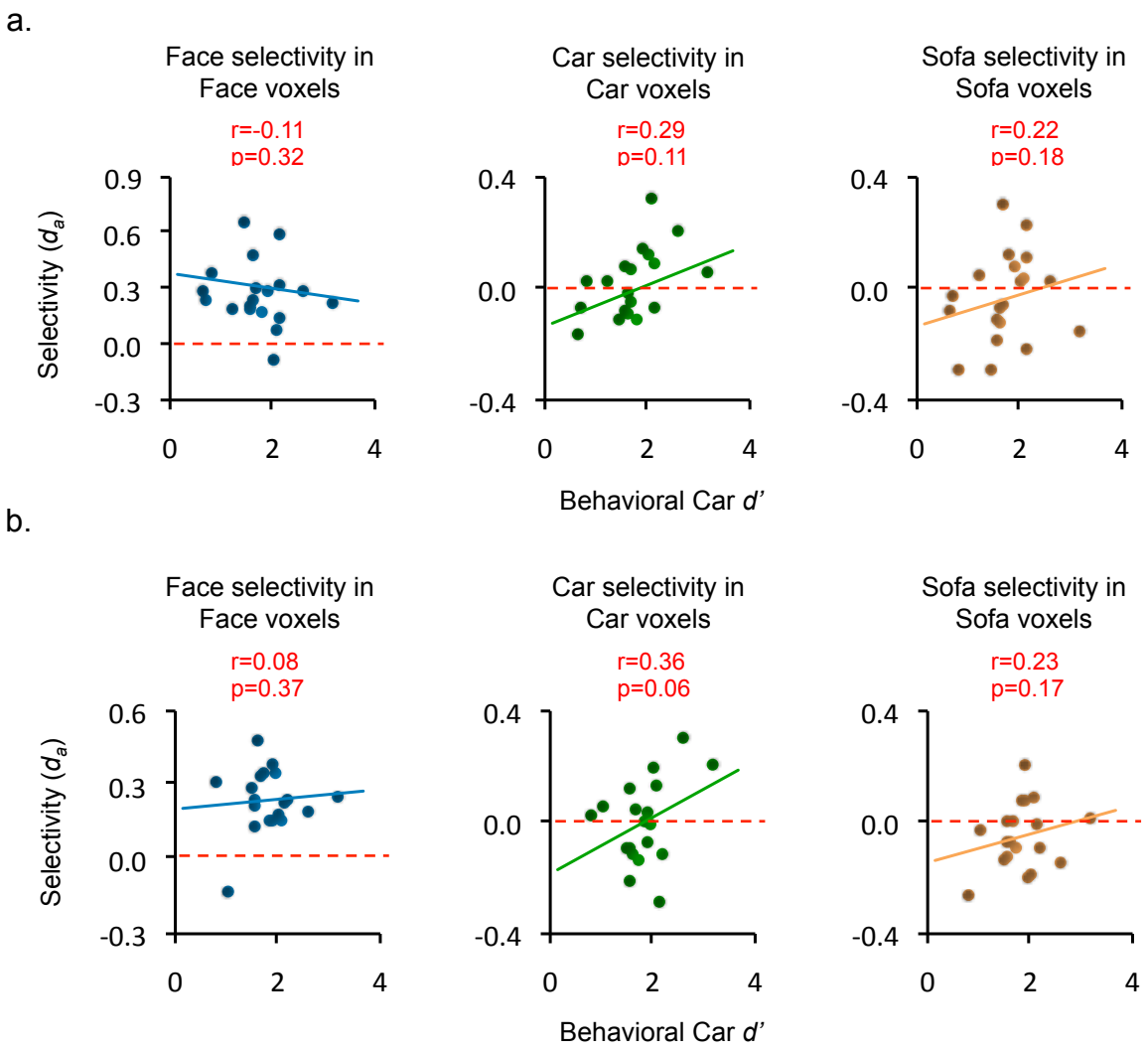

Figure 38. Scatterplots showing the correlations between behavioral car expertise and voxel selectivity, d_a, in sorted voxels for (a) the left aFG and (b) the left pFG. Pearson's moment correlation (r) and statistical significance (p) are given. The horizontal red line depicts zero reliability.

Table 28. For the left aFG and pFG, the zero-order correlations with Car *d'* (in white rows) and partial correlations with Car *d'* controlled for Bird *d'* (in grey rows) for face, car and sofa selectivity (d_a). Significant correlations are shown in bold ($\alpha = 0.05$).

	ROI d_a		
	***Face* d_a**	***Car* d_a**	***Sofa* d_a**
Left aFG (N=20)	-0.11	0.285	0.217
	-0.102	0.265	0.258
Left pFG (N=19)	0.082	0.357	0.233
	0.084	0.358	0.234

HR amplitude selectivity: We tested whether the PSC to cars in sorted voxels was predicted by behavioral car expertise. In the left aFG, behavioral car expertise (regressed for bird performance) predicted the PSC for cars-faces only in car voxels (r=0.380, p=0.053). Similarly, the left pFG showed an expertise effect for the car-face signal in car voxels (r=0.464, p=0.025), but also in sofa voxels (r=0.427, p=0.038). As in the right hemisphere, here too we observed an increase in the raw neural response to sofas with car expertise. Thus, in some cases where voxels showed an expertise effect for cars – faces, they were also likely to show an effect in the opposite direction with a face – sofa comparison, as in the left aFG car voxels (r=-0.408, p=0.041) and the left pFG sofa voxels (r=-0.451, p=0.029). Also see APPENDIX D.

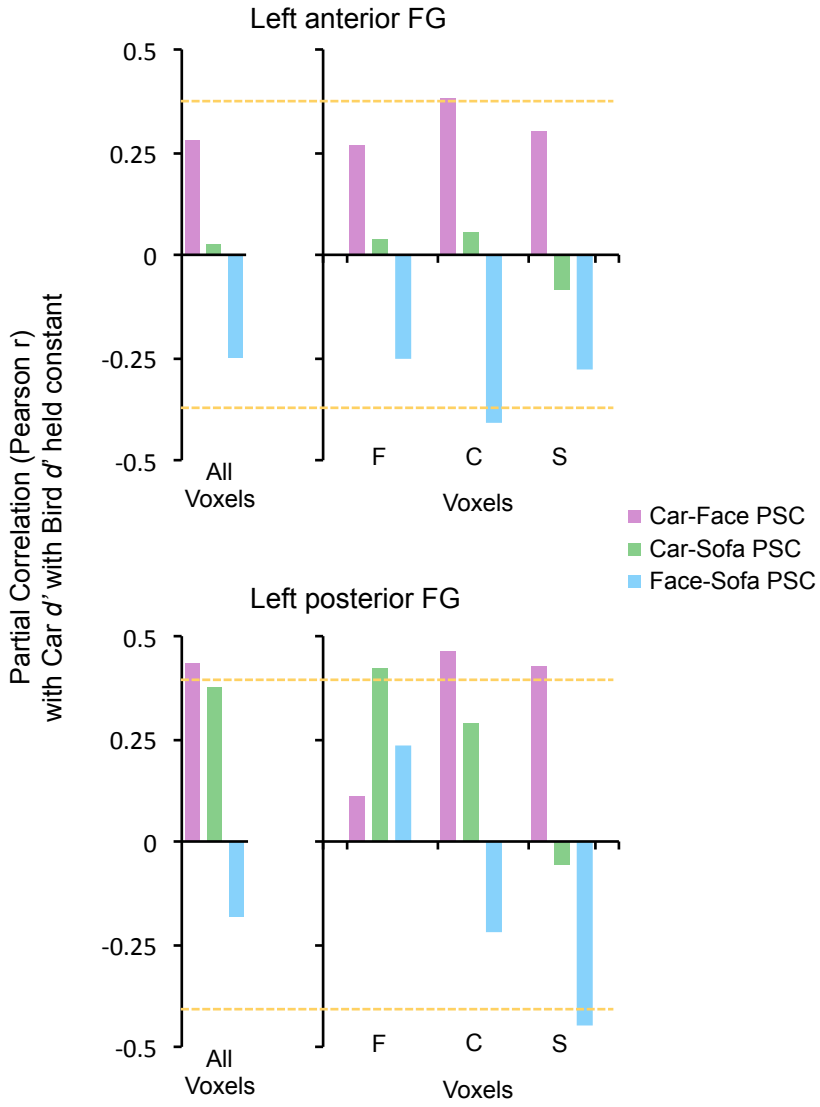

Figure 39. The partial correlations (Pearson r) between behavioral Car *d*' (with Bird *d*' regressed out) and Car–Face PSC, Car–Sofa PSC, and Face–Sofa PSC in all activated voxels (left most bars graphs) and voxels maximally responsive to faces (F), cars (C), and sofas (S) for the left aFG (N=20; top) and the left pFG (N=19; bottom). The horizontal dotted yellow lines mark the critical r-values for the aFG (r_{crit} = 0. 389) and pFG (r_{crit} = 0. 378) using a 1-tail test and *N-3* degrees of freedom for partial regression analysis.

Face-selective occipital regions

Expertise effects in face-selective occipital areas have received less focus than those in the fusiform areas, especially in the left occipital areas. In two SR-fMRI studies, however, training with novel objects and expertise with familiar objects recruited the right OFA, while the left OFA showed no effect (Gauthier et al., 1999; 2000). Consistent with these findings, using HR-fMRI in E1, we

observed marginal effects of expertise in the right OFA, but no such evidence in the left OFA. Thus, we predicted similar results here.

To generally summarize our results, we find expertise effects bilaterally in the OFA. Perhaps surprisingly, these effects were stronger in the left region. Interestingly, whereas car expertise in the rOFA lead to a tradeoff in face selectivity, car expertise in the lOFA lead to a tradeoff with neural selectivity for *sofas*.

One-way ANOVAs performed on mean PSC values (Figures 40a, 41a) revealed a main effect of Category (right OFA: $F_{1,15}$=5.09, p=0.013; left OFA: $F_{1,12}$=5.67, p=0.010), carried by greater response for faces relative to sofas (Scheffé Post-hoc tests, right OFA: p=0.013; left OFA: p=0.010). The mean car-face PSC over all activated right OFA voxels was significantly correlated with behavioral car expertise with Bird *d*' controlled for (r=0.496, p=0.029) (Figure 40a; Table 29), supporting previous work at SR. However, here, the left OFA also showed evidence of an expertise effect, but in the car-sofa PSC only (r=0.519, p=0.039) (Figure 41a; Table 29). The right OFA pattern of expertise effects resembled that observed in bilateral FG, where the neural response for cars and sofas is correlated. Surprisingly, mean responses for cars and sofas in the left OFA, however, do not show this correlation.

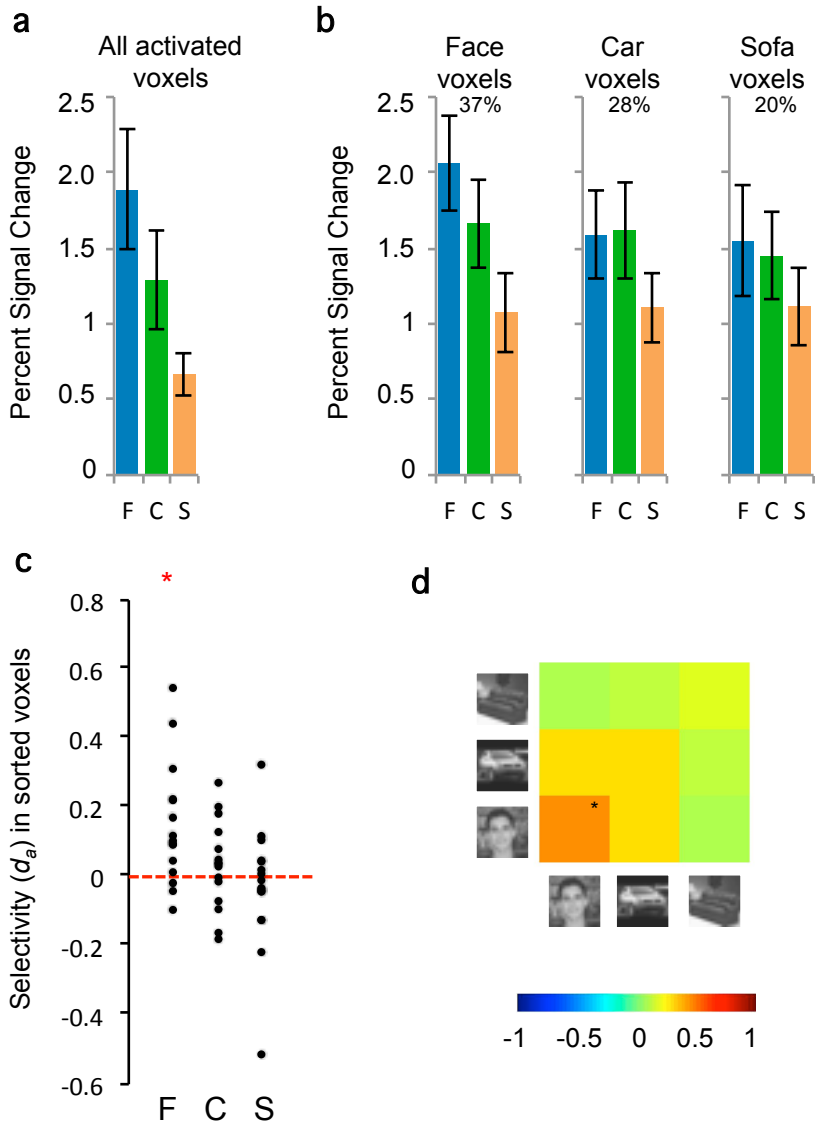

Figure 40. Category-specific response in the right OFA (n=16). (a) Average percent signal change (PSC) to faces, cars and sofas averaged over all HR voxels that were more active for objects than scrambled matrices. This is roughly equivalent to an SR-fMRI signal. (b) HR voxels were grouped by the category that elicited the maximal response in 1/3 of the data, and PSC for each category relative to scrambled matrices was plotted for the other 2/3 of the data. Error bars show SEM. (c) Voxel selectivity across participants measured using the signal detection theory measure d_a in sorted voxels, for half the data based in voxels sorted in the other half. (d) Cross-correlation for the voxel-by-voxel pairwise contrasts between within-category and between-category correlations, computed across independent datasets and averaged. Asterisks denote cases where, after a Fisher transformation, the within-category (on-diagonal) correlation was significantly larger than the between-category (off-diagonal) correlations.

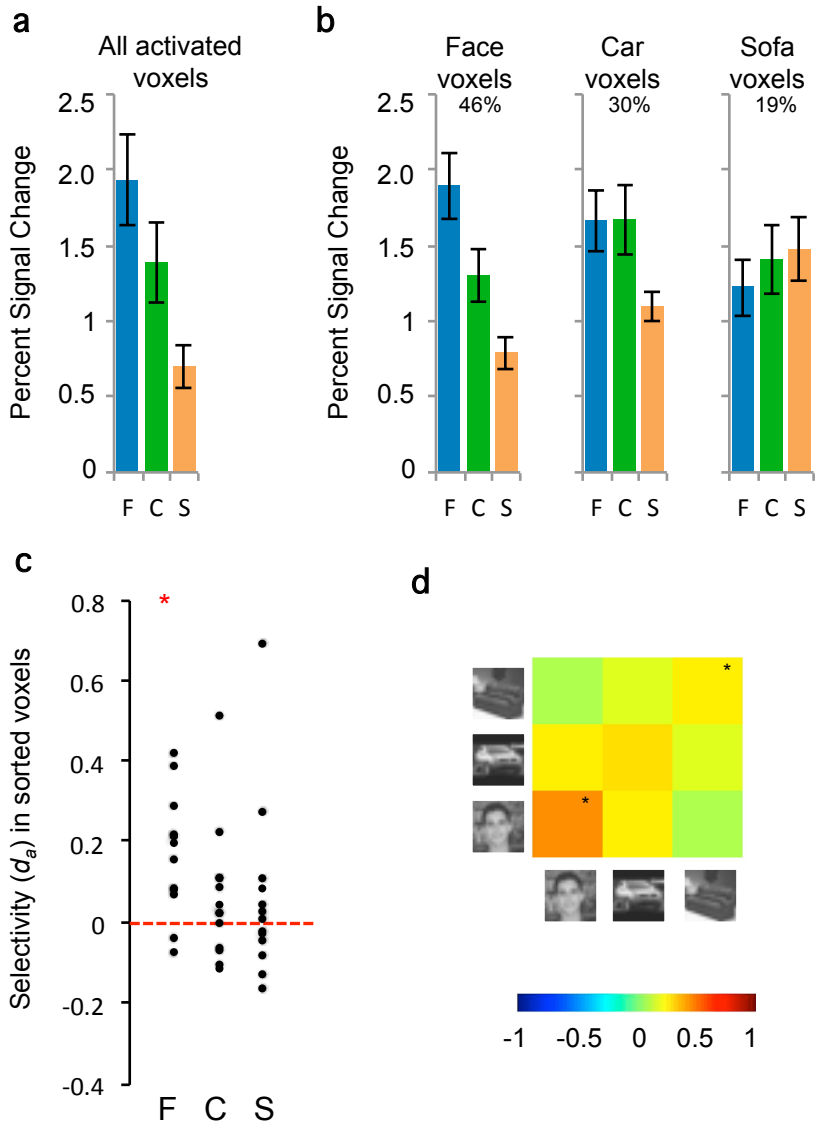

Figure 41. Category-specific response in the left OFA (n=13). (a) Average percent signal change (PSC) to faces, cars and sofas averaged over all HR voxels that were more active for objects than scrambled matrices. This is roughly equivalent to an SR-fMRI signal. (b) HR voxels were grouped by the category that elicited the maximal response in 1/3 of the data, and PSC for each category relative to scrambled matrices was plotted for the other 2/3 of the data. Error bars show SEM. (c) Voxel selectivity across participants measured using the signal detection theory measure d_a in sorted voxels, for half the data based in voxels sorted in the other half. (d) Cross-correlation for the voxel-by-voxel pairwise contrasts between within-category and between-category correlations, computed across independent datasets and averaged. Asterisks denote cases where, after a Fisher transformation, the within-category (on-diagonal) correlation was significantly larger than the between-category (off-diagonal) correlations.

Table 29. For bilateral OFA, the zero-order correlations with Car *d'* (in white rows) and partial correlations with Car *d'* controlled for Bird *d'* (in grey rows) for the relationship between the mean PSC response to cars–faces, cars-sofas, and faces-sofas in the whole ROI. Significant correlations are shown in bold (α = 0.05).

	ROI PSC		
	Av Car-Face PSC	***Av Car-Sofa PSC***	***Av Face-Sofa PSC***
Right OFA (N=16)	**0.446**	0.069	**-0.463**
	0.496	0.032	**-0.565**
Left OFA (N=13)	0.336	**0.61**	0.162
	0.258	**0.519**	0.143

HR-analyses of mean selectivity in face-selective occipital regions showed a similar pattern of response to that observed in face-selective fusiform areas (Figure 40b, 41b). As before, we compared responses for preferred and non-preferred categories within HR-sorted voxels, finding reliable selectivity for faces in face voxels, but not for cars or sofas in car or sofa voxels, respectively: Right OFA (*Face voxels* ($F_{1,15}$=10.37, p=0.006*)*, Car *voxels* ($F_{1,15}$=3.19, n.s.), Sofa *voxels* ($F_{1,15}$=2.07, n.s.); Left OFA (*Face voxels* ($F_{1,12}$=24.41, p=0.0003*)*, Car *voxels* ($F_{1,12}$=3.00, n.s.), Sofa *voxels* ($F_{1,12}$=0.94, n.s.). Moreover, in both right and left occipital face-selective regions, reliable selectivity of response (d_a > 0, red asterisks) emerged for faces (right OFA: t=3.14, p=0.007; left OFA: t=4.38, p=0.001), but not cars or sofas (Figure 40c, 41c). In comparison to the right OFA studied in E1, the present region demonstrates greater face selectivity through a variety of measures. E1 rOFA demonstrated very robust selectivity for animals, which could have affected mean comparisons that used animal activation as a baseline (Figure 18). The left OFA results here replicate those observed in E1, whereby selectivity is found for animate objects only.

Despite this apparent uniformity of face-selective responses in bilateral OFA, we employed MVPA techniques as a sensitive test for replicable patterns of response for non-preferred categories. MVPA decoding in E1 for bilateral face-selective occipital regions suggested the potential for face and non-face information in these regions. As expected, MVPA on HR-FCS data in E2 accurately decoded faces in both the right OFA (planned contrast: $F_{1,14}$=36.12, p<0.0001) and the left OFA (planned contrast: $F_{1,12}$=17.71, p=0.001) (Figure 40d and 41d). MVPA in the left OFA also

demonstrated successful decoding of sofas ($F_{1,12}$=6.49, p=0.026). Even despite relatively small sample sizes for the occipital regions relative to the fusiform regions, we still observe evidence for the existence of face *and* non-face information in at least one face-selective occipital region, which was not present in amplitude or d_a analyses.

Testing selectivity of HR voxels for objects with expertise in SR-OFA

Behavioral car expertise predicted the proportion of voxels maximally selective to cars in the right OFA (r=0.418, p=0.052) and the left OFA (r=0.497, p=0.040), regardless of whether we considered Car *d*' alone or Car *d*' with Bird *d*' held constant (Table 30). Interestingly, the left OFA shows a decrease in the proportion of sofa voxels with car expertise. This trend is unique from the other ROIs, in which car expertise predicted sofa selectivity. This evidence suggests that the lOFA is less influenced by visual similarity, an idea we will pursue in the final discussion.

We did not find a significant effect of car expertise on HR neural selectivity**,** d_a, for cars in either OFA (Table 30).

Table 30. For bilateral OFA, the zero-order correlations with Car *d*' (in white rows) and partial correlations with Car *d*' controlled for Bird *d*' (in grey rows) for the proportion of voxels maximally selective to faces, cars, and sofas, and category neural selectivity, d_a. Significant correlations are shown in bold (α = 0.05).

	ROI PROPORTION			ROI d_a		
	Face %	***Car %***	***Sofa %***	***Face d_a***	***Car d_a***	***Sofa d_a***
Right OFA (N=16)	**-0.516**	**0.413**	0.386	-0.226	-0.043	0.106
	-0.607	**0.418**	**0.523**	-0.242	-0.059	0.131
Left OFA (N=13)	0.088	**0.59**	**-0.563**	0.24	0.36	-0.066
	0.132	**0.497**	**-0.466**	0.207	0.398	-0.037

Next, we looked at HR effects of expertise in sorted voxels. A HR expertise effect was only observed in car voxels of the left OFA for the neural response to cars relative to sofas (r=0.604, p=0.017) (Figure 42; APPENDIX D).

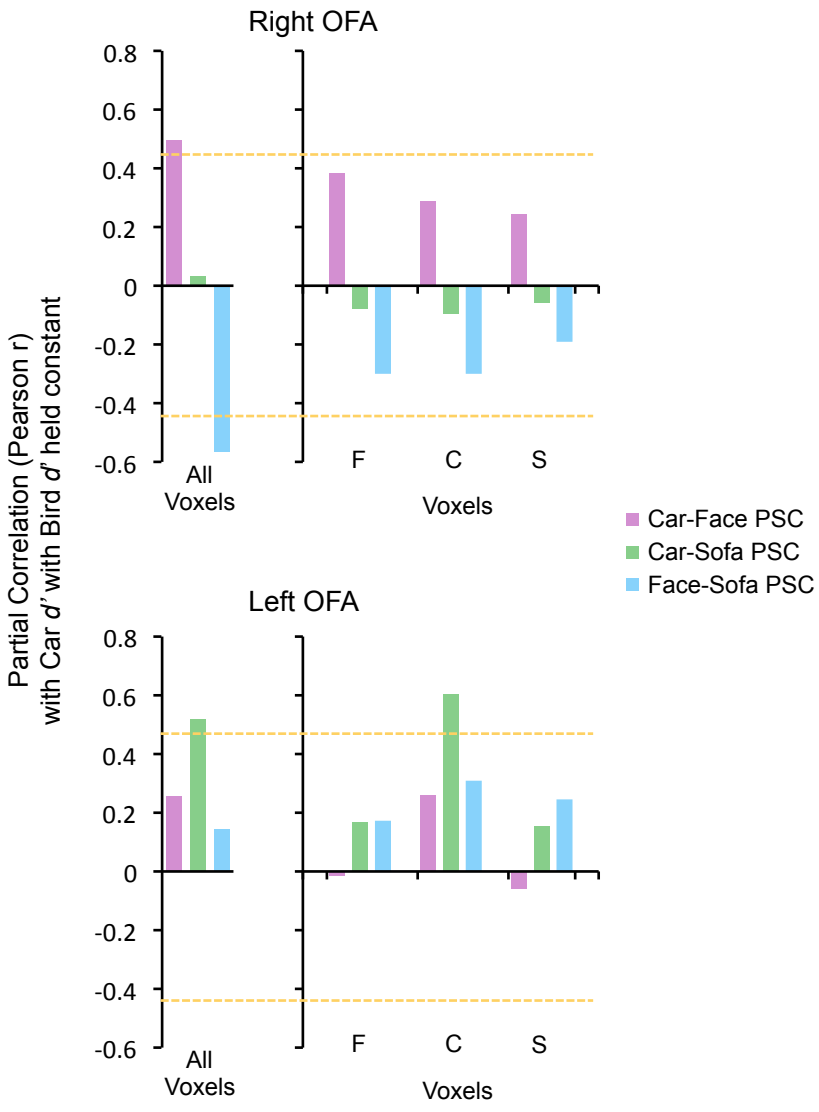

Figure 42. The partial correlations (Pearson r) between behavioral Car *d*' (with Bird *d*' regressed out) and Car–Face PSC, Car–Sofa PSC, and Face–Sofa PSC in all activated voxels (left most bars graphs) and voxels maximally responsive to faces (F), cars (C), and sofas (S) for the right OFA (N=16; top) and the left OFA (N=13; bottom). The horizontal dotted yellow lines mark the critical r-values for the right OFA (r_{crit} = 0. 441) and pFG (r_{crit} = 0. 497) using a 1-tail test and *N-3* degrees of freedom for partial regression analysis.

Object selective parahippocampal regions

We also localize bilateral object-selective regions, however their location in E2 was slightly more anterior relative to the localized object-selective regions in E1. Specifically, these regions fell along the parahippocampal gyri in E2, rather than the medial surface of the fusiform gyri in E1.

To summarize our results, we find evidence of expertise effects on car selectivity bilaterally in the PHG object-selective areas, though stronger in the right PHG. For example, in the most face-selective voxels of the right PHG, we observe an increase in the PSC for cars versus sofas.

First, we examined the mean PSC values in bilateral object-selective ROIs. One-way ANOVAs performed on mean PSC values (Figure 43, 44) revealed a main effect of Category (right PHG: $F_{1,25}$=9.46, p=0.0003; left PHG: $F_{1,23}$=13.60, p<0.0001), carried by greater response for sofas relative to faces (Scheffé Post-hoc tests, right PHG: p=0.0005; left PHG: p<0.0001) *and* cars (Scheffé Post-hoc tests, right PHG: p=0.013; left PHG: p=0.011), with no difference between faces and cars (Figure 43a, 44b). Expertise effects have been observed bilaterally in object-selective regions of the parahippocampal gyrus with SR-fMRI (Gauthier et al., 2000), and in medial fusiform gyrus with HR-fMRI (E1). Here, in contrast, we did not find effects of car expertise on the simulated mean response to cars in the right or left PHG region (Table 31).

Table 31. For bilateral PHG regions, the zero-order correlations with Car *d*' (in white rows) and partial correlations with Car *d*' controlled for Bird *d*' (in grey rows) for the relationship between the mean PSC response to cars–faces, cars-sofas, and faces-sofas in the whole ROI. Significant correlations are shown in bold (α = 0.05).

	ROI PSC		
	Av Car-Face PSC	***Av Car-Sofa PSC***	***Av Face-Sofa PSC***
Right PHG (N=26)	0.237	0.143	-0.046
	0.237	0.144	-0.053
Left PHG (N=24)	0.242	-0.062	-0.258
	0.239	-0.073	-0.265

We performed HR-analyses of selectivity in sorted voxels from bilateral object-selective regions. A trend opposite that observed for face-selective ROIs emerged in the right and left PHG: a one-way ANOVA comparison of preferred to non-preferred responses in the sorted voxels demonstrated reliable selectivity for sofas in sofa voxels, but not faces or cars in face and car voxels, respectively: Right PHG (Face voxels ($F_{1,25}$=1.41, n.s.), Car voxels ($F_{1,25}$=0.36, n.s.), *Sofa* voxels *($F_{1,25}$=38.14, p*<0.0001) (Figure 43b); Left PHG (Face voxels ($F_{1,23}$=0.98, n.s.), Car voxels ($F_{1,23}$=0.67, n.s.), *Sofa* voxels *($F_{1,23}$=30.97, p*<0.0001) (Figure 44b). These regions also showed an opposite trend in selectivity as measured using d_a: reliable selectivity of response ($d_a > 0$, red asterisks) was found for sofas (right PHG: t=5.79, p<0.0001; left PHG: t=5.22, p<0.0001), but not faces or cars (Figure 43c, 44c). Similarly, selectivity analyses from E1 also failed to find voxel selectivity, d_a, for faces or cars in bilateral object-selective regions.

In MVPA analyses, we compared replicability to confusability across category-specific voxel-by-voxel activation maps. MVPA successful decoded Faces and Sofas, respectively, in the right PHG ($F_{1,25}$=17.74, p=0.0003; $F_{1,25}$=32.91, p<0.0001) (Figure 43d) and the left PHG ($F_{1,23}$=14.67, p=0.0009; $F_{1,23}$=28.34, p<0.0001) (Figure 44d). In neither region were Cars successful decoded.

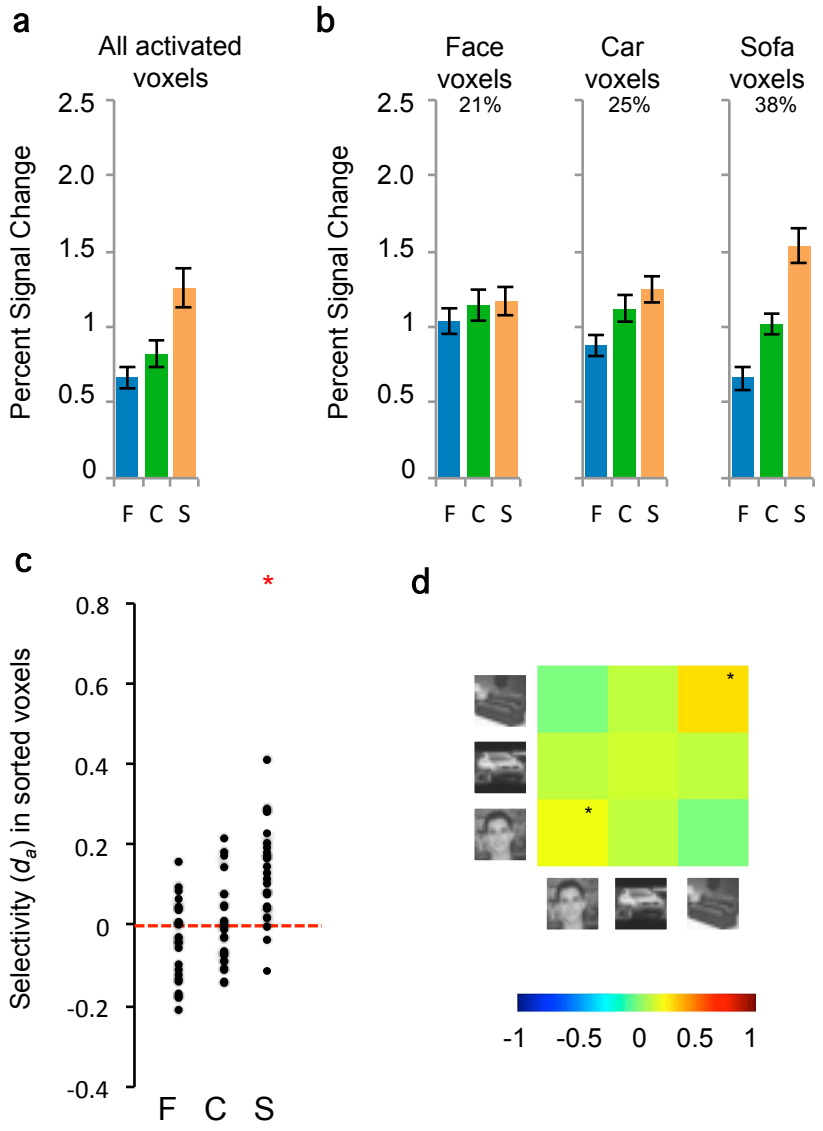

Figure 43. Category-specific response in the right PHG (n=26). (a) Average percent signal change (PSC) to faces, cars and sofas averaged over all HR voxels that were more active for objects than scrambled matrices. This is roughly equivalent to an SR-fMRI signal. (b) HR voxels were grouped by the category that elicited the maximal response in 1/3 of the data, and PSC for each category relative to scrambled matrices was plotted for the other 2/3 of the data. Error bars show SEM. (c) Voxel selectivity across participants measured using the signal detection theory measure d_a in sorted voxels, for half the data based in voxels sorted in the other half. (d) Cross-correlation for the voxel-by-voxel pairwise contrasts between within-category and between-category correlations, computed across independent datasets and averaged. Asterisks denote cases where, after a Fisher transformation, the within-category (on-diagonal) correlation was significantly larger than the between-category (off-diagonal) correlations.

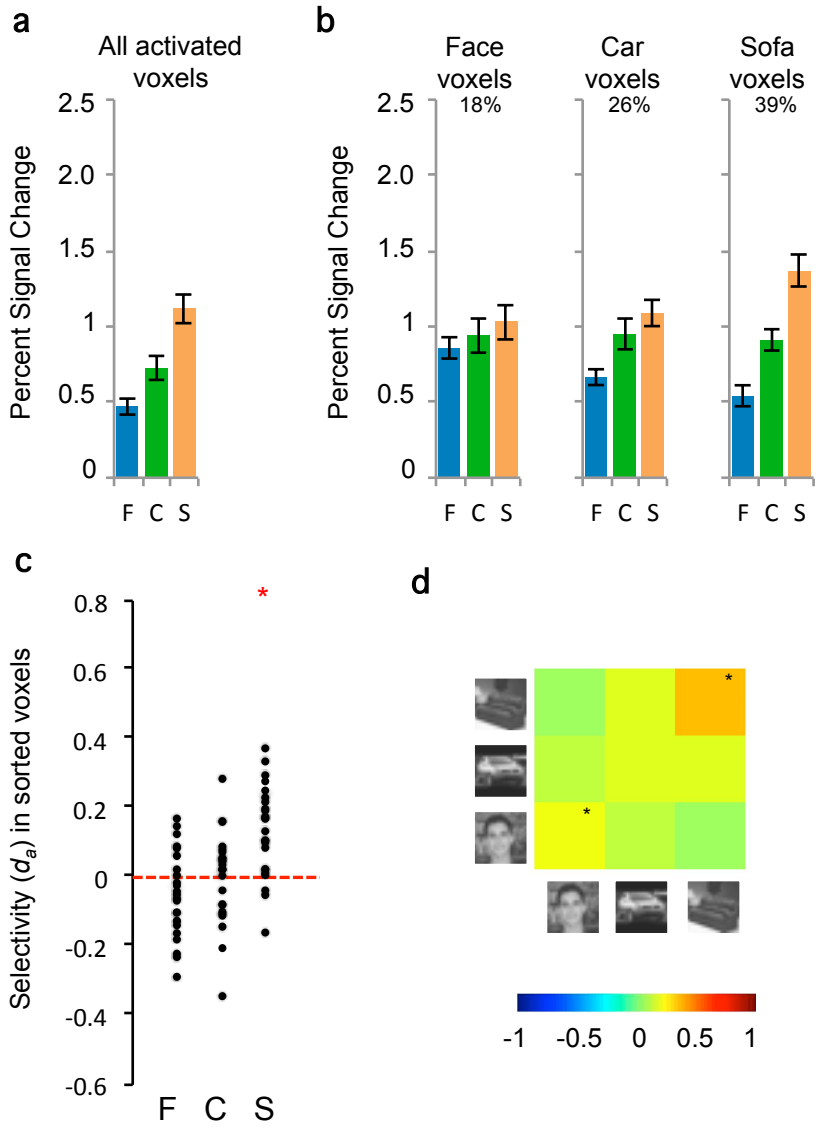

Figure 44. Category-specific response in the left PHG (n=24). (a) Average percent signal change (PSC) to faces, cars and sofas averaged over all HR voxels that were more active for objects than scrambled matrices. This is roughly equivalent to an SR-fMRI signal. (b) HR voxels were grouped by the category that elicited the maximal response in 1/3 of the data, and PSC for each category relative to scrambled matrices was plotted for the other 2/3 of the data. Error bars show SEM. (c) Voxel selectivity across participants measured using the signal detection theory measure d_a in sorted voxels, for half the data based in voxels sorted in the other half. (d) Cross-correlation for the voxel-by-voxel pairwise contrasts between within-category and between-category correlations, computed across independent datasets and averaged. Asterisks denote cases where, after a Fisher transformation, the within-category (on-diagonal) correlation was significantly larger than the between-category (off-diagonal) correlations.

We did not find evidence for an effect of expertise on the proportional representation of car voxels in bilateral PHG regions (Table 32). When considering neural selectivity (d_a,) of car voxels,

however, the right PHG region showed greater car selectivity with individual car expertise, regardless of whether we regressed out the influence of Bird *d*' or not (Table 32).

Table 32. For the right aFG and pFG, the zero-order correlations with Car *d*' (in white rows) and partial correlations with Car *d*' controlled for Bird *d*' (in grey rows) for the proportion of voxels maximally selective to faces, cars, and sofas, and category neural selectivity, d_a. Significant correlations are shown in bold ($\alpha = 0.05$).

	ROI PROPORTION			ROI d_a		
	Face %	***Car %***	***Sofa %***	***Face d_a***	***Car d_a***	***Sofa d_a***
Right PHG (N=26)	-0.067	0.291	-0.139	-0.008	**0.348**	0.1
	-0.079	0.297	-0.142	-0.01	**0.348**	0.106
Left PHG (N=24)	-0.331	-0.018	0.119	-0.143	0.221	0.135
	-0.026	-0.331	0.134	-0.142	0.221	0.132

Moreover, we observed a car expertise effects on the PSC response in HR sorted voxels bilaterally in the PHG regions (Figure 45; APPENDIX D). In the right PHG area, car expertise predicted the neural response for car – sofa in face voxels (r=0.371, *p*=0.033) and car – face in sofa voxels (r=0.367, *p*=0.035). A different pattern emerged in the left PHG, revealing an effect of car expertise on the car-face PSC in car voxels (r=0.388, *p*=0.033).

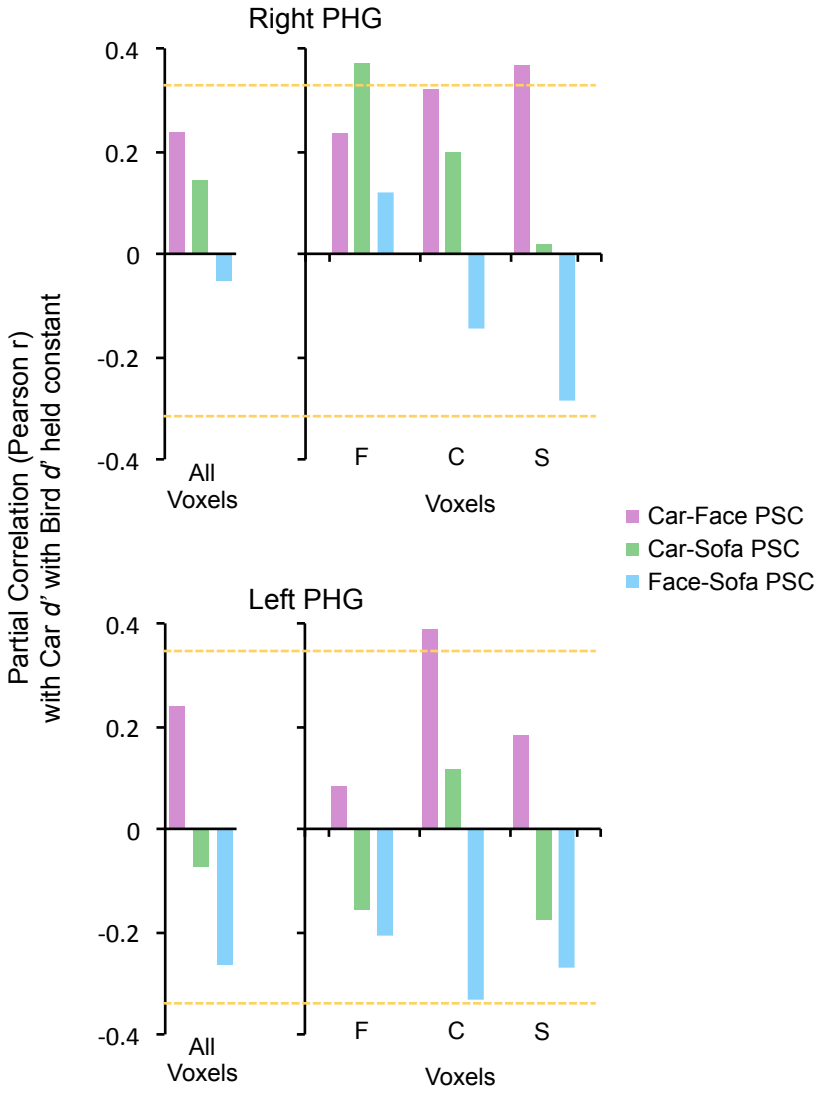

Figure 45. The partial correlations (Pearson r) between behavioral Car *d*' (with Bird *d*' regressed out) and Car–Face PSC, Car–Sofa PSC, and Face–Sofa PSC in all activated voxels (left most bars graphs) and voxels maximally responsive to faces (F), cars (C), and sofas (S) for the right PHG (N=26; top) and the left PHG (N=24; bottom). The horizontal dotted yellow lines mark the critical r-values for the right PHG (r_{crit} = 0. 337) and the left PHG (r_{crit} = 0. 352) using a 1-tail test and *N-3* degrees of freedom for partial regression analysis.

Interim discussion of E2 HR-FCS data

Our results replicate those from E1 and support earlier work using HR-fMRI (Grill-Spector et al., 2006; Baker et al., 2007) in finding no reliable response to non-face objects across all participants in face selective regions of the fusiform gyrus. However, although mean activation of

HR-face voxels shows no car-selective response, we find significant reliability for cars when we examine how the response to cars depends on car expertise (even we regress out the behavioral effect of bird matching performance). We find that selectivity for non-face objects in the FFA can go undetected at high resolution without considering the influence of individual differences in object expertise. Using less than half the data per participant, HR-FCS analyses from E2 replicate the results obtained with E1.

We once again find some evidence that car expertise is associated with reductions in the number and/or magnitude of face-selective neural representations in the lateral FG. For example, car expertise led to an increase in the proportion of voxels maximally selective to cars in both E1 and E2, which was associated with a corresponding decrease in the proportion of *animal* voxels in E1, or *face* voxels in E2 (and possibly in E1, once an outlier was removed). These results suggest that expertise with an object category may limit the representation of faces (or other categories) in the FFA when they demand the same processing mechanisms.

While these results demonstrate competition for spatial representation within object-selective cortex, we can also investigate how objects from different domains of expertise compete in terms of on-line functional dependencies. When dual experts simultaneously process objects from multiple domains of expertise, competition occurs (McGugin et al., 2010; McKeeff et al., 2010; Wong et al., 2011). HR imaging can detect this signal by examining the pattern of response across functionally heterogeneous voxels. In the second part of E2, neural competition was probed using an RSVP design that demanded concurrent processing of objects from two unique categories. This task was very difficult, with the goal of pushing the bounds of perceptual processing. We have seen that neural selectivity for cars – when presented in isolation – increases with car expertise. Now we will ask how the brain responds when cars are presented in the context of other objects: faces or sofas. Faces represent a category of ubiquitous expertise, while sofas are a relatively neutral category. Thus, we were able to compare the contextual influence of expert- and non-expert-object categories on car processing, as a function of individual differences in behavioral car expertise.

Results – HR-RSVP runs

For all participants, 6 HR-RSVP runs immediately followed the SR face-object localizer and 3 HR-FCS localizer runs (Figure 26). Effects of competition were probed in the same 8 ROIs discussed above, using three presentation conditions: alternating faces and cars (FC), alternating faces and sofas (FS), or alternating cars and sofas (CS) (Figure 27). As with the single-category HR-FCS runs, we will compare each condition to each of the other conditions as a high-level baseline, allowing us to investigate three comparisons of interest: Car – Face in the context of Sofas (C–F)S, Car – Sofa in the context of Faces (C–S)F, and Face – Sofa in the context of Cars (F–S)C. We compared neural responses in ROIs identified using an independent SR localizer and in voxels classified with independent HR-FCS data.

We will begin by considering our data without taking into account individual differences in car expertise. First, we computed the mean signal across all voxels of the ROI, representing the response obtained before HR voxel sorting. Next, we will investigate effects of competition in voxels sorted based on their maximal response in HR-FCS runs. HR-FCS analyses showed that classification of face voxels, alone, is reliable; thus, we focus our discussion of competitive influences (independent of expertise) on this subset of FG voxels, which are more likely to constitute the FFA proper.

In the HR-FCS data we found that during non-competitive conditions, faces alone yielded a reliable neural response in the right aFG and pFG. Thus, if face processing is robust to contextual effects, we may expect reliable signal when faces are present relative to when they are absent, regardless of context. Indeed, since the mean response for cars and sofas presented in isolation was not reliable, we would expect minimal influence of these categories on neural face representation during the concurrent processing induced in mixed-category RSVP runs. Relative to the three

comparisons tested, we would predict a negative mean response for (C–F)S, a positive mean response for (F–S)C, and no difference for (C–S)F.

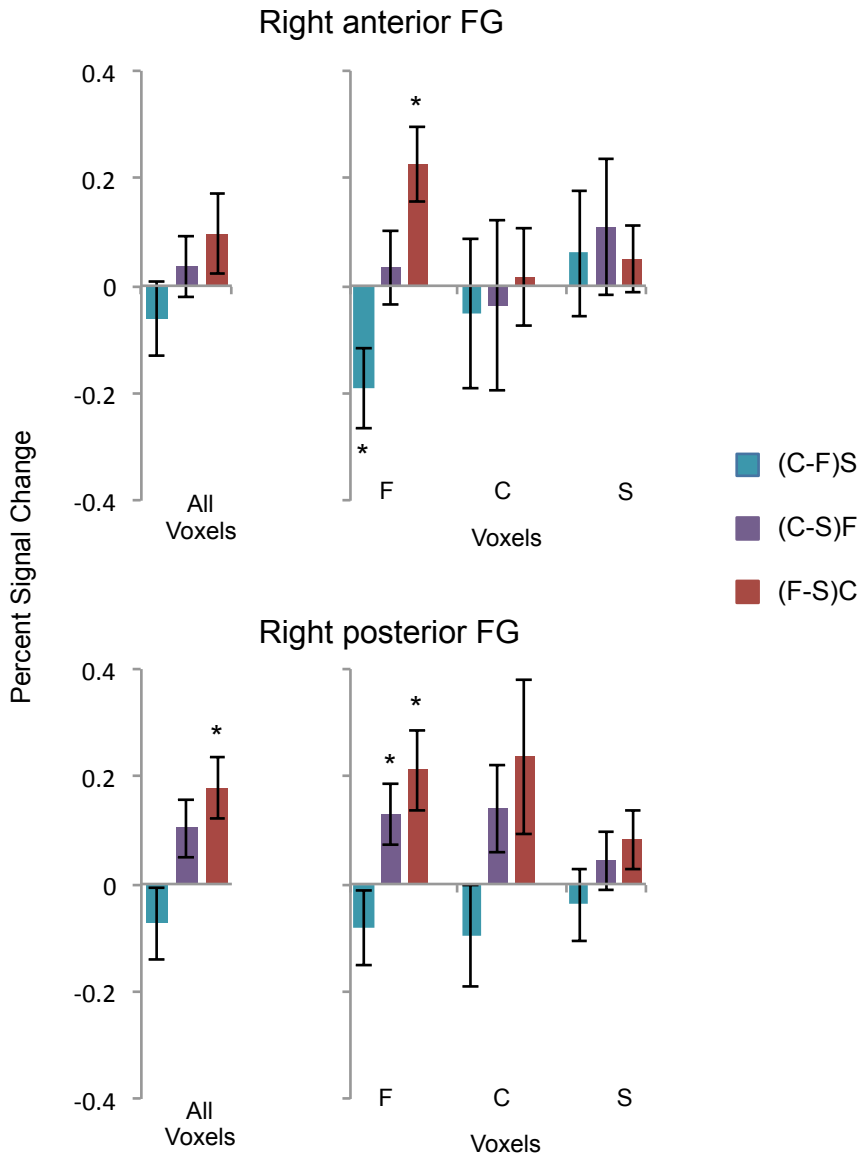

Figure 46. Percent signal change mean response amplitudes during the HR-RSVP runs for the right anterior FG (N=21) and the right posterior FG (N=23). The neural response evoked by each RSVP condition is compared to the other two, yielding three variables of interest. The leftmost bar graphs show the averages over all activated voxels, simulating the response we'd see with SR. Bar graphs to the right plot the mean response amplitudes in voxels sorted based on their maximum response during HR-FCS runs. Error bars represent the sem. Asterisks denote significant effects from one-sample t-tests comparing each condition value to zero. Inferential statistics are given in APPENDIX E.

Mixed-category RSVP data without considering expertise

Contextual effects were indexed as the PSC difference between two conditions: (C–F)S, (C–S)F and (F–S)C. In the absence of car- or sofa-induced contextual effects on face processing, we'd expect a significant signal when face-present conditions are compared to a face-absent condition ((C–F)S and (F–S)C). On the other hand, there may be no difference in the raw neural signal between conditions in which faces are present, (C–S)F. We assessed whether mean differences were significantly different from 0 in all activated voxels and in voxels sorted into category-specific bins based on HR-FCS data. In general, the predicted patterns of response were observed in the average over all voxels, the face voxels for both right FG regions of interest, and the car voxels in the right pFG (Figure 46; APPENDIX E). These results suggest that all face voxels, and the car voxels in right pFG are the most face-selective voxels in the FG under these mixed conditions. Interestingly, in the pFG region, we also observed an increase in the PSC signal for cars – sofas in the context of faces. This may be evidence of a context effect, since the neural response in pFG is greater when faces are shown with cars than when faces are shown with sofas.

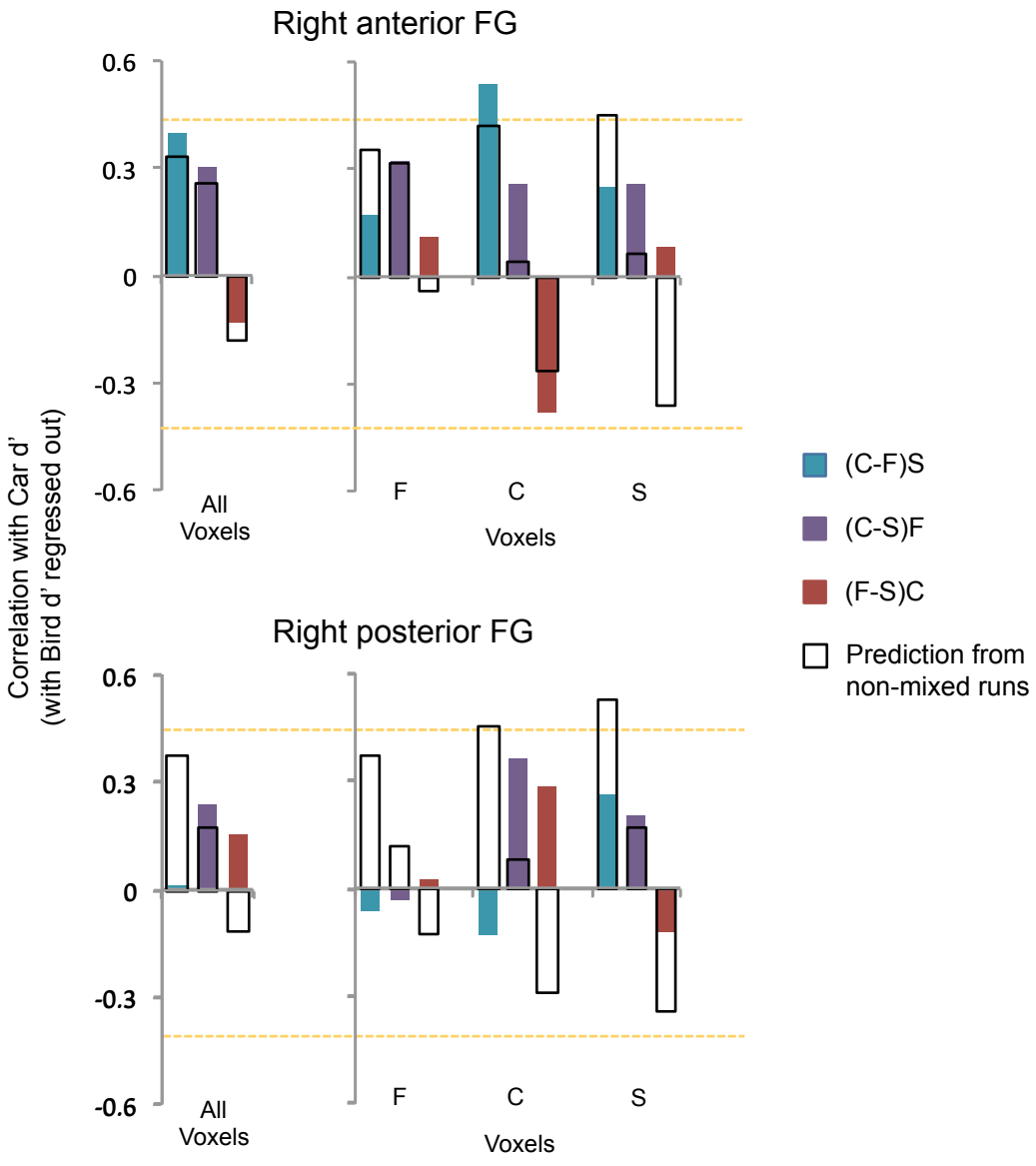

Figure 47. Partial correlations between the neural response during RSVP sequences and behavioral expertise for cars with bird performance regressed out, for the right aFG (N=21) and the right pFG (N=23). The leftmost bar graphs show correlations with the neural response from all activated voxels, while bar graphs on the right depict correlations with activation in HR-sorted voxels. Hollow black bars indicate the corresponding correlations observed in the non-mixed HR-FCS runs. Mixed conditions (C–F)S, (C–S)F and (F–S)C are compared to non-mixed conditions (C–F), (C–S), and (F–S), respectively. The horizontal yellow dotted line represents the critical Pearson's r at which the neural response is significantly correlated with behavioral expertise for the mixed conditions. We used a 2-tail partial correlation with N-3 degrees of freedom: right aFG (r_{crit}=0.444), right pFG (r_{crit}=0.423). Note, this critical value does not mark significance for the non-mixed runs, in which a 1-tail test was applied. See APPENDIX E for all zero-order and partial correlations.

Comparing non-mixed and mixed conditions relative to expertise

We will now consider mixed-category RSVP PSCs, taking into account individual variability in car expertise. Based on data from the non-mixed FCS runs, we predicted that the neural response for cars versus faces shown in the context of sofas would increase as function of behavioral car expertise (Figure 47). This *car – face* trend observed for non-mixed conditions would persist in mixed conditions if showing images in the context of sofas has no influence on the respective car- and face-evoked neural responses (as was suggested by the group mean analyses).

The solid bars in Figure 47 show the partial correlations for RSVP PSC values and Car *d*' when we control for Bird *d*' (APPENDIX E). First considering only these solid bars (ignoring the hollow bars), we can see a significant expertise effect in the right aFG region car voxels, revealing an increase in (C–F)S with increasing car expertise. Neither (C–S)F nor (F–S)C were significantly correlated with car expertise, and the expertise effect for (C–F)S appears to be a combination of signals for cars increasing with car expertise and signals for faces decreasing with car expertise. However, the greatest impact appears to be the decrease in the face response, since (F–S)C in car voxels is marginally significant (r=-0.379, p=0.098).

Here, as in E1, we see that a mere consideration of mean amplitudes is insufficient in grasping a complete picture of patterned neural response. Without considering expertise with cars, there appears to be a general preference in PSC response when faces are present versus not present. When individual differences are taken into account, however, this difference is reduced as a function of car expertise, especially for (C–F)S in the maximally selective car voxels.

A very different pattern emerges when we consider the right posterior FG region. Although mean amplitude differences suggested very similar expertise effects for aFG and pFG, illustrated by the hollow bars in Figure 47, taking into account car expertise extracted a surprising dissociation: no expertise effect in the posterior region (Figure 47). When objects were presented in category-specific blocks, both aFG and pFG showed effects of car expertise. But in mixed-category blocks,

while the effect of expertise remains significant at least in the in aFG car voxels, it is no longer present in pFG.

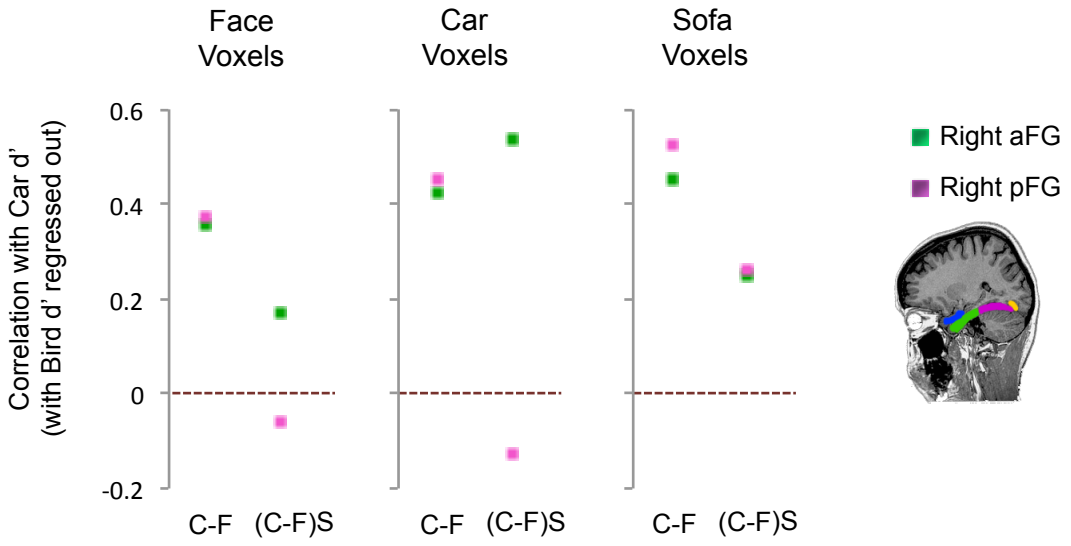

Figure 48. Contrasting the effects of expertise for non-mixed- and mixed-category runs in the right anterior and posterior FG regions. Points represent partial correlations with Car *d'* when we regress out the influence of Bird *d'*. Car expertise for non-mixed data is represented by the cars versus faces PSC (C-F) and, for a comparable contrast, mixed-category expertise is represented by the neural response for cars versus faces all in the context of sofas (C–F)S. The aFG and pFG demonstrate similar effects of expertise during non-mixed runs in face, car and sofa voxels. On the other hand, for mixed-category runs expertise is only found in the aFG car voxels. Horizontal dotted lines depict 0 correlation with car expertise.

Figure 48 illustrates large differences in the expertise effects observed in HR-sorted voxels of the aFG and pFG during non-mixed- and mixed-category runs. This figure shows correlations with car expertise for one relevant comparison from the non-mixed- or mixed-category conditions: cars versus faces from the non-mixed condition or cars versus faces in the context of sofas from the mixed-category condition. When car images are presented in isolation (C–F), both the anterior and the posterior FG regions show positive correlations with behavioral car expertise, in all sorted voxels. However, when cars and faces are presented in the context of sofas (C–F)S, only the aFG expertise effect in car voxels persists. As discussed in the next session, the reduction of the expertise effect for mixed-category RSVP runs appears to be a general phenomenon present in all regions except the right aFG.

Regions outside the right FG

Left anterior and posterior FG

In general, the left aFG and pFG regions showed similar patterns of response compared to their right counterparts. Namely, the magnitude of PSC reflected a preference for face-present relative to face-absent conditions. Although, not significant, car expertise marginally predicted (C–S)F in the left aFG, but no such evidence for expertise emerged in the left pFG region.

Mixed-category RSVP data without considering expertise

We also investigated context effects in mixed-category RSVP data in left FG regions without considering individual differences in car performance and, again, focusing on the face voxels. First, we looked at the PSC averaged over all activated voxels in the left aFG and left pFG, as done before. In both regions, face-present conditions yielded greater activation relative to face-absent conditions (aFG: (C–F)S: t=-2.170, p=0.043; pFG: (C–F)S: t=-3.500, p=0.003 and (F–S)C: t=2.367, p=0.029), while there was no difference in overall activation when faces were shown with cars versus sofas (APPENDIX E).

This pattern of face preference is also reflected in the HR voxels maximally selective to faces in both the left aFG ((C–F)S: t=-3.806, p=0.001 and (F–S)C: t=3.712, p=0.002; (C–S)F: *n.s.*), as well as the left pFG ((C–F)S: t=-3.515, p=0.003 and (F–S)C: t=2.807, p=0.022; (C–S)F: *n.s.*) (APPENDIX E). As expected, mean amplitude responses in the left FG regions follow a similar pattern to those observed in the right FG regions.

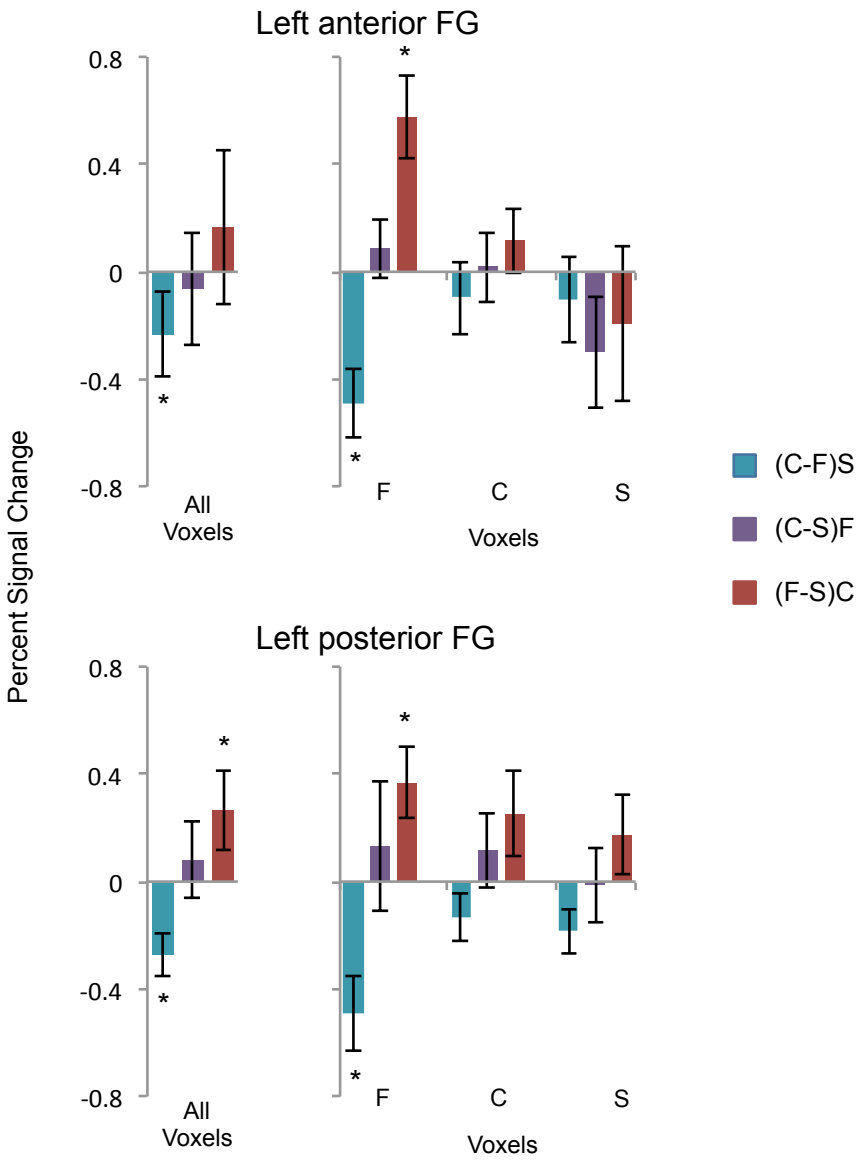

Figure 49. Percent signal change mean response amplitudes during the HR-RSVP runs for the left anterior FG (N=20) and the left posterior FG (N=19). The leftmost bar graphs show the averages over all activated voxels. Bar graphs to the right plot the mean response amplitudes in voxels sorted based on their maximum response during HR-FCS runs. Error bars represent the sem. Asterisks denote means significantly different from zero. Inferential statistics given in APPENDIX E.

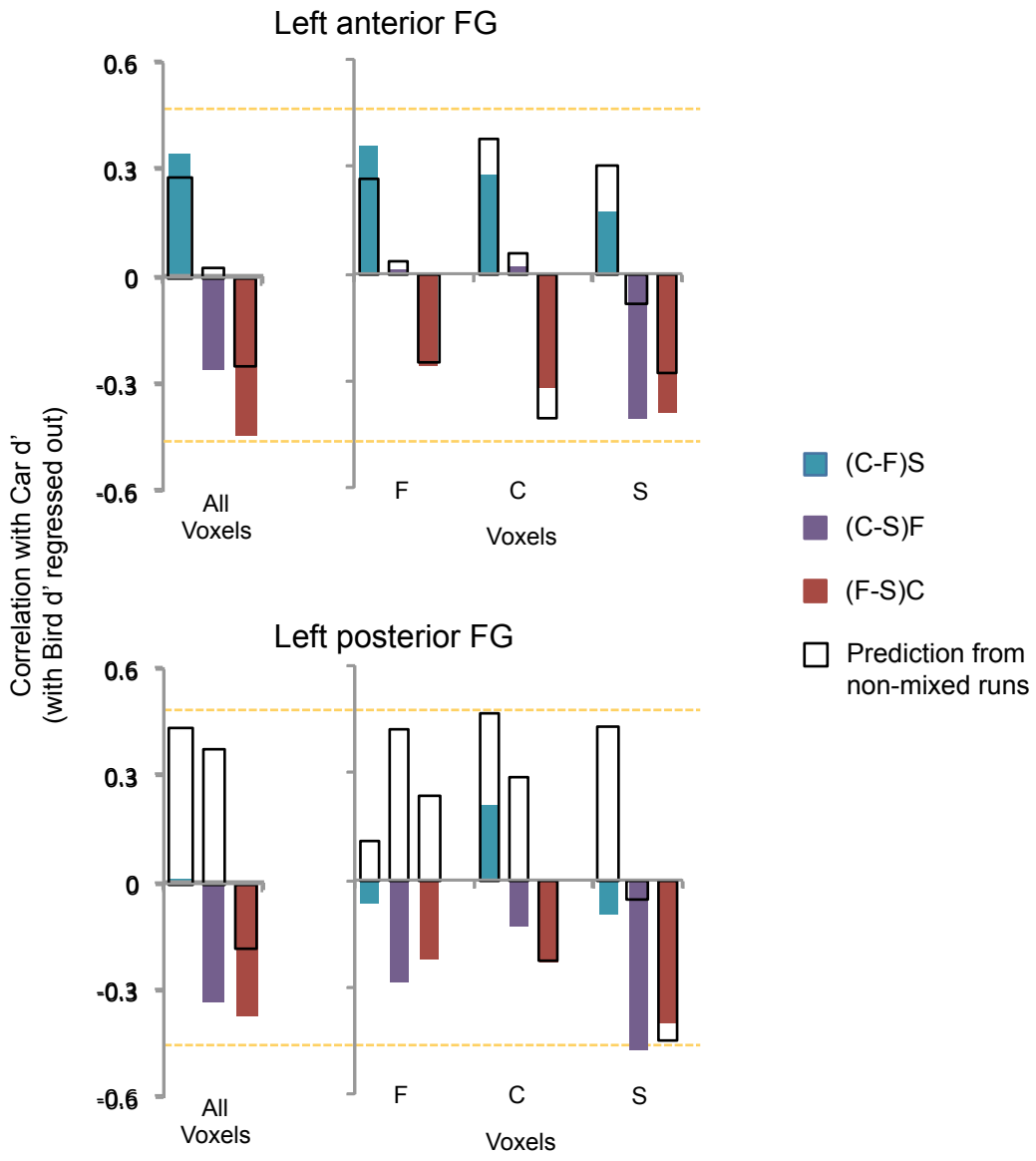

Figure 50. Partial correlations between the neural response during RSVP sequences and behavioral expertise for cars with bird performance regressed out, for the left aFG (N=20) and the left pFG (N=19). The leftmost bar graphs show correlations with the neural response from all activated voxels, while bar graphs on the right depict correlations with activation in HR-sorted voxels. Hollow black bars indicate the corresponding correlations observed in the non-mixed HR-FCS runs. The horizontal yellow dotted line represents the critical Pearson's r at which the neural response is significantly correlated with behavioral expertise for the mixed conditions. We used a 2-tail partial correlation with N-3 degrees of freedom: left aFG (r_{crit}=0.456), left pFG (r_{crit}=0.486). Recall, this critical value does not mark significance for the non-mixed runs, in which a 1-tail test was applied. Zero-order and partial correlations given in APPENDIX E.

Comparing non-mixed and mixed conditions relative to expertise

As in the right FG regions, we can also explore expertise effects in the left aFG and pFG ROIs.

We considered responses during HR-RSVP blocks as a function of individual differences in

behavioral car expertise, with behavioral performance for birds regressed out. Although car expertise was not significantly associated with response magnitudes from mixed-category RSVP comparisons in the left FG regions (Figure 50), trends suggest an interesting dissociation relative to the non-mixed FCS data. While in the left aFG the trend for an expertise effect for C – F only increases when the objects are shown in the context of sofas, in the left pFG, placing cars and faces in the context of sofas entirely abolished any trend of a correlation with expertise (Figure 51).

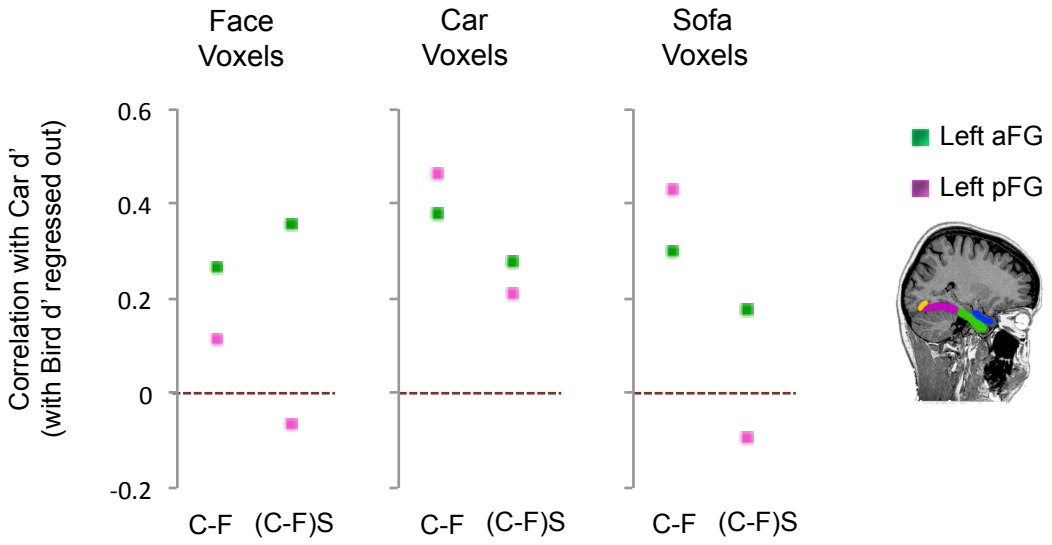

Figure 51. Contrasting the effects of expertise for non-mixed- and mixed-category runs in the left anterior and posterior FG regions. Points represent partial correlations with Car *d'* when we regress out the influence of Bird *d'*. Car expertise for non-mixed data is represented by the cars versus faces PSC (C-F) and, for a comparable contrast, mixed-category expertise is represented by the neural response for cars versus faces all in the context of sofas (C–F)S. Horizontal dotted lines depict 0 correlation with car expertise.

Left OFA and Right OFA

In general, we find greater face preference in the lOFA than the rOFA for mean amplitude responses without considering expertise. When taking into account individual differences in car performance, the rOFA reveals trends in the expected directions (i.e., car expertise predicts increases in the neural response for (C–F)S, while the lOFA does not show evidence of expertise effects.

Mixed-category RSVP data without considering expertise

Next we investigated context effects in mixed-category RSVP data within the right and left OFA, without considering individual differences in car performance. Although the right OFA condition means suggested a similar pattern, only the left OFA showed preference towards the RSVP conditions in which a face was present (Figure 52; APPENDIX E). When averaging over all activated OFA voxels, the left OFA shows only a marginal face preference for (C–F)S (t=-1.903, p=0.081), which is also only marginally significant we look at the HR face voxels (t=-1.920, p=0.079). In the face voxels, (F–S)C suggests a significantly enhanced response for face-present blocks relative to blocks of alternating sofas and cars (t=2.139, p=0.054). As observed in bilateral FG regions, bilateral OFA mean PSC responses do no differentiate faces shown in the context of cars versus faces (all (C–S)F*s n.s.*).

Comparing non-mixed and mixed conditions relative to expertise

We do not find expertise effects during mixed-category HR-RSVP runs in bilateral OFA (Figure 53; APPENDIX E). In neither the right OFA nor the left OFA do individual differences in car expertise predict the neural response evoked during mixed-category presentations. Figure 53 represents the effects of behavioral car expertise for mixed conditions ((C–F)S, (C–S)F and (C–S)F) and non-mixed conditions (C–F, C–S and F–S) in overlapping bar graphs.

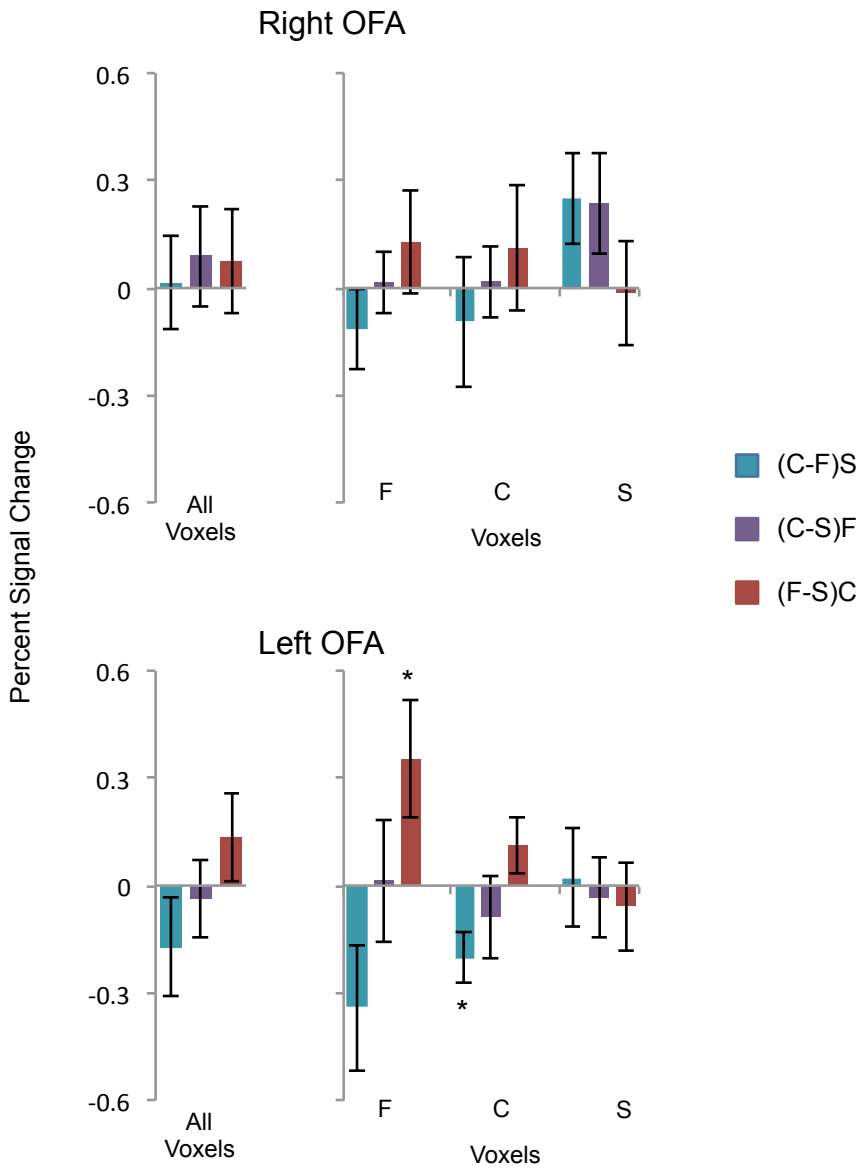

Figure 52. Percent signal change mean response amplitudes during the HR-RSVP runs for the right OFA (N=16) and the left OFA (N=13). The leftmost bar graphs show the averages over all activated voxels. Bar graphs to the right plot the mean response amplitudes in voxels sorted based on their maximum response during HR-FCS runs. Error bars represent the sem. Asterisks denote means significantly different from zero. Inferential statistics given in APPENDIX E.

Making this comparison highlights an interesting dissociation between right and left occipital regions. On one hand, the right OFA demonstrates a similar pattern of response for the mixed as for the non-mixed conditions, though the magnitude of expertise effects is weakened (but primarily remain in the same direction). For example, considering the expertise effect for cars relative to faces in the HR voxels maximally selective to faces, the positive trend observed with non-

mixed data (r=0.383, *n.s.*) becomes weaker when cars and faces both shown in the context of sofas (r=0.255, *n.s.*), but remains in the same direction.

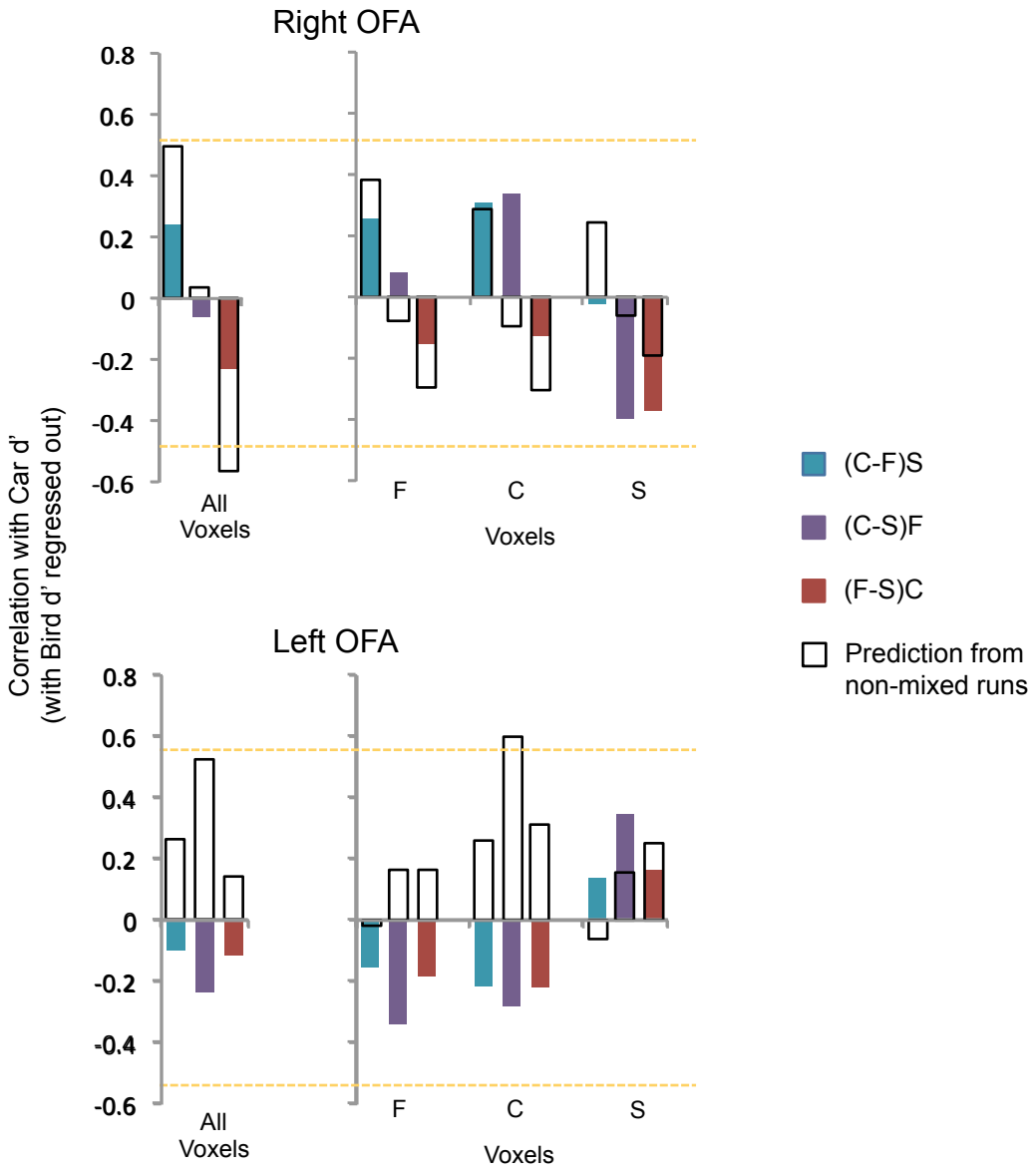

Figure 53. Partial correlations between the neural response during RSVP sequences and behavioral expertise for cars with bird performance regressed out, for the right OFA (N=16) and the left OFA (N=13). The leftmost bar graphs show correlations with the neural response from all activated voxels, while bar graphs on the right depict correlations with activation in HR-sorted voxels. Hollow black bars indicate the corresponding correlations observed in the non-mixed HR-FCS runs. The horizontal yellow dotted line represents the critical Pearson's r at which the neural response is significantly correlated with behavioral expertise for the mixed conditions; 2-tail partial correlation with N-3 degrees of freedom: left aFG (r_{crit}=0.514), left pFG (r_{crit}=0.576). Recall, this critical value does not mark significance for the non-mixed runs, in which a 1-tail test was applied.

On the other hand, the left OFA shows a very different pattern of response for mixed and non-mixed runs. Whereas non-mixed FCS data revealed an increase in the PSC for cars versus sofas, which was especially pronounced in the lOFA car voxels (r=0.604, p=0.017), mixed RSVP data actually suggested the opposite trend in car voxels for cars versus sofas when both categories were presented in the context of alternating faces (C–S)F: r=-0.284, *n.s.*). Together, these data suggest that the right OFA expertise effects may be more stable relative to the context of image presentation, whereas the left OFA response relative to expertise is more susceptible to interference from context. The left posterior FG region demonstrated similar susceptibility, whereas the left anterior FG showed relatively robust effects of expertise regardless of context. Thus as we move from posterior to anterior regions, the influences of context become weaker (it is the case when comparing aFG to pFG in the right hemisphere, and aFG to pFG and OFA in the left hemisphere).

Bilateral PHG regions

The left PHG region, in particular, showed a preference towards RSVP conditions that included the presentation of sofa images. When expertise was considered, neither the right nor the left PHG showed evidence for an effect of car expertise on patterns of neural response. This will be contrasted to the expertise effects observed in these areas during non-competitive image presentations.

Mixed-category RSVP data without considering expertise

Finally, we considered context effects in object-selective regions of the parahippocampal gyri. First, when averaging HR-RSVP responses over all activated voxels of right or left PHG regions, no significant relations appeared. Next, we examined the HR pattern of response in sorted voxels. Non-mixed HR-FCS data showed reliable responses in bilateral PHG regions that were restricted to the sofas: d_a analyses revealed reliable sofa selectivity (mean $d_a > 0$) in sofa voxels, but not the

equivalent for faces or cars (e.g., Figures 43, 44). Thus, we will test for similar sofa selectivity from the mixed-category results of PHG voxels in both hemispheres.

In contrast to results obtained in face-selective ROIs, the right PHG showed a PSC preference during sofa-present conditions for (C–S)F in face voxels (t=-2.096, p=0.046) and marginally so for (F–S)C in car voxels (t=-1.813, p=0.082) (Figure 54; APPENDIX E). Moreover, the left PHG showed a preference for sofas as revealed by a significant effect for (F–S)C in sofa voxels (t=-2.494, p=0.020), which was the only comparison that reached significance for this left ROI.

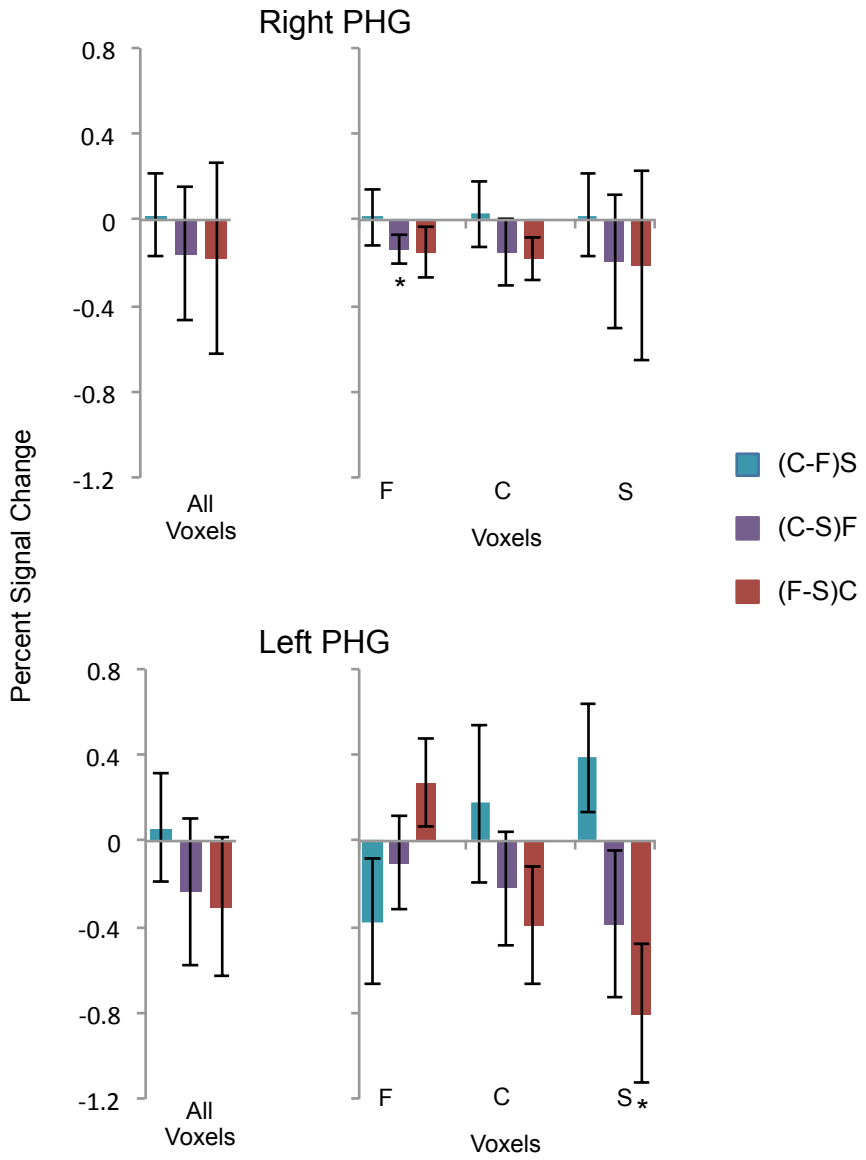

Figure 54. Percent signal change mean response amplitudes during the HR-RSVP runs for the right PHG (N=26) and the left PHG (N=24). The leftmost bar graphs show the averages over all activated voxels. Bar graphs to the right plot the mean response amplitudes in voxels sorted based on their maximum response during HR-FCS runs. Error bars represent the sem. Asterisks denote means significantly different from zero. Inferential statistics given in APPENDIX E.

Neither the right nor left PHG region showed an effect of context for sofas: there was no difference in the magnitude of PSC response for when sofas were presented in the context of cars versus faces ((C–F)S; APPENDIX E).

Comparing non-mixed and mixed conditions relative to expertise

We do not find evidence for expertise effects during mixed-category runs in bilateral PHG regions (Figure 55; APPENDIX E). Figure 55 highlights critical differences in expertise effects – or lack thereof – for bilateral PHG regions during non-mixed and mixed category presentations. For non-mixed FCS runs, the right PHG revealed significant effects of car expertise for cars versus sofas in face voxels (r=0.371, p=0.033) and car versus faces in sofa voxels (r=0.367, p=0.035) and marginally in car voxels (r=0.320, p=0.059). Most interestingly, when cars were shown in the context of faces or sofas, the effects of car expertise disappeared in the right PHG.

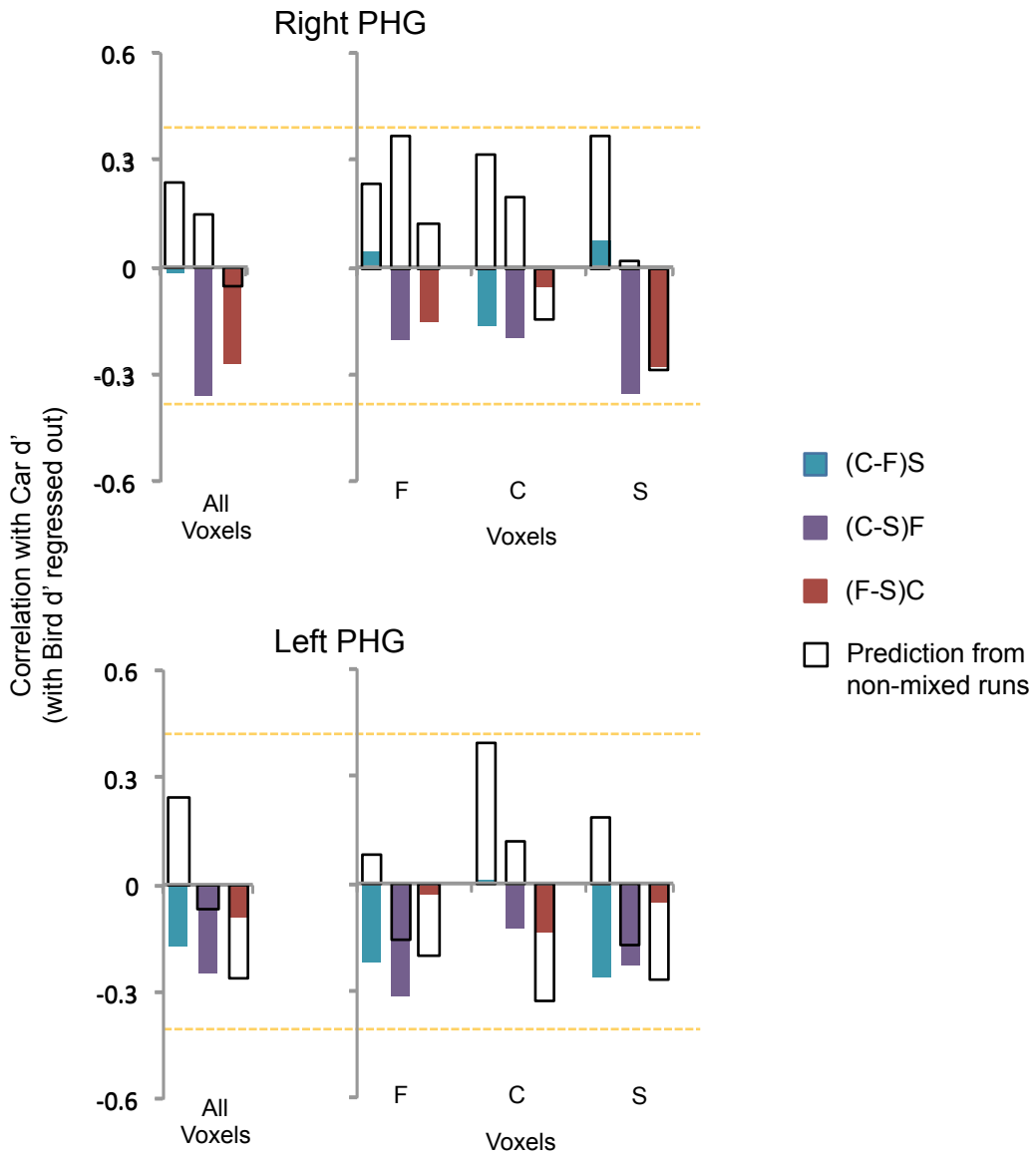

Figure 55. Partial correlations between the neural response during RSVP sequences and behavioral expertise for cars with bird performance regressed out, for the right PHG (N=26) and the left PHG (N=24). The leftmost bar graphs show correlations with the neural response from all activated voxels, while bar graphs on the right depict correlations with activation in HR-sorted voxels. Hollow black bars indicate the corresponding correlations observed in the non-mixed HR-FCS runs. The horizontal yellow dotted line represents the critical Pearson's r at which the neural response is significantly correlated with behavioral expertise for the mixed conditions. We used a 2-tail partial correlation with N-3 degrees of freedom: left aFG (r_{crit}=0.396), left pFG (r_{crit}=0.413). Recall, this critical value does not mark significance for the non-mixed runs, in which a 1-tail test was applied.

The left PHG area as well, which revealed a more limited spatial extent of expertise effects during non-mixed category runs (cars versus faces in car voxels, r=0.388, p=0.033), showed no evidence for an influence of car expertise when cars were presented in the context of either faces or sofas. These data from object-selective cortices reflect a general pattern observed in the face-

selective regions: car expertise effects observed when cars are presented in isolation disappear when cars are presented with other categories of objects. The single exception to this trend was the right anterior FG.

Discussion of E2 results

Replication of E1

In E2 we used HR-fMRI to investigate the fine-grain patterns of neural response in six face-selective ROIs and 2 object-selective ROIs. Once ROIs were defined, HR-FCS runs were used to sort the voxels into bins based on maximal response to faces, cars, or sofas. We tested reliability and replicability of category-specific responses in the HR-FCS data, with and without considering the influence of individual differences in car expertise. In general, results from these analyses on the right aFG and pFG supported E1 rFFA data. Critically, when we consider category means in HR-sorted voxels, we see no evidence for car selectivity, and it is only through consideration of car expertise that a complete picture of neural response in these regions becomes clear. The magnitude of response and neural selectivity for cars increases in relation to car expertise. Expertise effects are found even in the most face-selective voxels of the FG, and they are predicted by variance unique to performance with cars relative to another category (birds). We also replicated effects of expertise in areas outside the face-selective right-lateralized FG regions.

Individual differences in face expertise

All participants completed the Cambridge Face Memory Test (CFMT), and accuracy on this test was used as an index for individual face recognition skill (Duchaine & Nakayama, 2006). In a recent study, Furl et al. (2010) found increased neural selectivity for Faces vs. Cars in bilateral FG regions for individuals with better face identification. They further demonstrated that better performance in facial identity processing tasks was positively associated with the size of the right

FFA. Using the CFMT as an index of face identification ability, we tested whether face selectivity and/or the size of the face-selective fusiform regions would increase as a function of face identification. Contrary to Furl et al. (2010), we found no evidence for increased face selectivity with better face matching accuracy on the CFMT in either face-selective fusiform region. We did, however, observe an overall increase in the size of the right pFG as a function of CFMT accuracy, but not for the right aFG or either left FG ROI.

There are several reasons why our results diverge from those of Furl et al. (2010). First, Furl et al. assessed face identification ability not with a single test, as done here, but rather using CFMT in the context of a factor analysis. They administered 11 behavioral tests and the CFMT loaded strongly on a face processing factor, together with 4 other tests. Relative to the CFMT used alone, that method allowed for a more reliable and more valid measure of individual differences in face processing, ensuring that the emergent variability is orthogonal to the variability linked to other factors. It is possible that our putative identity-related measure was confounded by variability attributed to more general visual processes. Nonetheless, in Furl et al. the CFMT had a very high loading (.86) with the factor that predicted FFA activity, which led us to expect a correlation with that measure, given that car expertise, here and before, successfully predicted FFA activity with a single test.

In addition, the sample size studied in Furl et al. (2010) included 35 participants, 17 of which were Developmental Prosopagnosics with self-reported face recognition difficulties in everyday life and test-validated performance on behavioral measures of face processing. Across all 35 participants, performance of the CFMT ranged from~25% correct to ~75% correct. Our study, on the other hand, considered 26 individuals with normal face processing: CFMT performance ranged from 57% correct to 96% correct. The reduced range and potential ceiling effect in the current population may have restricted our correlations. Furthermore, our sample may also differ from Furl et al.'s because half our participants were car experts, which was associated with reduced face activity. Given these constraints, it is difficult to draw conclusion based on our null result.

Neural effects of competition

In addition to replication, HR-FCS runs served another critical purpose: they were used to localize maximally face-, car-, and sofa-selective voxels in which to test effects of competition. We first explored mean PSC amplitudes in sorted voxels. In SR face-selective ROIs, we found a general trend towards greater response for face-present RSVP conditions relative to conditions that did not show faces. Moreover, this effect was present regardless of the alternating non-face category, suggesting that the face response evoked by face images in face-selective regions is not contingent upon the context in which the face image is presented. An opposite pattern was observed in object-selective ROIs, in which sofa-present conditions elicited the greatest neural response, regardless of whether sofas were shown in the context of faces or cars. These data alone do not suggest effects of on-line neural competition induced by simultaneous processing of very rapidly alternating images from unique categories.

However, by considering individual differences in car expertise, we unveiled critical effects of expertise on the influence of context during mixed-category RSVP presentations. Specifically, by comparing car expertise effects for non-mixed FCS data with those observed for mixed RSVP data, we find an influence of context. While non-mixed data showed evidence for expertise effects in many different brain regions, the right anterior FG was the only area to show similar expertise effects during mixed category runs. This idea is explored in more depth in the following section.

Distributed versus focal effects of expertise

As we've seen, by taking into account individual variability in car expertise, E2 results highlight important differences in the patterns of neural response evoked by single-category presentations relative to mixed-category displays throughout the ventral temporal cortex. The task-intensive mixed sequences demanded the monitoring of many different objects shown at a rate of 6 images/s and alternating amongst two categories. The non-mixed runs, on the other hand, only

required a binary decision (present/absent) for images shown at a rate of 1 image/s from a single category. Our data suggest that when we tax the perceptual system, the right aFG alone shows significant effects of expertise. We observed distributed effects of expertise in the brain for single-category blocks (in both E1 and E2), but only a focal effect restricted to the aFG during mixed-category blocks and, more specifically, to the *car voxels* of the aFG. This suggests that under stressful conditions, expertise becomes more specific to the right aFG.

Table 33 shows single-category expertise effects with Car PSC – Face PSC and mixed-category expertise effects with the neural response for cars versus faces in the context of sofas, for HR sorted voxels for all ROIs. Table values represent the Pearson's partial correlation coefficient with behavioral car *d*' with bird *d*' regressed out. Bold values show significant correlations. In many voxel types of most ROIs (except the right OFA and right PHG), behavioral expertise was positively associated with the single-category Car–Face neural response. In contrast, when these objects were shown in the context of sofas, the relative Car–Face difference is no longer significantly related to car expertise in any ROIs save the right anterior FG region. These data suggest something unique may be operating in this anterior area.

Table 33. Car expertise effects (partial correlations with Car *d*' after regressing out the influence of Bird *d*') for the PSC response for cars versus faces during non-mixed category runs, and for cars versus faces in the context of sofas during mixed category runs. Partial correlations for all eight ROIs are given for the average ROIs response, as well as the response in face, car and sofa sorted voxels. Significant correlations are shown in bold.

	Non-mixed: C-F				**Mixed: (C-F)S**			
	All	Face	Car	Sofa	All	Face	Car	Sofa
Right aFG	0.334	0.355	**0.425**	**0.454**	0.398	0.171	**0.536**	0.249
Right pFG	**0.379**	**0.371**	**0.452**	**0.524**	0.009	-0.06	-0.127	0.263
Left aFG	**0.496**	0.383	0.288	0.243	0.24	0.255	0.307	-0.022
Left pFG	0.237	0.235	0.32	**0.367**	-0.014	0.043	-0.166	0.072
Right OFA	0.279	0.267	0.38	0.3	0.339	0.358	0.278	0.174
Left OFA	**0.435**	0.112	**0.464**	**0.427**	0.006	-0.066	0.211	-0.095
Right PHG	0.258	-0.014	0.259	-0.06	-0.096	-0.155	-0.218	0.134
Left PHG	0.239	0.082	**0.388**	0.182	-0.169	-0.219	0.011	-0.26

Interestingly, earlier work has investigated the influence of distractors or visual 'clutter' on category-specific responses in the FFA and demonstrated a robust face response regardless of distractors (Reddy & Kanwisher, 2007). On the other hand, the FFA response to non-face objects was severely degraded when these objects were presented simultaneously with others. If the response to faces is robust to conditions of interference or competition within face-selective regions because of their 'expert' status, then we may expect non-face objects of expertise to show similar resilience in taxed conditions, and we would expect greatest resilience where selectivity is greatest. Our mixed-category RSVP data show expertise effects with the neural signal for cars in the context of sofas (relative to faces with sofas) that were restricted to the right aFG, suggesting that here lies the hub of the truest expert-object processing. Moreover, our HR analysis showed that effects of car expertise were only preserved in the right aFG voxels maximally selective to *cars*.

We may speculate that under perceptually stressful or attention-demanding conditions, not only do face and car responses (in car experts) outside of FFA subside, but within the FFA, the face and car signals become more separated. As a caveat, we would have expected similar expertise effects for cars versus sofas in the context of faces, but these results were less clear due to some regions responding to sofa as they did cars. These issues will have to be revisited in future studies. It is striking, however, that while we expected selectivity for cars in car experts to suffer under conditions of competition with faces mainly in the FFA, we obtained a drastically different picture, whereby under more taxing conditions, the response everywhere *but* the right aFG (and to some extent the same qualitative pattern is found in left aFG and right OFA) suffers. It is worth contemplating that the expertise-specific behavioral competition (McGugin et al., 2010; McKeeff et al., 2010; Wong et al., 2010), just like the more general contextual effects we uncovered here, could be associated with relatively small and distributed changes in activity outside of the classic face-selective areas.

CHAPTER IV

CONCLUDING REMARKS

In this dissertation I have explored effects of perceptual expertise on the fine-grain neural organization and patterns of response for functionally defined regions of the ventral temporal brain. To date, there are only a couple studies of the FFA at high resolution, and CHAPTER II presented the first study (E1) using high resolution to investigate the spatial distribution of expertise effects within the FFA. CHAPTER III presented the first fMRI study (E2) to examine effects of neural competition between objects of expertise.

Challenging claims of domain-specificity

The goal of E1 was to explore HR effects of perceptual expertise within the SR-defined right FFA. Earlier studies using SR-fMRI have shown that expertise effects can be obtained in or around the FFA, but how these effects would be spatially organized at high resolution was unclear. Would the expertise effect only come from non-face selective voxels interspersed among face-selective voxels? Would expertise effects be a general effect obtained throughout the FFA? Would the expertise effects be limited to the SR-fMRI region or reflect a general effect in the visual system? E1 specifically investigated patterns of FFA response to cars, planes, animals and faces as a function of individual differences in expertise with cars and planes.

Our results challenge three critical assertions made in support of the domain-specificity of FFA responses. First, there have been claims that the only category-selective neurons in FFA are selective for faces (Baker et al., 2007, Tsao et al., 2006). Second, there have been claims that expertise effects do not encroach on the truly face-selective core of

the FFA, or in other words that SR-expertise effects only overlap with face-selectivity because of spatial blurring (McKone, Kanwisher & Duchaine, 2007). Third, there have been claims that if an expertise effect is obtained in the FFA, it may only been because of overall increases in activity due to attention to objects of expertise (McKone et al., 2007; Harel et al., 2010).

To address these claims, we localized the FFA at standard resolution and within this region, sorted high-resolution voxels according to selectivity for various categories. Our analyses are compatible with those used in Grill-Spector et al (2006) and Baker et al. (2007) and, indeed, our results – when expertise is *not* taken into account – supported these earlier reports: we found reliable face-selectivity and no reliable response for non-face objects. However, for the first time we demonstrate that this is no longer true when expertise is considered, since within the classical FFA there are face-, car- and plane-selective voxels in a participant who has expertise for all three categories. This finding discounts the first claim implicating exclusivity of face-selective responses in the FFA.

Another claim for domain specificity of FFA response suggests that expertise effects are only found in FFA because of spatial blurring between truly face-selective neurons and non-face selective regions (Kanwishwer, 2000). This argument is supported by studies conducted with the highest available resolution – single-cell recording. Tsao et al. (2006) targeted a "middle face patch" thought to correspond to human FFA in two monkeys using fMRI, then used single-unit recording and found that 97% of visually responsive cells in this area were highly face-selective. Here we cannot achieve single-cell responses and, indeed, it must be acknowledged that even our high-resolution fMRI voxel contains millions of neurons. While this makes it difficult to claim that a given area responding in two conditions does not hide two intermingled but distinct populations, claims for domain specificity are nonetheless proclaimed at this spatial scale (Grill-Spector et al., 2006; Baker et al., 2007).

Consider that in the Tsao et al. study, the monkey patch found to consist almost exclusively of "face cells" was 16 mm^2 in size, which is smaller than the putative homologue human FFA, and much larger than our 1.56 mm^2 voxels (1.25 x 1.25). Therefore, once we find highly face selective voxels at this scale, we can only postulate that using the exact methods used by Tsao and colleagues (ignoring expertise), we would detect primarily face selectivity. Therefore, we can be confident that at this scale, we address expertise effects at the scale at which claims of selectivity have been made for faces.

Our results address the concern of spatial blurring well within the scale at which face-selectivity has been found in these studies. We localized the peak of face selectivity in the right fusiform gyrus and placed concentric ROIs on this peak. We then demonstrated that the expertise effects are observed within the most face-selective voxels inside the 25 mm^2 peak of face-selectivity. This suggests that if there are pockets of uniquely face-selective neurons in FFA, they are smaller than the size of one of our voxels and are intermingled with populations of cells selective for other objects of expertise.

Finally, by measuring expertise effects as a function of the distance to the peak of face selectivity in the FG, we can ask whether increased attention for objects of expertise is a sufficient explanation for our results. Our results demonstrated that the expertise effect in the fusiform gyrus is centered on the peak of face selectivity and restricted to a 200 mm^2 region. While expertise-related attention could explain the magnitude of the FFA response to cars or planes, it cannot explain why attention would specifically increase signals in the center of the FFA.

Moreover, in a recent study, Harel et al. (2010) reported that expertise effects disappear when car experts are not instructed to pay attention to cars. Although we did not directly address this question, we show in E2 that even when effects of expertise are reduced in most participants as a result of a taxing task, they remain in the FFA.

In sum, our novel findings of car and plane expertise at high-resolution directly refute claims that have been made about the strict face-selectivity of the FFA.

Expertise effects in HR sorted voxels

Given that we have found expertise effects up to a 200 mm^2 size ROI centered on the peak of face selectivity, but not beyond (within the FG), the investigation in E1 could have yielded several different results. First, we could have found a car expertise effect only in HR-"car" voxels. This would have shown that within the FFA – at high resolution – face and car selectivity can be separated. Alternatively, the current results could have revealed a car expertise effect only in HR-"face" voxels. This would have shown first, that the "real" FFA may simply be smaller than what we see at SR-fMRI and, second, that at the present resolution we cannot separate face and car selectivity.

In contrast, we actually observed a car expertise effect that was present in most types of HR sorted voxels within the FFA, within an area limited to 200 mm^2. Specifically, the results in E1 show that within this 200 mm^2 region, there are face selective neurons in all participants, car selective neurons as a function of car expertise and plane-selective neurons as a function of plane expertise. This suggests that face neurons are intermingled within an area where neurons are being recruited for any category of expertise (assuming that expertise requires individuation that can be achieved holistically – Wong et al., 2009). This account suggests that the only difference for the representation of faces may be that there are, on average, more face neurons.

Do the populations of cells representing face and non-face categories actually overlap in the FFA? Several single-cell recording studies have shown a scattered clustering of face-selective cells in the temporal lobe of monkey (Desimone et al., 1984; Perrett et al.,

1982; 1985), implicating a distributed underlying architecture of face-preferring cells. Our data similarly suggest the existence of HR category-selective clusters in SR-defined face-selective regions. However, the question remains whether the same clusters of cells represent faces and non-face objects.

If face and non-face object representations overlap, then susceptibility to competition during stressed conditions increases. Reddy and Kanwisher (2007) argue that our ability to simultaneously perceive a face and a place without the two representations interfering occurs because faces and places are represented by neural codes that do not overlap. In that vein, Kanwisher (2000) suggested that inferotemporal neurons should be tuned to two very different stimulus types. However, there are counter-examples. For instance, when Sigala and Logothetis (2002) recorded single-cell activity from the anterior inferior temporal lobe in monkeys trained to categorize line drawings of faces and fish, they found that some neurons were tuned to diagnostic dimensions for trained categories, for both faces *and* fish. This would suggest that training to individuate cars could recruit some cells also involved in face processing.

Limitations to tests of neural competition

E1 revealed that when face and non-face objects are presented in isolation, objects of expertise recruit voxels that are spatially intermixed with maximally face-preferring voxels. E2 extended upon these findings to make predictions for neural competition during concurrent processing of expert objects that simultaneously call upon the mechanisms of holistic processing. Boutet and Chaudhuri (2001) suggest that only one holistic representation can be encoded at a time. Using a sequential matching paradigm with images composed of two superimposed faces (at 45 degree angles), they showed that participants

were only able to recognize one face when the two superimposed faces were upright (but not inverted) and presented for 1 s. These results suggest a perceptual bottleneck of holistic processing.

In E2 RSVP runs, images were presented at a rate of 6 images per second while participants sometimes had to search for both a face and another object of expertise, suggesting competition for holistic processing would abound. Specifically, for car experts processing faces and cars holistically, we expected the greatest competition during sequences of alternating face and car images. However, when considering results from E2, it is important to consider that unfortunately, the strong response for sofa images in car experts made it difficult to assess on-line neural competition in the RSVP sequences. Theoretically, the competition hypothesis would have predicted that the cars–sofas comparison would have been relatively less dependent on expertise when images were shown in the context of faces, (C–S)F, versus when they were presented alone. On the one hand, car expertise may have predicted the neural response for cars versus sofas in non-mixed runs (i.e., as a positive correlation between the two variables). On the other hand, car expertise would not have predicted on the neural response for cars versus sofas when shown in mixed-category runs in the context of faces. This is because faces may selectively interfere with the perception of cars in car experts (Gauthier et al., 2003; McGugin et al., 2010; McKeeff et al., 2010; Rossion et al. 2004; 2007).

However, behavioral experiments have shown that in addition to perceptual competition based on similar processing (Gauthier et al. 2003; McGugin et al., 2010; McKeeff et al., 2010), there can also be competition in working memory for visually similar objects (Cheung & Gauthier, 2010). For example, holistic processing for baby faces was more reduced by a working memory load of baby than adult faces (Cheung & Gauthier, 2010). Rapidly alternating cars and sofas may have looked particularly similar to

participants, as they were trying to hold a car and a sofa target in working memory. Critically, however, not all areas showed the same relationship between expertise with cars versus sofas. Most profoundly, the left OFA actually showed a significant decline in the representation of maximally sofa-preferring voxels as a function of car expertise. This will need to be investigated further, but it may be related to either the spatial scale of representations in different areas or to the temporal resolution of processing at different points in the visual system (McKeeff, Remus & Tong, 2007).

To better address competition in a future experiment we might employ an object category control that is visually very dissimilar from cars. By eliminating or reducing low-level visual confounds, we may be better able to isolate the source of the competition observed in behavioral studies.

Given this confound between car and sofa responses, it is perhaps not surprising that our strongest effects of expertise in E2 were obtained when comparing the neural response for cars versus faces both in the context of sofas. This contrast yielded the strongest effect perhaps in part due to the low-level visual differences between cars and faces (relative to cars and sofas), but also as a result of the tradeoffs between car and face responses.

Expertise effects under conditions of divided attention

An interesting dissociation was obtained when we compared the extent of expertise effects obtained when objects were presented in non-mixed runs versus when they were presented in very rapid sequences of alternating categories. This later condition required simultaneous processing of mixed-category presentations. In particular, we considered the neural response for cars versus faces outside of and within the context of sofas. Whereas

this comparison does not address the on-line neural competition upon which our hypotheses were formulated, it allows us to examine the stability of expertise effects under conditions of divided attention. We found that the distributed effects of HR expertise obtained during non-mixed presentations become far more focal under mixed-category presentations of divided attention, whereby participants are forced to simultaneously process objects from different domains. Specifically, when car images are shown in non-competitive conditions (E1 and first part of E2, as well as prior studies), we observe a distributed pattern of expertise effects in several areas of the ventral temporal cortex. In contrast, when car images are shown in conditions of divided attention, expertise effects are far less distributed and focally preserved only in the anterior FG region.

Indeed, Harel et al. (2010) observed no "conspicuous" differences in patterns of activity between car experts and car novices when attention was divided (i.e., participants were instructed to *only* attend to the planes and to ignore the intermixed car images). These results suggest that effects of car expertise, just like category-specific effects for faces and houses (Reddy & Kanwisher, 2007), are less distributed under taxing perceptual conditions and, as we show in E2, are only preserved in the anterior FFA region. Similarly, using a simultaneous presentation task where only one category is attended and attention is divided, Reddy and Kanwisher (2007) suggest that information about faces and houses – domains that selectively activate certain cortical regions – is robust to cases of divided attention, while classification performance for other non-preferred categories is drastically impaired by mixed-category presentations of divided attention.

Although the current experimental design departs from Reddy and Kanwisher (2007) in significant ways (for example, they use *simultaneous* image presentations and specific instructions to only attend to *one* category), their results highlight a critical aspect of our current data. Specifically, in light of Reddy and Kanwisher (2007), our findings

suggest that the stability of category-specific responses is not domain-specific for so-called "special" classes, but rather is a characteristic of objects of expertise.

What are the implications of a limited distribution of activity during conditions of competition or stress? Are the distributed patterns of response observed under non-taxing conditions important for the perceptual judgment, or are they merely epiphenomenal (Williams et al., 2007)? Our evidence suggests reliable responses for faces and non-face objects outside of the FFA. When perceptual constraints are applied through mixed-category presentations, however, this reliability drastically shrinks. Thus, it is possible that our findings suggest that under divided attention or difficult conditions, judgments are based on polling fewer neurons. Note, assessing cases of divided of attention relative to perceptual expertise is inherently confounded by the combination of top-down attentional requirements with bottom-up differences in attention between experts and novices.

Our findings, along with those from Harel et al. (2010), suggest that much more research needs to be done to investigate the interactions between top-down and bottom-up attention. These mechanisms are typically studied separately, but in cases such as expertise, it will be critical to investigate how they interact. In a recent fMRI study, McMains and Kastner (2011) sought to isolate bottom-up and top-down processes, showing that these processes interact dynamically during competitive situations when stimuli are presented simultaneously. These findings are consistent with physiological reports suggesting dynamic interactions between top-down and bottom-up processes in monkey V4 (Reynolds & Desimone, 2003; Ogawa & Komatsu, 2006). Future work should investigate how top-down and bottom-up processes interact in the case of perceptual expertise.

We have shown that car expertise effects become less distributed when car experts view cars in competitive mixed-category presentations. These data suggest that the behavioral limitations associated with concurrent processing of multiple objects that

demand overlapping processing resources may be related to the decreased distribution of cortical activation. Holistic processing, in particular, may become spatially restricted under perceptually demanding circumstances.

In addition, an intriguing possibility is that under stress, not only do expertise effects become more specific to the right aFG, but face and car populations may actually become more distinct within this region. This is suggested by the finding that mixed-category car expertise effects were only observed in the right aFG voxels maximally selective to cars, and not in the most face-selective voxels. In contrast, in non-stressful blocked conditions, expertise effects were observed in voxels maximally selective to other categories as well.

A future experiment should further investigate this finding. For example, we could compared HR patterns of activity in sorted voxels for conditions where categories A and B are seen in the context of objects that more closely resemble category A (A') or category B (B'). Thus, we would compare the neural response and relationship to expertise for A or B in contrasts for (A–B)A' and (A–B)B'. This would allow us to address how expertise effects in different areas depend on the similarity of the context. For an area that represents many different categories – especially in an individual with non-face expertise – the aFG may resolve competition among visually similar items by recruiting only those voxels maximally selective for the current job (e.g., car voxels for processing cars).

Future directions

Simultaneous versus sequential visual presentations

Future work investigating effects of neural competition should consider competition during simultaneous image displays. In the present experiment, stimuli were presented sequentially in rapidly alternating streams. Although the rate of image presentation was fast enough to demand overlapping processing of sequentially shown images, a simultaneous display may be more sensitive to competitive effects. Indeed, it has been suggested that perceptual competition related to holistic processing in occipito-temporal areas may be greatest when the competing stimulus is still generating neural activity at the time in which the target face is presented (Rossion et al., 2007). Rossion et al. (2007) showed that the decrease of the face-selective N170 response when car experts viewed faces in the context of cars was no longer significant when a 200 ms gap intervened between the face and car stimuli. This work suggests that visual perceptual competition between faces and objects of expertise occurs during a limited time window in occipito-temporal areas. Indeed, a recent study suggests that the source of this competition does not have its locus in later stages of working memory, since the encoding of objects of expertise did not interfere with holistic processing of faces (Cheung & Gauthier, 2010).

During simultaneous image presentations, we could more carefully control what people see. When images are shown at a rate of 6 images per second, it is difficult to know whether changes in neural activation reflect competition from different images within a category, across categories, or both. For example, when faces are shown in the context of cars at this rate, it is hard to decipher whether alternating faces compete with previously seen faces (Boutet, Gentes- Hawn, & Chaudhuri, 2002; Palermo & Rhodes, 2002), or whether alternating *cars* compete with the faces (McKeeff et al., 2010). In simultaneous display conditions, we can contrast competition for holistic processing of two faces versus a face with a non-face object of expertise.

Levels of perceptual expertise

Our findings demonstrate that even at high-resolution, it is critical to take into account levels of perceptual expertise when probing for selectivity for objects. Perceptual expertise as measured here likely occurs in most people as they learn to individuate objects related to professional activities or hobbies. Thus, most people's FFA probably contains several populations of neurons selective for objects of expertise. It is an open question, however, whether there is a limit to the number of object categories with which an individual can be an expert. This dissertation presents evidence of competition for spatial representation of expert categories in face-selective regions, suggesting that there may be a limit in the extent to which the FFA can represent these expert categories. We tested individuals with a maximum of three categories of expertise (faces, cars, and planes; although individuals are likely expert with other untested domains as well). Plane expertise likely represented the least extensive skill in our participants, and effects of plane expertise were observed in the outermost ROI-ring encompassing the FFA. This suggests that as new expert skills develop, they may initially recruit peripheral regions of face-selective cortex. Effects for planes in our participants may reflect neural changes following relatively limited experience (Wong et al., 2009), or visual abilities without the considerable semantic associations that may arise in a domain with which one claims expertise. It is only when these non-face domains achieve face-like holistic representations that their neural representations will encroach upon the true FFA.

Kanwisher (2010) suggests that because of the domain specificity of the FFA, learning can occur for new faces without affecting the stored information for non-face objects that is separately localized. If, as our data suggest, face and non-face object representations are not necessarily separate, then interference with learning may result. In future experiments, it would be interesting to push the bounds of expert recognition. How

many different visual domains can we learn to process holistically, and how are neural representations for diverse expert categories organized in the FFA? E1 did not explicitly recruit plane experts, so a more concrete assessment of individuals with expertise for several visual domains (whether trained or naturally-occurring) is necessary to answer this question.

Effects of laterality

Another important direction for future research expands upon E2 laterality effects. We observed an interesting dissociation between the right and left OFA regions when considering the proportional representation of category-selective voxels. Specifically, in the right OFA, car expertise led to increasing representations of cars but, also, increasing representations of sofa voxels. This trend was generally observed – at least marginally so – across most face-selective ROIs. However, a very different pattern emerged in the left OFA region, where car expertise recruited car voxels with a *cost* to the proportional representation of voxels maximally selective to sofas. These data show that the increase in neural selectivity for sofas with car expertise is not observed ubiquitously across cortex.

The direction of the laterality effect observed in the OFA is surprising, however, since we would expect greater effects of holistic processing in the right region and greater parts-based processing in the left (McCarthy et al., 1997; Rossion et al., 2000). In addition, the left OFA, but not the right OFA, showed an increase in the neural response for cars versus sofas in car voxels. The Car – Sofa amplitude effect is also found in the left pFG region, but not the corresponding right pFG. These data provide evidence that face-selective areas of the left hemisphere process cars and sofas as separable categories, whereas corresponding areas of the right hemisphere seem to process cars and sofas on the basis of their low-level visual similarities. Future studies can explore this hypothesis more directly,

for instance comparing right and left hemisphere car expertise effects for cars among visually similar objects vs. visually dissimilar objects.

Conclusion

Prior studies revealing only face-selective responses in the FFA (Grill-Spector et al., 2006) or in face patches (Tsao et al., 2006) relied on non-face categories that their participants likely had little experience individuating. While our results do not rule out an influence of genetics on specialization of the FFA (Wilmer et al., 2010), they suggest that the function itself is not specific to the face domain but rather supports learning more generally. Our effects of divided attention, which are spatially constrained to the right FFA, further implicate generality of FFA functioning. The work in the dissertation demonstrates that non-face object selectivity increases with expertise, in several visual areas including in the heart of the highly face-selective FFA and that under conditions of highly taxed perceptual processing, the right FFA becomes the main focus of these expertise effects in the ventral pathway.

APPENDIX A

LIST OF 34 STUDIES PRESENTED IN THE HISTOGRAM OF FIGURE 5.

1. Andrews, T.J., Clarke, A., Pell, P., & Hartley, T. (2010). Selectivity for low-level features of objects in the human ventral stream. *NeuroImage, 49(1)*, 703-711.

2. Op de Beeck, H.P., Brants, M., Baeck, A., & Wagemans, J. (2009). Distributed subordinate specificity for bodies, faces, and buildings in human ventral visual cortex. *Neuroimage, 49(4),* 1-12.

3. Carlson, T., Hogendoom, H., Fonteijn, H., & Verstraten, F.A. (2011). Spatial coding and invariance in object-selective cortex. *Cortex, 47(1)*, 14-22.

4. Downing, P.E., Chan, A.W.-Y., Peelen, M.V., Dodds, C.M., & Kanwisher, N. (2006). Domain specificity in visual cortex. *Cerebral Cortex, 16(10),* 1453-1461

5. Downing, P.E., Chan, A.W.-Y., Peelen, M.V., Dodds, C.M., & Kanwisher, N. (2006). Domain specificity in visual cortex. *Cerebral Cortex, 16(10),* 1453-1461.

6. Dricot, L., Sorger, B., Schiltz, C., Goebel, R., & Rossion, B. (2008). The roles of "face" and "non-face" areas during individual face perception: Evidence by fMRI adaptation in a brain-damaged prosopagnosic patient. *NeuroImage, 40(1),* 318-332.

7. Druzgal, T.J. & D'Esposito, M. (2003). Dissecting contributions of prefrontal cortex and fusiform face area to face working memory. *Journal of Cognitive Neuroscience, 15(6),* 771-784.

8. Golarai,G., Ghahremani, D.G., Whitfield-Gabrieli, S., Reiss, A., Eberhardt, J.L., Gabrieli, J.D.E., & Grill-Spector, K. (2007). Differential development of high-level visual cortex correlates with category-specific recognition memory. *Nature Neuroscience, 10(4),* 512-522.

9. Grill-Spector, K., Sayres, R., & Ress, D. (2006). High-resolution imaging reveals highly selective nonface clusters in the fusiform face area. *Nature Neuroscience, 9,* 1177-1185.

10. Grill-Spector, K., Knouf, N., & Kanwisher, N. (2004). The fusiform face area subserves face perception, not generic within-category identification. *Nature Neuroscience, 7(5),* 555-562.

11. Harley, E.M., Pope, W.B., Villablanca, J.P., Mumford, J., Suh, R., Mazziotta, J.C., Enxmann, D., & Engel, S.A. (2009). Engagement of fusiform cortex and disengagement of lateral occipital cortex in the acquisition of radiological expertise. *Cerebral Cortex, 19(11),* 2746-2754.

12. Haxby, J.V., Ungerleider, L.G., Clark, V.P., Schouten, J.L., Hoffman, E.A., & Martin, A. (1999). The effect of face inversion on activity in human neural systems for face and object perception. *Neuron, 22(1),* 189-99.

13. Ishai, A., Ungerleider, L.G., & Haxby, J.V. (2000). Distributed neural systems for the generation of visual images. *Neuron, 28(3),* 979-90.

14. Ishai, A., Haxby, J.V., & Ungerleider, L.G. (2002). Visual imagery of famous faces: Effects of memory and attention revealed by fMRI. *Neuroimage, 17(4),* 1729-1741.

15. Joseph, J.E., & Gathers, A.D. (2002). Natural and manufactured objects activate the fusiform face area. *Neuroreport, 13(7),* 935-938.

16. Kanwisher, N., McDermott, J., Chun, M.M. (1997). The fusiform face area: A module in human extrastriate cortex specialized for face perception. *Journal of Neuroscience, 17(11),* 4302-4311.

17. Kung, C.C., Peissig, J.J., & Tarr, M.J. (2007). Is region-of-interest overlap comparison a reliable Measure of category specificity? *Journal of Cognitive Neuroscience, 19(12),* 2019-2034.

18. Lehmann, C., Mueller, T., Federspiel, A., Hubi, D., Schroth, G., Huber, O., Strik, W., & Dierks, T. (2004). Dissociation between overt and unconscious face processing in the fusiform face area. *Neuroimage, 21(1),* 75-83.

19. McCarthy, G., Puce, A., Gore, J.C., & Allison, T. (1997). Face-specific processing in the human fusiform gyrus. *Journal of Cognitive Neuroscience, 9,* 605-610.

20. O'Craven, K.M., & Kanwisher, N. (2000). Mental imagery of faces and places activates corresponding stimulus-specific brain regions. *Journal of Cognitive Neuroscience, 12(6),* 1013-1023.

21. Peelen, M.V., & Downing, P.E. (2005). Selectivity for the human body in the fusiform gyrus. *Journal of Neurophysiology, 93(1),* 603-608.

22. Pourtois, G., Schwartz, S., Seghier, M.L., Lazeyras, F., & Vuilleumier, P. (2005). View-independent coding of face identity in frontal and temporal cortices is modulated by familiarity: An event-related fMRI study. *NeuroImage, 24(4),* 1214-1224.

23. Rhodes, G., Byatt, G., Michie, P.T., & Puce, A. (2004). Is the fusiform face area specialized for faces, individuation, or expert individuation? *Journal of Cognitive Neuroscience, 16(2),* 189-203.

24. Rossion, B., Caldara, R., Seghier, M., Schuller, A.M., Lazeyras, F., & Mayer, E. (2003). A network of occipito-temporal face-sensitive areas besides the right middle fusiform gyrus is necessary for normal face processing. *Brain, 126(11),* 2381-2395.

25. Schiltz, C., Sorger, B., Caldara, R., Ahmed, F., Mayer, E., Goebel, R., & Rossion, B. (2005). Impaired face discrimination in acquired prosopagnosia is associated with abnormal response to individual faces in the right middle fusiform gyrus. *Cerebral Cortex, 16(4),* 574-586.

26. Schwarzlose, R.F., Swisher, J.D., Dang, S., & Kanwisher, N. (2008). The distribution of category and location information across object-selective regions in human visual cortex. *Proceedings of the National Academy Sciences of the USA*, *105(11),* 4447-4452.

27. Schwarzlose, R.F., Baker, C.I., & Kanwisher, N. (2005). Separate face and body selectivity on the fusiform gyrus. *Journal of Neuroscience, 25(47),* 11055-11059.

28. Steeves, J., Dricot, L., Goltz, H.C., Sorger, B., Peters, J., Milner, A.D., Goodale, M.A., Goebel, R., & Rossion, B. (2009). Abnormal face identity coding in the middle fusiform gyrus of two brain-damaged prosopagnosic patients. *Neuropsychologia, 47(12),* 2584-2592.

29. Van den Stock, J., van de Riet, W.A.C., Righart, R., & de Gelder, B. (2008). Neural correlates of perceiving emotional faces and bodies in developmental prosopagnosia: An event-related fMRI-study. *PLoS ONE, 3(9),* e3195. doi:10.1371/journal.pone.0003195.

30. Xu, X., Yue, X., Lescroart, M.D., Biederman, I., Kim, J.G. (2009). Adaptation in the fusiform face area (FFA): Image or person? *Vision Research, 49(23),* 2800-2807.

31. Xu, X., Yue, X., Lescroart, M.D., Biederman, I., Kim, J.G. (2009). Adaptation in the fusiform face area (FFA): Image or person? *Vision Research, 49(23),* 2800-2807.

32. Yoon, J.H., D'Esposito, M., & Carter, C.S. (2006). Preserved function of the fusiform face area in schizophrenia as revealed by fMRI. *Psychiatry Research: Neuroimaging, 148 (2-3),* 205-216.

33. Yovel, G., & Kanwisher, N. (2004). Face perception domain specific, not process specific. *Neuron, 44(5),* 889-898.

34. Yovel, G., Tambini, A., & Brandman, T. (2008). The asymmetry of the fusiform face area is a stable individual characteristic that underlies the left-visual-field superiority for faces. *Neuropsychologia, 46(13),* 3061-3068.

SPATIAL EXTENT OF EXPERTISE EFFECTS IN E1.

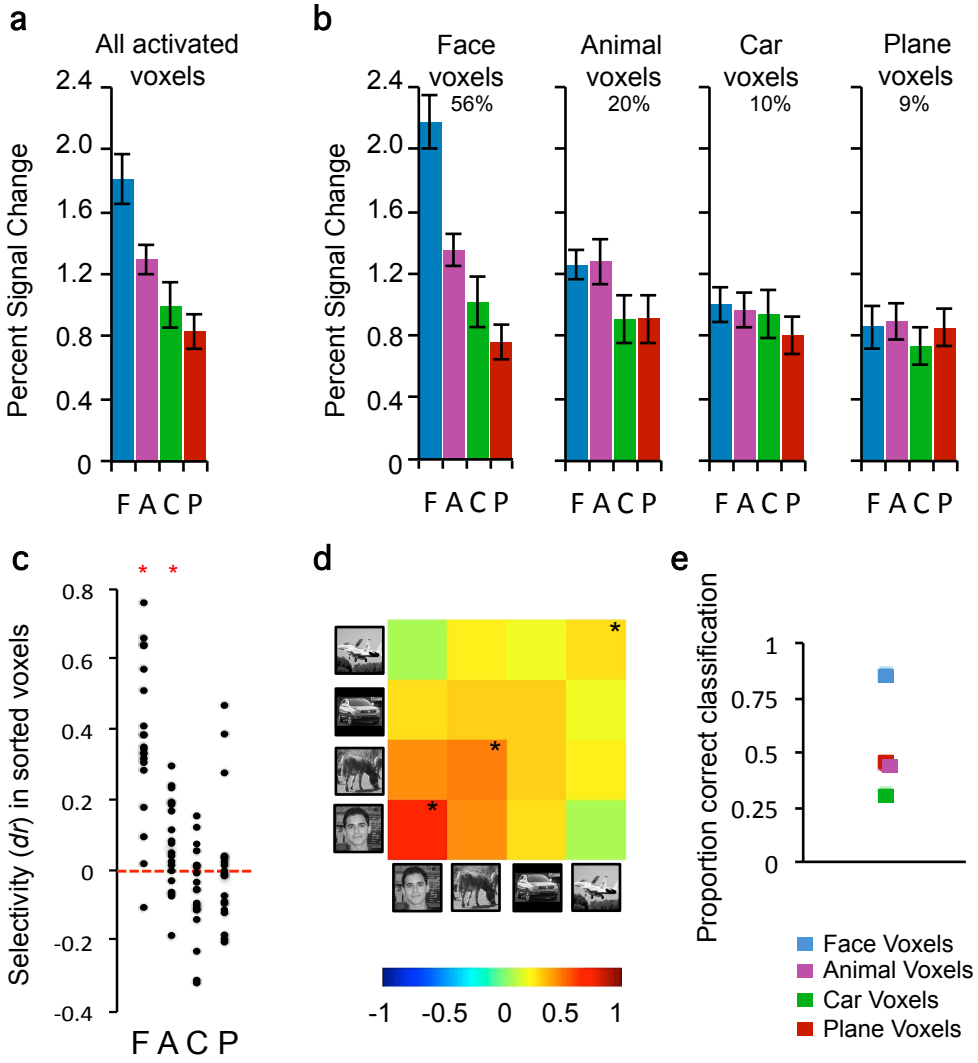

a. Category-specific response in 25 mm² area centered on peak of the right FFA. (a) Average percent signal change (PSC) to faces, animals, cars and planes averaged over all HR voxels that were more active for objects than scrambled matrices. (b) HR voxels were grouped by the category that elicited the maximal response in half of the data, and PSC for each category relative to scrambled matrices was plotted for the other half of the data. Error bars show SEM. (c) Voxel selectivity across participants measured using the signal detection theory measure d_a in sorted voxels, for half the data based in voxels sorted in the other half. (d) Cross-correlation for the voxel-by-voxel pairwise contrasts between within-category and between-category correlations, computed across independent halves of the data and averaged. Asterisks denote cases where, after a Fischer transformation, the within-category (on-diagonal) correlation was significantly larger than the between-category (off-diagonal) correlations. (e) Winner-take-all (WTA) classifier hit rate as a function of ROI size. The WTA is trained with the distributed response profile for each category

based on half the data, then computes the cross correlation between training set and the input to determine the winning category for the other half of the data. Chance is 25%.

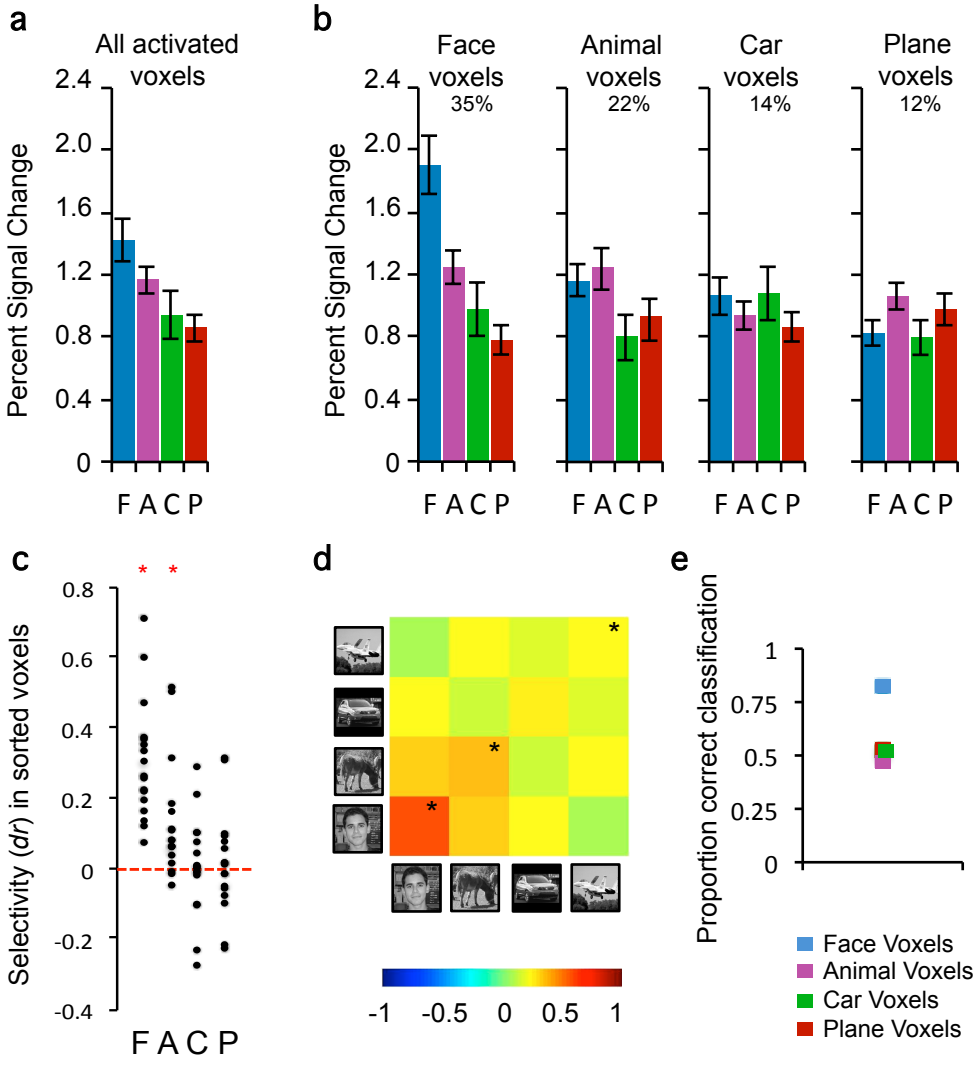

b. Equivalent to (a) for the 200 - 100 mm² ROI-ring surround the right FFA.

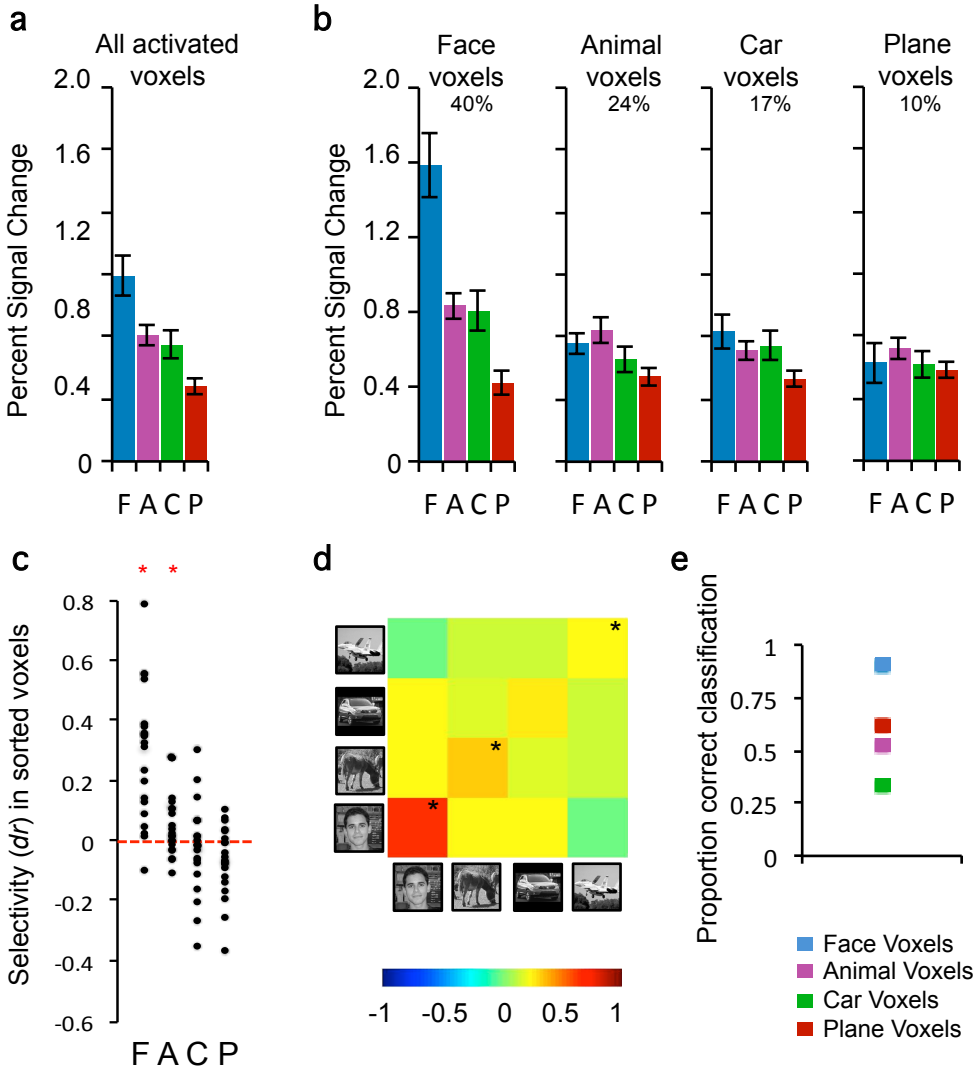

c. Equivalent to (a) for the 25 mm^2 area centered on peak of the left FFA.

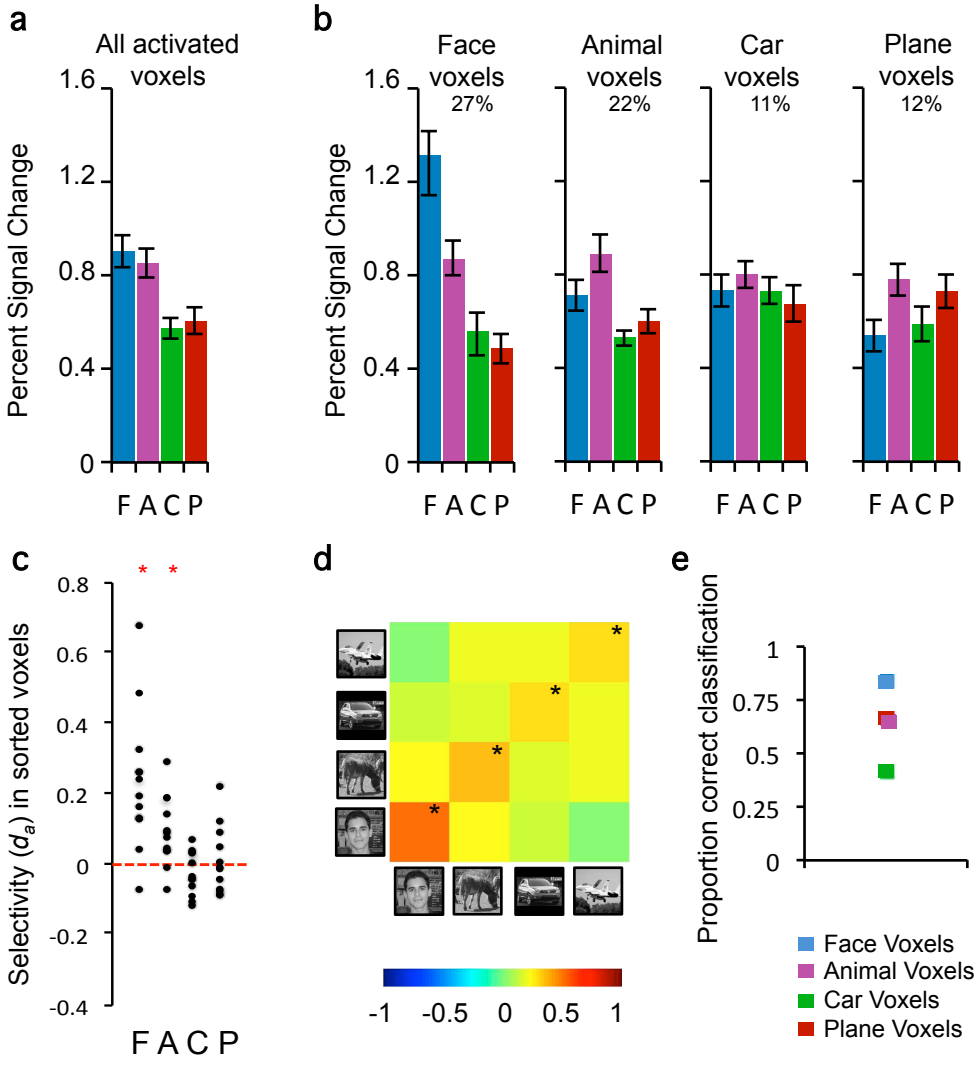

d. Equivalent to (a) for the 200 - 100 mm² ROI-ring surround the left FFA.

APPENDIX C

EDINBURGH HANDEDNESS INVENTORY[1]

Your Initials:_____

Please indicate with a check (✓) your preference in using your left or right hand in the following tasks.

Where the preference is so strong you would never use the other hand, unless absolutely forced to, put two checks (✓✓).

If you are indifferent, put one check in each column (✓ | ✓).

Some of the activities require both hands. In these cases, the part of the task or object for which hand preference is wanted is indicated in parentheses.

Task / Object	Left Hand	Right Hand
1. Writing		
2. Drawing		
3. Throwing		
4. Scissors		
5. Toothbrush		
6. Knife (without fork)		
7. Spoon		
8. Broom (upper hand)		
9. Striking a Match (match)		
10. Opening a Box (lid)		
Total checks:	LH =	RH =
Cumulative Total	CT = LH + RH =	
Difference	D = RH – LH =	
Result	R = (D / CT) × 100 =	
Interpretation: (Left Handed: R < -40) (Ambidextrous: -40 ≤ R ≤ +40) (Right Handed: R > +40)		

[1] Oldfield, R. C. (1971). The assessment and analysis of handedness: The Edinburgh inventory. *Neuropsycholollgia*, *9*, 97-113.

APPENDIX D

ZERO-ORDER CORRELATIONS WITH CAR d' AND PARTIAL CORRELATIONS WITH CAR d' WITH BIRD d' REGRESSED OUT FOR CATEGORY-SELECTIVE RESPONSES IN E2 SORTED VOXELS

a. For the right aFG and pFG, the zero-order correlations with Car *d'* (in white rows) and the partial correlations with Car *d'* with Bird *d'* regressed out (in grey rows), between the response for cars–faces, cars–sofas, and faces–sofas in voxels sorted into face, car and sofa voxels using independent data. Significant correlations are shown in bold (α = 0.05).

	Face Voxels			Car Voxels			Sofa Voxels		
	car-face	***car-sofa***	***face-sofa***	***car-face***	***car-sofa***	***face-sofa***	***car-face***	***car-sofa***	***face-sofa***
Right aFG (N=21)	**0.375**	0.311	-0.073	**0.442**	0.034	-0.288	**0.471**	0.057	**-0.381**
	0.355	0.32	-0.04	**0.425**	0.038	-0.264	**0.454**	0.063	-0.36
Right pFG (N=23)	**0.377**	0.104	-0.144	**0.462**	0.084	-0.303	**0.465**	0.151	-0.319
	0.371	0.113	-0.131	**0.452**	0.082	-0.297	**0.524**	0.171	-0.344

b. Equivalent of Table (a) for the left aFG and pFG.

	Face Voxels			Car Voxels			Sofa Voxels		
	car-face	***car-sofa***	***face-sofa***	***car-face***	***car-sofa***	***face-sofa***	***car-face***	***car-sofa***	***face-sofa***
Left aFG (N=20)	0.276	0.085	-0.228	**0.474**	0.054	**-0.403**	0.323	-0.04	-0.252
	0.267	0.037	-0.251	0.38	0.055	**-0.408**	0.3	-0.084	-0.276
Left pFG (N=19)	0.112	**0.391**	0.221	**0.458**	0.284	-0.201	**0.425**	-0.057	**-0.45**
	0.112	**0.423**	0.232	**0.464**	0.289	-0.223	**0.427**	-0.057	**-0.451**

b. Equivalent of Table (a) for the right OFA and left OFA.

	Face Voxels			Car Voxels			Sofa Voxels		
	car-face	***car-sofa***	***face-sofa***	***car-face***	***car-sofa***	***face-sofa***	***car-face***	***car-sofa***	***face-sofa***
Right OFA (N=16)	0.333	0.02	-0.191	0.278	-0.02	-0.224	0.258	-0.002	-0.166
	0.383	-0.08	-0.296	0.288	-0.094	-0.303	0.243	-0.059	-0.187
Left OFA (N=13)	-0.019	0.236	0.237	0.256	**0.579**	0.293	0.157	0.309	0.24
	-0.014	0.169	0.17	0.259	**0.604**	0.312	-0.06	0.155	0.249

b. Equivalent of Table (a) for the right PHG and left PHG.

	Face Voxels			Car Voxels			Sofa Voxels		
	car-face	***car-sofa***	***face-sofa***	***car-face***	***car-sofa***	***face-sofa***	***car-face***	***car-sofa***	***face-sofa***
Right PHG (N=26)	0.227	**0.369**	0.119	0.32	0.198	-0.142	**0.365**	0.022	-0.267
	0.235	**0.371**	0.12	0.32	0.198	-0.144	**0.367**	0.018	-0.286
Left PHG (N=24)	0.083	-0.142	-0.195	**0.384**	0.112	-0.332	0.186	-0.173	-0.27
	0.082	-0.158	-0.206	**0.388**	0.116	-0.332	0.182	-0.176	-0.268

APPENDIX E

INFERENTIAL STATISTICS FOR MIXED-CATEGORY RSVP MEANS AND ZERO-ORDER AND PARTIAL CORRELATIONS WITH EXPERTISE

a. For the right aFG and pFG, the t-statistic (in white rows) and the associated p-value (italicized in grey rows) for a one-sample t-test comparing each mean condition value to zero, for (C–F)S, (C–S)F and (F–S)C within all activated voxels (left) and voxels maximally activated to faces, cars and sofas (bottom). Significant effects are shown in bold (α = 0.05).

		All voxels		
ROI	N	***(C-F)S***	***(C-S)F***	***(F-S)C***
Right aFG	21	-0.608	0.339	1.763
		0.55	*0.738*	*0.093*
Right pFG	23	-1.074	1.941	**2.187**
		0.295	*0.065*	*0.04*

		Face voxels			Car voxels			Sofa voxels		
ROI	N	***(C-F)S***	***(C-S)F***	***(F-S)C***	***(C-F)S***	***(C-S)F***	***(F-S)C***	***(C-F)S***	***(C-S)F***	***(F-S)C***
Right aFG	21	**-2.555**	0.497	**3.234**	-0.372	-0.233	0.173	0.514	0.867	0.802
		0.019	*0.625*	*0.004*	*0.714*	*0.818*	*0.864*	*0.613*	*0.397*	*0.432*
Right pFG	23	-1.201	**2.298**	**2.817**	-1.039	1.735	1.645	-0.575	0.8	1.45
		0.242	*0.031*	*0.01*	*0.31*	*0.097*	*0.114*	*0.571*	*0.432*	*0.161*

b. For the right aFG and pFG, the zero-order correlations with Car *d'* (in white rows) and the partial correlations with Car *d'* with Bird *d'* regressed out (in grey rows), between the response for (C–F)S, (C–S)F and (F–S)C in all activated voxels (top) and in face, car and sofa voxels sorting using independent data. Significant correlations are shown in bold (α = 0.05).

		All voxels		
ROI	N	***(C-F)S***	***(C-S)F***	***(F-S)C***
Right aFG	21	0.416	0.328	-0.132
		0.398	0.303	-0.131
Right pFG	23	0.017	0.23	0.138
		0.009	0.237	0.151

		Face voxels			Car voxels			Sofa voxels		
ROI	N	***(C-F)S***	***(C-S)F***	***(F-S)C***	***(C-F)S***	***(C-S)F***	***(F-S)C***	***(C-F)S***	***(C-S)F***	***(F-S)C***
Right aFG	21	0.203	0.343	0.122	**0.551**	0.282	-0.369	0.278	0.28	0.046
		0.171	0.322	0.109	**0.536**	0.257	-0.379	0.249	0.259	0.081
Right pFG	23	-0.057	-0.041	0.022	-0.111	0.362	0.274	0.265	0.188	-0.133
		-0.06	-0.029	0.026	-0.127	0.363	0.287	0.263	0.205	-0.12

c. For the left aFG and pFG, the t-statistic (in white rows) and the associated p-value (italicized in grey rows) for a one-sample t-test comparing each mean condition value to zero, for (C–F)S, (C–S)F and (F–S)C within all activated voxels (left) and voxels maximally activated to faces, cars and sofas (bottom). Significant effects are shown in bold (α = 0.05).

		All voxels		
ROI	N	***(C-F)S***	***(C-S)F***	***(F-S)C***
Left aFG	20	**-2.17**	-0.636	1.134
		0.043	*0.532*	*0.271*
Left pFG	19	**-3.499**	0.519	**2.367**
		0.003	*0.61*	*0.029*

		Face voxels			Car voxels			Sofa voxels		
ROI	N	***(C-F)S***	***(C-S)F***	***(F-S)C***	***(C-F)S***	***(C-S)F***	***(F-S)C***	***(C-F)S***	***(C-S)F***	***(F-S)C***
Left aFG	20	**-3.806**	0.793	**3.712**	-0.728	0.143	0.96	-0.643	-1.431	-0.682
		0.001	*0.438*	*0.002*	*0.476*	*0.888*	*0.349*	*0.528*	*0.169*	*0.503*
Left pFG	19	**-3.515**	0.552	**2.807**	-1.565	0.842	1.58	**-2.29**	-0.079	1.188
		0.003	*0.588*	*0.012*	*0.135*	*0.411*	*0.132*	*0.034*	*0.938*	*0.25*

d. For the left aFG and pFG, the zero-order correlations with Car *d'* (in white rows) and the partial correlations with Car *d'* with Bird *d'* regressed out (in grey rows), between the response for (C–F)S, (C–S)F and (F–S)C in all activated voxels (top) and in face, car and sofa voxels sorting using independent data. Significant correlations are shown in bold (α = 0.05).

		All voxels		
ROI	N	***(C-F)S***	***(C-S)F***	***(F-S)C***
Left aFG	20	0.277	-0.224	-0.355
		0.339	-0.265	**-0.448**
Left pFG	19	0.006	-0.33	-0.367
		0.006	-0.336	-0.377

		Face voxels			Car voxels			Sofa voxels		
ROI	N	***(C-F)S***	***(C-S)F***	***(F-S)C***	***(C-F)S***	***(C-S)F***	***(F-S)C***	***(C-F)S***	***(C-S)F***	***(F-S)C***
Left aFG	20	0.218	0.003	-0.179	0.236	0.049	-0.21	0.176	-0.357	-0.358
		0.358	*0.012*	*-0.258*	*0.278*	*0.022*	*-0.318*	*0.174*	*-0.406*	*-0.389*
Left pFG	19	-0.065	-0.283	-0.22	0.211	-0.127	-0.225	-0.095	**-0.472**	-0.398
		-0.066	*-0.287*	*-0.223*	*0.211*	*-0.13*	*-0.23*	*-0.095*	***-0.475***	*-0.401*

e. For bilateral OFA, the t-statistic (in white rows) and the associated p-value (italicized in grey rows) for a one-sample t-test comparing each mean condition value to zero, for (C–F)S, (C–S)F and (F–S)C within all activated voxels (left) and voxels maximally activated to faces, cars and sofas (bottom). Significant effects are shown in bold (α = 0.05).

		All voxels		
ROI	N	***(C-F)S***	***(C-S)F***	***(F-S)C***
Right OFA	16	0.125	0.994	0.534
		0.902	*0.336*	*0.601*
Left OFA	13	-1.903	-0.475	1.628
		0.081	*0.643*	*0.129*

		Face voxels			Car voxels			Sofa voxels		
ROI	N	***(C-F)S***	***(C-S)F***	***(F-S)C***	***(C-F)S***	***(C-S)F***	***(F-S)C***	***(C-F)S***	***(C-S)F***	***(F-S)C***
Right OFA	16	-1.012	0.165	0.896	-0.512	0.174	0.638	1.944	1.682	-0.092
		0.327	*0.872*	*0.385*	*0.616*	*0.864*	*0.533*	*0.071*	*0.113*	*0.928*
Left OFA	13	-1.92	0.082	**2.139**	**-2.732**	-0.773	1.428	0.164	-0.314	-0.458
		0.079	*0.936*	*0.054*	*0.018*	*0.455*	*0.179*	*0.872*	*0.759*	*0.655*

f. For the bilateral OFA, the zero-order correlations with Car *d'* (in white rows) and the partial correlations with Car *d'* with Bird *d'* regressed out (in grey rows), between the response for (C–F)S, (C–S)F and (F–S)C in all activated voxels (top) and in face, car and sofa voxels sorting using independent data. No correlations were significant (α = 0.05).

		All voxels		
ROI	N	***(C-F)S***	***(C-S)F***	***(F-S)C***
Right OFA	16	0.188	-0.07	-0.198
		0.24	-0.059	-0.23
Left OFA	13	0.021	-0.162	-0.17
		-0.096	-0.234	-0.112

		Face voxels			Car voxels			Sofa voxels		
ROI	N	***(C-F)S***	***(C-S)F***	***(F-S)C***	***(C-F)S***	***(C-S)F***	***(F-S)C***	***(C-F)S***	***(C-S)F***	***(F-S)C***
Right OFA	16	0.223	0.07	-0.132	0.259	0.316	-0.092	-0.058	-0.4	-0.332
		0.255	*0.079*	*-0.15*	*0.307*	*0.337*	*-0.125*	*-0.022*	*-0.397*	*-0.368*
Left OFA	13	-0.086	-0.279	-0.196	-0.127	-0.285	-0.295	0.221	0.392	0.103
		-0.155	*-0.342*	*-0.186*	*-0.218*	*-0.284*	*-0.221*	*0.134*	*0.344*	*0.161*

g. For the right PHG, the t-statistic (in white rows) and the associated p-value (italicized in grey rows) for a one-sample t-test comparing each mean condition value to zero, for (C–F)S, (C–S)F and (F–S)C within all activated voxels (left) and voxels maximally activated to faces, cars and sofas (bottom). Significant effects are shown in bold ($\alpha = 0.05$).

		All voxels		
ROI	N	***(C-F)S***	***(C-S)F***	***(F-S)C***
Right PHG	26	0.146	-1.106	-0.972
		0.885	*0.279*	*0.341*
Left PHG	24	0.251	-0.985	-1.38
		0.804	*0.335*	*0.181*

		Face voxels			Car voxels			Sofa voxels		
ROI	N	***(C-F)S***	***(C-S)F***	***(F-S)C***	***(C-F)S***	***(C-S)F***	***(F-S)C***	***(C-F)S***	***(C-S)F***	***(F-S)C***
Right PHG	26	0.09	**-2.096**	-1.213	0.179	-0.968	-1.813	0.102	-0.62	-0.48
		0.929	*0.046*	*0.237*	*0.86*	*0.342*	*0.082*	*0.92*	*0.541*	*0.635*
Left PHG	24	-1.278	-0.479	1.317	0.473	-0.818	-1.419	1.54	-1.14	**-2.494**
		0.214	*0.637*	*0.201*	*0.641*	*0.422*	*0.169*	*0.137*	*0.266*	*0.02*

h. For bilateral PHG, the zero-order correlations with Car *d'* (in white rows) and the partial correlations with Car *d'* with Bird *d'* regressed out (in grey rows), between the response for (C–F)S, (C–S)F and (F–S)C in all activated voxels (top) and in face, car and sofa voxels sorting using independent data. No correlations were significant ($\alpha = 0.05$).

		All voxels		
ROI	N	***(C-F)S***	***(C-S)F***	***(F-S)C***
Right PHG	26	-0.013	-0.354	-0.267
		-0.014	*-0.359*	*-0.268*
Left PHG	24	-0.172	-0.246	-0.082
		-0.169	*-0.247*	*-0.089*

		Face voxels			Car voxels			Sofa voxels		
ROI	N	***(C-F)S***	***(C-S)F***	***(F-S)C***	***(C-F)S***	***(C-S)F***	***(F-S)C***	***(C-F)S***	***(C-S)F***	***(F-S)C***
Right PHG	26	0.044	-0.206	-0.157	-0.167	-0.198	-0.058	0.073	-0.353	-0.28
		0.043	-0.205	-0.156	-0.166	-0.199	-0.057	0.072	-0.356	-0.281
Left PHG	24	-0.222	-0.314	-0.016	0.009	-0.125	-0.133	-0.261	-0.222	-0.047
		-0.219	-0.314	-0.028	0.011	-0.123	-0.134	-0.26	-0.228	-0.053

REFERENCES

Allison, T., Ginter, H., & McCarthy, G. (1994). Face recognition in human extrastriate cortex. *Journal of Neurophysiology*, *71*(2), 821–825.

Ambady, N., Bernieri, F.J., & Richeson, J.A. (2000). Toward a histology of social behavior: Judgmental accuracy from thin slices of the behavioral stream. In M.P. Zanna (Ed.), *Advances in Experimental Social Psychology*, 32, 201–272.

Baker, C.I., Hutchison, T.L., & Kanwisher, N. (2007). Does the fusiform face area contain subregions highly selective for nonfaces? *Nature Neuroscience*, *10*(1), 3–4.

Bar, M., Neta, M., & Linz, H. (2006). Very first impressions. *Emotion*, *6*(2), 269–278.

Beauchamp, M.S., Lee, K.E., Argall, B.D., & Martin, A. (2004). Integration of auditory and visual information about objects in superior temporal sulcus. *Neuron, 41,* 809-823.

Behrmann, M., Marotta, J., Gauthier, I., Tarr, M.J, & McKeeff, T.J. (2005). Behavioral change and its neural correlates in visual agnosia after expertise training. *Journal of Cognitive Neuroscience*, *17*(4), 554–568.

Bentin, S., Allison, T., Puce, A., Perez, E., & McCarthy, G. (1996). Electrophysiological studies of face perception in humans. *Journal of Cognitive Neuroscience*, *8*(6), 551–565.

Bilalic, M., Langner, R., Ulrich, R., & Grodd, W. (2011). Many faces of expertise: Fusiform face area in chess experts and novices. *Journal of Neuroscience, 31*(28)*,* 10206-10214.

Bodamer, J. (1947). Die Prosop-Agnosie. *European Archives of Psychiatry and Clinical Neuroscience, 179,* 6–53.

Boggan, A.L., Bartlett, J.C., & Krawczyk, D.C. (2011). Chess masters show a hallmark of face processing with chess. *Journal of Experimental Psychology: General*, 1-6.

Boutet, I., & Chaudhuri, A. (2001). Multistability of overlapped face stimuli is dependent upon orientation. Perception, 30, 743–753.

Boutet, I., Gentes Hawn, A., & Chaudhuri, A. (2002). The influence of attention on holistic face encoding. *Cognition*, *84*, 321–341.

Bouvier, S.E., & Engel, S.A. (2006). Behavioral deficits and cortical damage loci in cerebral achromatopsia. *Cerebral Cortex, 16*(2)*,* 183-191.

Brainard, D.H. (1997). The psychophysics toolbox. *Spatial Vision, 10*(4)*,* 433-436.

Bruce, C., Desimone, R., & Gross, C.G. (1981). Visual properties of neurons in a polysensory area in superior temporal sulcus of the macaque. *Journal of Neurophysiology, 46,* 369-384.

Bukach, C.M., Gauthier, I., & Tarr, M.J. (2006). Beyond faces and modularity: The power of an expertise framework. *Trends in Cognitive Sciences*, *10*(4), 159–166.

Bukach, C.M., Phillips, S.W., Gauthier, I. (2010). Limits of generalization between categories and implications for theories of category specificity. *Attention, Perception & Psychophysics*, *17*(7), 1865-1874.

Busey, T.A., & Vanderkolk, J.R. (2005). Behavioral and electrophysiological evidence for configural processing in fingerprint experts. *Vision Research, 45,* 431-448.

Cheung, O.S., & Gauthier, I. (2010). Selective Interference on the holistic processing of faces in working memory. *Journal of Experimental Psychology: Human Perception and Performance*, *36*(2), 448-461.

Cox, D.D., & Savoy, R.L. (2003). Functional magnetic resonance imaging (fMRI) "brain reading": Detecting and classifying distributed patterns of fMRI activity in human visual cortex. *NeuroImage, 19,* 261-270.

Curby, K.M., Glazek, K., & Gauthier, I. (2009). A visual short-term memory advantage for objects of expertise. *Journal of Experimental Psychology: Human Perception and*

Performance, 35, 94-107.

Dehaene, S., Pegado, F., Braga, L.W., Ventura, P., Nunes Filho, G., Jobert, A., Dehaene-Lambertz, G., et al. (2010). How learning to read changes the cortical networks for vision and language. *Science*, *330*(6009), 1359–1364.

Desimone, R. (1991). Face-selective cells in the temporal cortex of monkeys. *Journal of Cognitive Neuroscience, 3*, 1–8.

Desimone, R., Albright, T.D., Gross, C.G., & Bruce, C. (1984). Stimulus-selective properties of inferior temporal neurons in the macaque. *Journal of Neuroscience, 4,* 2051-2062.

Dicarlo, J., & Cox, D. (2007). Untangling invariant object recognition. *Trends in Cognitive Sciences*, *11*(8), 333–341.

Downing, P.E., Chan, A. W.-Y., Pellen, M.V., Dodds, C. M., & Kanwisher, N. (2005). Domain specificity in visual cortex. *Cerebral Cortex*, *16*(10), 1453-1461.

Downing, P.E., Jiang, Y., Shuman, M., & Kanwisher, N. (2001). A cortical area selective for visual processing of the human body. *Science*, *293*(5539), 2470–2473.

Duchaine, B., & Nakayama, K. (2005). Dissociations of face and object recognition in developmental prosopagnosia. *Journal of Cognitive Neuroscience, 17,* 249-261.

Duchaine, B., & Nakayama, K. (2006). The Cambridge Face Memory Test: Results for neurologically intact individuals and an investigation of its validity using inverted face stimuli and prosopagnosic patients. *Neuropsychologia, 44,* 576-585.

Epstein, R., & Kanwisher, N. (1998). A cortical representation of the local visual environment. *Nature*, *392*(6676), 598–601.

Farah, M., Wilson, K., & Drain, M. (1998). What is“ special” about face perception? *Psychological Review*, *105*(3), 482–498.

Fodor, J. (1983). *Modularity of Mind*. Cambridge, MA: MIT Press.

Fodor, J. (2000). *The mind doesn’t work that way.* Cambridge, MA: MIT Press.

Furl, N., Garrido, L., Dolan, R.J., Driver, J., & Duchaine, B. (2011). Fusiform gyrus face selectivity relates to individual differences in face recognition ability. *Journal of Cognitive Neuroscience, 23*(7), 1723-1740.

Gauthier, I. (2000). What constrains the organization of the ventral temporal cortex. *Trends in Cognitive Sciences*, *4*(1), 1–2.

Gauthier, I., & Bukach, C. (2007). Should we reject the expertise hypothesis? *Cognition*, *103*(2), 322–330.

Gauthier, I., Curby, K.M., Skudlarski, P., & Epstein, R. (2005). Individual differences in FFA activity suggest independent processing at different spatial scales. *Cognitive and Affective Behavioral Neuroscience, 5*(2)*,* 222-234.

Gauthier, I., Curran, T., Curby, K.M., & Collins, D. (2003). Perceptual interference supports a non-modular account of face processing. *Nature Neuroscience*, *6*(4), 428–432.

Gauthier, I., Skudlarski, P., Gore, J.C., & Anderson, A.W. (2000). Expertise for cars and birds recruits brain areas involved in face recognition. *Nature Neuroscience*, *3*(2), 191–197.

Gauthier, I., & Tarr, M.J. (1997). Becoming a "Greeble" expert: Exploring mechanisms for face recognition. *Vision Research*, *37*(12), 1673–1682.

Gauthier, I., & Tarr, M.J. (2002). Unraveling mechanisms for expert object recognition: Bridging brain activity and behavior. *Journal of Experimental Psychology: Human Perception & Performance*, *28*(2), 431–446.

Gauthier, I., Tarr, M.J., Anderson, A.W., Skudlarski, P., & Gore, J.C. (1999). Activation of the middle fusiform "face area" increases with expertise in recognizing novel objects. *Nature Neuroscience*, *2,* 568–573.

Gauthier, I., Tarr, M.J., Moylan, J., Skudlarski, P., Gore, J. C., & Anderson, A.W. (2000). The fusiform "face area" is part of a network that processes faces at the individual level. *Journal of Cognitive Neuroscience*, *12*(3), 495–504.

Gauthier, I., Wong, A.C., Hayward, W.G., & Cheung, O.S. (2006). Font tuning associated with expertise in letter perception. *Perception, 35,* 541-559.

Grill-Spector, K., Knouf, N., & Kanwisher, N. (2004). The fusiform face area subserves face perception, not generic within-category identification. *Nature Neuroscience*, *7*(5), 555–562.

Grill-Spector, K., Sayres, R., & Ress, D. (2006). High-resolution imaging reveals highly selective nonface clusters in the fusiform face area. *Nature Neuroscience*, *9*(9), 1177–1185.

Hanson, S.J., & Schmidt, A. (2010). High-resolution imaging of the fusiform face area (FFA) using multivariate non-linear classifiers shows diagnosticity for non-face categories. *Neuroimage, 54,* 1715-1734.

Harel, A., Gilaie-Dotan, S., Malach, R., & Bentin, S. (2010). Top-down engagement modulates the neural expressions of visual expertise. *Cerebral Cortex, 20,* 2304-2318.

Harley, E.M., Pope, W.B., Villablanca, J.P., Mumford, J., Suh, R., Mazziotta, J.C., Enzmann, D., et al. (2009). Engagement of fusiform cortex and disengagement of lateral occipital cortex in the acquisition of radiological expertise. *Cerebral Cortex*, *19*(11), 2746–2754.

Hasselmo, M.E., Rolls, E.T., & Baylis, G.C. (1989). The role of expression and identity in the face-selective responses of neurons in the temporal visual cortex of the monkey. *Behavioral Brain Research, 32*, 203–218.

Haxby, J.V., Gobbini, M.I., Furey, M.L., Ishai, A., Schouten, J.L., & Pietrini, P. (2001). Distributed and overlapping representations of faces and objects in ventral temporal cortex. *Science*, *293*(5539), 2425–2430.

Haxby, J., Hoffman, E., & Gobbini, M. (2000). The distributed human neural system for face perception. *Trends in Cognitive Science*, *4*(6), 223–233.

Haxby, J. V., Horwitz, B., Ungerleider, L. G., Maisog, J. M., Pietrini, P., & Grady, C. L. (1994).

The functional organization of human extrastriate cortex: A PET-rCBF study of selective attention to faces and locations. *Journal of Neuroscience*, *14*, 6336–6353.

Haxby, J.V., Ungerleider, L.G., Horwitz, B., Maisog, J.M., Rapoport, S.I., & Grady, C.L. (1996). Face encoding and recognition in the human brain. *Proceedings of the National Academy of Sciences USA*, *93*, 922–927.

Hoffman, E.A., & Haxby, J.V. (2000). Distinct representations of eye gaze and identity in the distributed human neural system for face perception. *Nature Neuroscience*, *3*(1), 80–84.

Hole, G.J. (1994). Configural factors in the perception of unfamiliar faces. *Perception, 23,* 65-74.

Kanwisher, N. (2000). Domain specificity in face perception. *Nature Neuroscience*, *3*(8), 759–763.

Kanwisher, N., Chun, M.M. & Ledden, P. (1996): Functional imaging of human visual recognition. *Cognitive Brain Research,* 5, 55–67.

Kanwisher, N., McDermott, J., & Chun, M.M. (1997). The fusiform face area: A module in human extrastriate cortex specialized for face perception. *Journal of Neuroscience*, *17*(11), 4302–4311.

Kriegeskorte, N., Formisano, E., Sorger, B., & Goebel, R. (2007). Individual faces elicit distinct response patterns in human anterior temporal cortex. *Proceedings of the National Academy of Sciences USA*, *104*(51), 20600–20605.

Ku, S.P., Gretton, A., Macke, J., & Logothetis, N.K. (2008). Comparison of pattern recognition methods in classifying high-resolution BOLD signals obtained at high magnetic field in monkeys. *Magnetic Resonance Imaging, 26,* 1007-1014.

Malach, R., Reppas, J., & Benson, R. (1995). Object-related activity revealed by functional magnetic resonance imaging in human occipital cortex. *Proceedings of the National Academy of Sciences USA*, *92*, 8135–8139.

Martin, A., Wiggs, C.L., Ungerleider, L.G., & Haxby, J.V. (1996). Neural correlates of category-specific knowledge. *Nature*, *379*(6566), 649–652.

McAdams, C.J., & Maunsell, J.H. (1999). Effects of attention on the reliability of individual neurons in monkey visual cortex. *Neuron, 23,* 765-773.

McCarthy, G., Puce, A., & Gore, J. (1997). Face-specific processing in the human fusiform gyrus. *Journal of Cognitive Neuroscience*, *9*(5), 605–610.

McGugin, R.W., McKeeff, T.J., Tong, F., & Gauthier, I. (2010). Irrelevant objects of expertise compete with faces during visual search. *Attention, Perception & Psychophysics*, *73*(2), 309–317.

McKeeff, T.J., McGugin, R.W., Tong, F., & Gauthier, I. (2010). Expertise increases the functional overlap between face and object perception. *Cognition*, *117*(3), 355–360.

McKeeff, T.J., Remus, D.A., & Tong, F. (2007). Temporal limitations in object processing across the human ventral visual pathway. *Journal of Neurophysiology*, *98*, 382-393.

McKone, E., Kanwisher, N., & Duchaine, B. C. (2007). Can generic expertise explain special processing for faces. *Trends in Cognitive Sciences*, *11*(1), 8–15.

McMains, S.A., & Kastner, S. (2011). Interactions of top-down and bottom-up mechanisms in human visual cortex. *Journal of Neuroscience*, *31*, 587-597.

Ogawa, T., & Komatsu, H. (2006). Neuronal dynamics of bottom-up and top-down processes in area V4 of macaque monkeys performing a visual search. *Experimental Brain Research*, *173,* 1–13.

Op de Beeck, H.P., & Baker, C.I. (2009). The neural basis of visual object learning. *Trends in Cognitive Sc*ience, *14*(1), 22-30.

Op de Beeck, H.P., Baker, C.I., DiCarlo, J.J., & Kanwisher, N.G. (2006). Discrimination training alters object representations in human extrastriate cortex. *Journal of Neuroscience, 26,* 13025-13026.

O'Toole, A.J., Jiang, F., Abdi, H., & Haxby, J.V. (2005). Partially distributed representations of objects and faces in ventral temporal cortex. *Journal of Cognitive Neuroscience*, *17*(4), 580–590.

Palermo, R., & Rhodes, G. (2002). The influence of divided attention on holistic face perception. *Cognition*, *82*, 225-257.

Pelli, D.G. (1997). The VideoToolbox software of visual psychophysics: Transforming numbers into movies. *Spatial Vision, 10,* 437-442.

Perrett, D., & Mistlin, A. (1990). Perception of facial characteristics by monkeys. In W. Stebbins & M. Berkley (Eds.), *Comparative Perception (Vol. 2)* (187–215). New York: Wiley.

Perrett, D.I., Rolls, E.T., & Cann, W. (1982). Visual neurons responsive to faces in the monkey temporal cortex. *Experimental Brain Research, 47*, 329–342.

Perrett, D.I., Smith, P.A.J., Potter, D.D., Mistlin, A.J., Head, A.S., Milner, A.D., & Jeeves, M.A. (1985). Visual cells in the temporal cortex sensitive to face view and gaze direction. *Proceedings of the Royal Society of London. Series B, Biological Sciences, 223*, 293–317.

Puce, A., Allison, T, Asgari, M., & Gore, J. (1996). Differential sensitivity of human visual cortex to faces, letterstrings, and textures: A functional magnetic resonance imaging study. *Journal of Neuroscience*, *16*(16), 5205–5215.

Puce, A., Allison, T., Bentin, S., Gore, J.C., & McCarthy, G. (1998). Temporal cortex activation of humans viewing eye and mouth movements. *Journal of Neuroscience, 18*, 2188–2199.

Puce, A., Allison, T., Gore, J., & McCarthy, G. (1995). Face-sensitive regions in human extrastriate cortex studied by functional MRI. *Journal of Neurophysiology, 74*(3), 1192–1199.

Puri, A.M., Wojciulik, E., & Ranganath, C. (2009). Category expectation modulates baseline

and stimulus-evoked activity in human inferotemporal cortex. *Brain Research, 1301,* 89-99.

Reddy, L., & Kanwisher, N. (2007). Category selectivity in the ventral visual pathway confers robustness to clutter and diverted attention. *Current Biology, 17,* 2067-2072.

Reynolds, J.H., & Desimone, R. (2003). Interacting roles of attention and visual salience in V4. *Neuron, 37,* 853–863.

Richler, J.J., Cheung, O.S., & Gauthier, I. (2011). Holistic processing predicts face recognition. *Psychological Science, 22,* 464-471.

Robbins, R., & McKone, E. (2003). Can holistic processing be learned for inverted faces? *Cognition*, *88*(1), 79–107.

Rossion, B., Collins, D., Goffaux, V., & Curran, T. (2007). Long-term expertise with artificial objects increases visual competition with early face categorization processes. *Journal of Cognitive Neuroscience, 19*, 543-555.

Rossion, B., Dricot, L., Devolder, A., Bodart, J.M., Crommelinck, M., de Gelder, B., & Zoontjes, R. (2000). Hemispheric asymmetries for whole-based and part-based face processing in the human fusiform gyrus. *Journal of Cognitive Neuroscience, 12*(5*),* 793-802.

Rossion, B., Gauthier, I., Tarr, M.J., Despland, P., Bruyer, R., Linotte, S., et al. (2000). The n170 occipito-temporal component is delayed and enhanced to inverted faces but not to inverted objects: An electrophysiological account of face-specific processes in the human brain. *NeuroReport: For Rapid Communication of Neuroscience Research*, *11*, 69–74.

Rossion, B., Kung, C.-C., & Tarr, M.J. (2004). Visual expertise with nonface objects leads to competition with the early perceptual processing of faces in the human occipitotemporal cortex. *Proceedings of the National Academy of Science USA, 101*(40), 14521–14526.

Seidemann, E., & Newsome, W.T. (1999). Effect of spatial attention on the responses of area MT neurons. *Journal of Neurophysiology, 81,* 1783–1794.

Sergent, J., Ohta S., & Macdonald, B. (1992). Functional neuroanatomy of face and object processing: A positron emission tomography study. *Brain*, *115*, 15–36.

Sigala, N. & Logothetis, N.K. (2002). Visual categorization shapes feature selectivity in the primate temporal cortex. *Nature, 415*, 318-320.

Simmons, W.K., Bellgowan, P.S., & Martin, A. (2007). Measuring selectivity in fMRI data. *Nature Neuroscience, 10,* 4-5.

Talairach, J., & Tournoux, P. (1988). *Co-Planar Stereotaxic Atlas of the Human Brain*. New York, NY: Thieme Medical Publishers.

Tanaka, J.W., & Farah, M.J. (1993). Parts and wholes in face recognition. *Quarterly Journal of Experimental Psycholo*gy, *46*(2), 225–245.

Tarr, M.J., & Gauthier, I. (2000). FFA: A flexible fusiform area for subordinate-level visual processing automatized by expertise. *Nature Neuroscience*, *3*(8), 764–769.

Thomas, C.P., Avidan, G., Humphreys, K., Jung, K.J., Gao, F., & Behrmann, M. (2006). Reduced structural connectivity in ventral visual cortex in congenital prosopagnosia. *Nature Neuroscience*, *12*, 29-31.

Tong, F., Nakayama, N., Moscovitch, M., Weinrib, O., & Kanwisher, N. (2000). Response properties of the human fusiform face area. *Cognitive Neuropsychology*, *17,* 257–280.

Treue, S., & Martınez-Trujillo, J.C. (1999). Feature-based attention influences motion processing gain in macaque visual cortex. *Nature, 399,* 575–579.

Tsao, D.Y., Freiwald, W.A., Tootell, R.B.H., & Livingstone, M.S. (2006). A cortical region consisting entirely of face-selective cells. *Science*, *311*(5761), 670–674.

Tsao, D.Y., & Livingstone, M.S. (2008). Mechanisms of face perception. *Annual Reviews in Neuroscience*, *31*(1), 411–437.

Weiner, K.S., & Grill-Spector, K. (2010). Sparsely-distributed organization of face and limb activations in human ventral temporal cortex. *Neuroimage*, *52*(4), 1559–1573.

Williams, M.A., Berberovic, N. & Mattingley, J.B. (2007). Abnormal fMRI adaptation to unfamiliar faces in a case of developmental prosopagnosia. *Current Biology, 17,* 1259–1264.

Willis, J., & Todorov, A. (2006). First impressions: Making up your mind after a 100-ms exposure to a face. *Psychological Science*, *17*(7), 592–598.

Wilmer, J., Germine ,L., Chabris, C., Chatterjee, G., Nakayama, K., Williams, M., Loken, E., & Duchaine, B. (2010). Human face recognition ability is highly heritable. *Proceedings of the National Academy of Sciences USA, 107*, 5238–5241.

Wojciulik, E., Kanwisher, N., & Driver, J. (1998). Covert visual attention modulates face-specific activity in the human fusiform gyrus: fMRI study. *Journal of Neurophysiology, 79,* 1574-1578.

Wong, A.C., Palmeri, T.J., Rogers, B.P., Gore, J.C., & Gauthier, I. (2009). Beyond shape: How you learn about objects affects how they are represented in visual cortex. *Plos ONE*, 4(12), e8405.

Wong, A.C., Qu, Z., McGugin, R.W., & Gauthier, I. (2011). Interference in character processing reflects common perceptual expertise across writing systems. *Journal of Vision, 11,* 15.

Wong, Y., & Gauthier, I. (2010). A multimodal neural network recruited by expertise with musical notation. *Journal of Cognitive Neuroscience*, *22*(4), 695–713.

Xu, Y. (2005). Revisiting the role of the fusiform face area in visual expertise. *Cerebral Cortex*, *15*(8), 1234–1242.

Young, A.W., Hellawell, D., & Hay, D. (1987). Configural information in face perception. *Perception, 10,* 747–759.

Yue, X., Tjan, B.S., & Biederman, I. (2006). What makes faces special. *Vision Research*, *46*(22), 3802–3811.